Charles University

Faculty of Science

Department of Experimental Plant Biology

Modulation of Cytokinin Distribution Between Roots and Shoots

Ph.D. Thesis

Daniel Nedvěd

Supervisor: Bc. Ing. Klára Hoyerová, PhD.
Consultant: RNDr. Jan Petrášek, PhD.

2024

Abstract

Cytokinins are adenine derivatives and a group of plant hormones that regulate many physiological processes, including cell division, root and shoot growth, and senescence delay. Cytokinins transported via xylem have a specific role; they act as messengers of nitrate availability in soil. Precise regulation of cytokinin distribution between roots and shoots thus allows effective communication among various parts of the plant body. In my thesis, I address two mechanisms contributing to this regulation. First, I present findings about the kinetics of cytokinin transport across the biomembranes. I characterize EQUILIBRATIVE NUCLEOSIDE TRANSPORTER 3 (ENT3) as a membrane-bound carrier recognizing cytokinin nucleobases and ribosides. Using computational methods, I estimate which ENT3 residues interact with cytokinins and discuss the conservation of these residues within the ENT family. I further show that the *ent3* mutation alters shoot phenotype and the expression of the cytokinin-induced transcription factor *WUSCHEL*. These findings indicate that ENT3 contributes to the regulation of cytokinin distribution in plants via the uptake of root-borne cytokinins from the xylem in shoots. Second, I show that CYTOKININ DEHYDROGENASE (CKX), a cytokinin-degrading enzyme, is active in the xylem sap and thus negatively regulates cytokinins travelling from roots to shoots via their metabolism. The CKX activity in the xylem sap is stimulated by cytokinin, and cytokinin concentration in turn increases in response to nitrate supply. These findings indicate that CKX in the xylem sap contributes to the overall cytokinin distribution by mediating negative feedback to the increased cytokinin flux from roots to shoots.

Abstrakt

Cytokininy jsou deriváty adeninu a skupinou rostlinných hormonů, které regulují široké spektrum fyziologických procesů včetně buněčného dělení, růstu kořenů i nadzemní části a oddálení senescence. Cytokininy transportované skrze xylém mají specifickou roli; nesou informaci o dostupnosti dusičnanů v půdě. Přesná regulace rozdělení cytokininů mezi kořeny a nadzemní část tudíž umožňuje účinnou komunikaci napříč různými částmi rostlinného těla. Ve své práci se věnuji dvěma mechanismům přispívajícím k této regulaci. Za prvé představuji zjištění o kinetice cytokininového transportu přes biomembrány. Popisuji EKVILIBRATIVNÍ NUKLEOSIDOVÝ TRANSPORTÉR 3 (ENT3) jako membránový přenašeč cytokininových nukleobází a ribosidů. Pomocí výpočetních metod odhaduji, které zbytky ENT3 interagují s cytokininy, a diskutuji jejich konzervaci v rámci ENT rodiny. Dále ukazuji, že mutace *ent3* mění fenotyp nadzemní části a expresi transkripčního faktoru *WUSCHEL*, která je indukována cytokiny. Tato zjištění ukazují, že ENT3 přispívá k regulaci rozdělení cytokininů v rostlinách tím, že v nadzemní části přijímá z xylému cytokininy původem z kořene. Za druhé ukazuji, že CYTOKININ DEHYDROGENÁZA (CKX), enzym degradující cytokininy, je aktivní v xylémovém exudátu, a tedy že negativně reguluje cytokininy putující z kořene do nadzemní části prostřednictvím jejich metabolismu. Aktivita CKX v xylémovém exudátu je stimulována cytokininy a koncentrace cytokininů se zase zvyšuje spolu s dostupností dusičnanů. Tato zjištění ukazují, že CKX v xylému přispívá k celkové distribuci cytokininů tím, že zprostředkovává negativní zpětnou vazbu na zvýšení cytokininového toku z kořene do nadzemní části.

Declarations

I hereby declare that I wrote this thesis by myself, using data from my own research and the research I have participated in and that I have properly cited all information sources. This thesis has not been submitted as candidature for any other degree.

Daniel Nedvěd
26. 6. 2024, Horoušany

On behalf of the co-authors of the publications and manuscripts included in this thesis, I hereby confirm their consent with the inclusion. The candidate's contributions to each publication or manuscript are explicitly listed in the corresponding chapters.

Klára Hoyerová
25. 6. 2024, Prague

Acknowledgement

I thank my supervisor and consultant for their guidance, Roman Pleskot, Martin Lepšík, and Stanislav Vosolsobě for their consultations about computational and bioinformatical methods, Julie Talpová, Roberta Vaculíková, and Anita Birošíková for their professional assistance, and Václav Motyka for his critical proof-reading of the thesis. Last but not least, I thank my colleagues and family for their support.

Table of Contents

1 Abbreviation List

ABC	ATP-BINDING CASSETTE
ADP	adenosine diphosphate
AK	adenosine kinase
AP	APETALA
ATP	adenosine triphosphate
AZG	AZA-GUANINE RESISTANT
BA	benzyladenine
BAR	benzyladenosine
CCCP	cyanide carbonyl-3-chlorohydrazone
CHASE	cyclases/histidine kinase-associated sensory extracelular
CK	cytokinin
CKI	CYTOKININ-INSENSITIVE
CKX	CYTOKININ DEHYDROGENASE
CLV	CLAVATA
CPN	CYTOKININ/PURINE RIBOSIDE NUCLEOSIDEASE
CRF	CYTOKININ RESPONSE FACTOR
CYP	cytochrome P450 monooxygenase
cZ	*cis*-zeatin
DHZ	dihydrozeatin
DHZR	dihydrozeatin riboside
DMAPP	dimethylallyl pyrophosphate
DNA	deoxyribonucleic acid
DNP	dinitrophenol
ENT	EQUILIBRATIVE NUCLEOSIDE TRANSPORTER
HK	HISTIDINE KINASE
HP	HISTIDINE-CONTAINING PHOSPHOTRANSFER PROTEIN
HPLC	high-performance liquid chromatography
iP	isopentenyladenine
iPR	isopentenyladenosine
iPRDP	isopentenyladenosine diphosphate
iPRMP	isopentenyladenosine monophosphate
iPRTP	isopentenyladenosine triphosphate
IPT	ADENYLATE ISOPENTENYLTRANSFERASE
LOG	LONELY GUY (cytokinin riboside 5'-monophosphate phosphoribohydrolase)
mmT	*meta*-methoxytopolin
MPP	6-(3-methylpyrrol-1-yl)purine
mT	*meta*-topolin
NAA	1-naphthylacetic acid
NADP(H)	nicotinamide adenine dinucleotide phosphate (reduced)
NBTI	*S*-(4-nitrobenzyl)-6-thioinosine
NIGT	NITRATE-INDUCIBLE GARP-TYPE TRANSCRIPTIONAL REPRESSOR

NIN	NODULE INCEPTION PROTEIN
NLP	NIN-LIKE PROTEIN
NPF	NRT1/ PTR FAMILY
NRT	NITRATE TRANSPORTER
omT	*ortho*-methoxytopolin
oT	*ortho*-topolin
Phy	PHYTOCHROME
pT	*para*-topolin
PTR	PEPTIDE TRANSPORTER
PUP	PURINE PERMEASE
RAP2.6L	RELATED TO AP2 6L
RR	RESPONSE REGULATOR
SAM	shoot apical meristem
SWEET	SUGARS WILL EVENTUALLY BE EXPORTED TRANSPORTER
TCS	two-component system
tZ	*trans*-zeatin
tZR	*trans*-zeatin riboside
tZRDP	*trans*-zeatin riboside diphosphate
tZRMP	*trans*-zeatin riboside monophosphate
tZRTP	*trans*-zeatin riboside triphosphate
UDP	uridine diphosphate
UGT	UDP GLYCOSYLTRANSFERASE
WUS	WUSCHEL

2 Introduction

2.1 Cytokinins: Occurrence, Function, and History of Research

Cytokinins (CKs) are a class of plant hormones, signalling molecules mediating plant responses to internal and external stimuli. Their most prominent functions regulated by CKs include cell cycle and proliferation (Miller et al., 1956; Schaller et al., 2014), growth and branching of shoots and roots (Chang et al., 2015; Dello Ioio et al., 2012; Schaller et al., 2014; Skoog and Miller, 1957; Werner et al., 2001), chlorophyll retention and senescence delay (Dobránszki and Mendler-Drienyovszki, 2014; Richmond and Lang, 1957; Talla et al., 2016) or differentiation of vascular elements (Bishopp et al., 2011; De Rybel et al., 2014; Mähönen et al., 2006). However, the actual scope of CK effects is much larger thanks to CK interacting with other hormones and signalling cues (El-Showk et al., 2013; Liu et al., 2017; Zdarska et al., 2015).

CK research dates back to 1913, when Gottlieb Haberlandt induced proliferation of non-dividing potato parenchyma cells by treatment with phloem sap and proposed the existence of a proliferation-inducing hormone (Haberlandt, 1913; Kamínek, 2015). In 1955, Folke Skoog, Carlos O. Miller, and colleagues prepared the first such compound, a nucleobase 6-furfuryladenine or kinetin, by DNA cleavage (Miller et al., 1955b, 1955a). In 1963, David Letham and colleagues discovered the first naturally occurring CK. The substance was isolated from maize (*Zea mays*) kernels and named zeatin (Letham, 1963). Since then, CK research has provided insight into novel CK molecules, their metabolic conversions, transport processes involving CK-specific carriers, molecular basis of CK signalling cascades, and CK-mediated physiological processes (Kamínek, 2015; Kieber and Schaller, 2010). Besides plants, CKs are also produced by some bacterial strains (Arkhipova et al., 2005; Islam et al., 2016; Sun et al., 2024) and in the form of modified nucleotides in tRNA of various species, where they presumably serve to stabilize codon-anticodon interactions (Hall, 1970; Kline et al., 1969; Schweizer et al., 2017). CK research has also practical aspects; CKs have been studied and applied as agrochemicals (Khablak et al., 2024; Koprna et al., 2016), anti-oxidative agents in cosmetics (Cronin and Draelos, 2010; Othman et al., 2016), and potential anti-cancer drugs (Voller et al., 2019, 2010).

2.2 Chemical Diversity of Cytokinins

From the chemical point of view, CKs are N6-substituted derivatives of adenine, a canonical nucleobase found in nucleic acids, macroergic compounds or cofactors. CKs are classified as isoprenoid or aromatic according to the character of the N6-bound substituent, the so-called side chain. Isoprenoid CKs contain five-carbon side chains derived from the dimethylallyl (2-methyl-buten-2-yl) moiety. Isopentenyladenine (iP) contains a plain dimethylallyl side chain (Laloue et al., 1977). Terminal hydroxylation of iP yields zeatin. Due to the double bond in the side chain of iP, there are two possible zeatin isomers: *trans*-zeatin (tZ) and *cis*-zeatin (cZ). Both isomers exist and occur in nature (Hall et al., 1967; Leonard et al., 1971; Letham, 1963). Saturating the double bond in the side chain of tZ or cZ yields dihydrozeatin (DHZ) (Letham, 1973; Wang and Horgan, 1978). While tZ, cZ, and iP (and their derivatives) are found in most plant tissues (Corbesier et al., 2003; Gajdošová et al., 2011), DHZ-type CKs seem to be restricted to seeds, flowers, and fruits (Arnau et

al., 1999; Emery et al., 2000; Ionescu et al., 2017), suggesting they might play a specific role in plant reproduction. Various bacterial strands produce even more types of isoprenoid CKs. Some of these bacteria-produced CKs mimic the physiological effects of CK in plants and are employed by plant pathogens to facilitate invasions into their hosts (Evidente et al., 1991; Gibb et al., 2020; Pertry et al., 2010, 2009; Radhika et al., 2015).

Aromatic CKs contain side chains derived from the benzyl moiety. The simplest aromatic CK with no other side chain modifications is benzyladenine (BA) (Leopold and Kawase, 1964). Monohydroxylation of the aromatic core of the BA side chain yields three isomeric CKs: *meta*-topolin (mT), *ortho*-topolin (oT), and *para*-topolin (pT) (Horgan et al., 1975; Strnad, 1997; Strnad et al., 1994). Other types of aromatic CKs comprise methoxylated derivatives of BA, *ortho*-methoxytopolin (omT) and *meta*-methoxytopolin (mmT) (Tarkowská et al., 2003). The grain pathogen *Fusarium pseduograminerum* produces CK-like substances whose aromatic side chains are formed by the condensation of isoprenoid side chains of tZ or iP (Haidoune et al., 1990; Sørensen et al., 2017). One of these compounds, 6-(3-methylpyrrol-1-yl)purine (MPP), can also be formed in maize through a conversion from tZ (Hluska et al., 2016).

So-called synthetic CKs trigger CK-like effects in biological assays but are not produced naturally. The synthetic CKs include kinetin, already presented as the first isolated compound with CK-like effects (Miller et al., 1955b, 1955a), and some phenylurea derivatives: diphenylurea, *N*-(2-chloro-4-pyridyl)-*N'*-phenylurea or thidiazuron (Kieber and Schaller, 2018; Mok et al., 2005; Spíchal, 2012). As previously summarized, the diversity of CK side chains can significantly alter their hydrophobicity and thus modulate their ability to pass through the biological membranes or bind to various proteins (Nedvěd et al., 2021).

Apart from the differences in their side chains, the N6-substituted nucleobases are further modified by conjugation with endogenous molecules. CK ribosides are CK nucleobases with a ribosyl moiety attached to the N9 atom with an *N*-glycosylic bond. Phosphorylation of the O5' atom of a CK riboside yields CK monophosphates, diphosphates, and triphosphates. CK glucosides are formed by conjugating a CK nucleobase with glucose. This glycosylation can occur at the N3, N7 or N9 position through an *N*-glycosylic bond or an *O*-glycosylic bond at the side-chain hydroxyl group of tZ, DHZ or topolins (Mok et al., 2005; Vylíčilová et al., 2020). These different CK forms vary in their roles: nucleobases are the main form of biologically active CKs, CK ribosides and monophosphates are the main CK form transported over long distances (as well as biochemical precursors of other CK nucleobases, together with di- and triphosphates), and glycosides are predominantly the storage form of CKs (Hoyerová and Hošek, 2020; Lomin et al., 2015; Sakakibara, 2021).

A specific conjugate of tZ called lupinic acid has been identified in the blue lupine (*Lupinus angustifolius*). Lupinic acid contains an N-C bond between the N9 atom of tZ and the C3 atom of an alanyl residue, representing a CK conjugate with an amino acid (MacLeod et al., 1975). It is likely formed from tZ and *O*-acetylserine via a mechanism corresponding to that of cysteine synthase, but the conformation of this reaction and the role of lupinic acid in CK homeostasis remain to be explained (Entsch et al., 1983; Murakoshi et al., 1977; Wirtz and Hell, 2006).

2.3 Cytokinin Signalling Pathways

Being signalling molecules, CKs execute their physiological effects by binding to their molecular receptors and triggering a signalling cascade, resulting in changes in gene expression.

The CK signalling cascade shares some features with the two-component system (TCS), the predominant signalling pathway in bacteria (Zschiedrich et al., 2016). Akin to the TCS, CKs bind to dimeric membrane-bound receptors from the HISTIDINE KINASE (HK) family. HKs interact with CKs via the cyclases/histidine kinase-associated sensory extracellular (CHASE) domain located at the exoplasmic side of the membrane (Anantharaman and Aravind, 2001; Mougel and Zhulin, 2001). CK binding to the CHASE domain results in phosphorylation of a conserved His residue and subsequent relay of the phosphate group as follows: from the conserved His residue to an Asp residue at the receiver domain of HK, then to a His residue of a HISTIDINE-CONTAINING PHOSPHOTRANSFER PROTEIN (HP), and ultimately to an Asp residue of a RESPONSE REGULATOR (RR), which effectuates the CK response (Argueso and Kieber, 2024; Heyl and Schmülling, 2003; Hutchison and Kieber, 2002; Kieber and Schaller, 2010).

In mouse-ear cress (*Arabidopsis thaliana*), the CK-binding HKs comprise AHK2 (from *Arabidopsis* HK), AHK3, and AHK4 (Higuchi et al., 2004; Nishimura et al., 2004). Earlier reports on the subcellular localization of CK receptors have shown that all three AHKs are mainly associated with endomembranes (Caesar et al., 2011; Wulfetange et al., 2011). Later findings have revealed that CK signalling mediated by AHK3 and AHK4 also occurs from the plasma membrane and proposed dual-localization or cycling of CK receptors (Antoniadi et al., 2020; Kubiasová et al., 2020; Zürcher et al., 2016). The three AHKs differ in their affinities for various CK nucleobases, suggesting that their functions are not fully redundant (Lomin et al., 2015; Romanov et al., 2006; Spíchal et al., 2004; Stolz et al., 2011). Another member of the HK family, CYTOKININ-INSENSITIVE 1 (CKI1), was initially identified as a putative CK receptor (Kakimoto, 1996), but later studies have shown that CKI1 acts independently of CK dose (Hwang and Sheen, 2001; Yamada et al., 2001). Nevertheless, CKI1 acts upstream of the TCS components and affects CK-responding genes, indicating its involvement in CK signalling (Deng et al., 2010; Dobisova et al., 2017; Hejátko et al., 2009).

A. thaliana possesses six HPs, denoted AHP1-6. Of these, AHP1-5 shuttle between the cytoplasm and nucleus to mediate the phosphate transfer (Hradilová et al., 2007; Hutchison et al., 2006; Punwani et al., 2010). AHP6 lacks the phosphotransfer-mediating His residue and cannot propagate CK signalling. Instead, AHP6 acts as a CK signal repressor (Besnard et al., 2014; Mähönen et al., 2006).

Most RRs fall into two main categories: type-A and type-B. Type-A RRs are negative regulators of CK signalling. Their overexpression reduces plant sensitivity to exogenous CKs and vice versa (Kiba et al., 2003; To et al., 2007, 2004). *A. thaliana* RR3 (ARR3), 4 and 9, all of which are type-A ARRs, contribute to the regulation of the circadian rhythm (Ishida et al., 2008a; Salomé et al., 2005; Zheng et al., 2006), and ARR4 further interacts with PHYTOCHROME B (PhyB), a receptor for red light (Sweere et al., 2001), indicating links between the light and CK signalling pathways. Type-B RRs are transcription factors that regulate the expression of CK-responding genes (Argyros et al., 2008; Ishida et al., 2008b). The targets of type-B RRs include type-A RRs, which means that the transcription of type-A *RRs* is positively regulated by CKs and that type-A RRs mediate negative feedback to the CK signal (Hwang and Sheen, 2001; Kieber and Schaller, 2018; Sakai et al., 2001).

A minor group of RRs, called type-C RRs, comprise ARR22 and ARR24 in *A. thaliana*. Type-C ARRs do not possess a DNA-binding domain (thus do not act as transcription factors), and their transcription does not respond to CK stimuli, which makes them distinct from their type-A and

B counterparts (Horák et al., 2008; Kang et al., 2013; Kiba et al., 2004; Pils and Heyl, 2009). Alongside RRs, CK signal can be executed via CYTOKININ RESPONSE FACTORs (CRFs), transcription factors that directly interact with HPs and regulate a range of CK-related physiological responses (Cutcliffe et al., 2011; Raines et al., 2016; Rashotte et al., 2006; Zwack et al., 2016).

2.4 Metabolism of Cytokinins

To precisely regulate the output of CK signalling, plants modulate the availability of biologically active CK nucleobases through enzyme-catalysed biochemical reactions (i.e. CK metabolism) and carrier-mediated transport of CKs across biological membranes. CK metabolism comprises the biosynthesis of CK nucleobases, their conjugations yielding inactive CK forms, CK reactivation by the release of CK nucleobases from their conjugates, and irreversible CK degradation.

Biosynthesis of isoprenoid CKs iP and tZ begins with a reaction catalysed by ADENYLATE ISOPENTENYLTRANSFERASES (IPTs), in which adenosine diphosphate (ADP) or triphosphate (ATP) reacts with dimethylallyl pyrophosphate (DMAPP), yielding nucleotides isopentenyladenosine diphosphate (iPRDP) or isopentenyladenosine triphosphate (iPRTP), respectively (Kakimoto, 2001; Takei et al., 2001a). iP nucleotides can be hydroxylated by CYTOCHROME P450 MONOOXYGENASES (CYP) from the 85A subfamily, CYP85A1 and CYP85A2, to produce the corresponding nucleotides of tZ, i.e. *trans*-zeatin riboside diphosphate (tZRDP) or *trans*-zeatin riboside triphosphate (tZRTP). The reaction requires the reduced form of nicotinamide adenine dinucleotide phosphate (NADPH) as the reducing agent (Takei et al., 2004b). Considering the typical reaction mechanism of CYPs, the source of oxygen for the tZ ribotides is likely a dioxygen molecule (Esteves et al., 2021; Meunier et al., 2004). The plant pathogen *Agrobacterium tumefaciens* can synthesize tZ nucleotides directly from adenine species by an IPT-catalysed reaction that uses 1-hydroxy-2-methyl-2-(*E*)-butenyl 4-diphosphate (HMBDP) as a co-substrate. Upon plant infection, *A. tumefaciens* activates this pathway in its host, which contributes to the formation of tumours called crown galls (Åstot et al., 2000; Sakakibara et al., 2005).

The iP and tZ nucleotides can be converted to the respective CK nucleobases in a reaction catalysed by LONELY GUY (LOG) enzymes, which hydrolyse the *N*-glycosylic bond between the nucleobase and the phosphorylated ribosyl moiety (Kurakawa et al., 2007; Kuroha et al., 2009). Alternatively, iP and tZ ribosides can be hydrolysed to their respective ribosides, isopentenyladenosine (iPR) and *trans*-zeatin riboside (tZR) (Chen and Kristopeit, 1981a), followed by hydrolysis of the ribosides to the nucleobases (Chen and Kristopeit, 1981b). The latter reaction can be catalysed by a cell wall-bound enzyme CYTOKININ/PURINE RIBOSIDE NUCLEOSIDEASE 1 (CPN1) identified in rice (*Oryza sativa*) (Kojima et al., 2023) or nucleoside hydrolases that primarily target inosine, uridine, and xanthosine but that recognize CK ribosides as well (Kopečná et al., 2013). The enzyme or enzymes catalysing dephosphorylation of CK nucleotides remain to be characterized.

Biosynthesis of cZ involves IPT-mediated prenylation of tRNA followed by its degradation (Armstrong et al., 1969; Golovko et al., 2002). Of the nine IPTs of *A. thaliana*, AtIPT2 and 9 catalyse prenylation of tRNA, whereas the remaining isoforms catalyse the formation of iP nucleotides (Kasahara et al., 2004; Miyawaki et al., 2006). An enzymatic extract from bean (*Phaseolus vulgaris*) stimulated the conversion of tZ to cZ in the presence of flavin cofactors and the light, suggesting that cZ is also formed by a putative *cis-trans* isomerase (Bassil et al., 1993).

However, a later study showed that the light-dependent isomerization in the presence of flavin mononucleotide (FMN) occurs non-enzymatically and that the observed enzyme activity might stimulate FMN formation from flavin adenine dinucleotide (FAD) rather than the tZ-to-cZ conversion itself (Hluska et al., 2017). Biosynthesis of DHZ might involve NADPH-dependent reduction of tZ species catalysed by a putative zeatin reductase (Gaudinová et al., 2005; Martin et al., 1989). However, the enzyme remains to be identified. The biosynthesis of aromatic CKs is currently unknown.

CK nucleobases can undergo several types of conjugations producing biologically inactive compounds. CK glycosylation is catalysed by UDP GLYCOSYLTRANSFERASES (UGTs). In *A. thaliana*, *N*-glycosylated CKs are formed by AtUGT76C1 and AtUGT76C2, while *O*-glycosylated CKs by AtUGT85A1 (Chen et al., 2021; Hou et al., 2004; Jin et al., 2013; Šmehilová et al., 2016; Wang et al., 2013, 2011). *O*-glycosyltransferases AtUGT73C1 and AtUGT73C2 have also been shown to glycosylate CKs (Hou et al., 2004) but not as their preferred substrate (Chen et al., 2021; Jin et al., 2013). *O*-glucosylated CKs can be hydrolysed back to CK nucleobases by β-glucosidase activity (Brzobohatý et al., 1993). Hydrolysis of *N*-glycosylated CKs has been reported too (Hošek et al., 2020), but the details of this reaction remain to be explained.

Besides glycosylation, CK nucleobases can be converted to their biologically inactive precursors. Enzymes from the ADENINE PHOSPHORIBOSYLTRANSFERASE (APT) family catalyse the formation of CK nucleotides from the corresponding nucleobases, i.e. the opposite reaction than LOGs (Allen et al., 2002; Zhang et al., 2013). Enzymes from the ADENOSINE KINASE (ADK) family phosphorylate CK ribosides and produce nucleotides as well (Moffatt et al., 2000; Schoor et al., 2011).

Another way of CK inactivation is their oxidative degradation, catalysed by CYTOKININ DEHYDROGENASES (CKXs). The CKX reaction consists of two steps. First, the CK side chain becomes oxidized and forms an intermediate with an additional double bond (Kopečný et al., 2016, 2008; Popelková et al., 2006). The oxidizing agent in this step is FAD, which is covalently bound to a conserved His residue (Frébortová et al., 2004; Malito et al., 2004). The oxidized intermediate gets subsequently hydrolysed to adenine (or its conjugate such as adenosine) and an aldehyde derived from the CK side chain (Brownlee et al., 1975; Hare and van Staden, 1994; Pačes et al., 1971). The net result of the CKX reaction is the cleavage of the bond between the N6 atom and the side chain. CKXs cleave CK nucleobases, ribosides, nucleotides, and *N9*-glycosides derived from tZ and iP but not DHZ or BA. Substrate preferences of various CKX isoforms vary (Galuszka et al., 2007; Kowalska et al., 2010; Šmehilová et al., 2009; Zalabák et al., 2014).

2.5 Membrane Transport of Cytokinins

Another factor affecting CK homeostasis is CK transport across biological membranes. Membrane transport regulates CK distribution between the intracellular and extracellular space, as well as CK compartmentalization within the cell. Like all substances, CKs can be transported via simple diffusion, facilitated diffusion or active transport. In the case of simple diffusion, substances physically pass through the lipid component of the membrane. Due to the hydrophobic nature of the membrane interior, simple diffusion is restricted to small and non-polar molecules. Among CKs, simple diffusion is mostly relevant to CK nucleobases. Facilitated diffusion and active transport occur in the presence of a membrane-bound carrier. The two transport modes differ in their energy requirements. Facilitated diffusion occurs in the direction that diminishes the concentration

gradient, whereas active transport can increase this gradient thanks to coupling to another, exergonic process, such as the hydrolysis of macroergic substances or balancing out the membrane proton gradient (Nedvěd et al., 2021). The mode of transport mediated by a particular carrier can be assessed from homology, responses to a change of pH or treatment with a protonophore such as cyanide carbonyl-3-chlorohydrazone (CCCP) (Wormit et al., 2004).

CK-recognizing carriers comprise proteins from several families. PURINE PERMEASES (PUPs) are a family of plant-specific transporters. They mainly transport purine nucleobases, cytosine, and their derivatives, such as CKs or caffeine, but they show significantly lower affinities for the corresponding ribosides (Bürkle et al., 2003; Cedzich et al., 2008; Gillissen et al., 2000; Hu and Shani, 2023; Szydlowski et al., 2013). There is evidence of several PUPs being directly involved in the regulation of CK-mediated physiological responses. In *A. thaliana*, AtPUP14 acts as an importer of tZ from the extracellular space to the cytoplasm. The AtPUP14-mediated influx of tZ makes tZ inaccessible for the CHASE domain of the plasma membrane-bound CK receptors, which leads to a decrease in the CK signalling output. This AtPUP14 activity contributes to the establishment of CK signalling gradients, which are necessary for proper embryonic development (Zürcher et al., 2016). AtPUP8 is a plasma membrane-localized carrier that mediates tZ efflux. Its close relatives, AtPUP7 and AtPUP21, reside on the tonoplast and mediate tZ uptake from the cytoplasm into the vacuole. Triple mutants *atpup7,8,21* have smaller leaves and display reduced CK signalling output in the shoot apical meristem (Hu et al., 2023). In rice, OsPUP4 (also known as Big Grain3) transports CKs from apoplast to cytoplasm (Xiao et al., 2019), from where they can be further transported to the endoplasmic reticulum via OsPUP7 (Qi and Xiong, 2013) and further distributed in a cell-to-cell manner through plasmodesmata. OsPUP1 is a CK transporter localized on the endoplasmic reticulum membrane of vascular cells, suggesting its involvement in the symplastic unloading of CKs (Xiao et al., 2020). OsPUP11 can be translated from two transcripts with distinct tissue-specific and subcellular localizations. Loss of OsPUP11 function alters the expression of type-A *RR* genes in grains (Rong et al., 2024).

AZA-GUANINE RESISTANT (AZG) is a family of purine nucleobase transporters closely related to the azgA permease from the fungus *Aspergillus nidulans*. In *A. thaliana*, this family comprises two proteins, AtAZG1 and AtAZG2 *(Mansfield et al., 2009)*. Both these proteins mediate the uptake of tZ, BA, and kinetin into the cytoplasm (Tessi et al., 2023, 2020). Structural assessment of AtAZG1 has further revealed that the protein adopts a homodimeric structure and that tZ, BA, and kinetin bind at the same position as adenine (Xu et al., 2024). Both AtAZG1 and AtAZG2 regulate the lateral root emergency via CK uptake. Moreover, AtAZG1 stabilizes PIN-FORMED 1 (AtPIN1), an exporter of plant hormone auxin, and directly influences auxin-CK interactions during the shaping of the root architecture (Marhavý et al., 2014; Tessi et al., 2023, 2020).

ATP-BINDING CASSETTE (ABC) is a large family of carriers. It is present in diverse species and involved in the transport of a great variety of compounds. ABC proteins mediate transport coupled to the ATP hydrolysis (Wilkens, 2015). Plants possess proteins from eukaryotic ABC subfamilies A-G and also ABCIs, which are related to prokaryotic ABC subunits (Hwang et al., 2016; Verrier et al., 2008). AtABCG14 exports CK nucleobases and ribosides from the cytoplasm to the apoplast. Losing the transport activity of AtABCG14 causes CK accumulation in roots and lowers CK concentrations in xylem sap, demonstrating the role of AtABCG14 in the loading of CKs to the xylem and their subsequent root-to-shoot translocation (Ko et al., 2014; Zhang et al., 2014; Zhao et al., 2023). Similar roles are played by AtABCG11 (Yang et al., 2022)

and OsABCG18 in rice (Zhao et al., 2019). AtABCG11 and AtABCG14 can form heterodimers, suggesting they might cooperate in CK transport (Le Hir et al., 2013). AtABCI19, AtABCI20, and AtABCI21 are endoplasmic reticulum-localized proteins modulating CK-mediated responses, but their involvement in CK transport remains to be shown (Hu and Shani, 2023; Kim et al., 2020). MtABCG40 and MtABCG56 are CK transporters regulating root nodulation in barrel medic (*Medicago truncatula*) (Jamruszka et al., 2024; Jarzyniak et al., 2021).

A member of the SUGARS WILL EVENTUALLY BE EXPORTED TRANSPORTER (SWEET) family in barley (*Hordeum vulgare*), HvSWEET11b, transports CKs alongside sugars, the typical substrate of SWEET proteins (Chen, 2014; Radchuk et al., 2023). HvSWEET11b-mediated CK transport is necessary for proper grain development (Radchuk et al., 2023).

The EQUILIBRATIVE NUCLEOSIDE TRANSPORTER (ENT) family comprise nucleoside (i.e. ribosylated nucleobases) carriers that are widespread among all domains of life (Boswell-Casteel and Hays, 2017; Girke et al., 2014; Li et al., 2003). In *A. thaliana*, loss of AtENT3 and 8 reduces the uptake of ribosylated CKs by hypocotyl explants. The *atent8* mutant is also less sensitive towards exogenously applied iPR but not iP (Sun et al., 2005). AtENT3 further contributes to the regulation of CK distribution between roots and shoots via CK retention in roots (Korobova et al., 2021). AtENT6 (and to a lesser extent AtENT3 and 7) mediates adenosine uptake that decreases in the presence of tZR and iPR (Hirose et al., 2008). Similarly, iPR inhibits adenosine uptake mediated by OsENT2. OsENT2 has also been directly shown to transport tZR and iPR (Hirose et al., 2005).

2.6 Cytokinin Distribution in Plants and Long-Distance Transport

CKs are present in both phloem and xylem, the vascular systems responsible for the distribution of various substances among different tissues and organs. CKs transported through the vasculature act as a long-distance signal and contribute to the coordination of diverse physiological processes (Osugi et al., 2017; Sakakibara, 2021). While not further discussed in this text, it should be noted that short-range (paracrine) CK signalling exists too (Faiss et al., 1997; Kurakawa et al., 2007; Poitout et al., 2018; Werner and Schmülling, 2009).

The CK contents in the phloem and xylem differ. The former contains mostly iP- and cZ-derived species, with iPR, iPRMP, and cZR being the most abundant ones (Corbesier et al., 2003; Hirose et al., 2008). In the xylem, the CK fraction mostly consists of tZR and tZ (Hirose et al., 2008; Ko et al., 2014). The differential composition of CK fractions in the two vascular pathways is consistent with the expression pattern of *AtCYP735A2*, which is predominantly localized in roots. *AtCYP735A1* is expressed in roots and flowers but to a lesser extent than *AtCYP735A2* (Takei et al., 2004b). Mutating both *AtCYP735A* genes shifts the composition of the CK fraction in the xylem sap, roots, and shoots. In each of these plant parts, iP-derived CKs become the dominant CK type, while the absolute CK amounts remain comparable with the wild type (Kiba et al., 2013; Ko et al., 2014). The deficiency of tZ-type CKs results in a retardation of shoot growth, indicating that hydroxylation of CKs in the xylem is a necessary feature of CK long-distance signalling (Kiba et al., 2013). The diverse compositions of the CK fractions in the xylem and phloem could also be related to the differential expression patterns of *AtIPTs*. Notably, *AtIPT1* is expressed in the xylem-surrounding procambium cells, *AtIPT5* in the primary root columella, xylem-radius pericycle cells

developing into root primordia and subsequently in the lateral root caps, whereas *AtIPT3* is expressed in the phloem and to a lesser extent in the root pericycle (Miyawaki et al., 2004). These distributions indicate that CKs found in the phloem and xylem might be synthesized by different IPT isoforms. Interestingly, *AtIPT2* and *9* are expressed ubiquitously (Miyawaki et al., 2004), suggesting that cZ-type CKs are synthesized throughout the whole plant, making them good candidates for the mediators of short-range CK signalling.

The root-to-shoot flow of CK positively responds to the nitrate availability in the plant's environment. Increased nitrate supply boosts CK concentration in the xylem sap (Takei et al., 2001b) as well as the expression of *AtIPT3*, *AtIPT5*, *AtCYP735A2*, and *AtABCG14* (Abualia et al., 2022; Maeda et al., 2018; Ramireddy et al., 2014; Takei et al., 2004a). While *AtIPT3* expression increases as soon as one hour after the increase of nitrate supply, the increase in *AtIPT5* expression is only visible in long-term treatments (Takei et al., 2004a). Conversely, *atipt3,5,7* and *atabcg14* mutants cannot properly respond to an increase in nitrate supply (Poitout et al., 2018), indicating that the tZ-type CKs travelling from roots to shoots carry the message about nitrate availability. Transcription factors involved in the induction of the CK-related genes in response to nitrate include NIN-LIKE PROTEIN 7 (NLP7) and NITRATE-INDUCIBLE GARP-TYPE TRANSCRIPTIONAL REPRESSOR 1 (NIGT1) (Alvarez et al., 2020; Maeda et al., 2018; Marchive et al., 2013). Nitrate-dependent *AtIPT3* expression is also mediated by the NRT1/ PTR FAMILY 6.3 (NPF6.3) protein, which functions as a nitrate transporter and sensor at the same time (Krouk et al., 2010). AtIPT3 being downstream of NPF6.3 is consistent with the fast enhancement of the *AtIPT3* expression following the nitrate treatment (Abualia et al., 2023; Miyawaki et al., 2004; Takei et al., 2004a; Wang et al., 2003). Interestingly, targets of NLP7 also include CK transporters AtPUP14 and AtPUP18, whose roles in the response to nitrate remain to be explained (Abualia et al., 2023).

CK distribution between roots and shoots also depends on the amount of available sugars and the carbon dioxide concentration. *A. thaliana* plants grown in carbon dioxide-enriched atmosphere accumulate CKs in shoots, which results in larger shoots. In the roots of such treated plants, the expression of *AtCYP735A2* and *AtIPT3* increases, whereas the expression of *AtIPT5* decreases in roots and shoots alike, possibly due to the negative regulation of AtIPT5 by CK (Kiba et al., 2019; Miyawaki et al., 2004; Sakakibara, 2021).

CKs travelling from roots to the shoot apex activate WUSCHEL (WUS), the regulator of stem cells of the shoot apical meristem (SAM) (Gordon et al., 2009; Lopes et al., 2021). *WUS* expression and the associated phenotype (the meristem size and leaf emergency rate) in *A. thaliana* respond positively to nitrate. In the *atipt1,3,4,7* and *atcyp735a1,2* mutants, the meristem size decreases compared to the control, but this phenotype can be rescued by grafting mutant scions onto wild-type stocks, indicating that the SAM activity is regulated by root-borne tZ-type CKs (Landrein et al., 2018). Of the two most abundant CK species in the xylem, tZR and tZ, only the former can control SAM-associated physiological traits. Grafting the *atlog1-7* mutant scion onto the wild-type stock does not rescue the reduced meristem size, indicating that the root-borne CKs need to be activated in the shoot apex by LOGs to properly induce *WUS* expression (Davière and Achard, 2013; Osugi et al., 2017; Sakakibara, 2021). The cytoplasmic localization of the LOG enzymes (Kuroha et al., 2009) implies that prior to its activation, the root-borne tZR has to be transported from the apoplast into the cell by a membrane-bound carrier (or multiple carriers) recognizing ribosylated CKs.

3 Aims

CK distribution between roots and shoots is mediated by a complex network involving CK transport across membranes and over long distances, CK metabolic conversions, and regulation of these processes by external cues as well as interactions with other signalling pathways. CKs travelling from roots to shoots are an indispensable marker of nutrient availability.

Since my arrival at the Institute of Experimental Botany, I have participated on several projects focused on the transport and metabolic processes that participate on the regulation of CK homeostasis. In one project, we have addressed the cellular uptake of CK ribosides. Ribosylated CKs are the major CK form transported from roots to shoots, so it can be assumed that their uptake from the xylem in the shoot is mediated by a system of membrane-bound carriers (Sakakibara, 2021). Good candidates for such transporters are members of the ENT family (Girke et al., 2014), which has prompted us to systematically examine the transport activity of *A. thaliana* ENTs towards CKs. In another project, we have addressed CKX activity that my colleagues had previously detected in the xylem sap of oats (*Avena sativa*). The presence of a CK-degrading enzyme in the xylem might be an important factor in the CK root-to-shoot flux, possibly contributing to a negative feedback loop triggered by an increase of CK concentration in the xylem due to increased nitrate supply. My aims in this thesis are:

1. To evaluate the kinetics of the cellular uptake of CK ribosides, characterize the CK transport activity of AtENT3 (a representative of the *A. thaliana* ENTs) in direct assays, and assess the impact of the membrane transport of CK ribosides on shoot development.
2. To characterize CKX isoforms in oats and CKX activity in the oat xylem sap and to examine whether this activity responds to increased nitrate supply.

These objectives represent unknown links in the working scheme of CK distribution between roots and shoots (**Figure 1**).

▼**Figure** 1: A schematic representation of CK distribution between roots and shoots in response to nitrate supply. Carriers such as NPF6.3 transport nitrate from soil across the plasmatic membrane (PM). The nitrate stimulates transcription factor NLP7, which upregulates CK biosynthetic genes in roots, *IPTs* (catalysing formation of iP-type CKs) and *CYP735A1, 2* (catalysing formation of tZ-type CKs). In addition, NLP7 stimulates NIGT1, a repressor of further CK synthesis. Root-borne *trans*-zeatin riboside monophospahate (tZRMP) is activated by LOG enzymes to tZ or dephosphorylated to tZR. Both tZ and tZR are exported into the xylem by ABCG14 and can be re-uptaken by ENT3. In shoots, root-borne tZ and tZR (after being converted to tZ) regulate leaf size through the CK signal cascade (denoted as the two-component system: *TCS*). In the shoot apex, tZR is transported from the apoplast to the cytoplasm, then activated by AK and LOG, and as tZ stimulates the expression of *WUS*, which regulates further physiological traits, such as SAM size and leaf emergency rate. Non-ribosylated root-borne tZ cannot trigger such response, presumably due to its degradation (depicted as three arrows in a circle) catalysed by CKX in the apex area. In my thesis, I address the impact and possible identity of the membrane-bound carrier responsible for the uptake of root-borne tZR from the apoplast and the possible degradation of tZ throughout its entire travel from roots. Both these issues are marked with a question mark (?). Adapted from (Abualia et al., 2023; Qi and Xiong, 2013; Sakakibara, 2021; Xiao et al., 2020).

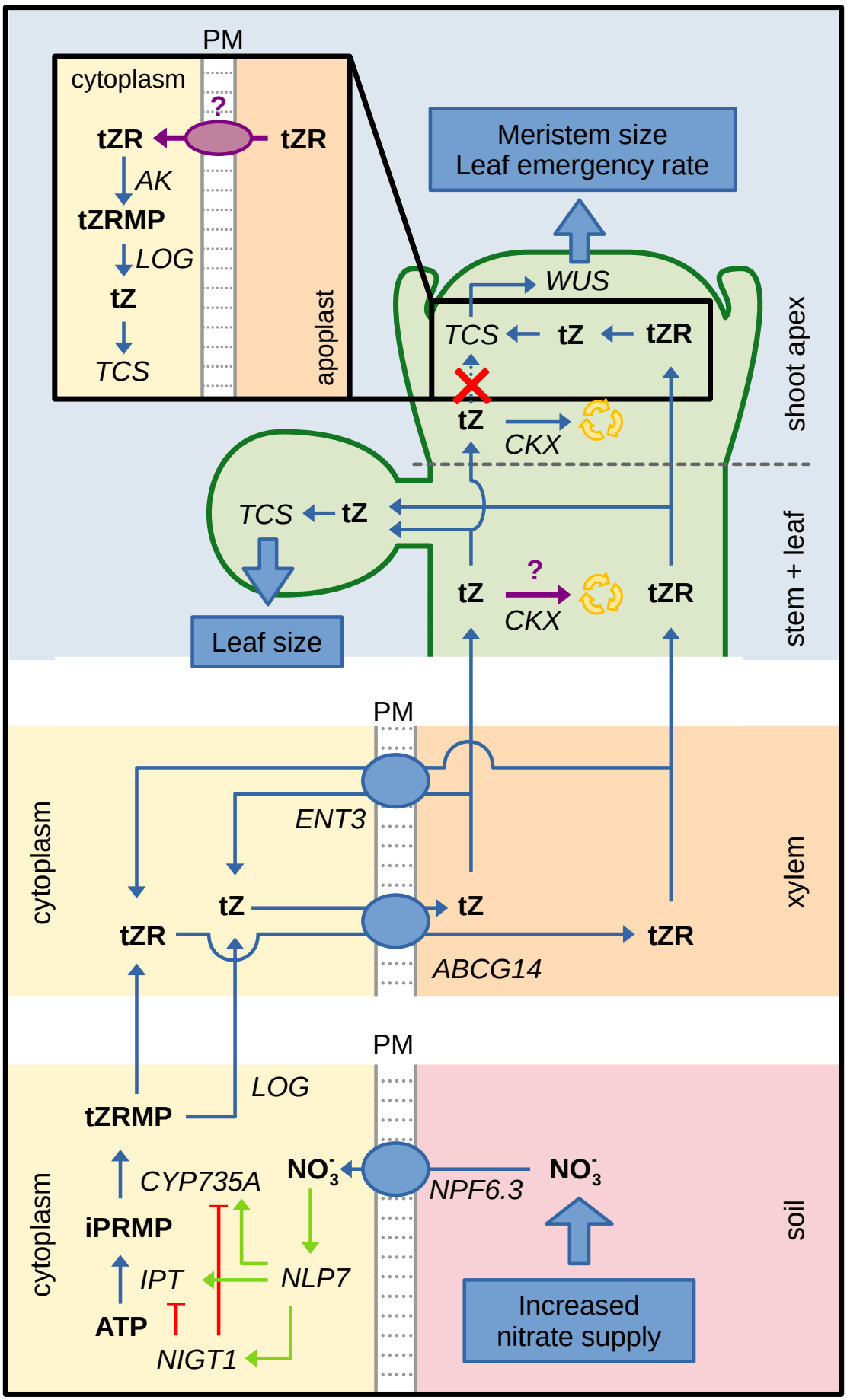
PM
cytoplasm
?
tZR
tZR
AK
tZRMP
LOG
tZ
TCS
apoplast
Meristem size
Leaf emergency rate
WUS
TCS
tZ
tZR
shoot apex
tZ
CKX
TCS
tZ
stem + leaf
?
tZ
CKX
tZR
Leaf size
PM
ENT3
cytoplasm
tZ
tZ
tZR
tZR
ABCG14
xylem
PM
LOG
tZRMP
CYP735A
NO3-
NPF6.3
NO3-
cytoplasm
iPRMP
IPT
NLP7
ATP
NIGT1
Increased
nitrate supply
soil

4 Results

4.1 Differential Subcellular Distribution of Cytokinins: How Does Membrane Transport Fit into the Big Picture?

In this review article, my colleagues and I summarize the recent development in the research of CK membrane transport in the context of chemical properties of the CK molecules and the implications of the CK-specific membrane-bound carriers for CK homeostasis at the subcellular level. We begin with an overview of the CK structural variety with respect to the N6 atom substitution and the formation of CK conjugates. Next, we examine how chemical diversity affects the hydrophobicity of CK molecules. Hydrophobicity is a physicochemical property that determines how readily a molecule diffuses across the phospholipid bilayer and interacts with proteins. It follows that CK species with different hydrophobicities should be recognized by different carriers or bind to the same carrier with significantly different affinities. We present structure-based predictions of CK hydrophobicities (in terms of their octanol-water partition coefficients) according to Wildman and Crippen (1999) and predictions by Molinspiration Property Calculation Service (https://www.molinspiration.com, last accessed on 11 June 2024) compared with elution times on a high-performance liquid chromatography (HPLC) column publishes by Šimura and colleagues (2018). Both predictions show, among others, that the partition coefficients of iP and iPR are about ten times greater than those of tZ and tZR, respectively, suggesting that plants might have different carriers for iP- and tZ-type CKs (Figure 2 in the publication). Depiction of individual atoms to the Wildman-Crippen partition coefficient estimates supports that the difference in hydrophobicities between iP and tZ is due to the side chain compositions (Figure 3 in the publication).

We continue by summarizing the CK distribution between the intracellular and extracellular spaces or among various cellular compartments since the concentration gradient of a molecule can be a marker of its regulated membrane transport. We point out the predominantly extracellular localization of tZ-type CKs, which is consistent with their occurrence in the xylem sap, and the discrepancy between the cytoplasmic localization of CK-recognizing UGTs and the significant extracellular concentration of CK glucosides, implying the existence of one or more transporters recognizing CK glucosides. Next, we provide an overview of the basic kinetic and thermodynamic aspects of membrane transport. Subsequently, we discuss these aspects in relation to the ENT and PUP families, whose members are known or hinted to be involved in CK membrane transport, as well as carriers that affect plant physiological responses by regulation of CK membrane transport: AtPUP14, AtABCG14, AtAZG1 and AtAZG2. Based on the reviewed findings, we present an exhaustive scheme of processes mediating the CK distribution at the cellular level and propose additional transport processes that might connect existing CK pools in different compartments (Figure 4 in the publication). The scheme includes an assumed influx of CK ribosides from the extracellular space to the cytoplasm that I aim to characterize in this thesis.

Personal contribution: I contributed to the first manuscript draft, calculated the estimates of the partition coefficients, and designed the figures.

International Journal of
Molecular Sciences

MDPI

Review

Differential Subcellular Distribution of Cytokinins: How Does Membrane Transport Fit into the Big Picture?

Daniel Nedvěd [1,2], Petr Hošek [1], Petr Klíma [1,*] and Klára Hoyerová [1,*]

[1] The Czech Academy of Sciences, Institute of Experimental Botany, 165 02 Prague, Czech Republic; dan@nedved.eu (D.N.); hosek@ueb.cas.cz (P.H.)
[2] Department of Biochemistry, Faculty of Science, Charles University, 128 00 Prague, Czech Republic
* Correspondence: klima@ueb.cas.cz (P.K.); hoyerova@ueb.cas.cz (K.H.)

Abstract: Cytokinins are a class of phytohormones, signalling molecules specific to plants. They act as regulators of diverse physiological processes in complex signalling pathways. It is necessary for plants to continuously regulate cytokinin distribution among different organs, tissues, cells, and compartments. Such regulatory mechanisms include cytokinin biosynthesis, metabolic conversions and degradation, as well as cytokinin membrane transport. In our review, we aim to provide a thorough picture of the latter. We begin by summarizing cytokinin structures and physicochemical properties. Then, we revise the elementary thermodynamic and kinetic aspects of cytokinin membrane transport. Next, we review which membrane-bound carrier proteins and protein families recognize cytokinins as their substrates. Namely, we discuss the families of "equilibrative nucleoside transporters" and "purine permeases", which translocate diverse purine-related compounds, and proteins AtPUP14, AtABCG14, AtAZG1, and AtAZG2, which are specific to cytokinins. We also address long-distance cytokinin transport. Putting all these pieces together, we finally discuss cytokinin distribution as a net result of these processes, diverse in their physicochemical nature but acting together to promote plant fitness.

Keywords: cytokinin transport; membrane transport; ABCG14; PUP14; AZG1; AZG2; cytokinin distribution; cytokinin hydrophobicity

check for updates

Citation: Nedvěd, D.; Hošek, P.; Klíma, P.; Hoyerová, K. Differential Subcellular Distribution of Cytokinins: How Does Membrane Transport Fit into the Big Picture? *Int. J. Mol. Sci.* **2021**, *22*, 3428. https://doi.org/10.3390/ijms22073428

Academic Editor: Karen Skriver

Received: 4 January 2021
Accepted: 22 March 2021
Published: 26 March 2021

Publisher's Note: MDPI stays neutral with regard to jurisdictional claims in published maps and institutional affiliations.

Copyright: © 2021 by the authors. Licensee MDPI, Basel, Switzerland. This article is an open access article distributed under the terms and conditions of the Creative Commons Attribution (CC BY) license (https://creativecommons.org/licenses/by/4.0/).

1. Introduction

Cytokinins (CKs), a group of phytohormones, mediate sensitive and potent regulation of wide variety of growth and developmental processes in plants [1,2]. To keep the CK signal intensity at the desired level, plants need efficient mechanisms to regulate the concentration of active CK forms at specific cellular sites. These mechanisms comprise biochemical reactions (including both formation of biologically active CKs from their precursors and their subsequent metabolic inactivation) and transport processes occurring at biological membranes. Distribution of different enzymes involved in the former varies throughout the subcellular compartments. This fact accounts for compartmentalization of diverse CK species and their enzymatic reactions [3].

Biosynthesis of the most prominent CKs in plants begins with prenylation of adenosine diphosphate (ADP) or triphosphate (ATP). This reaction is catalysed by ADP/ATP isopentenyltransferases (ADP/ATP IPTs) [4,5]. The isoprenoid moiety can be hydroxylated by specific cytochrome P450 (CYP) monooxygenases CYP735A1 and 2 [6]. Such intermediates are converted to free CK bases, which can interact with CK receptors, triggering a cellular response to the CK signal [7]. Chen and Kristopeit isolated purine-specific nucleotidases [8] and nucleosidases, respectively [9]. These findings hint that CK activation could occur via two subsequent reactions. Later, Kurakawa et al. discovered an enzyme family dubbed "Lonely Guy" (LOG), the members of which are able to activate CKs on their own, i.e., with no other enzymes involved in the pathway [10]. Further research suggested that the LOG-mediated CK activation pathway is dominant in plants [11,12].

CKs in the form of free bases can be inactivated either by oxidative degradation or via covalent conjugation with another low-molecular-weight compound, thus forming CK derivatives. The former reaction is catalysed by CK oxidases/dehydrogenases (CKXs). CK degradation yields adenine and an oxidized form of the corresponding side-chain. The oxidative degradation of CKs is irreversible [13,14]. The most prominent CK conjugates are those containing a glucose moiety, i.e., glucosides. Reactions converting free CK bases to glucosides (or glycosylation reactions) are catalysed by UDP glycosyl transferases (UGTs) [15]. While CK *O*-glucosides are readily converted back to free bases by a β-glucosidase [16], *N*-glycosylation is often considered irreversible. However, a recent work published by Hošek et al. suggests otherwise [17]. Apart from CK nucleosides, nucleotides, and glucosides, conjugates with disaccharides or amino acids have been described as well [18].

Biologically active CKs trigger physiological plant responses through a series of transcriptional events mediated via canonical two-component signalling system typically consisting of a sensory histidine kinase (HK) and response regulators (RRs). In *Arabidopsis*, a multi-step phosphorelay system including CK receptors AHK2, AHK3, CRE1/AHK4/WOL1, histidine phosphotransfer proteins (AHP1-5 and AHP6 lacking His residue), and type-A and type-B ARRs was described [2,19].

Indeed, the localization of CK perception system determines the sites of ignition of CK signalling cascade once the active CK is present. However, there is a discrepancy concerning the subcellular localization of the CK receptors as well as HK substrate preferences. Initially, extracellular localization has been proposed for CRE1/AHK4/WOL1 [20,21] and AHK3 [22]. On the other hand, later experiments have shown that fusion constructs of these two AHKs with green fluorescent protein (GFP) reporter reside mainly on the endoplasmic reticulum (ER) membrane [23,24]. The preferential role of ER-localized HKs has been further supported [19,25]. However, recent studies clearly demonstrated that *Arabidopsis* CK receptors localize to plasma membrane as well [26,27], supporting an earlier hypothesis that depletion of CKs from apoplast dampens CK signalling output [28].

Furthermore, it was shown that AHK4 localization depends on the cell type [27]. It might be expected that other, so far unknown factors affect CK receptor distribution too. Considering that HKs substrate preference varies [29] it is hard to connect CK metabolism and transport with direct signalling output.

CK membrane transport consists of several processes with diverse thermodynamic and kinetic aspects, tightly linked to the chemical properties of individual CK species. Recent findings also suggest particular roles of CK-specific membrane-bound carriers during certain developmental events. This review aims to summarize the results of CK transport research so far and to put them within a frame of basic physicochemical principles of membrane transport mechanisms.

2. The Structural Variety of Naturally Occurring and Synthetic Cytokinins

Various mechanisms of CK transport closely tie to their structural and functional diversity. Naturally occurring CKs can be characterized as derivatives of adenine. Their molecules bear a side-chain moiety bound to the N6 atom (i.e., the primary amine group of adenine). The composition and structure of the said side-chain play a pivotal role in chemical diversity among major CKs (Figure 1). Regarding the general chemical character of their side-chains, naturally occurring CKs can be further classified as isoprenoid or aromatic [30,31].

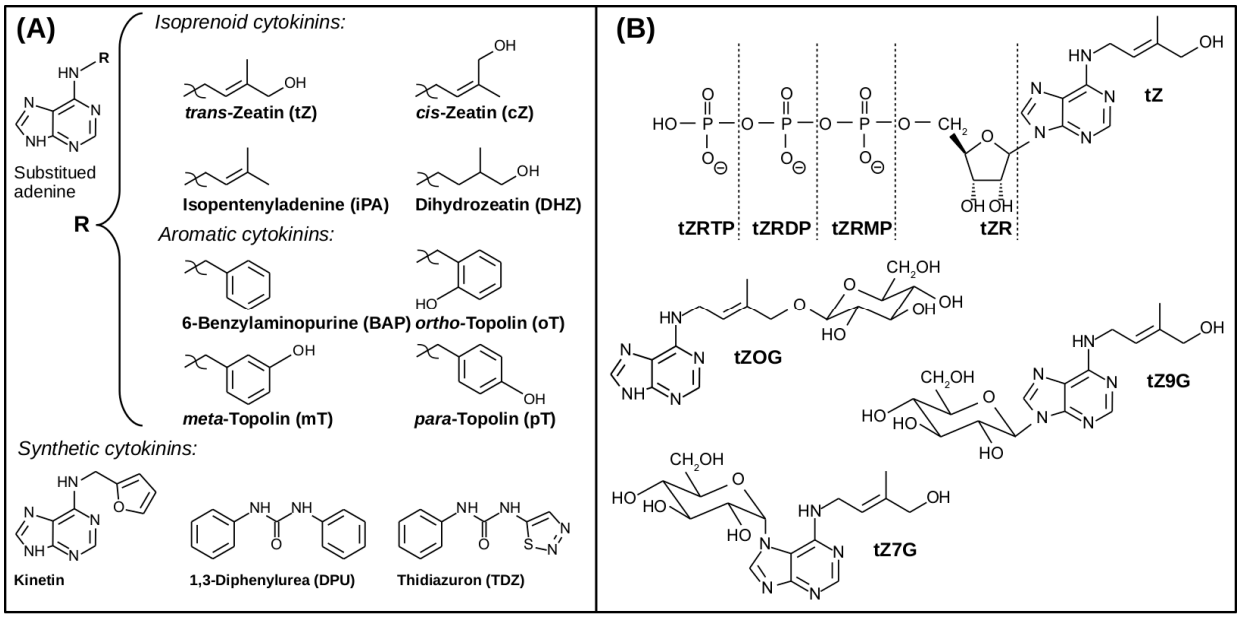

Figure 1. Structures of major cytokinins (CKs) in form of free bases (**A**) and different forms of *trans*-zeatin (**B**). Taken from [32]; tZR: *trans*-zeatin riboside; tZRMP: *trans*-zeatin riboside monophosphate; tZRDP: *trans*-zeatin riboside diphosphate; tZRTP: *trans*-zeatin riboside triphosphate; tZOG: *trans*-zeatin *O*-glucoside; tZ7G: *trans*-zeatin N^7-glucoside; tZ9G: *trans*-zeatin N^9-glucoside. Remaining abbreviations are explained in the figure.

Isoprenoid CKs' side-chain derives from a dimethylallyl moiety—a five-carbon atomic group bearing a double bond. Dimethylallyl pyrophosphate is a common precursor of isoprenoid CKs and secondary plant metabolites [33]. Isopentenyladenine (iP) contains a dimethylallyl side-chain with no further modifications. Terminal hydroxylation of the dimethylallyl side-chain yields zeatins. Due to the stereochemistry of double bonds, two zeatin isomers exist—*cis*-zeatin (cZ) and *trans*-zeatin (tZ). Both these isomers occur in plants. The relative amounts of cZ-type and tZ-type CKs vary throughout different plant species and during different developmental stages within a plant's lifetime [34]. Despite their structural similarity, CK-specific enzymes and receptors can discriminate between the two zeatin isomers [35].

Bassil et al. isolated an enzyme supposed to catalyse the *cis-trans* isomerization of zeatin [36]. However, a later study published by Hluska et al. challenged this view. The authors showed that no significant change of cZ to tZ ratio occurred in *Arabidopsis* plants expressing the said enzyme. They suggested that the putative cis-trans isomerase actually catalysed hydrolysis of flavin adenine dinucleotide (FAD) to flavin adenine mononucleotide (FMN). FMN could be then readily excited by light and induce non-enzymatic photoisomerization of zeatin [37].

Gajdošová et al. studied the *cis-trans* isomerization as a potential source of artefacts in CK profiling. They have concluded that such a reaction in plant samples requires either photochemical or thermal catalysis, due to its relatively high activation energy [34].

Until now the only source of cZ seems to be degraded tRNA as shown by Miyawaki et al. Using *ipt2ipt9* double mutant they demonstrated complete lack of cZ-type metabolites in the mutant pointing at tRNA IPT as a key enzyme in cZ biosynthesis [38].

Another known type of isoprenoid CKs is dihydrozeatin (DHZ). Its side-chain is hydroxylated, similarly to cZ or tZ, and fully saturated. Martin et al. purified a putative zeatin reductase, supposed to produce DHZ by hydrogenation of zeatins [39]. The authors observed DHZ formation in a mixture containing the isolated enzyme, radiolabelled tZ, and nicotinamide adenine dinucleotide phosphate (NADPH). They saw no such reaction with cZ, tZR, *O*-xylosyl zeatin or iP as substrates. Later, NADPH-dependent conversion of cZ to DHZ was shown in pea leaf [40]. Recently, a correlation analysis of CK metabolites

in potato suggested there might be interconversions between DHZ riboside and tZR with possible involvement of cZ-type CKs [41].

The side-chains of naturally occurring aromatic CKs are based on a benzyl moiety. The simplest aromatic CK, whose side-chain is not further modified, is called 6-benzylaminopurine (BAP). BAP can be both prepared synthetically and isolated from *Arabidopsis* and poplar [31,42]. Formal monohydroxylation of the aromatic ring at the side-chain of BAP yields topolins. The monohydroxylation can occur at three sites, yielding three possible topolin isomers, called *ortho*- (oT), *meta*- (mT), and *para*-topolin (pT). All three topolins, as well as their metabolites, have been found in plants [31,43]. Methyl ethers of oT (*ortho*-methoxytopolin—MeoT), mT (*meta*-methoxytopolin—MemT), and their respective nucleosides were identified too [42]. Another class of aromatic CKs, 6-(3-methylpyrrol-1-yl)purine (MPP) and its derivatives, has been identified as a metabolic product of tZ. Formation of MPP has been observed in maize [44] as well as in cereal pathogen *Fusarium pseudograminearum* [45]. Interestingly, chemical synthesis of MPP from tZR had been already carried out years ago [46].

As pointed out by Hluska et al., the current knowledge of aromatic CK metabolism is sparse [29]. Still, there have been few reports on aromatic CK glycosylation; BAP has been *N*-glycosylated by UGT76C1 and 2 [15] and topolins have been *O*-glycosylated by recombinant *O*-glucosyl transferases [47]. Oxidative cleavage of pT by several AtCKXs has been observed too [48]. Biosynthesis of aromatic CKs remains unknown, with the exception of MPP and its derivatives [44,45].

Some other naturally occurring CKs are synthesized not by plants themselves, but rather by plant pathogens. These include various methylated, thiomethylated, and deoxyribosylated variants of iP and zeatin-type CKs [49–52]. These compounds have been shown to mimic physiological CK activity, effectively disrupting the hormonal balance in host plants and facilitating the infection.

Kinetin is an example of a synthetic CK. It is a derivative of adenine, like its naturally occurring counterparts. Its side-chain consists of an aromatic furan moiety linked to the N6 amino group via a methylene bridge. Another type of synthetic CKs comprises derivatives of phenylurea, such as diphenylurea (DPU), *N*-(2-chloro-4-pyridyl)-*N*′-phenylurea (CPPU), thidiazuron (TDZ), and its monohydroxylated derivatives [5,31,47]. Chemical synthesis is also employed to produce novel CK derivatives [18,53].

3. Cytokinin Structures Affect Their Physical and Chemical Properties

Structures of CKs govern both their physicochemical and biological properties (such as ability to trigger cellular response via CK signalling system). Different properties of naturally occurring free CK bases can be accounted to the differences in their side-chain compositions. Similarly, metabolites or precursors of a given free base vary in their properties due to different moieties present in their molecules.

One of the important chemical features of CKs to be discussed is their hydrophobicity. This property can be characterized by octanol-water partition coefficient, *P*, or its logarithm. Wildman and Crippen published a method to predict log(*P*) of a given molecule by summing up individual contributions of all its atoms [54]. The value of each contribution depends both on the atom type and its surroundings. To demonstrate this prediction method, log(*P*) values of various CKs have been estimated and listed in Figure 2 (in comparison with another prediction method and retention times of internal HPLC CK standards provided by Šimura et al. in [55]). Additionally, individual atomic contributions to the net log(*P*) values of selected CKs, evaluated according to Wildman and Crippen [54], are depicted in Figure 3.

Cytokinin Name	Log(P) Prediction (dimensionless)		HPLC Retention Time [Minutes] (Šimura et al., 2018)
	Wildman and Crippen	Molinspiration Model	
Adenosine monophosphate (AMP)	-2.495	-4.455	N/A
Adenosine (Ado)	-1.980	-0.854	N/A
trans-Zeatin N^7-glucoside (tZ7G)	-1.851	-2.018	2.15
cis-Zeatin N^7-glucoside (cZ7G)	-1.851	-2.018	N/A
trans-Zeatin N^9-glucoside (tZ9G)	-1.851	-1.211	3.82
cis-Zeatin N^9-glucoside (cZ9G)	-1.851	-1.211	3.89
Dihydrozeatin N^7-glucoside (DHZ7G)	-1.771	-2.068	4.15
Dihydrozeatin N^9-glucoside (DHZ9G)	-1.771	-1.261	4.15
cis-Zeatin riboside monophosphate (cZRMP)	-1.727	-3.767	N/A
trans-Zeatin riboside monophosphate (tZRMP)	-1.727	-3.767	N/A
Dihydrozeatin riboside monophosphate (DHZRMP)	-1.647	-3.816	N/A
cis-Zeatin *O*-glucoside (cZOG)	-1.472	-0.663	2.53
trans-Zeatin *O*-glucoside (tZOG)	-1.472	-0.663	2.53
Dihydrozeatin *O*-glucoside (DHZOG)	-1.393	-0.712	2.53
cis-Zeatin riboside (cZR)	-1.212	-0.045	6.97
trans-Zeatin riboside (tZR)	-1.212	-0.045	6.97
Dihydrozeatin riboside (DHZR)	-1.132	-0.095	7.05
meta-Topolin N^9-glucoside (mT9G)	-0.884	-0.751	7.09
ortho-Topolin N^9-glucoside (oT9G)	-0.884	-0.307	7.82
meta-Topolin N^7-glucoside (mT7G)	-0.884	-1.557	N/A
para-Topolin N^7-glucoside (pT7G)	-0.884	-1.533	N/A
ortho-Topolin N^7-glucoside (oT7G)	-0.884	-1.113	N/A
para-Topolin N^9-glucoside (pT9G)	-0.884	-0.727	6.77
meta-Topolin *O*-glucoside (mTOG)	-0.856	-0.282	N/A
para-Topolin *O*-glucoside (pTOG)	-0.856	-0.258	N/A
ortho-Topolin *O*-glucoside (oTOG)	-0.856	-0.306	N/A
Isopentenyladenine N^7-glucoside (iP7G)	-0.823	-0.776	6.78
Isopentenyladenine N^9-glucoside (iP9G)	-0.823	0.030	7.9
meta-Topolin riboside monophosphate (mTRMP)	-0.760	-3.306	N/A
para-Topolin riboside monophosphate (pTRMP)	-0.760	-3.282	N/A
ortho-Topolin riboside monophosphate (oTRMP)	-0.760	-2.862	N/A
Isopentenyladenine riboside monophosphate (iPRMP)	-0.699	-2.525	N/A
6-Benzylaminopurine N^7-glucoside (BAP7G)	-0.589	-1.054	6.78
6-Benzylaminopurine N^9-glucoside (BAP9G)	-0.589	-0.247	8.04
6-Benzylaminopurine riboside monophosphate (BAPRMP)	-0.465	-2.803	N/A
meta-Topolin riboside (mTR)	-0.245	0.416	7.84
para-Topolin riboside (pTR)	-0.245	0.440	7.63
ortho-Topolin riboside (oTR)	-0.245	0.859	8.49
Isopentenyladenine riboside (iPR)	-0.184	1.197	8.63
Adenine (Ade)	-0.065	0.235	N/A
6-Benzylaminopurine riboside (BAPR)	0.050	0.919	8.74
trans-Zeatin (tZ)	0.703	1.044	2.61
cis-Zeatin (cZ)	0.703	1.044	3.3
Dihydrozeatin (DHZ)	0.783	0.994	2.7
meta-Topolin (mT)	1.671	1.505	6.75
para-Topolin (pT)	1.671	1.529	5.46
ortho-Topolin (oT)	1.671	1.949	7.85
Isopentenyladenine (iP)	1.731	2.286	7.67
6-Benzylaminopurine (BAP)	1.965	2.008	8.04
Monomethylated isopentenyladenine (1MeiP)	2.121	2.555	N/A
Dimethylated isopentenyladenine (2MeiP)	2.511	2.824	N/A

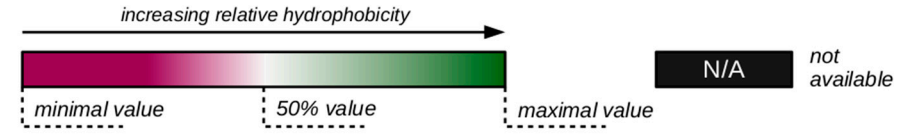

Figure 2. Hydrophobicity of various cytokinin species (CK) has been predicted using cheminformatics tools. In the second column, log(*P*) values are estimated according to [54]; this method yields log(*P*) as a sum of individual Wildman-Crippen atomic contributions. Calculation of Wildman-Crippen contributions has been done using RDKit: Open-source cheminformatics software (http://www.rdkit.org, accessed on 4 January 2021). In the third column, log(*P*) values are estimated using a method provided by Molinspiration Cheminformatics free web services (https://www.molinspiration.com, accessed on 4 January 2021). To compare these predictions with actual experimental data, retention times of internal standards for high-performance liquid chromatography (HPLC) separation of CKs taken from [55] are given in the last column. For all three datasets, relative hydrophobicity range is visualized using the colour scale given below the table. The colour range is normalized within each column. Note that not all of the listed CKs were analysed in [55], as indicated by missing values ("N/A").

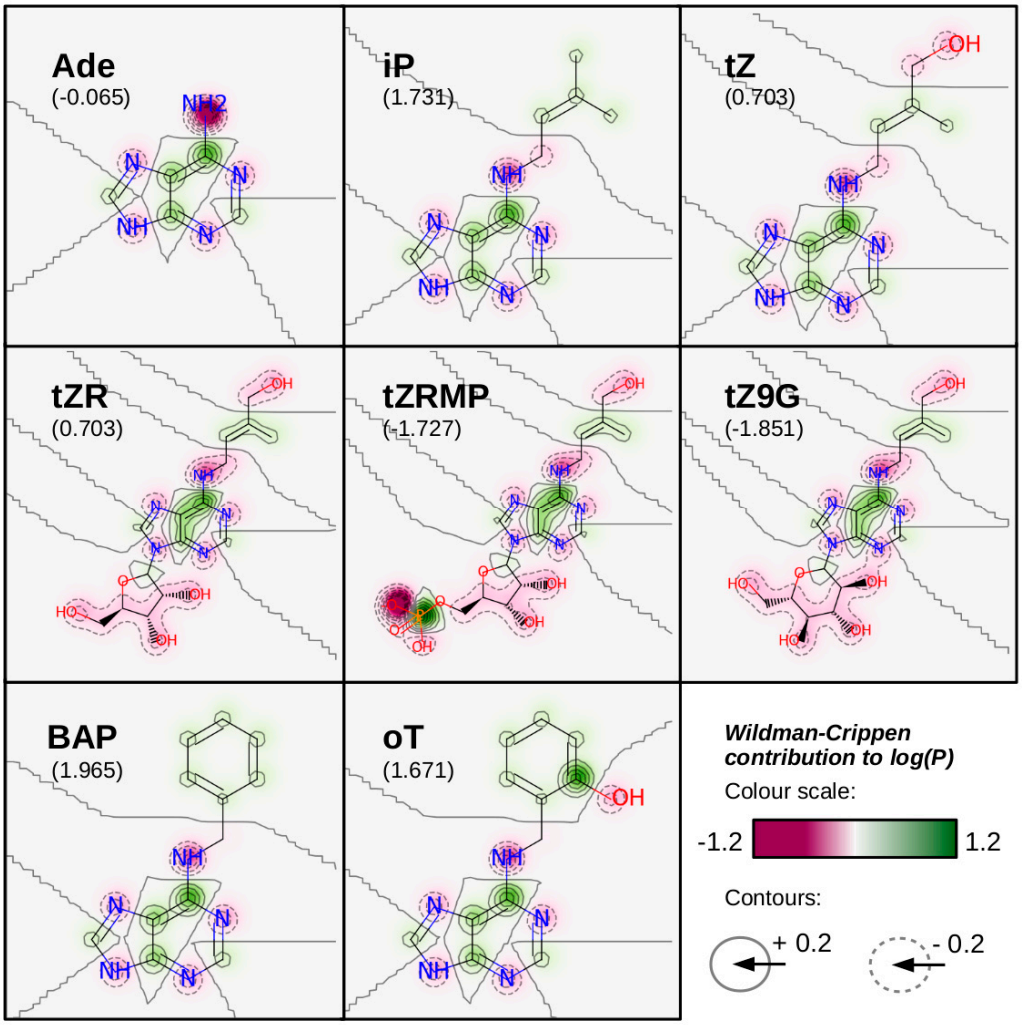

Figure 3. For selected CKs, Wildman-Crippen contributions of individual atoms to the value of log(*P*) have been predicted according to [54]. Gaussian distribution of the contributions have been visualized and juxtaposed with the corresponding molecular structures. Negative contributions (which decrease the overall hydrophobicity of the molecule) are depicted in shades of pink, while positive contributions (which increase the overall hydrophobicity) are depicted in shades of green (refer to the colour-bar in the bottom right corner of the figure). Increments of Wildman-Crippen contribution levels are also expressed by solid (above zero levels) and dashed contours (below zero levels). For each molecule, the Wildman-Crippen value of log(*P*) is given in the parentheses. Note that contributions of hydrogen atoms, which have been included in predicting total log(*P*) values, are not shown. Calculation and visualization of the Wildman-Crippen contributions have been performed using RDKit: Open-source cheminformatics software (http://www.rdkit.org, accessed on 4 January 2021). Ade: adenine; iP: isopentenyl adenine; tZ: *trans*-zeatin; tZR: *trans*-zeatin riboside; tZRMP: *trans*-zeatin riboside monophosphate; tZ9G: *trans*-zeatin N^9-glucoside; BAP: 6-benzylaminopurine; oT: *ortho*-topolin; *P*—octanol-water partition coefficient.

Molecular hydrophobicity governs, for instance, the kinetics of diffusion across biological membranes, which is one of the basic mechanisms of cellular transport. Furthermore, hydrophobic interactions play their part in interactions between low-molecular substances (such as CKs) and proteins (including CK-specific receptors, transporters, and enzymes) [56]. Naturally occurring CKs possess relatively hydrophobic side-chains, which has proved useful for CK isolation from plant material by solid-phase extraction (SPE) and their further analysis by HPLC [55,57–59].

Several observations can be made considering Figure 2 data. For instance, while both prediction methods agree that hydrophobicities of tZ and cZ should be equal, the HPLC

data show that tZ is eluted slightly earlier, suggesting that other molecular properties, such as double bond stereochemistry, could also play their roles in the interaction between analytes and HPLC columns. However, this effect is observed only for free zeatin bases and not the other forms. One can also notice that while Wildman-Crippen method predicts all free topolin bases to be of equal hydrophobicity, the Molinspiration model considers oT slightly more hydrophobic than the other two, which better corresponds to the HPLC data.

Both predictions generally consider CK glucosides less hydrophobic than the corresponding ribosides and the ribosides less hydrophobic than the corresponding free bases. This pattern suggests that discrimination among free CK bases, ribosides or glucosides observed for some membrane-bound transporters [28,60–62], enzymes [15,48] or CK receptors [63–65] could be at least partly caused by the differences in substrate hydrophobicity. Interestingly, in the HPLC data, zeatin-type ribosides are shown to be more hydrophobic than both free bases and glucosides.

Aromatic and iP-type CKs are shown to be more hydrophobic than their zeatin-type counterparts in both predictions and HPLC data. Following the idea presented in the previous paragraph, this hydrophobicity differences might be an explanation for different apparent affinities towards zeatin-type and iP-type substrates observed for some membrane-bound transporters [61,66–68], enzymes [15,48] or CK receptors [47,64].

CKs can also act as acids or bases, undergoing deprotonation or protonation in various pH. The N6 amino group, which binds the specific side-chains, is mostly protonated at pH < 3, bearing a positive charge. The N9 imine group can be deprotonated at pH > 11, becoming negatively charged. Similarly, the 2′-hydroxyl groups present on ribosyl moieties in CK nucleosides and nucleotides become mostly deprotonated at pH > 12. The phosphate group of CK nucleotides is neutral at pH < 1, once deprotonated at pH < 6, and twice deprotonated at pH < 12 [69].

Most of these proton transfer reactions occur at non-physiological pH values, which makes them irrelevant to CK transport processes. Still, CK nucleotides remain negatively charged at neutral pH, which effectively disables their diffusion across biological membranes under physiological conditions.

4. Cytokinin Content Varies in Different Subcellular Compartments

Differential distribution of CKs affects their transport, as both its thermodynamics and kinetics depend on CK concentration in various cellular compartments, as well as in the apoplast. Conversely, knowledge of CK subcellular localization can help to decide whether CK transport is expected to be involved in specific situations as a regulatory process. Important findings in this field, as well as the methodology of CK subcellular fractionation are reviewed in [3].

A comprehensive study of CK distribution in *Arabidopsis* (a dicot) and barley (a monocot) leaf cells was carried out by Jiskrová et al. [70]. In *Arabidopsis*, tZ was mostly extracellular, with a small fraction localized in cytoplasm, similarly to tZR and tZ-type glucosides; tZRMP was found in the cytoplasm as well. iP and iPR were predominantly localized in the cytoplasm, while most of iPRMP was found in the extracellular space. The iP-type glucosides were found in both the extracellular space and vacuoles. cZ was extracellular, cZR intracellular, cZRMP was found in both extracellular space and cytoplasm, and cZ-type glucosides were localized in the extracellular space and vacuoles. Of DHZ-type CKs, only DHZ7G was detected in a significant amount; it was localized in the extracellular space and vacuoles. In barley, apoplast was dominated by tZ9G and cZOG with a noticeable presence of the active bases iP and tZ as well as iPRMP. In contrast to *Arabidopsis*, vacuolar content was enriched in iP and cytoplasmic content in iPR. cZ forms made up for over 60% of both the cytoplasmic and the vacuolar cytokinins content in barley [70].

The extracellular localization of tZR reported by Jiskrová et al. [70] is in agreement with results of CK profiling in xylem sap, where tZR was the major CK species [67,71–73]. In phloem sap, iP-type nucleosides and nucleotides were the dominant species [67,74]. A

notable spatial discrepancy appears to exist between the reported extracellular localization of CK glucosides [70] and the described cytoplasmic localization of CK-specific glycosyl transferases [75,76].

In chloroplasts from tobacco and wheat, a wide range of CKs has been detected. The results of CK profiling varied in samples collected at the end of light and dark periods, both in the total CK amount and in the composition of the CK fraction. Notably, dark-treated chloroplasts contained much larger amounts of CK glucosides, compared to their light-treated counterparts [77].

Another CK content analysis has been carried out in *Arabidopsis* root cell protoplast, as well as in apoplastic and symplastic fractions. Interestingly, CK glucosides have been found in high abundance in both symplastic fraction and protoplast. On the other hand, free bases and ribosides were more or less equally abundant in both symplastic and apoplastic fractions [26].

Until now endogenous cytokinin compartmentalization is still far from being unified. The development of more sensitive analytical methods as well as cell and organelle sorting [78] should lead to more precise determination of minute amounts of CK derivatives within the cell compartments.

5. Cytokinin Transport at the Cellular Level Occurs via Thermodynamically and Kinetically Diverse Processes

Compounds moving between apoplast and cytoplasm, two cells, or different compartments at the subcellular level have to cross biological membranes. These membranes consist of an amphiphilic lipid bilayer and many proteins varying in size, shape, and function.

The means of transport across the biological membrane comprise simple diffusion, facilitated diffusion, primary, and secondary active transport. In this part, we summarize these processes, their basic mathematical description, and discuss them in terms of CK cellular transport.

From the thermodynamic point of view, membrane transport processes can be classified as either passive, if they can occur spontaneously, or active, if they require an external energy source. At a constant temperature and pressure, the energy balance of a transport process can be quantified using Gibb's free energy, ΔG. For a transport process between two compartments, ΔG can be expressed as:

$$\Delta G = RTln\frac{c_t}{c_s} + zFV \quad (1)$$

Here, R is the universal gas constant (approx. 8.3145 J $\times$ K^{-1} $\times$ mol^{-1}), T is thermodynamic temperature, c_s and c_t are concentrations of the transported compound in the source and the target compartment, respectively, z is the charge number of the compound, F is the Faraday constant (approx. 96,485 C $\times$ mol^{-1}), and V is the voltage between the two compartments. Translocation processes characterized by negative ΔG can occur via passive routes, whereas those characterized with positive ΔG are realized by means of active transport. The latter utilizes energy provided by an exergonic process. According to the type of this process, active transport is further classified as primary or secondary.

The primary active transport is directly coupled to the hydrolysis of adenosine triphosphate (ATP). Both the hydrolysis and the translocation are catalysed by multi-domain membrane carriers belonging to the "ATP-Binding Cassette" (ABC) family. A typical ABC protein is composed of two nucleotide-binding domains (NBDs) and two transmembrane domains (TMDs). Some ABCs are expressed as either homodimers or heterodimers, with each protomer containing one NBD and one TMD [79]. In plants, ABCs are further divided into eight subfamilies (ABCA—ABCG and ABCI). They recognize a wide range of substrates, including some phytohormones [80].

The secondary active transport employed by most members of plant ENT and PUP families utilizes energy gained from passive translocation of another substrate [81]. Both

substrates are transported by the same carrier. In plants, the secondary active transport is often linked to the proton gradient, which can be also expressed as a difference of pH between two compartments.

While the thermodynamics help us to discuss the energy balance, it does not tell us how fast the transport processes occur. To access this kind of information, we need kinetic equations describing the transport flux and/or the resulting temporal changes in the concentrations of the transported substances. Passive transport occurs via simple or facilitated diffusion. The latter is mediated by membrane-bound carriers, which results in different kinetic descriptions of the two diffusion types. Active transport always requires the membrane carries, and therefore it shares its kinetic characteristics with facilitated diffusion. However, the thermodynamic difference remains—facilitated diffusion, a passive process, cannot occur if ΔG is positive.

The kinetics of simple diffusion is described by classical Fick's laws [82]. The first law describes the relationship between the diffusion flux, $\vec{J}$, and the concentration gradient, ∇c. It states that:

$$\vec{J} = -D\nabla c \tag{2}$$

where D is the mass diffusivity, a parameter depending on both environment and the properties of the transported substance. Note that ∇ (pronounced "nabla") is a vector of partial derivatives with respect to all three spatial coordinates, denoted as x, y, and z:

$$\nabla = \left(\frac{\partial}{\partial x}, \frac{\partial}{\partial y}, \frac{\partial}{\partial z}\right) \tag{3}$$

In other words, the diffusion flux is proportional to the concentration gradient and it occurs in the opposite direction. Considering a system, where c changes only due to diffusion, Fick's first law can be used to derive the temporal change of concentration as:

$$\frac{\partial c}{\partial t} = D\nabla^2 c \tag{4}$$

where t is the time. This is a formulation of Fick's second law. The square of ∇, or the Laplace operator, can be expressed as:

$$\nabla^2 = \frac{\partial^2}{\partial x^2} + \frac{\partial^2}{\partial y^2} + \frac{\partial^2}{\partial z^2} \tag{5}$$

Models based on simple diffusion and Fick's laws have been used to describe short-distance apoplastic movements and membrane transport of various plant hormones, including CKs [83–85]. Simple diffusion across biological membranes is generally allowed to small, hydrophobic, and non-charged molecules. In Figure 2, hydrophobicity of some CKs is predicted in terms of log(P), which the molecular affinity towards hydrophobic and hydrophilic environments. CKs able to readily diffuse through the biological membrane should have relatively high log(P) to be able to pass through its lipid core. Considering both Figure 2 predictions, log(P) of free CK bases ranges from approximately 0.7 to 2.0; in other words, their affinities to hydrophobic environments are predicted to be 5 to 100 times higher in comparison with the hydrophilic ones. Therefore, it is worth considering that free CK bases are able to cross biological membranes, unless proved otherwise. Other data from Figure 2 (both Molinspiration prediction and HPLC internal standard elution times) suggest that simple diffusion might be relevant for topolin ribosides as well.

As discussed by Radhika et al., plant pathogen *Rhodococcus fascians* produces mono- and dimethylated derivatives of iP which are fairly hydrophobic, and therefore easily diffuse through membranes, facilitating the bacterial infection [51]. In Figure 2, both these derivatives are predicted to be more hydrophobic than the free CK bases produced by plants.

Weak acids and bases may cross the membrane only non-dissociated. The dissociation equilibrium of a weak acid or base is characterized by a certain value of pK_A. The ratio between concentrations of the dissociated, $c(A^-)$, and non-dissociated form of the given compound, $c(HA)$, can be written using one of the Henderson-Hasselbalch equations:

$$log\frac{c(A^-)}{c(HA)} = pH - pK_A \quad (6)$$

While this equilibrium does not play a significant role in regulating CK transport, it is crucial for the polar distribution of auxins, weakly acidic phytohormones. As reviewed by Zažímalová et al. [86], a significant portion of auxin molecules is protonated in the apoplast, due to its mildly acidic pH (5.5). In such form, it readily diffuses to the cytoplasm, which is rather neutral (7.0). There, the transported molecules deprotonate, becoming negatively charged and therefore trapped within the cells.

Kramer modelled the apoplastic diffusion of several weakly acidic phytohormones: auxin, abscisic acid, and gibberellins [87]. In this model, the weak acid travels through the apoplast in one direction from the transmitter cell to the receiver one. A portion of the protonated acid molecules is continuously trapped by surrounding sink cells. Each weak acid can be characterized by its decay length, L_{apo}, indicating how far it can travel before its apoplastic concentration decreases to 10% of its initial value. The decay length is defined as:

$$L_{apo} \approx 1.63\frac{\sqrt{Dh}}{P_{eff}} \quad (7)$$

where h is the width of the apoplastic route, and P_{eff} is effective permeability of the sink cell membranes, depending on the dissociation constant of the given weak acid. The dissociation constant determines the rate of constant depletion of the travelling weak acid molecules from the apoplast, which is required in the model. In contrast to the acids, CK dissociation is not a relevant source of this behaviour and CK diffusion from the cytoplasm back to apoplast cannot be ruled out. However, a similar model could be derived, based, for example, on continuous cleavage of CK molecules by apoplastic CKXs [48]. CK degradation rate could be therefore implemented in a similar fashion, with consideration of CKX apoplastic distribution.

Facilitated diffusion is mediated by membrane-bound carriers, such as AtENT7 in the case of CK transport [81,88]. The thermodynamics remains the same as in the case of the simple diffusion (i.e., passive transport). However, a different kind of kinetic model is required to characterize this process. Carrier-mediated transport, including both facilitated diffusion and active transport, can be described using Michaelis-Menten kinetics [89] (English translation and additional commentary provided by Johnson and Goody in [90]). This model expresses the relationship between the transport rate, v, and the concentration of the transported compound, or the substrate, as:

$$v = \frac{V_{max}c}{K_M + c} \quad (8)$$

where V_{max} is the limit rate (achieved at complete saturation of the given membrane carrier) and K_M is the substrate concentration at which the transport rate is equal to half V_{max} (K_M therefore characterize the affinity of the carrier toward the substrate). In the presence of a competitive inhibitor, which binds to the same site of the carrier as the substrate does, the kinetic equation expands into:

$$v = V_{max}\frac{c}{K_M + \frac{K_M}{K_I}c_i + c} \quad (9)$$

where c_i is the inhibitor concentration and K_I is the dissociation constant of inhibitor-enzyme complex.

Carrier-mediated transport can be approximated with first-order kinetics if the substrate concentration is relatively low, simplifying Michaelis-Menten equation as follows:

$$c \ll K_M \Rightarrow K_M + c \approx K_M \tag{10}$$

$$v \approx \frac{V_{max}}{K_M} c \tag{11}$$

The ratio of $\frac{V_{max}}{K_M}$ is equivalent to the first-order rate constant and it can be also interpreted as membrane permeability. More complex models of hormonal homeostasis may express membrane transport with first-order kinetics, considering the requirement of low substrate concentration fulfilled [83,84,87].

On the other side of the concentration range, i.e., when the substrate concentration permanently remains at levels corresponding to practical saturation of the carrier, the transport kinetics become independent of it. In such situation, the Michaelis-Menten equation simplifies to:

$$c \gg K_M \Rightarrow K_M + c \approx c \tag{12}$$

$$v \approx V_{max} \tag{13}$$

This is an example of zero-order kinetics.

6. Equilibrative Nucleoside Transporters Mediate Proton-Dependent Transport of Cytokinin Ribosides

CKs (and some other derivatives of adenine) are recognized as non-specific substrates by some membrane-bound transporters of nitrogenous bases and nucleosides. One family of such carriers is called the "Equilibrative Nucleoside Transporters" (ENTs). As the name suggests, ENTs recognize various nucleosides [81]. ENTs are present within genomes of most eukaryotes. In plants, they were identified for the first time thanks to the homology with their human counterparts [81,91,92].

In the *Arabidopsis* genome, eight *ENT* genes have been predicted. Five of them (*AtENT1*, *3*, *4*, *6*, and *7*) have been characterized in terms of their products' substrate specificities and transport mechanisms [62,67,81,88,91–96]. In addition, three function products of *ENT* genes found in rice (*Oryza sativa*) were biochemically characterized [66].

Most plant ENTs mediate secondary active transport coupled to the proton gradient [81]. This fact was confirmed in several studies, in which dependence of the ENT activity on pH was studied [88,94,96]. In other studies, effects of protonophores, which erase the proton gradient and disable proton-dependent membrane transport processes were examined [88,92]. Examples of such protonophores include carbonyl cyanide *m*-chlorophenyl hydrazone (CCCP) or 2,4-dinitrophenol (DNP). However, AtENT7 did not respond to either a change of pH or application of a protonophore [88,94]. Therefore, ENT7 likely mediates facilitated diffusion, rather than secondary active transport, remaining true to the "equilibrative" part of its name. Analogously, the best-characterized human ENTs, hENT1 and 2, mediate facilitated diffusion as well. However, two other hENTs are suggested to mediate secondary active transport, possibly coupled to the proton gradient [97,98].

AtENT1 was the first identified plant ENT. It was shown to recognize common nucleosides, except for uridine, while the corresponding free bases were not recognized as substrates at all [91,92]. AtENT1 localizes to both plasma membrane and tonoplast, mediating the release of nucleosides and RNA breakdown products from vacuole to cytoplasm. Therefore, AtENT1 could contribute to the CK homeostasis by providing adenosine for cytosolic CK biosynthetic pathways [93]. However, *atent1* mutation did not produce any significant change of either CK response or CK uptake by *Arabidopsis* hypocotyl explants [62].

In contrast, the *atent3* loss-of-function mutation led to a decrease in the accumulation of tZR and iPR in *Arabidopsis* hypocotyl explants. The accumulation of the corresponding free bases remained unchanged [62]. In another experiment, *AtENT3* was expressed in yeast

cells accumulating adenosine. Upon addition of either tZR or iPR, only a weak decrease of adenosine uptake was observed [67]. Similar results were obtained for AtENT7. On the contrary, in yeast cells expressing *AtENT6*, significant inhibition of adenosine uptake by iPR was observed, while inhibition by tZR was comparable to that in yeast cells expressing *AtENT3* and *7* [67]. The authors suggest that AtENT6 may be involved in tZR and iPR compartmentalization. Both AtENT3 and 6 are localized to plasma membrane [88,95].

AtENT8 was originally identified as a suppressor of AtIPT8. Subsequently, it was found that the *atent8* loss-of-function mutation reduces plants' sensitivity towards exogenously supplied CK ribosides, while the sensitivity towards the corresponding free bases remains unchanged. Uptake of iPR by *atent8* hypocotyl explants also decreased (although tZR uptake was not altered). Conversely, upon over-expression of *AtENT8*, sensitivity of plants towards exogenous CK ribosides (but not free bases) was increased [62].

Expression patterns of *AtENTs* in five organs (root, stem, leaf, flower, and silique) were examined by [95]. The expression pattern of *AtENT8* throughout various developmental stages was later studied in greater detail [62]. The expression of *AtENT6* was further found to be confined to the vasculature, suggesting a possible involvement of AtENT6 in long-distance nucleoside transport [67]. Expression patterns of ENTs relevant to CK transport are summarized in Table S1.

OsENT2 from rice was implied to act as a CK transporter as well. When expressed in yeast cells accumulating adenosine, a drop in adenosine uptake was observed in presence of iPR (but not in presence of tZR). Similarly to most AtENTs, OsENT2-mediated adenosine uptake depends on pH and is partially hindered by CCCP. Direct uptake of tZR and iPR in transgenic yeast cells was also observed. The affinity of OsENT2 towards tZR was significantly lower than towards iPR. *OsENT2* is expressed mainly in roots and to a lesser extent in stems and leaf sheaths [66].

7. Purine Permeases Are Involved in Proton-Dependent Transport of Free Cytokinin Bases

Another protein family contributing to the CK membrane transport is that of "Purine Permeases" (PUPs). Most PUPs recognizing CKs are non-specific, similarly to the ENTs discussed above. However, unlike ENTs, PUPs recognize their substrates in the form of free bases, as reviewed in [81]. Hildreth et al. used bioinformatics search tools to predict PUPs to be only found in vascular plants [99]. In the *Arabidopsis* genome, 23 *PUP* genes have been found, though only a few of them have been isolated and biochemically characterized [28,60,61,81,100–102]. Thirteen other PUPs have been found in rice [68] and two in tobacco (*Nicotiana tabacum*) [99].

The first discovered PUP was AtPUP1. It was identified via complementation of a yeast mutant deficient in adenine uptake. The AtPUP1-mediated uptake of adenine was hindered upon addition of cytosine, hypoxanthine, nicotine, caffeine, and also two CKs—kinetin and tZ. Corresponding nucleosides and nucleotides were not recognized as AtPUP1 substrates. The inhibition of adenine uptake by both CKs was shown to be competitive. The adenine and cytosine uptakes were dependent on pH and sensitive to the use of protonophores [60]. Based on its function and expression pattern (summarized in Table S1), the authors suggest that the role of AtPUP1 is to import various substrates, such as nucleobases or CKs, from xylem to shoot tissues. Bürkle et al. conducted direct measurements of tZ uptake in yeast cells expressing *AtPUP1*, confirming that AtPUP1 acts as a CK transporter. Furthermore, they found that iP is another substrate of AtPUP1 [61]. Szydlowski et al. showed that AtPUP1 is also involved in the uptake of pyridoxine (vitamin B6), which can be inhibited, among others, by tZ. They also traced AtPUP1 subcellular localization to the plasma membrane [103].

Similar experiments were carried out on AtPUP2. When expressed in yeast cells, *AtPUP2* mediated proton-dependent adenine uptake inhibited by iP, kinetin, BAP, and to a lesser extent by tZ and cZ. The adenine uptake obeyed Michaelis-Menten kinetics, but its rate was significantly lower than upon expression of *AtPUP1*. Expression of *AtPUP2* did

not complement mutant yeast deficient in adenine uptake. In contrast, AtPUP3 did not display any transport activity at all [61].

Three PUPs have been suggested to be involved in CK transport in rice: OsPUP1, 4, and 7. OsPUP1 and 7 localize to ER and OsPUP4 to plasma membrane [68,104,105].

OsPUP1 overexpression in rice plants led to a decrease of tZ, tZR, iP, and DHZ concentrations in shoots; while tZR concentration decreased in roots as well, those of cZ, cZR, and DHZR increased. In panicles, iP, iPR, and cZR concentrations decreased, while those DHZ and DHZR increased. These findings hinted that *OsPUP1* overexpression impairs root-to-shoot CK translocation, which was further confirmed by showing that treating overexpressor roots with endogenous CKs triggers much less pronounced response in shoots that in the wild type. Interestingly, *ospup1* mutants exhibited no significant differences from the wild type, suggesting redundancy among the *OsPUP* genes [105].

OsPUP4 was identified as a gene responsible for *bg3-D* ("big grain") phenotype. As the name implies, the phenotype includes larger grains but also taller shoots, shorter roots, and longer leaves in mature plants. The *bg3-D* phenotype corresponded to that caused by *OsPUP4* overexpression. *OsPUP4* expression was reduced by exogenous application of BAP, iP, tZ, and cZ, hinting that the gene is involved in modulating response to CK signal. CK profiling in *bg3-D* plants revealed that iP content decreased in shoots but increased in roots, while cZ and tZ increased in both parts of the plant, suggesting that OsPUP4 is involved in shoot-to-root translocation of iP. This was further confirmed by showing that *bg3-D* plants are more sensitive to exogenous application of CKs to shoots than wild type [104].

The *ospup7* mutant displayed several phenotype alterations, which were explained as results of CK transport impairment and accumulation of CKs in their source organs. Higher amounts of iP and iPR were found in the mutant plants, while the content of tZ-type CKs remained the same as in the wild type. Expression of *OsPUP7* in yeast led to phenotype rescue of mutants deficient in caffeine uptake [68].

In tobacco, PUP-like transporters NUP1 and 2 ("Nicotine Uptake Permease") were identified thanks to their similarity to AtPUP1. NUP1 was expressed in yeast cells and characterized as a nicotine-specific transporter. Addition of kinetin did not inhibit the nicotine uptake. NUP1 was found to be expressed mostly in root tips and localized to the plasma membrane. While its sensitivity to protonophores was not studied, it was assumed that NUP1 mediates secondary active transport coupled to the proton gradient, based on its homology with AtPUP1 [99].

8. Recent Findings Suggest That Proteins AtPUP14, AtABCG14, AtAZG1, and AtAZG2 Are Cytokinin-Specific Transporters with an Important Role in Cytokinin Signalization

All the transporters discussed so far have been non-specific to CKs, meaning that they recognize a wider range of substrates and their exact involvement in CK-mediated processes remains unclear. However, the transport activities of four proteins—AtPUP14, AtABCG14, AtAZG1, and AtAZG2—are linked to distinct features of CK physiology. This fact suggests that CK transport and distribution is an important part of the complex hormonal network in plants.

The role of AtPUP14 was identified by Zürcher et al. [28]. They used CK-specific reporter *TCSn::GFP* (Two Component Signalling Sensor new::Green Fluorescent Protein) developed earlier [106] to find out that prospective cotyledons in *Arabidopsis* embryos did not respond to CK signal, even though CK receptors were actively expressed there. These results led to a hypothesis that members of the PUP family may be involved in precise CK distribution, thus regulating the CK signalization by limiting the availability of biologically active CKs at specific sites. AtPUP14 turned out to be the aptest candidate for such task, given its ubiquitous expression [28,100].

Introduction of AtPUP14-targeting artificial microRNA (*amiRPUP14*) caused ectopic CK signalization in *Arabidopsis* plants, which manifested in several phenotype alterations, such as lateral root suppression or increase in shoot branching. Conversely, inducible

expression of *AtPUP14* in *Arabidopsis* embryos reduced endogenous CK response and promoted morphological defects in embryo roots. Visualizing *AtPUP14* and *TSCn::GFP* expression produced complementary patterns. All these results suggest that AtPUP14 down-regulates CK signalling [28].

Uptake assays in mesophyll protoplasts and tobacco microsomes were used to study the biochemical properties of AtPUP14. Transient expression of *AtPUP14* led to an increase in tZ uptake and its rate turned out to be dependent on ATP. Contrarily, tZ uptake in *amiRPUP14* seedlings was hindered. AtPUP14-mediated tZ uptake was inhibited by iP, BAP, and adenine, but not by tZR. Further experiments showed that AtPUP14 is localized to the plasma membrane [28].

The role of another CK-specific transporter, AtABCG14, was reported by two groups within one year. Ko et al. identified AtABCG14 as a transporter potentially involved in root-to-shoot communication via CK transport, given its co-localization with IPTs. Several experiments conducted on *atabcg14* mutants confirmed this hypothesis. Mutant plants displayed growth retardation, which has been rescued by applying exogenous tZ. Mutant shoots also contained less tZ-type CKs than those of the wild type. Grafting *atabcg14* shoots on wild type roots rescued their phenotype while grafting wild type shoots on *atabcg14* roots had no effect. All these results suggest that AtABCG14 is involved in root-to-shoot CK translocation. The authors also tried to study direct CK uptake in yeast cells expressing *AtABCG14*, but they could not detect any transport activity. They hypothesized that the reason for the negative result could be a heterodimeric quaternary structure of biologically active AtABCG14 [107]. As reviewed by Kang et al., some ABC transporters are indeed composed of two different protomers [80]. Le Hir et al. had also shown that AtABCG14 forms heterodimers with AtABCG11, rather than homodimers [108]. However, Ko et al. pointed out that the expression of *AtABCG11* in roots is low, which makes the involvement of said heterodimer in CK shoot-to-root transport unlikely. They tried to identify putative AtABCG14 dimerization partners by scanning the remaining *atabcg* single-gene mutants, but none of them displayed a phenotype similar to that of *atabcg14* [107].

At the same time, Zhang et al. were systematically studying the AtABCG subfamily. Similarly, to the authors of the previous study, they noticed that *atabcg14* mutants had a characteristic phenotype, which manifested as CK deficiency in shoots and an increase in CK concentration in roots. Expressing a CK signal reporter in *Arabidopsis* seedlings confirmed that in *atabcg14*, most CKs accumulated in roots. Conversely, CK concentration in *atabcg14* cotyledons remained lower than in the wild type. Feeding both wild-type and *atabcg14* seedlings with radiolabelled tZ-type CKs yielded the same results [109]. Put together, these results show that AtABCG14 contributes to the long-distance CK transport by exporting tZ-type CKs from roots to xylem. As proved in both works, the loss of its function leads to significant changes in CK distribution [107,109].

In rice, OsABCG18 is the closest ortholog to AtABCG14 and its properties and function are comparable. The *osabcg18* mutants accumulated tZ, tZR, and DHZ in roots, while their respective concentrations in shoots decreased. Experiments employing radiolabelled tZ directly demonstrated that the *osabcg18* mutation lowers root-to-shoot CK translocation. It was further shown that OsABCG18 is also involved in the export of iP, iPR, and cZR [110]. Both AtABCG14 and OsABCG18 are localized to plasma membrane [107,109,110].

Recent studies have revealed that CK membrane transport might be also mediated by two members of the "Aza-Guanine Resistant" (AZG) family—AtAZG1 and 2, previously identified as adenine and guanine importers [111–113].

Biochemical characterization of AtAZG1 in yeast expression system has revealed its particular affinity towards adenine (the mean K_M value has been reported as 1.62 μM). In the same system, AtAZG1-mediated adenine uptake was strongly inhibited by kinetin, tZ, BAP, and to a lesser extent also by iP. Overexpression of *AtAZG1* in *Arabidopsis* seedlings enhanced their ability to accumulate adenine, although the uptake rate in seedlings bearing *atazg1* loss-of-function mutation remained similar to the wild type. Furthermore, adenine uptake mediated by the overexpressor seedlings was inhibited by tZ, similarly to the

experiments in yeast. The *atazg1* mutant roots were on the other hand less sensitive to exogenously applied CKs. Another important feature of AtAZG1 is its interaction with PIN1 ("Pin-Formed"), an auxin cellular exporter. AtAZG1 was shown to co-localize with PIN1 and to stabilize it on the plasma membrane in *Arabidopsis* root cells, together with AtAZG2. Based on these results, it has been proposed that AtAZG1 modulates root cell architecture by regulating intracellular auxin:CK ratio [113].

AtAZG2 is found mainly in root primordia and is localized to plasma membrane and ER. Expression of *AtAZG2* gene is stimulated by auxins. In *AtAZG2*-expressing yeast cells, adenine uptake was strongly inhibited by iP, kinetin, BAP, and tZ. Upon ectopic expression of *AtAZG2* in *Arabidopsis* seedlings, an increase in tZ uptake was observed. However, tZ uptake in *atazg2* mutant plants was not impaired [112].

Expression of *TCSn::GFP* [106] in *Arabidopsis* has shown that CK signalling output is lowered in the proximity of *atazg2* lateral root primordia. It has been therefore proposed that AtAZG2 contributes to the inhibition of lateral root emergence by modifying CK distribution, similarly to AtPUP14 [112].

A brief summary of membrane transporters that had been studied in relation to CK transport is given in Table S1.

9. Cytokinin Paracrine Movement and Long-Distance Transport Open Up another Layer of Cytokinin Homeostasis Maintenance

Up to this point, CK homeostasis has been discussed in the context of isolated cells. In plant tissues, neighbouring cells are linked via symplast and apoplast. These connections enable, among other things, the paracrine hormonal signalization. Paracrine effects of CKs were studied in transgenic tobacco plants harbouring bacterial *IPT* gene under an inducible promoter [114]. Induction of this construct at a specific spot led to a local change of phenotype, suggesting CK overproduction. De Rybel et al. mention that CK biosynthesis and signalling do not necessarily occur in the same cells. For their model of auxin-CK crosstalk during vascular tissue formation, they consider paracrine movement of CKs between CK-producing xylem and CK-responsive neighbouring cambial cells [115].

At the level of whole plants, CKs are transported via vascular tissues. First pieces of evidence come from early studies focused on the distribution of radiolabelled CKs among different plant tissues and organs. Upon application of [^{3}H]-tZR to pea (*Pisum sativum*) root nodules and leaves, portions of the total radioactivity (comprising both the original tracer and its metabolites) were detected in other organs after eight days. The radiolabelled CKs were more readily transported from the root nodules than from the leaves [116]. Similarly, relocation of [^{14}C]-BAP applied to cocoa (*Theobroma cacao*) leaves at various stages of emergence was observed in both acropetal and basipetal direction [117].

Further information on CK long-distance transport has been obtained by means of CK profiling in vascular tissues. In xylem, the predominant CK species is tZR [67,71–73]. It has been also shown that the root-to-shoot translocation rate of CKs via xylem increases in plants treated with exogenous CK or with a protonophore, which impairs proton-dependent uptake of CKs by root cells [118]. Osugi et al. reported that tZ is transported from roots to shoots as well. They also suggested that both tZ and tZR may have their distinct roles as long-distance signalling molecules [119]. In phloem, both iPR and iPR monophosphate (iPRMP) are present in relatively high concentrations [67,74].

The long-distance CK transport was further examined using grafting experiments. Matsumoto-Kitano et al. focused on a quadruple *ipt* mutant, *atipt1;3;5;7*, which is strongly impaired in CK biosynthesis [38,120]. This mutant displayed a characteristic phenotype, including decreased shoot growth, increased root elongation, and decreased root perimeter (due to its inability to develop cambium), which could be recovered by applying exogenous tZ. Endogenous levels of both tZ-type and iP-type CKs were significantly lower in the mutant than in the wild type. Grafting a mutant shoot on a wild-type root restored the shoot phenotype. The level of tZ-type CKs in the shoot recovered too, while that of iP-type CKs remained decreased. An analogous observation was made after grafting a wild-type shoot on an *atipt1;3;5;7* mutant root—the root phenotype and iP-type CK contents became

comparable to the wild type, but tZ-type CK contents remained as low as in the mutant plants. Altogether, these results suggest that tZ-type CKs are mostly transported from roots via xylem as a shootward signal and iP-type CKs are mostly transported from shoots via phloem as a rootward signal [67,120].

As already mentioned, CK export to xylem is mediated by AtABCG14 [107,109]. Mechanisms of CK unloading, however, remain unknown so far. In relation to the role of AtABCG14, one may assume that sink tissues express another type of CK-specific transporter. Hot candidates for such position might be the members of families such as PUP, ENT, ABC or even AZG. On the other hand, we cannot rule out that xylem CKs are gradually depleted via unloading processes independent of membrane-bound carriers.

10. Future Perspectives

In this review, we address CK distribution among different compartments, cells, and tissues as well as the physical and chemical facets of the underlying transport processes. In a given subcellular compartment, concentrations of various CK species and forms are regulated by both membrane transport and metabolism. These two mechanisms are not completely independent of each other—membrane transport can provide substrates for enzyme-catalysed reactions and remove reaction products, both of which affect the thermodynamic equilibrium within the compartment. Similarly, metabolic conversions regulate concentrations of substrates available for different membrane-bound carriers. So far, it seems that CK recognition by membrane-bound carriers is governed by the substrate form (i.e., the moieties attached to the free base) rather than by their side-chain character. This can be demonstrated by the differential preferences of ENTs, which recognize CKs in the form of ribosides, and PUPs, which prefer free CK bases [81,102], similarly to the newly characterized AtAZG1 and 2 [112,113]. AtPUP14 has been characterized as a tZ-specific carrier; yet, when expressed in mesophyll protoplasts and tobacco microsomes, it displayed a slightly higher affinity towards other free CK bases (kinetin, BAP, iP) and adenine than towards tZR [28]. AtABCG14 has been shown to regulate the distribution of tZ-type CKs in various forms, but its biochemical characterization has not been successful [107,109]. It follows that biochemical conversions between different CK forms, such as glycosylation, phosphorylation, etc., affect both thermodynamic and kinetic aspects of carrier-mediated membrane transport.

A question arises whether there are membrane-bound transporters recognizing CK nucleotides and glucosides or whether these are converted to other CK types prior to translocation between compartments. As pointed out by Šmehilová et al., CK glucosylation in *Arabidopsis* is mostly confined to the cytoplasm, but most CK glucosides are to be found in the apoplast. Such situation advocates for the existence of a (so far unidentified) CK glucoside exporter [76]. Similarly, presence of CK glucoside carriers on tonoplast could explain relatively high abundance of CK glucosides in *Arabidopsis* vacuoles. Furthermore, *Arabidopsis* plastids contain high amounts of CK glucosides as well as of CK nucleotides [77]. It remains to be examined whether these CKs are transported between plastids and the cytoplasm or whether they rather play a role of buffer CK pools, balancing the levels of biologically active CKs in their particular compartments.

In Figure 4, we present a scheme of CK distribution in *Arabidopsis* at the cellular level. Different CK forms (i.e., free bases, ribosides, nucleotides, and glucosides) are grouped into pools. Depicted flows among these pools represent both confirmed and hypothetical CK transport pathways. This summary is meant to give a general idea of all possibilities of CK cellular traffic (and to demonstrate its complexity), it is not implied that all the depicted processes do necessarily occur. At the same time, one should note that even if certain transport process occurs, it does not have to be a sign of physiological importance, but also simply a result of physicochemical conditions at the given moment.

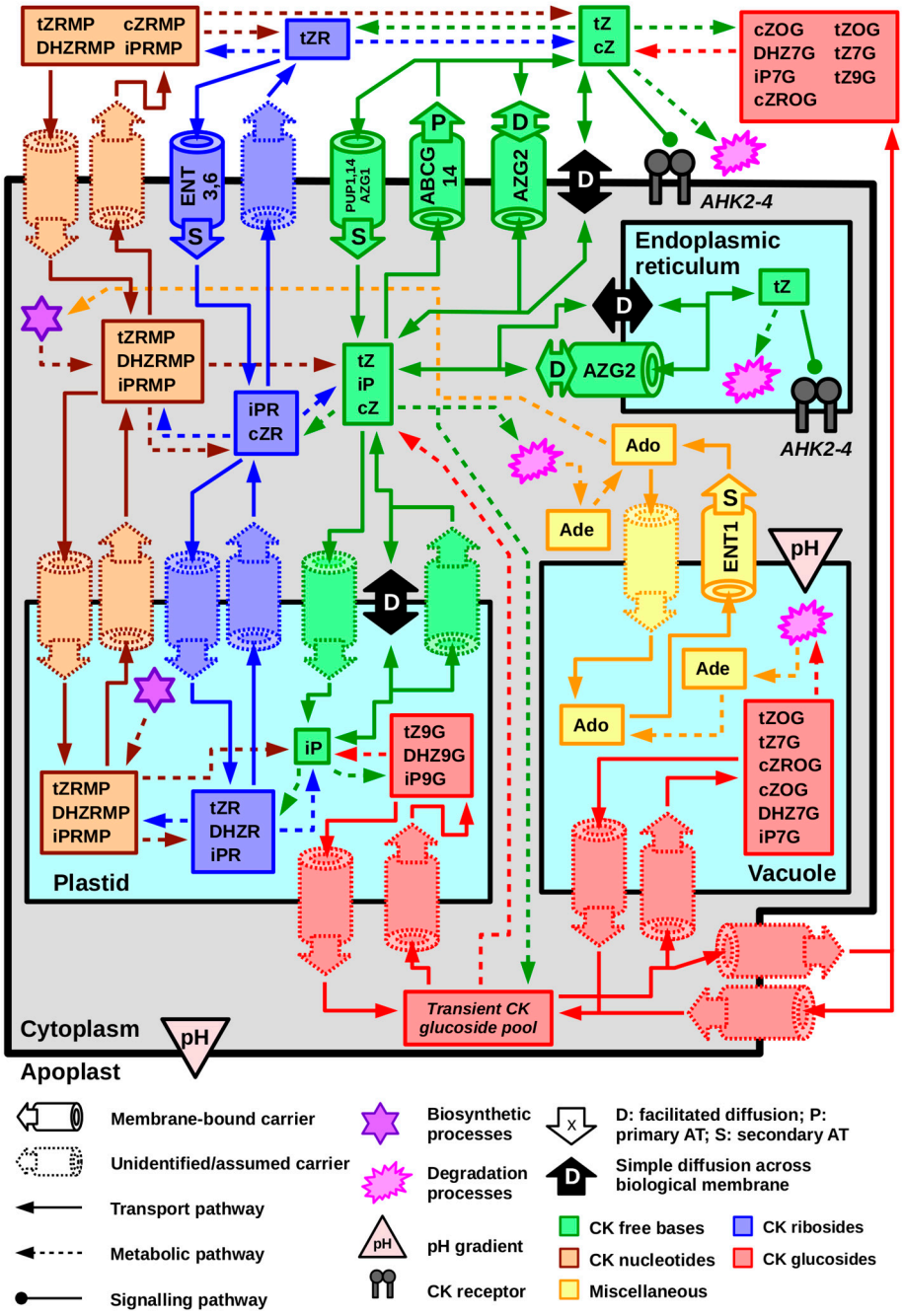

Figure 4. A proposition of a comprehensive scheme of cytokinin (CK) cellular homeostasis in *Arabidopsis* based on the current knowledge of cytokinin cellular trafficking in vascular plants. The plant cell is reduced to a simplified model depicting a plastid, a vacuole, endoplasmic reticulum, cytoplasm, and apoplast. Free CK bases, ribosides, nucleotides, and glucosides are grouped into their respective pools. Labels within the pools mark CK species that have been found in the given compartment in a significant amount [70,77]. Membrane-bound carriers with known subcellular localization are depicted together with a symbol indicating which kind of membrane transport process they mediate. Note that in case of free bases, which might be considered more hydrophobic than other CK species (refer to Figure 2), simple diffusion across the membrane is considered as well. Several putative membrane-bound carriers have been added to show possible transport routes that haven't been characterized or addressed yet. However, it is not implied that all of them have to be actually involved in CK trafficking. Light pink triangles indicate pH gradient, with the point located on the more acidic side of the membrane.

CK-recognizing transporters are classified as CK-specific or non-specific, based on how efficiently they discriminate among structurally similar substrates. The former comprise AtPUP14 [28], AtABCG14 [107,109], and possibly AtAZG1 and 2 [112,113], and the latter the remaining PUPs and ENTs [81,101].

While the importance of specific CK transport is hardly disputable, the role of non-specific membrane-bound carriers should not be overlooked. Even if further research finds no direct link between their function and CK signalization, they can be still involved in maintaining cellular CK balance in response to changes of CK-related enzyme activities and distribution of different CK metabolites.

In the very last part of the previous section, we also address the role of non-specific mechanisms in CK long-distance transport. While not ruling out the involvement of CK-specific membrane-bound carriers (such as AtABCG14-mediated tZ-type CK export to xylem), CK translocation via vascular tissues can be co-governed by source-sink relations. Source and sink powers are results of actual CK concentrations, which can be determined by enzyme-catalysed metabolism in the respective tissues.

Concerning long-distance CK transport, it is also worth further examining the distribution of radiolabelled CK tracers. In several studies, such tracers were applied on certain parts of intact plants, and subsequently, total radioactivity was measured in target tissues [107,109,116,117]. However, exact composition of the radioactive fraction was not analysed. Knowing which metabolites of the original tracer are distributed via long-distance transport would further help to determine which processes are relevant for CK distribution among source, vascular, and sink tissues. Moreover, it would be interesting to address whether molecules entering the vasculature from the source tissue (or at least a portion of them) travel to the sink, or whether long-distance CK translocation occurs in a relay manner. The latter means that the initial CK load acts as a paracrine signal, triggering CK production in the nearby cells and further propagation of the newly synthesized CK molecules.

CK transport processes contribute to the regulation of CK signalling activity. In Figure 4, we propose a scheme representing possible flows among intracellular and apoplastic CK pools. Regarding CK signalling, the complex scheme can be simplified to apoplast and ER, where binding of CKs to their receptors occurs [19,25–27,29], and cytoplasm. In such model, CK signalling is up-regulated by exporting CKs from cytoplasm to apoplast or ER and down-regulated by the opposite processes. Availability of biologically active CKs in apoplast and ER is also mediated metabolically, via enzyme reactions. As discussed above, these reactions can also affect transport rates by regulating CK concentration gradient between concerned compartments.

So far, two CK transporters have been shown to regulate CK signalling output—AtPUP14 and AtAZG2 [28,112]. AtPUP14 is localized to the plasma membrane and mediates energy-dependent CK uptake to cytoplasm, preventing apoplastic CKs from triggering cellular response. Compared to AtPUP14, AtAZG2 is more versatile—it is located to both the plasma membrane and ER and mediates bidirectional facilitated diffusion. It can follow, for instance, that the combination of active AtPUP14 and inactive AtAZG2 results in CK accumulation in cytoplasm and down-regulation of all CK receptors [112].

Considering the scheme in Figure 4, it is apparent that a large number of hypothetical pathways such as the one mentioned above could be designed. However, it is not implied that every CK movement has to ultimately result in the change of CK signallization output. As discussed throughout this paper, CK transport can also occur via processes driven by chemical properties of CK molecules and their transient concentration gradients. When discussing links between CK transport and signalling, it is therefore necessary to look for direct evidence and to keep in mind that correlation does not prove causality.

Supplementary Materials: The following is available online at https://www.mdpi.com/article/10.3390/ijms22073428/s1, Table S1: A summary of membrane-bound transport proteins which have been examined regarding the CK transport.

Author Contributions: D.N. and K.H. wrote the first draft of the manuscript; D.N. drew the figure; P.H. and P.K. contributed to manuscript revision. All authors have read and agreed to the published version of the manuscript.

Funding: The work was supported by The European Regional Development Fund-Project "Centre for Experimental Plant Biology" (No. CZ.02.1.01/0.0/0.0/16_019/0000738).

Acknowledgments: We would like to dedicate this review to Miroslav Kamínek, the long-time head of the Laboratory of Hormonal Regulations in Plants at the Institute of Experimental Botany, Prague, Czech Republic, our friend and teacher, who we have lost recently.

Conflicts of Interest: The authors declare no conflict of interest.

References

1. Schaller, G.E.; Bishopp, A.; Kieber, J.J. The Yin-Yang of Hormones: Cytokinin and Auxin Interactions in Plant Development. *Plant Cell* **2015**, *27*, 44–63. [CrossRef]
2. Kieber, J.J.; Schaller, G.E. Cytokinin Signaling in Plant Development. *Development* **2018**, *145*, dev149344. [CrossRef]
3. Skalický, V.; Kubeš, M.; Napier, R.; Novák, O. Auxins and Cytokinins—The Role of Subcellular Organization on Homeostasis. *Int. J. Mol. Sci.* **2018**, *19*, 3115. [CrossRef]
4. Akiyoshi, D.E.; Klee, H.; Amasino, R.M.; Nester, E.W.; Gordon, M.P. T-DNA of Agrobacterium Tumefaciens Encodes an Enzyme of Cytokinin Biosynthesis. *Proc. Natl. Acad. Sci. USA* **1984**, *81*, 5994–5998. [CrossRef]
5. Kieber, J.J.; Schaller, G.E. Cytokinins. *Arab. Book* **2014**, *12*, e0168. [CrossRef] [PubMed]
6. Takei, K.; Yamaya, T.; Sakakibara, H. Arabidopsis CYP735A1 and CYP735A2 Encode Cytokinin Hydroxylases That Catalyze the Biosynthesis of Trans-Zeatin. *J. Biol. Chem.* **2004**, *279*, 41866–41872. [CrossRef] [PubMed]
7. Lomin, S.N.; Krivosheev, D.M.; Steklov, M.Y.; Arkhipov, D.V.; Osolodkin, D.I.; Schmülling, T.; Romanov, G.A. Plant Membrane Assays with Cytokinin Receptors Underpin the Unique Role of Free Cytokinin Bases as Biologically Active Ligands. *J. Exp. Bot.* **2015**, *66*, 1851–1863. [CrossRef] [PubMed]
8. Chen, C.-M.; Kristopeit, S.M. Metabolism of Cytokinin: Dephosphorylation of Cytokinin Ribonucleotide by 5′-Nucleotidases from Wheat Germ Cytosol. *Plant Physiol.* **1981**, *67*, 494–498. [CrossRef]
9. Chen, C.-M.; Kristopeit, S.M. Metabolism of Cytokinin: Deribosylation of Cytokinin Ribonucleoside by Adenosine Nucleosidase from Wheat Germ Cells. *Plant Physiol.* **1981**, *68*, 1020–1023. [CrossRef]
10. Kurakawa, T.; Ueda, N.; Maekawa, M.; Kobayashi, K.; Kojima, M.; Nagato, Y.; Sakakibara, H.; Kyozuka, J. Direct Control of Shoot Meristem Activity by a Cytokinin-Activating Enzyme. *Nature* **2007**, *445*, 652–655. [CrossRef]
11. Kuroha, T.; Tokunaga, H.; Kojima, M.; Ueda, N.; Ishida, T.; Nagawa, S.; Fukuda, H.; Sugimoto, K.; Sakakibara, H. Functional Analyses of LONELY GUY Cytokinin-Activating Enzymes Reveal the Importance of the Direct Activation Pathway in Arabidopsis. *Plant Cell* **2009**, *21*, 3152–3169. [CrossRef]
12. Tokunaga, H.; Kojima, M.; Kuroha, T.; Ishida, T.; Sugimoto, K.; Kiba, T.; Sakakibara, H. Arabidopsis Lonely Guy (LOG) Multiple Mutants Reveal a Central Role of the LOG-Dependent Pathway in Cytokinin Activation. *Plant J.* **2012**, *69*, 355–365. [CrossRef]
13. Galuszka, P.; Frébort, I.; Šebela, M.; Sauer, P.; Jacobsen, S.; Peč, P. Cytokinin Oxidase or Dehydrogenase? *Eur. J. Biochem.* **2001**, *268*, 450–461. [CrossRef]
14. Schmülling, T.; Werner, T.; Riefler, M.; Krupková, E.; Bartrina y Manns, I. Structure and Function of Cytokinin Oxidase/Dehydrogenase Genes of Maize, Rice, Arabidopsis and Other Species. *J. Plant Res.* **2003**, *116*, 241–252. [CrossRef]
15. Hou, B.; Lim, E.-K.; Higgins, G.S.; Bowles, D.J. N-Glucosylation of Cytokinins by Glycosyltransferases of Arabidopsis Thaliana. *J. Biol. Chem.* **2004**, *279*, 47822–47832. [CrossRef] [PubMed]
16. Brzobohatý, B.; Moore, I.; Kristoffersen, P.; Bako, L.; Campos, N.; Schell, J.; Palme, K. Release of Active Cytokinin by a Beta-Glucosidase Localized to the Maize Root Meristem. *Science* **1993**, *262*, 1051–1054. [CrossRef]
17. Hošek, P.; Hoyerová, K.; Kiran, N.S.; Dobrev, P.I.; Zahajská, L.; Filepová, R.; Motyka, V.; Müller, K.; Kamínek, M. Distinct Metabolism of N-Glucosides of Isopentenyladenine and Trans-Zeatin Determines Cytokinin Metabolic Spectrum in Arabidopsis. *New Phytol.* **2020**, *225*, 2423–2438. [CrossRef] [PubMed]
18. Vylíčilová, H.; Bryksová, M.; Matušková, V.; Doležal, K.; Plíhalová, L.; Strnad, M. Naturally Occurring and Artificial N9-Cytokinin Conjugates: From Synthesis to Biological Activity and Back. *Biomolecules* **2020**, *10*, 832. [CrossRef] [PubMed]
19. Romanov, G.A.; Lomin, S.N.; Schmülling, T. Cytokinin Signaling: From the ER or from the PM? That is the Question! *New Phytol.* **2018**, *218*, 41–53. [CrossRef]
20. Inoue, T.; Higuchi, M.; Hashimoto, Y.; Seki, M.; Kobayashi, M.; Kato, T.; Tabata, S.; Shinozaki, K.; Kakimoto, T. Identification of CRE1 as a Cytokinin Receptor from Arabidopsis. *Nature* **2001**, *409*, 1060–1063. [CrossRef]
21. Ueguchi, C.; Koizumi, H.; Suzuki, T.; Mizuno, T. Novel Family of Sensor Histidine Kinase Genes in Arabidopsis Thaliana. *Plant Cell Physiol.* **2001**, *42*, 231–235. [CrossRef] [PubMed]

22. Kim, H.J.; Ryu, H.; Hong, S.H.; Woo, H.R.; Lim, P.O.; Lee, I.C.; Sheen, J.; Nam, H.G.; Hwang, I. Cytokinin-Mediated Control of Leaf Longevity by AHK3 through Phosphorylation of ARR2 in Arabidopsis. *Proc. Natl. Acad. Sci. USA* **2006**, *103*, 814–819. [CrossRef] [PubMed]
23. Caesar, K.; Thamm, A.M.K.; Witthöft, J.; Elgass, K.; Huppenberger, P.; Grefen, C.; Horak, J.; Harter, K. Evidence for the Localization of the Arabidopsis Cytokinin Receptors AHK3 and AHK4 in the Endoplasmic Reticulum. *J. Exp. Bot.* **2011**, *62*, 5571–5580. [CrossRef] [PubMed]
24. Wulfetange, K.; Lomin, S.N.; Romanov, G.A.; Stolz, A.; Heyl, A.; Schmülling, T. The Cytokinin Receptors of Arabidopsis are Located Mainly to the Endoplasmic Reticulum. *Plant Physiol.* **2011**, *156*, 1808–1818. [CrossRef]
25. Lomin, S.N.; Myakushina, Y.A.; Arkhipov, D.V.; Leonova, O.G.; Popenko, V.I.; Schmülling, T.; Romanov, G.A. Studies of Cytokinin Receptor-Phosphotransmitter Interaction Provide Evidences for the Initiation of Cytokinin Signalling in the Endoplasmic Reticulum. *Funct. Plant Biol.* **2018**, *45*, 192–202. [CrossRef]
26. Antoniadi, I.; Novák, O.; Gelová, Z.; Johnson, A.; Plíhal, O.; Simerský, R.; Mik, V.; Vain, T.; Mateo-Bonmatí, E.; Karady, M.; et al. Cell-Surface Receptors Enable Perception of Extracellular Cytokinins. *Nat. Commun.* **2020**, *11*, 4284. [CrossRef]
27. Kubiasová, K.; Montesinos, J.C.; Šamajová, O.; Nisler, J.; Mik, V.; Semerádová, H.; Plíhalová, L.; Novák, O.; Marhavý, P.; Cavallari, N.; et al. Cytokinin Fluoroprobe Reveals Multiple Sites of Cytokinin Perception at Plasma Membrane and Endoplasmic Reticulum. *Nat. Commun.* **2020**, *11*, 4285. [CrossRef]
28. Zürcher, E.; Liu, J.; di Donato, M.; Geisler, M.; Müller, B. Plant Development Regulated by Cytokinin Sinks. *Science* **2016**, *353*, 1027–1030. [CrossRef]
29. Hluska, T.; Hlusková, L.; Emery, R.J. The Hulks and the Deadpools of the Cytokinin Universe: A Dual Strategy for Cytokinin Production, Translocation, and Signal Transduction. *Biomolecules* **2021**, *11*, 209. [CrossRef]
30. Kieber, J.J. Cytokinins: Regulators of Cell Division. In *Plant Physiology*; Taiz, L., Zeiger, E., Eds.; Sinauer Associates, Inc.: Sunderland, MA, USA, 2002; pp. 493–517.
31. Spíchal, L. Cytokinins—Recent News and Views of Evolutionally Old Molecules. *Funct. Plant Biol.* **2012**, *39*, 267–284. [CrossRef]
32. Nedvěd, D. Transport and Metabolism of Radio-Labelled Cytokinins in Plant Cells and Tissues. Master's Thesis, Charles University, Prague, Czech Republic, 2020.
33. Vickers, C.E.; Bongers, M.; Liu, Q.; Delatte, T.; Bouwmeester, H. Metabolic Engineering of Volatile Isoprenoids in Plants and Microbes. *Plant Cell Environ.* **2014**, *37*, 1753–1775. [CrossRef]
34. Gajdošová, S.; Spíchal, L.; Kamínek, M.; Hoyerová, K.; Novák, O.; Dobrev, P.I.; Galuszka, P.; Klíma, P.; Gaudinová, A.; Žižková, E.; et al. Distribution, Biological Activities, Metabolism, and the Conceivable Function of Cis-Zeatin-Type Cytokinins in Plants. *J. Exp. Bot.* **2011**, *62*, 2827–2840. [CrossRef] [PubMed]
35. Heyl, A.; Riefler, M.; Romanov, G.A.; Schmülling, T. Properties, Functions and Evolution of Cytokinin Receptors. *Eur. J. Cell Biol.* **2012**, *91*, 246–256. [CrossRef]
36. Bassil, N.V.; Mok, D.W.S.; Mok, M.C. Partial Purification of a Cis-Trans-Isomerase of Zeatin from Immature Seed of Phaseolus Vulgaris L. *Plant Physiol.* **1993**, *102*, 867–872. [CrossRef]
37. Hluska, T.; Šebela, M.; Lenobel, R.; Frébort, I.; Galuszka, P. Purification of Maize Nucleotide Pyrophosphatase/Phosphodiesterase Casts Doubt on the Existence of Zeatin Cis–Trans Isomerase in Plants. *Front. Plant Sci.* **2017**, *8*. [CrossRef] [PubMed]
38. Miyawaki, K.; Tarkowski, P.; Matsumoto-Kitano, M.; Kato, T.; Sato, S.; Tarkowska, D.; Tabata, S.; Sandberg, G.; Kakimoto, T. Roles of Arabidopsis ATP/ADP Isopentenyltransferases and TRNA Isopentenyltransferases in Cytokinin Biosynthesis. *Proc. Natl. Acad. Sci. USA* **2006**, *103*, 16598–16603. [CrossRef]
39. Martin, R.C.; Mok, M.C.; Shaw, G.; Mok, D.W.S. An Enzyme Mediating the Conversion of Zeatin to Dihydrozeatin in Phaseolus Embryos. *Plant Physiol.* **1989**, *90*, 1630–1635. [CrossRef] [PubMed]
40. Gaudinová, A.; Dobrev, P.I.; Šolcová, B.; Novák, O.; Strnad, M.; Friedecký, D.; Motyka, V. The Involvement of Cytokinin Oxidase/Dehydrogenase and Zeatin Reductase in Regulation of Cytokinin Levels in Pea (Pisum Sativum L.) Leaves. *J. Plant Growth Regul.* **2005**, *24*, 188–200. [CrossRef]
41. Kolachevskaya, O.O.; Sergeeva, L.I.; Floková, K.; Getman, I.A.; Lomin, S.N.; Alekseeva, V.V.; Rukavtsova, E.B.; Buryanov, Y.I.; Romanov, G.A. Auxin Synthesis Gene Tms1 Driven by Tuber-Specific Promoter Alters Hormonal Status of Transgenic Potato Plants and Their Responses to Exogenous Phytohormones. *Plant Cell Rep.* **2017**, *36*, 419–435. [CrossRef]
42. Tarkowská, D.; Doležal, K.; Tarkowski, P.; Åstot, C.; Holub, J.; Fuksová, K.; Schmülling, T.; Sandberg, G.; Strnad, M. Identification of New Aromatic Cytokinins in Arabidopsis Thaliana and Populus × Canadensis Leaves by LC-(+)ESI-MS and Capillary Liquid Chromatography/Frit–Fast Atom Bombardment Mass Spectrometry. *Physiol. Plant* **2003**, *117*, 579–590. [CrossRef]
43. Strnad, M. The Aromatic Cytokinins. *Physiol. Plant* **1997**, *101*, 674–688. [CrossRef]
44. Hluska, T.; Dobrev, P.I.; Tarkowská, D.; Frébortová, J.; Zalabák, D.; Kopečný, D.; Plíhal, O.; Kokáš, F.; Briozzo, P.; Zatloukal, M.; et al. Cytokinin Metabolism in Maize: Novel Evidence of Cytokinin Abundance, Interconversions and Formation of a New Trans-Zeatin Metabolic Product with a Weak Anticytokinin Activity. *Plant Sci.* **2016**, *247*, 127–137. [CrossRef] [PubMed]
45. Sørensen, J.L.; Benfield, A.H.; Wollenberg, R.D.; Westphal, K.; Wimmer, R.; Nielsen, M.R.; Nielsen, K.F.; Carere, J.; Covarelli, L.; Beccari, G.; et al. The Cereal Pathogen Fusarium Pseudograminearum Produces a New Class of Active Cytokinins during Infection. *Mol. Plant Pathol.* **2017**, *19*, 1140–1154. [CrossRef] [PubMed]
46. Haidoune, M.; Mornet, R.; Laloue, M. Synthesis of 6-(3-Methylpyrrol-1-Yl)-9-β-D-Ribofuranosyl Purine, a Novel Metabolite of Zeatin Riboside. *Tetrahedron Lett.* **1990**, *31*, 1419–1422. [CrossRef]

47. Mok, M.C.; Martin, R.C.; Dobrev, P.I.; Vanková, R.; Ho, P.S.; Yonekura-Sakakibara, K.; Sakakibara, H.; Mok, D.W.S. Topolins and Hydroxylated Thidiazuron Derivatives are Substrates of Cytokinin O-Glucosyltransferase with Position Specificity Related to Receptor Recognition. *Plant Physiol.* **2005**, *137*, 1057–1066. [CrossRef]
48. Galuszka, P.; Popelková, H.; Werner, T.; Frébortová, J.; Pospíšilová, H.; Mik, V.; Köllmer, I.; Schmülling, T.; Frébort, I. Biochemical Characterization of Cytokinin Oxidases/Dehydrogenases from Arabidopsis Thaliana Expressed in Nicotiana Tabacum L. *J. Plant Growth Regul.* **2007**, *26*, 255–267. [CrossRef]
49. Evidente, A.; Fujii, T.; Iacobellis, N.S.; Riva, S.; Sisto, A.; Surico, G. Structure-Activity Relationships of Zeatin Cytokinins Produced by Plant PathogenicPseudomonades. *Phytochemistry* **1991**, *30*, 3505–3510. [CrossRef]
50. Pertry, I.; Václavíková, K.; Depuydt, S.; Galuszka, P.; Spíchal, L.; Temmerman, W.; Stes, E.; Schmülling, T.; Kakimoto, T.; Montagu, M.C.E.V.; et al. Identification of Rhodococcus Fascians Cytokinins and Their Modus Operandi to Reshape the Plant. *Proc. Natl. Acad. Sci. USA* **2009**, *106*, 929–934. [CrossRef] [PubMed]
51. Radhika, V.; Ueda, N.; Tsuboi, Y.; Kojima, M.; Kikuchi, J.; Kudo, T.; Sakakibara, H. Methylated Cytokinins from the Phytopathogen Rhodococcus Fascians Mimic Plant Hormone Activity. *Plant Physiol.* **2015**, *169*, 1118–1126. [CrossRef] [PubMed]
52. Gibb, M.; Kisiala, A.B.; Morrison, E.N.; Emery, R.J.N. The Origins and Roles of Methylthiolated Cytokinins: Evidence from Among Life Kingdoms. *Front. Cell Dev. Biol.* **2020**, *8*, 605672. [CrossRef]
53. Oshchepkov, M.S.; Kalistratova, A.V.; Savelieva, E.M.; Romanov, G.A.; Bystrova, N.A.; Kochetkov, K.A. Natural and Synthetic Cytokinins and Their Applications in Biotechnology, Agrochemistry and Medicine. *Russ. Chem. Rev.* **2020**, *89*, 787. [CrossRef]
54. Wildman, S.A.; Crippen, G.M. Prediction of Physicochemical Parameters by Atomic Contributions. *J. Chem. Inf. Comput. Sci.* **1999**, *39*, 868–873. [CrossRef]
55. Šimura, J.; Antoniadi, I.; Široká, J.; Tarkowská, D.; Strnad, M.; Ljung, K.; Novák, O. Plant Hormonomics: Multiple Phytohormone Profiling by Targeted Metabolomics. *Plant Physiol.* **2018**, *177*, 476–489. [CrossRef] [PubMed]
56. Buchanan, B.B.; Gruissem, W.; Jones, R.L. (Eds.) *Biochemistry & Molecular Biology of Plants*, 2nd ed.; Wiley-Blackwell: Hoboken, NJ, USA, 2015; ISBN 978-1-118-50219-8.
57. Chen, W.; Gai, Y.; Liu, S.; Wang, R.; Jiang, X. Quantitative Analysis of Cytokinins in Plants by High Performance Liquid Chromatography: Electronspray Ionization Ion Trap Mass Spectrometry. *J. Integr. Plant Biol.* **2010**, *52*, 925–932. [CrossRef] [PubMed]
58. Dobrev, P.I.; Hoyerová, K.; Petrášek, J. Analytical Determination of Auxins and Cytokinins. In *Auxins and Cytokinins in Plant Biology*; Dandekar, T., Naseem, M., Eds.; Methods in Molecular Biology; Springer: New York, NY, USA, 2017; Volume 1569, pp. 31–39. ISBN 978-1-4939-6829-9.
59. Hoyerová, K.; Gaudinová, A.; Malbeck, J.; Dobrev, P.I.; Kocábek, T.; Šolcová, B.; Trávníčková, A.; Kamínek, M. Efficiency of Different Methods of Extraction and Purification of Cytokinins. *Phytochemistry* **2006**, *67*, 1151–1159. [CrossRef]
60. Gillissen, B.; Bürkle, L.; André, B.; Kühn, C.; Rentsch, D.; Brandl, B.; Frommer, W.B. A New Family of High-Affinity Transporters for Adenine, Cytosine, and Purine Derivatives in Arabidopsis. *Plant Cell* **2000**, *12*, 291–300. [CrossRef]
61. Bürkle, L.; Cedzich, A.; Döpke, C.; Stransky, H.; Okumoto, S.; Gillissen, B.; Kühn, C.; Frommer, W.B. Transport of Cytokinins Mediated by Purine Transporters of the PUP Family Expressed in Phloem, Hydathodes, and Pollen of Arabidopsis. *Plant J.* **2003**, *34*, 13–26. [CrossRef]
62. Sun, J.; Hirose, N.; Wang, X.; Wen, P.; Xue, L.; Sakakibara, H.; Zuo, J. Arabidopsis SOI33/AtENT8 Gene Encodes a Putative Equilibrative Nucleoside Transporter That is Involved in Cytokinin Transport In Planta. *J. Integr. Plant Biol.* **2005**, *47*, 588–603. [CrossRef]
63. Spíchal, L.; Rakova, N.Y.; Riefler, M.; Mizuno, T.; Romanov, G.A.; Strnad, M.; Schmülling, T. Two Cytokinin Receptors of Arabidopsis Thaliana, CRE1/AHK4 and AHK3, Differ in Their Ligand Specificity in a Bacterial Assay. *Plant Cell Physiol.* **2004**, *45*, 1299–1305. [CrossRef]
64. Yonekura-Sakakibara, K.; Kojima, M.; Yamaya, T.; Sakakibara, H. Molecular Characterization of Cytokinin-Responsive Histidine Kinases in Maize. Differential Ligand Preferences and Response to Cis-Zeatin. *Plant Physiol.* **2004**, *134*, 1654–1661. [CrossRef]
65. Lomin, S.N.; Krivosheev, D.M.; Steklov, M.Y.; Osolodkin, D.I.; Romanov, G.A. Receptor Properties and Features of Cytokinin Signaling. *Acta Nat.* **2012**, *4*, 31–45. [CrossRef]
66. Hirose, N.; Makita, N.; Yamaya, T.; Sakakibara, H. Functional Characterization and Expression Analysis of a Gene, OsENT2, Encoding an Equilibrative Nucleoside Transporter in Rice Suggest a Function in Cytokinin Transport. *Plant Physiol.* **2005**, *138*, 196–206. [CrossRef] [PubMed]
67. Hirose, N.; Takei, K.; Kuroha, T.; Kamada-Nobusada, T.; Hayashi, H.; Sakakibara, H. Regulation of Cytokinin Biosynthesis, Compartmentalization and Translocation. *J. Exp. Bot.* **2008**, *59*, 75–83. [CrossRef] [PubMed]
68. Qi, Z.; Xiong, L. Characterization of a Purine Permease Family Gene OsPUP7 Involved in Growth and Development Control in Rice. *J. Integr. Plant Biol.* **2013**, *55*, 1119–1135. [CrossRef] [PubMed]
69. Dobrev, P.I.; Kamínek, M. Fast and Efficient Separation of Cytokinins from Auxin and Abscisic Acid and Their Purification Using Mixed-Mode Solid-Phase Extraction. *J. Chromatogr. A* **2002**, *950*, 21–29. [CrossRef]
70. Jiskrová, E.; Novák, O.; Pospíšilová, H.; Holubová, K.; Karády, M.; Galuszka, P.; Robert, S.; Frébort, I. Extra- and Intracellular Distribution of Cytokinins in the Leaves of Monocots and Dicots. *New Biotechnol.* **2016**, *33*, 735–742. [CrossRef]
71. Beveridge, C.A.; Murfet, I.C.; Kerhoas, L.; Sotta, B.; Miginiac, E.; Rameau, C. The Shoot Controls Zeatin Riboside Export from Pea Roots. Evidence from the Branching Mutant Rms4. *Plant J.* **1997**, *11*, 339–345. [CrossRef]

72. Kuroha, T.; Kato, H.; Asami, T.; Yoshida, S.; Kamada, H.; Satoh, S. A Trans-zeatin Riboside in Root Xylem Sap Negatively Regulates Adventitious Root Formation on Cucumber Hypocotyls. *J. Exp. Bot.* **2002**, *53*, 2193–2200. [CrossRef]
73. Takei, K.; Sakakibara, H.; Taniguchi, M.; Sugiyama, T. Nitrogen-Dependent Accumulation of Cytokinins in Root and TheTranslocation to Leaf: Implication of Cytokinin Species That Induces GeneExpression of Maize ResponseRegulator. *Plant Cell Physiol.* **2001**, *42*, 85–93. [CrossRef]
74. Corbesier, L.; Prinsen, E.; Jacqmard, A.; Lejeune, P.; van Onckelen, H.; Périlleux, C.; Bernier, G. Cytokinin Levels in Leaves, Leaf Exudate and Shoot Apical Meristem of Arabidopsis Thaliana during Floral Transition. *J. Exp. Bot.* **2003**, *54*, 2511–2517. [CrossRef] [PubMed]
75. Jin, S.-H.; Ma, X.-M.; Kojima, M.; Sakakibara, H.; Wang, Y.-W.; Hou, B.-K. Overexpression of Glucosyltransferase UGT85A1 Influences Trans-Zeatin Homeostasis and Trans-Zeatin Responses Likely through O-Glucosylation. *Planta* **2013**, *237*, 991–999. [CrossRef] [PubMed]
76. Šmehilová, M.; Dobrůšková, J.; Novák, O.; Takáč, T.; Galuszka, P. Cytokinin-Specific Glycosyltransferases Possess Different Roles in Cytokinin Homeostasis Maintenance. *Front. Plant Sci.* **2016**, *7*. [CrossRef]
77. Benková, E.; Witters, E.; Dongen, W.V.; Kolar, J.; Motyka, V.; Brzobohatý, B.; Onckelen, H.A.V.; Macháčková, I. Cytokinins in Tobacco and Wheat Chloroplasts. Occurrence and Changes Due to Light/Dark Treatment. *Plant Physiol.* **1999**, *121*, 245–252. [CrossRef] [PubMed]
78. Galbraith, D.; Loureiro, J.; Antoniadi, I.; Bainard, J.; Bureš, P.; Cápal, P.; Castro, M.; Castro, S.; Čertner, M.; Čertnerová, D.; et al. Best Practices in Plant Cytometry. *Cytom. Part. A* **2021**, 1–7. [CrossRef]
79. Wilkens, S. Structure and Mechanism of ABC Transporters. *F1000Prime Rep.* **2015**, *7*. [CrossRef]
80. Kang, J.; Park, J.; Choi, H.; Burla, B.; Kretzschmar, T.; Lee, Y.; Martinoia, E. Plant ABC Transporters. *Arab. Book* **2011**, *9*. [CrossRef] [PubMed]
81. Girke, C.; Daumann, M.; Niopek-Witz, S.; Möhlmann, T. Nucleobase and Nucleoside Transport and Integration into Plant Metabolism. *Front. Plant Sci.* **2014**, *5*. [CrossRef] [PubMed]
82. Paul, A.; Laurila, T.; Vuorinen, V.; Divinski, S.V. Fick's Laws of Diffusion. In *Thermodynamics, Diffusion and the Kirkendall Effect in Solids*; Paul, A., Laurila, T., Vuorinen, V., Divinski, S.V., Eds.; Springer International Publishing: Cham, Switzerland, 2014; pp. 115–139. ISBN 978-3-319-07461-0.
83. El-Showk, S.; Help-Rinta-Rahko, H.; Blomster, T.; Siligato, R.; Marée, A.F.M.; Mähönen, A.P.; Grieneisen, V.A. Parsimonious Model of Vascular Patterning Links Transverse Hormone Fluxes to Lateral Root Initiation: Auxin Leads the Way, While Cytokinin Levels Out. *PLoS Comput. Biol.* **2015**, *11*, e1004450. [CrossRef]
84. Hošek, P.; Kubeš, M.; Laňková, M.; Dobrev, P.I.; Klíma, P.; Kohoutová, M.; Petrášek, J.; Hoyerová, K.; Jiřina, M.; Zažímalová, E. Auxin Transport at Cellular Level: New Insights Supported by Mathematical Modelling. *J. Exp. Bot.* **2012**, *63*, 3815–3827. [CrossRef]
85. Moore, S.; Zhang, X.; Mudge, A.; Rowe, J.H.; Topping, J.F.; Liu, J.; Lindsey, K. Spatiotemporal Modelling of Hormonal Crosstalk Explains the Level and Patterning of Hormones and Gene Expression in Arabidopsis Thaliana Wild-Type and Mutant Roots. *New Phytol.* **2015**, *207*, 1110–1122. [CrossRef]
86. Zažímalová, E.; Murphy, A.S.; Yang, H.; Hoyerová, K.; Hošek, P. Auxin Transporters—Why So Many? *Cold Spring Harb. Perspect. Biol.* **2010**, *2*, a001552. [CrossRef]
87. Kramer, E.M. How Far Can a Molecule of Weak Acid Travel in the Apoplast or Xylem? *Plant Physiol.* **2006**, *141*, 1233–1236. [CrossRef]
88. Wormit, A.; Traub, M.; Flörchinger, M.; Neuhaus, H.E.; Möhlmann, T. Characterization of Three Novel Members of the Arabidopsis Thaliana Equilibrative Nucleoside Transporter (ENT) Family. *Biochem. J.* **2004**, *383*, 19–26. [CrossRef] [PubMed]
89. Michaelis, L.; Menten, M.L. Die Kinetik Der Invertinwirkung. *Biochemische Zeitschrift* **1913**, *49*, 333–369.
90. Johnson, K.A.; Goody, R.S. The Original Michaelis Constant: Translation of the 1913 Michaelis-Menten Paper. *Biochemistry* **2011**, *50*, 8264–8269. [CrossRef] [PubMed]
91. Li, J.; Wang, D. Cloning and in Vitro Expression of the CDNA Encoding a Putative Nucleoside Transporter from Arabidopsis Thaliana. *Plant Sci.* **2000**, *157*, 23–32. [CrossRef]
92. Möhlmann, T.; Mezher, Z.; Schwerdtfeger, G.; Neuhaus, H.E. Characterisation of a Concentrative Type of Adenosine Transporter from Arabidopsis Thaliana (ENT1,At). *FEBS Lett.* **2001**, *509*, 370–374. [CrossRef]
93. Bernard, C.; Traub, M.; Kunz, H.-H.; Hach, S.; Trentmann, O.; Möhlmann, T. Equilibrative Nucleoside Transporter 1 (ENT1) is Critical for Pollen Germination and Vegetative Growth in Arabidopsis. *J. Exp. Bot.* **2011**, *62*, 4627–4637. [CrossRef]
94. Girke, C.; Arutyunova, E.; Syed, M.; Traub, M.; Möhlmann, T.; Lemieux, M.J. High Yield Expression and Purification of Equilibrative Nucleoside Transporter 7 (ENT7) from Arabidopsis Thaliana. *Biochim. Biophys. Acta BBA Gen. Subj.* **2015**, *1850*, 1921–1929. [CrossRef] [PubMed]
95. Li, G.; Liu, K.; Baldwin, S.A.; Wang, D. Equilibrative Nucleoside Transporters of Arabidopsis Thaliana: CDNA Cloning, Expression Pattern, and Analysis of Transport Activities. *J. Biol. Chem.* **2003**, *278*, 35732–35742. [CrossRef]
96. Traub, M.; Flörchinger, M.; Piecuch, J.; Kunz, H.; Weise-Steinmetz, A.; Deitmer Joachim, W.; Ekkehard Neuhaus, H.; Möhlmann, T. The Fluorouridine Insensitive 1 (Fur1) Mutant is Defective in Equilibrative Nucleoside Transporter 3 (ENT3), and Thus Represents an Important Pyrimidine Nucleoside Uptake System in Arabidopsis Thaliana. *Plant J.* **2007**, *49*, 855–864. [CrossRef]

97. Boswell-Casteel, R.C.; Hays, F.A. Equilibrative Nucleoside Transporters—A Review. *Nucleosides Nucleotides Nucleic Acids* **2017**, *36*, 7–30. [CrossRef]
98. Young, J.D.; Yao, S.Y.M.; Baldwin, J.M.; Cass, C.E.; Baldwin, S.A. The Human Concentrative and Equilibrative Nucleoside Transporter Families, SLC28 and SLC29. *Mol. Asp. Med.* **2013**, *34*, 529–547. [CrossRef]
99. Hildreth, S.B.; Gehman, E.A.; Yang, H.; Lu, R.-H.; Ritech, C.K.; Harich, K.C.; Yu, S.; Lin, J.; Sandoe, J.L.; Okumoto, S.; et al. Tobacco Nicotine Uptake Permease (NUP1) Affects Alkaloid Metabolism. *Proc. Natl. Acad. Sci. USA* **2011**, *108*, 18179–18184. [CrossRef]
100. Cedzich, A.; Stransky, H.; Schulz, B.; Frommer, W.B. Characterization of Cytokinin and Adenine Transport in Arabidopsis Cell Cultures. *Plant Physiol.* **2008**, *148*, 1857–1867. [CrossRef] [PubMed]
101. Durán-Medina, Y.; Díaz-Ramírez, D.; Marsch-Martínez, N. Cytokinins on the Move. *Front. Plant Sci.* **2017**, *8*. [CrossRef] [PubMed]
102. Liu, C.-J.; Zhao, Y.; Zhang, K. Cytokinin Transporters: Multisite Players in Cytokinin Homeostasis and Signal Distribution. *Front. Plant Sci.* **2019**, *10*. [CrossRef] [PubMed]
103. Szydlowski, N.; Bürkle, L.; Pourcel, L.; Moulin, M.; Stolz, J.; Fitzpatrick, T.B. Recycling of Pyridoxine (Vitamin B6) by PUP1 in Arabidopsis. *Plant J.* **2013**, *75*, 40–52. [CrossRef] [PubMed]
104. Xiao, Y.; Liu, D.; Zhang, G.; Gao, S.; Liu, L.; Xu, F.; Che, R.; Wang, Y.; Tong, H.; Chu, C. Big Grain3, Encoding a Purine Permease, Regulates Grain Size via Modulating Cytokinin Transport in Rice. *J. Integr. Plant Biol.* **2019**, *61*, 581–597. [CrossRef]
105. Xiao, Y.; Zhang, J.; Yu, G.; Lu, X.; Mei, W.; Deng, H.; Zhang, G.; Chen, G.; Chu, C.; Tong, H.; et al. Endoplasmic Reticulum-Localized PURINE PERMEASE1 Regulates Plant Height and Grain Weight by Modulating Cytokinin Distribution in Rice. *Front. Plant Sci.* **2020**, *11*. [CrossRef]
106. Zürcher, E.; Tavor-Deslex, D.; Lituiev, D.; Enkerli, K.; Tarr, P.T.; Müller, B. A Robust and Sensitive Synthetic Sensor to Monitor the Transcriptional Output of the Cytokinin Signaling Network in Planta. *Plant Physiol.* **2013**, *161*, 1066–1075. [CrossRef]
107. Ko, D.; Kang, J.; Kiba, T.; Park, J.; Kojima, M.; Do, J.; Kim, K.Y.; Kwon, M.; Endler, A.; Song, W.-Y.; et al. Arabidopsis ABCG14 Is Essential for the Root-to-Shoot Translocation of Cytokinin. *Proc. Natl. Acad. Sci. USA* **2014**, *111*, 7150–7155. [CrossRef]
108. Le Hir, R.; Sorin, C.; Chakraborti, D.; Moritz, T.; Schaller, H.; Tellier, F.; Robert, S.; Morin, H.; Bako, L.; Bellini, C. ABCG9, ABCG11 and ABCG14 ABC Transporters are Required for Vascular Development in Arabidopsis. *Plant J.* **2013**, *76*, 811–824. [CrossRef] [PubMed]
109. Zhang, K.; Novak, O.; Wei, Z.; Gou, M.; Zhang, X.; Yu, Y.; Yang, H.; Cai, Y.; Strnad, M.; Liu, C.-J. Arabidopsis ABCG14 Protein Controls the Acropetal Translocation of Root-Synthesized Cytokinins. *Nat. Commun.* **2014**, *5*, 1–12. [CrossRef] [PubMed]
110. Zhao, J.; Yu, N.; Ju, M.; Fan, B.; Zhang, Y.; Zhu, E.; Zhang, M.; Zhang, K. ABC Transporter OsABCG18 Controls the Shootward Transport of Cytokinins and Grain Yield in Rice. *J. Exp. Bot.* **2019**, *70*, 6277–6291. [CrossRef]
111. Mansfield, T.A.; Schultes, N.P.; Mourad, G.S. AtAzg1 and AtAzg2 Comprise a Novel Family of Purine Transporters in Arabidopsis. *FEBS Lett.* **2009**, *583*, 481–486. [CrossRef]
112. Tessi, T.M.; Brumm, S.; Winklbauer, E.; Schumacher, B.; Pettinari, G.; Lescano, I.; González, C.A.; Wanke, D.; Maurino, V.G.; Harter, K.; et al. Arabidopsis AZG2 Transports Cytokinins in vivo and Regulates Lateral Root Emergence. *New Phytol.* **2020**, *229*, 979–993. [CrossRef]
113. Tessi, T.M.; Shahriari, M.; Maurino, V.G.; Meissner, E.; Novak, O.; Pasternak, T.; Schumacher, B.S.; Flubacher, N.S.; Nautscher, M.; Williams, A.; et al. The Auxin Transporter PIN1 and the Cytokinin Transporter AZG1 Interact to Regulate the Root Stress Response. *bioRxiv* **2020**. [CrossRef]
114. Faiss, M.; Zalubilová, J.; Strnad, M.; Schmülling, T. Conditional Transgenic Expression of the Ipt Gene Indicates a Function for Cytokinins in Paracrine Signaling in Whole Tobacco Plants. *Plant J.* **1997**, *12*, 401–415. [CrossRef]
115. De Rybel, B.; Adibi, M.; Breda, A.S.; Wendrich, J.R.; Smit, M.E.; Novák, O.; Yamaguchi, N.; Yoshida, S.; Isterdael, G.V.; Palovaara, J.; et al. Integration of Growth and Patterning during Vascular Tissue Formation in Arabidopsis. *Science* **2014**, *345*. [CrossRef]
116. Badenoch-Jones, J.; Letham, D.S.; Parker, C.W.; Rolfe, B.G. Quantitation of Cytokinins in Biological Samples Using Antibodies Against Zeatin Riboside. *Plant Physiol.* **1984**, *75*, 1117–1125. [CrossRef]
117. Abo-Hamed, S.; Collin, H.A.; Hardwick, K. Biochemical and Physiological Aspects of Leaf Development in Cocoa (Theobroma Cacao L.). *New Phytol.* **1984**, *97*, 219–225. [CrossRef]
118. Kudoyarova, G.R.; Korobova, A.V.; Akhiyarova, G.R.; Arkhipova, T.N.; Zaytsev, D.Y.; Prinsen, E.; Egutkin, N.L.; Medvedev, S.S.; Veselov, S.Y. Accumulation of Cytokinins in Roots and Their Export to the Shoots of Durum Wheat Plants Treated with the Protonophore Carbonyl Cyanide M-Chlorophenylhydrazone (CCCP). *J. Exp. Bot.* **2014**, *65*, 2287–2294. [CrossRef]
119. Osugi, A.; Kojima, M.; Takebayashi, Y.; Ueda, N.; Kiba, T.; Sakakibara, H. Systemic Transport of Trans-Zeatin and Its Precursor Have Differing Roles in Arabidopsis Shoots. *Nat. Plants* **2017**, *3*, 17112. [CrossRef]
120. Matsumoto-Kitano, M.; Kusumoto, T.; Tarkowski, P.; Kinoshita-Tsujimura, K.; Václavíková, K.; Miyawaki, K.; Kakimoto, T. Cytokinins are Central Regulators of Cambial Activity. *Proc. Natl. Acad. Sci. USA* **2008**, *105*, 20027–20031. [CrossRef]

Table S1. A summary of membrane-bound transport proteins which have been examined regarding the CK transport. For each transporter, a brief overview of its involvement in the CK transport (and possibly other functions) is provided. If available, measured K_M values for CKs are given as well. Respective transport mechanisms, expression patterns, and subcellular localizations are listed in the following columns. SAT: secondary active transport; PAT: primary active transport; *At*: *Arabidopsis thaliana* (mouse-ear cress); *Os*: *Oryza sativa* (rice); *Nt*: *Nicotiana tabacum* (tobacco); BAP: 6-benzylaminopurine, cZ: *cis*-zeatin, DHZ: dihydrozeatin, iP: isopentenyl adenine, iPR: isopentenyl adenine riboside, tZ: *trans*-zeatin, tZR: *trans*-zeatin riboside; *N/A*: not available.

Name	*Relation to CK Transport*	*Other Notable Properties*	*Transport Mechanism*	*Expression Pattern*	*Subcellular Localization*	*References*
AtPUP1	Adenine uptake was competitively inhibited by kinetin and tZ. Direct tZ uptake was observed; it was inhibited by kinetin and iP (both in yeast). Measured K_M values (μM) – **kinetin:** 20, **tZ:** 35 (both in yeast).	Uptake of adenine, cytosine, hypoxanthine, nicotine, and caffeine was observed (in yeast). Involved in uptake of pyridoxine (in *Arabidopsis* protoplasts).	Proton-coupled SAT	Flowers, leaves, petioles, siliques, stems, veins.	*Plasma membrane.*	[60,61,103]
AtPUP2	Adenine uptake was inhibited by iP, kinetin, BAP, tZ, and cZ (in yeast).	The adenine uptake rate was lower than that mediated by AtPUP1 (in yeast).	Proton-coupled SAT	Flowers, leaves, petioles, roots, veins.	*N/A*	[61]
AtPUP3	*N/A*	No transport activity observed.	*N/A*	Flowers.	*N/A*	[61]
AtPUP14	Ectopic expression alters CK response pattern. Direct of tZ was observed in mesophyll protoplasts and tobacco microsomes. This uptake was inhibited by iP, BAP, and adenine.	Abundant expression in whole plants throughout various developmental stages.	ATP-dependent transport	Flowers, roots, rosettes, seeds, stems.	*Plasma membrane.*	[28,100]
AtENT1	Mutation **did not** alter iPR nor tZR uptake by *Arabidopsis* hypocotyl explants.	Uptake of adenosine, guanosine, inosine, and cytidine was observed (in yeast). Involved in adenosine export from the vacuole to the cytoplasm.	Proton-coupled SAT	Flowers, leaves, siliques, stems, roots.	*Plasma membrane, tonoplast.*	[62,91–93,95]
AtENT3 (FUR1)	Mutation led to a decrease in iPR and tZR uptake by *Arabidopsis* hypocotyl explants. No significant inhibition of adenosine uptake was observed (in yeast).	Uptake of adenosine, guanosine, inosine, cytidine and uridine was observed (in yeast).	Proton-coupled SAT	Flowers, leaves, siliques, roots.	*Plasma membrane.*	[62,67,95]
AtENT6	Mutation led to a decrease in iPR and tZR uptake by Arabidopsis hypocotyl explants. Adenosine uptake inhibited by iPR and tZR (in yeast). Measured K_M values (μM) – **iPR:** 17, **tZR:** 630 (both in yeast).	Uptake of adenosine, guanosine, inosine, cytidine and uridine was observed (in yeast).	Proton-coupled SAT	Flowers, leaves, siliques, stems, roots.	*Plasma membrane.*	[67,88,95]
AtENT7	Mutation led to a decrease in iPR and tZR uptake by *Arabidopsis* hypocotyl explants. No significant inhibition of adenosine uptake was observed (in yeast).	Uptake of adenosine, guanosine, inosine, cytidine and uridine was observed (in yeast).	Facilitated diffusion	Flowers, leaves.	*N/A*	[67,95]
AtENT8 (SOI33)	Mutation led to a decrease in iPR and tZR uptake by Arabidopsis hypocotyl explants. Mutants were also less sensitive to exogenous CKs, compared to the wild type. Conversely, over-expressing plants were more sensitive to them.	N/A	Proton-coupled SAT	Flowers, leaves, roots, siliques, stems.	*N/A*	[62,95]

AtABCG14	Loss-of-fucntion mutants were unable to translocate tZ-type CKs from roots to shoots. Mutants were impaired in growth and lateral root emergence. Application of exogenous tZ and grafting mutant shoots on wild-type roots (but not vice versa) restored the wild-type phenotype. Transport activity in transgenic yeast cells was not observed.	Forms strict heterodimers with AtABCG11 in co-immunoprecipitation assays.	PAT	Mainly in roots.	*Plasma membrane.*	[107,109]
AtAZG1	Adenine uptake was inhibited by iP, kinetin, BAP and tZ (in yeast). tZ uptake was observed both in yeast and *Arabidopsis* seedlings. Overexpression led to uptake increase, while loss-of-function mutation led to decreased concentrations of tZ-type CKs after tZ treatment (both in *Arabidopsis* plants).	Both AtAZG1 and 2 stabilize PIN1, an auxin transporter, on plasma membrane.	Proton-coupled SAT	Cotyledons, flowers, leaves (rosette and cauline), stems, roots.	*Plasma membrane.*	[113]
AtAZG2	Adenine uptake was inhibited by iP, kinetin, BAP, and tZ (in yeast). Ectopic expression in Arabidopsis led to an enhanced uptake rate of tZ, while in loss-of-function mutants, the tZ uptake rate remained similar to that in the wild type. The mutants were less responsive to CK signalling, though. Measured KM values (nM) – tZ: 810 (in *Arabidopsis* cell suspension).	The loss-of-function mutation enhances the lateral root density in presence of nitrate.	Facilitated diffusion	Flowers, roots.	*Endoplasmatic reticulum, plasma membrane.*	[112]
OsPUP1	Overexpression in rice plants alters CK concentrations in shoots, roots, and panicles. Root-to-shoot translocation of CKS is impaired. Endogenous CK application to roots triggered less pronounced response in shoots.	OsPUP1 and 4 act antagonistically in several aspects. When simultaneously overexpressed, OsPUP4 overcame some phenotype traits typical for OsPUP1.	N/A	Leave blades and sheats, mature roots, panicles, stems.	*Endoplasmatic reticulum.*	[105]
OsPUP4	Overexpression in rice plants alters CK concentrations in shoots, roots, and panicles. Shoot-to-root translocation of CKs is impaired. Endogenous CK application to shoots triggered less pronounced response in roots.		N/A	Leave blades and sheats, mature roots, panicles, stems.	*Plasma membrane.*	[104,105]
OsPUP7	Higher amounts of iP and iPR were detected in mutant plants. The amounts of tZ-like CKs did not change. Mutant plants displayed phenotype suggesting CK transport impairment.	Ability to complement mutant yeast deficient in caffeine uptake.	N/A	Grains, leaves, pistil, spikelets, stems.	*Endoplasmatic reticulum.*	[68,104]
OsENT2	Adenosine uptake was inhibited by iPR, but not by tZR. Direct uptake of both iPR and tZR was observed (all in yeast). Measured KM values (μM) – iPR: 32, tZR: 660 (both in yeast).	Uptake of adenosine, guanosine, inosine, cytidine and uridine was observed (in yeast).	Proton-coupled SAT	Grains, leaves, roots, stems, veins.	*N/A*	[66]
OsABCG18	The loss-of-function mutants are impaired in their ability to translocate tZ, tZR, and DHZ from roots to shoots. When expressed in tobacco leave explants, iP, iPR, and cZR we recognized as substrates too.	The closest ortholog of AtABCG14 in rice.	Primary active transport.	Leaves, panicles, roots, stems.	*Plasma membrane.*	[110]

NtPUP1	A 10-fold excess of unlabelled kinetin did not significantly inhibited uptake of [14]-C nicotine (in yeast).	A nicotine-specific transporter; more than 50% homology with AtPUP1.	N/A	Mainly root tips.	*Plasma membrane.*	[99]

4.2 Comprehensive Model of Cell-to-Cell Cytokinin Transport Reveals A Specific Mode of Cytokinin Riboside Influx

In this manuscript, my colleagues and I address the specific kinetics of the cellular uptake of CK ribosides and its impact on shoot development. Firstly, we present a series of radio-accumulation assays performed in tobacco BY-2 cells (Nagata et al., 1992), in which we monitor the cellular uptake of four CK nucleobases - tZ, DHZ, iP, and BA - and four CK ribosides - tZR, dihydrozeatin riboside (DHZR), iPR, and benzyladenosine (BAR). We fit the measured data with an adapted version of a previously published mathematical model (Hošek et al., 2012) to estimate first-order rate constants for the uptake of all tested CK species. We show that the BY-2 cells accumulate CK nucleobases with isoprenoid side chains more readily than the corresponding ribosides, whereas the uptake rates of BA and BAR do not significantly differ (Figure 1 in the manuscript). To confirm that the observed CK uptake in the BY-2 cells is mediated by membrane-bound carriers, we perform another set of radio-accumulation assays, in which we show that the uptake of radio-labelled tZ, tZR, iP and iPR is inhibited by increasing concentrations of their non-labelled counterparts (i.e. the uptake is saturable, as expected of the transport proteins). This experimental setup also allows us to estimate the affinities of the transporters present on the BY-2 plasma membrane towards different CKs in terms of the IC_{50} values. We show that the net affinity of the BY-2 transporters is higher towards CK nucleobases than the corresponding ribosides. We further show that the uptake of tZ, tZR, iP, and iPR is significantly reduced in BY-2 cells treated with the protonophore CCCP, implying that CK cellular uptake largely depends on the proton gradient (Figure 2 in the manuscript).

These findings indicate that the BY-2 cells can effectively discriminate between CK nucleobases and ribosides and that they possess either one system of membrane-bound carriers with different affinities for the two forms or two separate systems, one for CK nucleobases and the other for CK ribosides. To resolve this matter, we perform a series of accumulation assays in which we pair radio-labelled tZ, tZR, iP, and iPR with a variety of non-labelled competitors. We demonstrate that the uptake of CK nucleobases is strongly reduced due to competition with other nucleobases and mildly reduced due to competition with ribosides. On the other hand, the uptake of CK ribosides only competes with other ribosides and does not respond to nucleobases. We conclude that CKs are transported by at least two independent systems of membrane-bound carriers, of which one transports both CK nucleobases and ribosides with a slight preference for the former, whereas the other strictly transports CK ribosides (Figure 3 in the manuscript).

We follow by determining the transport activity of AtENT3, a representative nucleoside transporter, towards tZ, tZR, iP, and iPR. We have picked this transporter because its homologs are expressed in the BY-2 cells (Figure 4 in the publication) and because AtENT3 itself affects CK homeostasis in *A. thaliana* plants (Korobova et al., 2021). We support the role of AtENT3 as a CK transporter by directly showing that it transports CK nucleobases and ribosides in the BY-2 cells. This wide substrate specificity of AtENT3 suggests that it does not belong among the strictly CK riboside-specific carriers, whose identity remains to be determined. We further show that the AtENT3-mediated uptake of tZR is sensitive to nucleoside uptake inhibitors *S*-(4-nitrobenzyl)-6-thioinosine (NBTI) and dipyridamole but not CCCP (Figure 4 in the manuscript).

The accumulation assays in the *AtENT3*-expressing BY2 cells suggest that AtENT3 slightly prefers tZR over iPR. We further address this preference through a computational approach consisting of molecular docking and molecular dynamic simulations. We show that the docked poses of tZR and iPR bind to the AlphaFold-predicted structure of AtENT3 (Jumper et al., 2021), similarly to NBTI in human ENT1 (Wright and Lee, 2019) and inosine in ENT1 from *Plasmodium falciparum* (Wang et al., 2023). By aligning sequences of ENTs from various species, we show that the ribosyl moieties of tZR and iPR interact with highly conserved residues. Conversely, the adenyl moiety and the side chains interact with more variable residues, indicating that diverse ENT proteins share common motifs for binding ribosylated substrates while being able to recognize specific aglycons. Our molecular dynamic simulations indicate stable interactions among the side-chain hydroxyl of tZR and the AtENT3 residues Tyr61 and Asp129, likely stabilized by a water bridge. Both Tyr61 and Asp129 are conserved among AtENTs but not among ENTs from animals, yeast or *P. falciparum*, suggesting that these two residues allow the plant ENTs to specifically stabilize hydroxylated CK ribosides as their substrates (Figure 5 in the manuscript). Their presence can also explain why AtENT3 prefers tZR over iPR.

We wrap the manuscript up by showing that AtENT3 contributes to the shoot development in *A. thaliana*. We show that *atent3* mutant plants aged 8 to 15 days (grown on agar or cultivation substrate) have significantly larger shoots than the wild type. This observation is consistent with the previously reported phenotype of the *wus* mutant (Hamada et al., 2000), suggesting that the loss of the AtENT3 function results in a decrease in the WUS activity and that AtENT3 could be involved in the implied uptake of root-borne tZR in the shoot apex that is necessary for its LOG-catalysed activation (Sakakibara, 2021). We provide additional support for this hypothesis by showing that *AtENT3* is expressed in the shoot apices of *A. thaliana* (together with *AtENT1*), that the *WUS* expression is down-regulated in *atent3* shoots, which can be partially reversed by treating the mutant plants with tZR, and that overexpression of *WUS* results in downregulation of *AtENT3* together with *AtLOG*s, and conversely, upregulation of *AtCKX7*, indicating negative feedback aimed to hinder the incoming CK signal (Figure 6 in the manuscript). Our findings advocate for further investigation of how AtENTs regulate SAM development and whether some of them could be responsible for CK riboside-specific transport.

Personal contribution: I performed some radio-accumulation assays, adapted the mathematical models, wrote Python scripts implementing the fitting of the models to the experimental data as well as scripts to evaluate the phenotypes of agar-grown plants via image processing, and performed molecular docking and molecular dynamic simulations. I contributed to writing the manuscript draft and designed the figures.

Comprehensive Model of Cell-to-Cell Cytokinin Transport Reveals A Specific Mode of Cytokinin Riboside Influx

Authors: Daniel Nedvěd[1,2], Martin Hudeček[3], Petr Klíma[1], Jozef Lacek[1], Karel Müller[1], Petr Hošek[1], Ján Šmeringai[4,5], Markéta Pernisová[4,5], Václav Motyka[1], Ondřej Plíhal[3*] & Klára Hoyerová[1*]

[1] Laboratory of Hormonal Regulations in Plants, Institute of Experimental Botany of the Czech Academy of Sciences, Rozvojová 263, 165 00, Prague, Czechia

[2] Department of Experimental Plant Biology, Faculty of Science, Charles University, Viničná 5, 128 44, Prague, Czechia

[3] Laboratory of Growth Regulators, Faculty of Science of Palacký University and Institute of Experimental Botany of the Czech Academy of Sciences, Šlechtitelů 27, CZ-78371 Olomouc, Czechia

[4] Laboratory of Functional Genomics and Proteomics, National Centre for Biomolecular Research, Faculty of Science, Masaryk University, Brno, Czechia

[5] Mendel Centre for Plant Genomics and Proteomics, Central European Institute of Technology, Masaryk University, Brno, Czechia

[*] Corresponding author

1 Abstract

Ribosylated forms of plant hormones cytokinins (CKs) are the dominant CK species translocated at long distances. Their particular roles in plant physiology imply the existence of a yet uncharacterized CK riboside-specific membrane transport system. In this work, we report significant differences in the kinetics of the membrane transport of CK nucleobases and ribosides and the overall affinity of membrane-bound carriers towards the two CK forms. We show that CK ribosides can inhibit the uptake of CK nucleobases in tobacco Bright Yellow 2 cell suspensions but not vice versa, confirming the existence of a membrane transport system that strictly recognizes CK ribosides.

We further characterize the membrane transport of CK nucleobases and ribosides mediated by AtENT3 (EQULIBRATIVE NUCLEOSIDE TRANSPORTER 3), showing its preference towards *trans*-zeatin riboside (tZR) over isopentenyl adenosine (iPR). With the molecular docking and molecular dynamics, we assess the interactions among the side chain of tZR and AtENT3 residues Tyr61 and Asp129, which are conserved in all AtENTs but not in the ENTs from non-plant species. Lastly, we show that *atent3* mutation affects shoot phenotype, demonstrating the impact of CK riboside membrane transport on shoot development.

Key words: cytokinin, cytokinin transport, cytokinin riboside, equilibrative nucleoside transporter, ENT3

2 List of Abbreviations

ABC	ATP-BINDING CASSETTE
ADFR	AutoDockFR software suite
ARR	ARABIDOPSIS RESPONSE REGULATOR
ANOVA	analysis of variance
At	mouse-ear cress (*Arabidopsis thaliana*)
AZG	AZA-GUANINE RESISTANT
BA	benzyladenine
BAR	benzyladenosine
Bt	cattle (*Bos taurus*)
BY-2	Bright Yellow 2
CCCP	carbonyl cyanide 3-chlorophenylhydrazone
CK	cytokinin
CKX	CYTOKININ DEHYDROGENASE
CMOS	complementary metal-oxide-semiconductor
Col-0	Columbia-0
cZ	*cis*-zeatin
DHZ	dihydrozeatin
DHZR	dihydrozeatin riboside
DiPy	dipyridamole
DMSO	dimethyl sulfoxide
Dr	zebrafish (*Danio rerio*)
ENT	EQULIBRATIVE NUCLEOSIDE TRANSPORTER
Hs	human (*Homo sapiens*)
iP	isopentenyl adenine
iPR	isopentenyl adenosine
LOG	LONELY GUY
MAD	median of absolute deviation
Mm	mouse (*Mus musculus*)
MS	Murashige-Skoog
NBTI	*S*-(4-nitrobenzyl)-6-thioinosine
NCBI	National Center for Biotechnology Information

Os	rice (*Oryza sativa*)
Pf	*Plasmodium falciparum*
PUP	PURINE PERMEASE
REL	relative expression level
Rn	rat (*Ratus norvegicus*)
SAM	shoot apical meristem
Sc	yeast (*Saccharomyces cerevisiae*)
SWEET	SUGAR WILL EVENTUALLY BE EXPORTED TRANSPORTER
TM	transmembrane helix
WUS	WUSCHEL
tZ	*trans*-zeatin
tZR	*trans*-zeatin riboside

3 Introduction

Cytokinins (CKs) are plant hormones that regulate a great variety of physiological processes, including cell cycle and proliferation (Miller et al., 1956; Schaller et al., 2014), growth and branching of both shoots and roots (Chang et al., 2015; Dello Ioio et al., 2012; Schaller et al., 2014; Skoog and Miller, 1957; Werner et al., 2001), chlorophyll retention and delay of senescence (Dobránszki and Mendler-Drienyovszki, 2014; Richmond and Lang, 1957; Talla et al., 2016) or differentiation of vascular elements (Bishopp et al., 2011; De Rybel et al., 2014; Mähönen et al., 2006).

As signalling molecules, CKs participate in communication between various parts of the plant. They are distributed among tissues and organs through the two vascular pathways - phloem and xylem - but the CK composition in each of them differs, and so presumably do their roles (Corbesier et al., 2003; Hirose et al., 2008; Osugi et al., 2017; Sakakibara, 2021). To reach their eventual destination, CKs have to pass through biological membranes. One possible meaning of membrane transport is simple diffusion, which is described by Fick's laws (Paul et al., 2014). Due to the hydrophobic character of the inner leaflets of the biological membrane, only small and non-polar molecules can cross the membrane this way. The required characterization applies to CK nucleobases, N^6-substituted derivatives of adenine, which are the biologically active CK form (Lomin et al., 2015). In contrast, CK ribosides, N^9-ribosylated conjugates of CK nucleobases and the dominant CK components found in the vasculature (Corbesier et al., 2003; Sakakibara, 2021), are bulky and polar, which implies that their diffusion would be inefficient (for more detailed comparison, see Nedvěd et al., 2021). CK nucleobases and ribosides are recognized by membrane-bound carriers, which significantly improves the kinetics of their membrane transport. These carriers belong to the families of PURINE PERMEASES (PUPs) (Hu et al., 2023; Qi and Xiong, 2013; Rong et al., 2024; Xiao et al., 2020, 2019; Zürcher et al., 2016), ATP-BINDING CASSETTES (ABCs) (Jamruszka et al., 2024; Jarzyniak et al., 2021; Kim et al., 2020; Ko et al., 2014; Yang et al., 2022; Zhang et al., 2014; Zhao et al., 2023, 2019), AZA-GUANINE RESISTANT

(AZG) (Tessi et al., 2023, 2020), SUGAR WILL EVENTUALLY BE EXPORTED TRANSPORTERS (SWEETs) (Radchuk et al., 2023), and EQUILIBRATIVE NUCLEOSIDE TRANSPORTERS (ENTs) (Girke et al., 2014; Hirose et al., 2008, 2005; Korobova et al., 2021; Sun et al., 2005).

Given that CK ribosides are the main form of CKs transported over long distances, the membrane transport of ribosylated CKs represents a link between the long-distance and cell-to-cell CK distribution. Unlike CK nucleobases, CK ribosides can travel from the root up to the shoot apex and regulate processes such as leaf emergency rate in response to nutrient availability, which likely requires involvement of CK riboside transporters (Davière and Achard, 2017; Landrein et al., 2018; Lopes et al., 2021; Osugi et al., 2017; Sakakibara, 2021).

The physiological importance of CK ribosides implies the existence of a CK riboside-specific system of membrane-bound carriers that are likely separated from the transport of CK nucleobases. Apparent candidates for these carriers are some members of the ENT family mentioned above. AtENT3, 6, 8 from mouse-ear cress (*Arabidopsis thaliana*, L.) (Hirose et al., 2008; Korobova et al., 2021; Sun et al., 2005) and OsENT2 from rice (*Oryza sativa*, L.) (Hirose et al., 2005) have been characterized as CK transporters although only OsENT2 has been shown to directly transport CKs across the biological membrane in a yeast model system.

In this work, we emphasize the importance of CK riboside transport by pin-pointing the different kinetics of CK nucleobase and riboside uptake in the BY-2 cell line (*Nicotiana tabacum*, L. cv Bright Yellow 2), a plant single-cell system (Nagata et al., 1992). Furthermore, we directly monitor AtENT3-mediated CK influx in BY-2, model interactions between AtENT3 and *trans*-zeatin riboside and demonstrate the involvement of AtENT3 in shoot development in *A. thaliana*.

4 Material and Methods

4.1 Plant Material

We maintained tobacco cell line BY-2 (*N. tabacum* L. cv Bright Yellow 2) in liquid Murashige and Skoog (MS) medium (30 g L^{-1} sucrose, 4.34 g L^{-1} MS salts, 100 mg L^{-1} myo-inositol, 1 mg L^{-1} thiamine, 0.2 mg L^{-1} 2,4-dichlorophenoxyacetic acid, 200 mg L^{-1} KH_2PO_4; pH = 5.8), in the dark, at 27 °C, under continuous shaking (150 rpm; orbital diameter 30 mm), and subcultured it every seven days. We cultured the *AtENT3*-expressing transgenic BY-2 cells and calli in the same medium supplemented with 100 mg mL^{-1} cefotaxime and 20 mg mL^{-1} hygromycin.

We grew *A. thaliana* ecotype Columbia 0 (Col-0) and *atent3* T-DNA insertion mutant, obtained from Nottingham Arabidopsis Stock Centre as N631585, on solid MS medium (2.17 g L^{-1} MS salts, 10 g L^{-1} agar; pH = 5.7) in Petri dishes and Klasmann TS-3 fine cultivation substrate (Klasmann-Deilmann GmbH, Germany) in 7.0×7.0×6.5 cm pots. We kept the seeds sown on solid MS medium in the darkness at 4 °C for three days and then cultivated them for eight days under long-day conditions (16 h light/8 h dark) at 20/22 ºC in the D-root system (Silva-Navas et al., 2015) using poly klima® climatic growth chambers (poly klima®, Germany). We randomly arranged the potted plants of different genotypes in transportable trays with a capacity of 20 pots (4×5 template) and grew them in cultivation chambers – phytotrons (CLF Plant Climatics, Germany) under long-day conditions at 21°C with a LED light intensity of 130 µM m^{-2} s^{-1} and 40-60% relative humidity. Unless stated otherwise, we obtained all chemicals and kits from Sigma–Aldrich Inc.

4.2 Transformation of BY-2 Cells

To construct the *XVE::AtENT3* inducible system, we amplified the 1939bp sequence of the *AtENT3* gene from genomic DNA using the forward and reverse *AtENT3* primers with attB1 and attB2 sites, respectively. The primer sequences are listed in Table S1. We cloned the amplified *AtENT3* gene flanked by attB sites into the pDONR207 vector using BP recombination. Subsequently, we transformed the *AtENT3* entry clone into the pMDC7 destination vector (Curtis and Grossniklaus, 2003) by LR recombination. We transformed BY-2 cells by co-cultivation with *Agrobacterium tumefaciens* strain GV2260 (An et al., 1985). We harvested transgenic lines after 4 weeks, cultured them on solid media with kanamycin, and tested for the presence of *AtENT3* via PCR.

4.3 Radio-Accumulation Assays

For the radio-accumulation assays, we used BY-2 cell suspensions two days after inoculation. We filtered away the liquid phase of the suspension, twice resuspended the cells in uptake buffer (20 mM 2-morpholin-4-ylethanesulfonic acid, 10 mM sucrose, 0.5 mM $CaSO_4$, pH = 5.7), and cultivated them in the dark for 45 and 90 minutes, respectively. The assay itself was initiated by applying a radio-labelled tracer into the cell suspension and terminated after 15-30 minutes. During the assay, we sampled 500 µL of the suspensions in regular intervals. For each sample, we filtered away the liquid phase and treated the cells with 500 µL of 96 % (v/v) ethanol for 30 minutes. Next, we added 4 mL of scintillation cocktail EcoLite(+)™ (MP Biomedicals, CA, USA) to each sample and mixed the samples for 20 min using orbital shaker KS 130 (IKA, Germany) at 480 rpm. The radioactivity in samples was measured using Tri-Carb 2900TR scintillation counter (PerkinElmer, CT, USA).

4.4 Mathematical Modelling of Transport Kinetics

To describe the kinetics of the CK membrane transport in BY-2 cell culture, we adapted the model published by Hošek et al. (2012). We introduced first-order rate constants I and E to characterize the influx and efflux of a radio-labelled tracer, respectively. To account for the tracer adsorption to the cell surfaces, we included a factor K. To estimate the values of I, E, and K, we fitted experimental data from radio-accumulation assays with equation:

$$c_I(t) = \frac{Ic_0}{fI+E}\left[1-e^{-t(fI+E)}\right](1-fK)+Kc_0, \quad (1)$$

where t and c_I are matrices of time points and measured intracellular concentrations, respectively (with each row composed of data points from one assay and different rows representing different assays), f is a factor correcting different sizes of the intra- and extracellular spaces, and c_0 is the initial extracellular concentration of the tracer. When comparing the effects of the *AtENT3* expression or a chemical treatment on the tracer influx, we constrained the model to keep common values of E and K for all assays in the dataset. For assays involving chemical treatment during the tracer accumulation (as opposed to the treatment before the tracer addition), we used an expanded form of equation (1):

$$c_I(t)=\begin{cases}\dfrac{Ic_0}{fI+E}\left[1-e^{-t(fI+E)}\right](1-fK)+Kc_0 & \text{if} \quad t\le t' \\ \left\{\dfrac{I'c_0}{fI'+E}\left[1-e^{(t'-t)(fI'+E)}\right]+\dfrac{Ic_0}{fI+E}\left[1-e^{-t'(fI+E)}\right]e^{(t'-t)(fI'+E)}\right\}(1-fK)+Kc_0 & \text{if} \quad t>t'\end{cases}, \quad (2)$$

where t' is the treatment time and I' is the influx rate constant after the treatment. For step-by-step derivations of equations (1) and (2), see the Supplementary methods.

To evaluate the affinity of the membrane transport system towards a tracer or the inhibition effect of a competitor, we adapted a saturation model published by Delbarre et al. (1996):

$$I(c_K)=\frac{v_{lim}}{IC_{50}+c_K}+D, \quad (3)$$

where c_K is the concentration of a competitor (either the non-labelled counterpart of the tracer or another chemical substance), v_{lim} is the limit transport rate, IC_{50} is a c_K value for which the transport rate equals to half of v_{lim}, and D is the rate constant of the influx that remains even when the transport system is fully saturated.

All fits were performed using the "curve_fit" method of the SciPy Python library (Virtanen et al., 2020) with arguments "ftol=1e-15" and "xtol=1e-15". The initial guesses were 10^{-3} for I and E, 0 for K, and 1 for v_{lim}, IC_{50} and D. All parameters were restricted to be non-negative. To visualize tracer accumulation in the cells, we used equation (1) with the optimized values of I and E, while setting K to 0.

4.5 Molecular Docking

For molecular docking, we downloaded AlphaFold-predicted structural models (Jumper et al., 2021) from the AlphaFold Protein Structure Database (https://alphafold.ebi.ac.uk/). We prepared the protein and ligand files and performed the docking procedure using the AutoDockFR (ADFR) software suite (Ravindranath et al., 2015; Zhao et al., 2006). The ligands were initially placed in the central cavity of the protein. The centre and dimension of the affinity grids were determined automatically by the ADFR program "agfr". Each docking consisted of 50 runs and each run performed 50 million evaluations. Residues Gln133, Arg312, Leu397, and Asp129 of AtENT3 were set flexible. To visualize the protein-ligand structures, we used ChimeraX (Goddard et al., 2018), PyMol (Schrödinger, LLC, 2015), and LigPlot+ software (Laskowski and Swindells, 2011). We used MAFFT with the automatic algorithm selection (Katoh and Standley, 2013) to align the ENT sequences and JalView for alignment visualization (Waterhouse et al., 2009).

4.6 Molecular Dynamics

For the molecular dynamic simulations, we built a rhombic dodecahedron-shaped simulation box consisting of the protein-ligand complex in 150 mM aqueous NaCl solution and additional ions to neutralize the electric charge. To prevent the complex from interacting with its own image, we set its distance from the box edges to 1.0 nm. We ran energy minimization using the steepest descent algorithm, a 100 ps-long simulation under the *NVT* ensemble (constant particle amount, volume, and temperature), a 100 ps-long simulation under the *NPT* ensemble (constant particle amount, pressure, and temperature), and finally 100 or 200 ns-long unbiased simulation. In the *NVT* and

NPT runs, we applied constraints with force constants of 1000 kJ mol^{-1} nm^2 to all non-hydrogen atoms. For all runs, we used the CHARMM36 force field (Best et al., 2012). For simulation parameters, see Table S2. We used the GROMACS software suite (Abraham et al., 2024, 2015; Páll et al., 2015) to parametrize the protein, build the simulation box, carry out the simulations, perform the cluster analysis, and calculate the distributions of distances and angles over the trajectories. Through GROMACS, we also used particle mesh Ewald method to evaluate long-range interactions (Essmann et al., 1995), LINCS algorithm to solve constraints (Hess, 2008), and SETTLE algorithm to treat water molecules (Miyamoto and Kollman, 1992). To parametrize the ligand, we used CGenFF program (Vanommeslaeghe et al., 2012; Vanommeslaeghe and MacKerell, 2012). To calculate fractional occupancies of the system by water molecules, we used VMD software (Humphrey et al., 1996).

4.7 Plant Phenotyping and Imaging

For phenotyping of 8 day-old *A. thaliana* plants grown on agar, we isolated their shoots, placed these shoots on Petri dishes and scanned them from top view using Epson Perfection V700 Photo (Epson, Japan). To image the potted plants, we used the PlantScreen™ Compact System (PSI, Czechia) equipped with PSI DUAL camera containing two 12.36-megapixel complementary metal-oxide-semiconductor (CMOS) sensors: a colour Sony IMX253LQR-C sensor for RGB structural imaging and a monochromatic Sony IMX253LLR-C for chlorophyll fluorescence measurement (Sony, Japan). For the fluorescence measurement, we used Quenching analysis protocol. Raw data were automatically processed using the PlantScreen™ Analyzer software (PSI). The imaging was performed according to a previously published protocol (Šmeringai et al., 2023).

4.8 Image Processing

To process images of agar-grown plants, we transformed the images of isolated plant shoots from the RGB to L*a*b* space and segmented the shoots by applying the thresholds $a^* <= -9.5$, $b^* >= -9.5$, and $L^* >= 18.5$, based on estimates obtained by multi-Otsu method (Liao et al., 2001). In the binary mask, we removed all objects smaller than 2048 pixels, performed morphological closing using a disk-shaped footprint with a radius of 8 pixels, and then removed all objects smaller than 8192 pixels. Finally, we measured the areas of all remaining objects in the image. To implement the techniques listed above, we used Python scikit-image library (van der Walt et al., 2014). We processed images of potted plants according to Šmeringai et al. (2023). For miscellaneous image manipulations, we used the GNU Image Manipulation Program (The GIMP Team, 2024).

4.9 Reverse Transcription Quantitative PCR

We isolated total RNA isolated from plant shoots using the RNeasy Plant Mini kit (Qiagen, Germany) and treated with DNA-Free kit (Thermo Fischer Scientific, MA, USA). We evaluated the purity, concentration, and integrity of RNA on 0.8% agarose gels (v/w) and by the RNA Nano 6000 Assay Kit using Bioanalyzer instrument (Agilent Technologies, CA, USA). For reverse transcription of approximately 1 mg of the DNAse-treated RNA, we used M-MLV Reverse Transcriptase, RNase H(-), Point Mutant (Promega, WI, USA). We performed the quantitative PCR using GoTaq qPCR Master Mix (Promega, WI, USA) at the annealing temperature of 58 °C on LightCycler480 instrument (Roche, Switzerland). PCR efficiency was estimated using serial dilution of template cDNA. We calculated the relative expression level, *REL*, as follows:

$$REL = \frac{\sqrt{2^{CP_{R1}+CP_{R2}}}}{2^{CP}}, \quad (4)$$

where CP_{R1} and CP_{R2} are the crossing points of the reference gene 1 and 2, respectively, and CP is the crossing point of the target gene. We used *A. thaliana* elongation factor 1a (AtEF1a) and actin 2 (AtACT2) as reference genes. We verified positive transcript levels and the quality of PCR by the melting curve analysis. The primer sequences are listed in Table S1.

5 Results

5.1 Transport of Cytokinin Ribosides in BY-2 Cells Occurs with Kinetics Distinct from Cytokinin Nucleobases and Depends on Proton Gradient

To find out whether the membrane transport kinetics of ribosylated CKs differ from the kinetics of CK nucleobases, the biologically active CK form, we measured the uptake of various radio-labelled CK tracers in tobacco Bright Yellow 2 (BY-2) cell cultures (Nagata et al., 1992), a model plant single-cell system. The radio-labelled tracers comprised four CK nucleobases: [3H]-*trans*-zeatin (tZ), [3H]-dihydrozeatin (DHZ), [3H]-isopentenyl adenine (iP), [3H]-benzyladenine (BA), and four CK ribosides: [3H]-*trans*-zeatin riboside (tZR), [3H]-dihydrozeatin riboside (DHZR), [3H]-isopentenyl adenosine (iPR), and [3H]-benzyladenosine (BAR). With this selection, we also included CKs with diverse characters of their side chains (N^9-bound moieties), namely those with unsaturated hydroxylated chains (tZ, tZR), saturated hydroxylated chains (DHZ, DHZR), unsaturated aliphatic chains (iP, iPR), and aromatic chains (BA, BAR).

To obtain comparable kinetic parameters for each tracer, we fitted the transport model given by equation (1) into the dataset of sampling time points and measured the radioactivities corresponding to the intracellular concentrations of accumulated CK tracers. We used the influx rate obtained by modelling, *I*, to compare the uptake kinetics of different CK tracers. Comparing the median values of *I* obtained for tZ (17.86×10^{-3} s^{-1}), DHZ (14.94×10^{-3} s^{-1}), and iP (11.58×10^{-3} s^{-1}) with the median *I* values obtained for tZR (3.45×10^{-3} s^{-1}), DHZR (2.38×10^{-3} s^{-1}), and iPR (5.44×10^{-3} s^{-1}) shows that BY-2 cells accumulate CK nucleobases with non-aromatic side chains more readily than their respective ribosides. Regarding the side chain composition, the differences in transport among tZ-type, DHZ-type, and iP-type CKs are less pronounced than the differences between CK nucleobases and ribosides. The median values of *I* obtained for BA (9.14×10^{-3} s^{-1}) and BAR (16.22×10^{-3}) show a difference between the uptake of the nucleobase and the riboside as well, but in this case, the more readily transported form is the riboside. The distributions of *I* values and the accumulation trends modelled for each assay are depicted in Figure 1. For the complete list of kinetic parameters and their statistical analysis, see Table S3 and Table S4, respectively.

To confirm that the observed uptake of CK nucleobases and ribosides occurs by carrier-mediated transport, we performed a series of assays in which we accumulated [3H]-tZ, [3H]-tZR, [3H]-iP or [3H]-iPR together with their non-labelled counterparts (so-called competitors) in concentrations of 0, 2 nM, 20 nM, 200 nM, 2 µM, and 20 µM. Each dataset, consisting of experiments performed with one tracer and all concentrations of the corresponding non-labelled competitor, was fitted with the constrained variant of equation (1), i.e. with single values of *E* and *K* for the whole dataset. The uptake of CK nucleobases and ribosides is subject to dose-dependent inhibition by their non-

labelled variant, as expected of the membrane-bound carriers becoming saturated (Figure 2A-D). To evaluate this inhibition effect numerically, we fitted the *I* parameter values obtained from the assays with competitors using the saturation model given by equation (3) (Delbarre et al., 1996). The estimated IC_{50} values obtained for tZ (112.21 nM), tZR (2.33 µM), iP (27.25 nM), and iPR (2.65 µM) show that CK nucleobases are transported with slightly higher affinity than the corresponding ribosides, which further indicates the distinct transport properties of the two CK forms (Figure 2E-H). For the complete list of kinetic parameters, see Table S5.

To assess the thermodynamic aspect of the uptake of tZ, tZR, iP, and iPR in the BY-2 cells, we performed a series of accumulation assays in suspensions treated with 50 µM protonophore carbonyl cyanide 3-chlorophenylhydrazone (CCCP) in dimethyl sulfoxide (DMSO). CCCP uncouples electron transfer from oxidative phosphorylation (Cavari et al., 1967; Cunarro and Weiner, 1975; Heytler, 1963), thus inhibiting proton gradient-dependent transport processes (Alexander et al., 2018; Culos and Watanabe, 1983; Stoffer-Bittner et al., 2018). We performed the same assays using cells treated with the corresponding amount of DMSO alone (mock treatment) as control. We fitted all data with equation (1) to obtain *I* values. The CCCP treatment decreased the medians of *I* (in comparison with the mock treatment) for all four tracers: from 24.24×10^{-3} to 8.89×10^{-3} s^{-1} for tZ, from 7.78×10^{-3} to 0.91×10^{-3} s^{-1} for tZR, from 9.89×10^{-3} to 1.46×10^{-3} for iP, and from 11.33×10^{-3} to 1.86×10^{-3} s^{-1} for iPR (Figure 2I-L), indicating that the uptake of both CK nucleobases and ribosides at least partially occurs in a proton gradient-dependent manner. For the complete list of kinetic parameters and their statistical analysis, see Table S6 and Table S7, respectively. To observe the immediate response of the CK influx to the uncoupling of the proton gradient, we performed another set of assays in which we treated the cells with 50 µM CCCP in DMSO seven minutes after the onset of the accumulation (i.e. after adding the tracer). We fitted the measured data with equation (2) to visualize the response (for the estimated kinetic parameters, see Table S8). The fits show that after the treatment, the intracellular concentrations of CK nucleobases start to decrease, while the concentrations of CK ribosides stop increasing and remain constant (Figure 2I-L). This trend could indicate the presence of CCCP-resistant exporters of CK nucleobases.

5.2 BY-2 Cells Possess a Riboside-Specific Transport System Not Recognizing Cytokinin Nucleobases as Substrates

The different affinities of the BY-2 membrane-bound carriers towards CK nucleobases and ribosides (Figure 2E-H) imply either that both CK types are recognized by the same set of carriers (with the nucleobases being slightly preferred) or that there are two sets of carrier, one for nucleobases and one for ribosides, that function independently of one another. To see which of these models characterizes the CK transport in BY-2 cells better, we paired nucleobase tracers with riboside competitors and vice versa (i.e. [3H]-tZ with tZR, [3H]-tZR with tZ, [3H]-iP with iPR, and [3H]-iPR with iP) and repeated the radio-accumulation assays with increasing concentrations of non-labelled CKs. We fitted the experimental data with equation (1) to assess kinetic parameters for each assay (Figure 3A-D) and the obtained values of *I* with equation (3) to estimate the IC_{50} for each competitor (Figure 3E-H). The estimated IC_{50} values are 18.77 µM ([3H]-tZ vs tZR), 90.82 µM ([3H]-tZR vs tZ), and 1.00 µM ([3H]-iP vs iPR). No saturation occurs for the [3H]-iPR vs iP variant (i.e. IC_{50} diverges towards infinity). For the complete list of kinetic parameters, see Table S5. These results show that the inhibition of the CK nucleobase uptake by CK ribosides is

significantly weaker than the inhibition by non-labelled nucleobases and vice versa, supporting the model of two independent carrier sets.

To confirm this trend, we tested the inhibitory effect of more CK- and adenine-based competitors (adenine, tZ, iP, BA, DHZ, kinetin, adenosine, tZR, iPR, BAR, and DHZR) on the uptake of [3H]-tZ, [3H]-tZR, [3H]-iP, [3H]-iPR, [3H]-BA, and [3H]-BAR. The concentration of all competitors was 20 μM. We fitted the measured data with the constrained variant of equation (1) and compared the median values of *I*. The uptake of [3H]-tZ and [3H]-BA decreases (two to four times) in the presence of all tested nucleobases, as well as tZR, adenosine, and iPR ([3H]-BAR only), whereas other tested ribosides cause mild to none uptake inhibition. The uptake of [3H]-iP is about three times reduced by its non-labelled variant but only mildly reduced by other tested compounds. The uptake of all three labelled ribosides is efficiently inhibited by all tested ribosides with a striking exception of adenosine and only mildly inhibited by tested nucleobases (Figure 3I; for the estimated kinetic parameters, see Table S9). The results presented so far indicate the existence of at least two systems mediating the CK membrane transport - one can recognize both CK nucleosides and ribosides (with a slight preference towards the former), while the other is strictly riboside-specific.

5.3 AtENT3 Transport Cytokinin Nucleobases and Ribosides, Preferring *trans*-Zeatin Riboside over Isopentenyl Adenosine

To see how our previous conclusions about the CK membrane transport as a whole apply to individual membrane-bound carriers, we decided to proceed with the expression of a previously characterized transporter of CK ribosides in BY-2 cells and measure its contribution to the uptake of tZ, iP, tZR, and iPR to assess its specificity. We have focused on members of the ENT family, as some of them have been linked to the transport of CK ribosides (Girke et al., 2014).

To determine whether tobacco ENTs could be responsible for the CK uptake in BY-2 cells, we searched for expression of *ENT* genes in a previously published BY-2 transcriptome (Müller et al., 2021). All tobacco ENTs listed in the UniProtKB database (The UniProt Consortium, 2023) are homologs of AtENT1, 3 or 8. Of these, only the homologs of *AtENT1* and *3* genes are expressed in BY-2 (Figure 4A; for numerical values, see Table S10), implying that measurements performed on AtENT1 or 3 may reflect the transport trends described above. We eventually decided to further work with AtENT3, given the previous reports on its effects on the CK homeostasis and plant sensitivity to exogenously applied CKs (Korobova et al., 2021; Sun et al., 2005).

To directly monitor the transport activity of AtENT3 towards CKs, we introduced the estradiol-inducible *XVE*::*AtENT3* gene construct to BY-2 cells. Using these transformed cells, we performed radio-accumulation assays with [3H]-tZ, [3H]-tZR, [3H]-iP, and [3H]-iPR as tracers. We performed each assay in non-induced (control) and induced cells to assess the contribution of AtENT3 to the overall CK uptake. The induced cells were treated with 1 μM estradiol in DMSO and the control cells with the corresponding amount of DMSO. The measured data were fitted with the constrained variant of equation (1) to estimate *I* values. The medians of *I* increased for all four tracers: from 24.56×10^{-3} to 50.03×10^{-3} s^{-1} for tZ, from 10.16×10^{-3} to 18.82×10^{-3} s^{-1} for tZR, from 21.34×10^{-3} to 44.27×10^{-3} s^{-1} for iP, and from 12.19×10^{-3} to 16.69×10^{-3} for iPR (Figure 4B-C). For the complete list of kinetic parameters and their statistical analysis, see Table S11 and Table S12, respectively. These results show that AtENT3 transports nucleobases and ribosides, implying that AtENT3 is likely not a part of the previously described CK riboside-specific system and that strict carriers of ribosylated

CKs remain to be identified. Focusing on the results obtained for the accumulation of tZR and iPR, we saw that AtENT3 boosts the influx rate of the former more than the latter. The influx rates of tZ and iP are boosted similarly, suggesting that CK nucleobases are transported with a different mechanism, which does not allow discrimination based on the character of the CK N^6-bound side chain.

To further confirm that AtENT3 is responsible for the increase in CK riboside uptake in the induced cells, we examined how AtENT3-mediated uptake of tZR changes after application of CCCP and two inhibitors of nucleoside uptake, *S*-(4-nitrobenzyl)-6-thioinosine (NBTI) (Karbanova et al., 2020; Ward et al., 2000; Wright and Lee, 2019) and dipyridamole (DiPy) (Newell et al., 1986; Woffendin and Plagemann, 1987). NBTI and DiPy inhibit the uptake of adenosine by AtENTs (Li et al., 2003; Möhlmann et al., 2001; Wormit et al., 2004). To assess the effects of the inhibitors, we performed accumulation assays with [3H]-tZR as a substrate, in non-induced (control) or induced cell lines and with or without CCCP, NBTI or DiPy. All inhibitor we dissolved in DMSO and used at the concentration of 10 μM. For mock treatment, we used the corresponding amount of DMSO alone. We fitted the measured data with the constrained variant of equation (1). In mock-treated cells, the uptake of tZR significantly increases (from 7.56×10^{-3} to 10.87×10^{-3} s^{-1}) due to the induction of *AtENT3* expression. In CCCP-treated cells, the overall tZR uptake drops, but there is still a difference between control and induced cells (the median of *I* increases from 0.85×10^{-3} to 2.05×10^{-3} s^{-1}). In NBTI-treated cells, there is no significant difference between the control and induced cells, indicating strong inhibition of AtENT3 by NBTI. Finally, in DiPy-treated cells, the median of *I* mildly increases from 7.73×10^{-3} to 9.39×10^{-3} s^{-1}, suggesting partial inhibition of AtENT3 (Figure 4D). For the complete list of kinetic parameters and their statistical analysis, see Table S13 and Table S14, respectively. The results of the competition assays show that AtENT3 is inhibited by NBTI and (to a lesser extent) DiPy, two typical inhibitors of adenosine uptake. However, it is resistant to CCCP, suggesting that AtENT3 mediates facilitated diffusion rather than active transport. The resistance of AtENT3 towards CCCP could also be related to the milder response of CK riboside uptake to the CCCP treatment (compared to CK nucleobases) in wild-type BY-2 cells (Figure 2I-L).

5.4 A Computational Approach Reveals A Non-Conserved tZR-Interacting Motif in AtENT Sequences

To assess the molecular interactions responsible for CK binding to AtENT3, we performed molecular docking of tZR into a predicted structure of AtENT3 obtained with AlphaFold (Jumper et al., 2021). The best-docked pose of tZR is located in a central cavity outlined by transmembrane helices (TMs) 1, 2, 4, 5, 7, 8, 10, and 11. The ENT3 residues interacting with the docked pose of tZR comprise Leu31, Trp34, Asn35, Tyr61, Gln62, Asp129, Gln133, Tyr272, Leu276, Tyr304, Asn305, Asp308, Lys312, Asn365, Leu396, Leu397, and Ile400 (Figure 5A). This pose roughly corresponds to the sites occupied by the adenosyl moiety of NBTI in human HsENT1 (Wright and Lee, 2019) (PDB code: 6OB6) and by inosine in PfENT1 from the parasite *Plasmodium falciparum* (Wang et al., 2023) (PDB code: 7WN1; see Figure 5C). Moreover, the CK-interacting residues Leu31, Trp34, Gln133, Tyr304, Asp308, and Lys312 correspond to residues reported to bind respective ligands in 6OB6 and 7WN1. We also performed docking of iPR, tZ, and iP. For all best-docked poses, see Figure S1-4.

To assess the conservation of the CK-binding residues among the known members of the ENT

family, we aligned sequences of the reviewed ENT proteins present in the UniProtKB database (The UniProt Consortium, 2023). These proteins are AtENT1-8, BtENT3 from cattle, DrENT4 from zebrafish, HsENT1-4, MmENT1-4 from mouse, PfENT1, RnENT1-3 from rat, and ScFUN26 from yeast. The alignment shows that the residues interacting with the ribosyl moiety of tZR are generally more conserved than those interacting with the heterocycle and the side chain (Figure 5B, D), suggesting that the binding cavities of different ENTs are all shaped to recognize nucleosides but with different specificities towards various aglycones.

To estimate the stability of predicted AtENT3-tZR interactions, we performed molecular dynamic simulations with a system consisting of the AtENT3-tZR complex in water and 150 mM NaCl. To equilibrate the system, we ran a single 200 ns-long simulation. Through cluster analysis of the 200 ns-long trajectory, we obtained a representative system conformation (corresponding to the frame at t = 177.72 ns). In this conformation, we observed interactions between the side-chain hydroxyl group of tZR and residues Trp34, Tyr61, and Asp129, mediated by a water molecule (Figure 5E). Tyr61 and Asp129 are conserved among AtENTs but not among ENTs from other species listed in Figure 5B, suggesting they might have a unique role in binding CK substrates.

Next, we ran three parallel 100 ns-long simulations, starting from the system conformation obtained through the cluster analysis. To confirm that a water bridge contributes to the stabilization the side-chain hydroxyl of tZR, we calculated the fractional occupancies of water molecules in the system during the simulations. In the space surrounded by the side-chain hydroxyl of tZR and the side chains of Tyr61 and Asp129, the fractional occupancy of water reaches a local maximum of approximately 90%, indicating that this space is occupied by water for the most simulation time and thus supporting the involvement of the water bridge in maintaining the interactions between AtENT3 and the tZR side chain (Figure 5F). To assess the stability of interactions among tZR, Trp34, Tyr61, and Asp129, we calculated the distributions of the distances between the interacting atom pairs (those visualized in Figure 5E) during the three 100 ns-long simulations. These distributions show that the distance between the hydrogen atom of the side-chain hydroxyl of tZR (H5) and the carboxylic oxygen of Asp129 (OD1), as well as the distance between H5 atom of tZR and the phenolic oxygen of Tyr61 (OH), oscillate around 4 Å. Assuming that the donor-acceptor distance in a typical hydrogen bond is less than 3.5 Å (Lemkul, 2019), the distribution of H5-OD1 and H5-OH distances supports the previous conclusion that the tZR-Asp129 and tZR-Tyr61 interactions are mediated by a water bridge, as the most likely distances are longer than the 3.5 Å threshold. The distribution of distances between the OD1 atom of Asp129 and the phenolic hydrogen (HH) of Tyr61 shows a sharp peak around 2 Å, indicating a stable hydrogen bond between these two atoms. This conclusion is also supported by the distribution of sizes of the angle formed by OD1, HH, and OH atoms, where the average angles are about 160°, i.e. close to a straight line (Figure S5). The distribution of distances between the oxygen of the side-chain hydroxyl of tZR (O5) and the nitrogen-bound hydrogen of Trp34 (HE1), ranging from 2 to 5 Å, does not show any significant peak, indicating that there are no stable interactions (Figure 5G). Distributions of distances involving the OD1 atom of Asp129 show a secondary peak, which is caused by the flipping of the Asp129 carboxyl group during the simulations. Altogether, the results from the docking and molecular dynamics show that Tyr61 and Asp129 of AtENT3 can stabilize AtENT3-tZR binding via interactions with the side-chain hydroxyl group of tZR, which might explain the preference of AtENT3 towards tZR over iPR (Figure 4C).

5.5 Loss of the AtENT3 Function Affects Shoot Development and *WUSCHEL* Expression in *A. thaliana*

To assess the physiological significance of the membrane transport of ribosylated CKs, we examined the phenotype of *A. thaliana* plants mutated in *atent3*, whose transport activity we have already characterized in this work. Given the previous report on the effects of *atent3* mutation on the primary root length (Korobova et al., 2021), we have focused on the plant shoots. We imaged shoots of 8-day-old wild-type *A. thaliana* plants and *anent3* mutants grown on the agar and 8, 11, and 15-day-old plants (wild type and *atent3*) grown on the cultivation substrate in pots. We processed the obtained image to measure the area of plant shoots from top view. The shoots of *atent3* plants are larger than the corresponding control in all cases (Figure 6A-B). For all measured parameters, see Table S15-16. For the statistical analysis of measured areas, see Table S17.

The effect of the *atent3* mutation on the shoot development might be related to the previously reported requirement of tZR for proper modulation of physiological responses in the shoot apex (Landrein et al., 2018; Lopes et al., 2021), which implies the presence of CK riboside-recognizing transporters responsible for supplying root-borne tZR to the the apex (Sakakibara, 2021). In the following experiments, we therefore investigated the possibility that one of these tZR-providing transporters is AtENT3.

To determine whether *AtENT* genes are expressed in the apex area, we examined transcriptomic data obtained from isolated apices or apex-enriched tissues of *A. thaliana* deposited to the GEO database under accessions of GSM4278593-95 (Yang et al., 2021), GSM2104466 and 71 (Mandel et al., 2016), and GSM7764635-36 (Incarbone et al., 2023). From these data, we extracted expression levels of *AtENT1-8*. In all samples, *AtENT1* and *3* are abundantly expressed, sometimes followed by *AtENT7* and *8* (Figure 6C), supporting the idea that AtENT3 supplies the shoot apex with root-borne tZR.

As it was previously shown that increased CK supply leads to upregulation of *WUSCHEL* (*WUS*) expression in the shoot apical meristem (SAM) (Landrein et al., 2018), we further examined a possible relationship between the expression of *WUS* and *AtENT3*. We examined transcriptional data under accession GSE122610, where the authors evaluate the effects of ectopic *WUS* overexpression in 5-day-old *A. thaliana* seedlings (Ma et al., 2019). In this dataset, we searched for genes related to CK metabolism, transport or signalling. Overexpression of *WUS* leads to downregulation of the transporters *AtENT3* and *4*, CK-activating genes from the LONELY GUY (LOG) family, *AtLOG5*, *6* and *8*, and CK-responsive genes from the ARABIDOPSIS RESPONSE REGULATOR (ARR) family, *ARR7* and *11*. Conversely, *ARR4*, *9*, and the CK-degrading CYTOKININ DEHYDROGENASE 7 (*AtCKX7*) are upregulated (Figure 6D).

Having seen that overexpression of *WUS* can affect the expression of *AtENT3*, we next examined the expression of *WUS* in the shoots of *atent3* mutant via quantitative PCR. To determine whether potential changes in *WUS* expression are due to a lack of ribosylated CKs in the shoot apex, we treated half of the wild-type plants and *atent3* mutants with 1 µM tZR in water and the remaining plants with the corresponding amount of water alone. The expression of *WUS* is lower in the water-treated *atent3* mutant than in the corresponding wild type plants. Treating the plants with tZR partially reduces this difference in *WUS* expression (Figure 6E). For the relative expression levels of *WUS* and their statistical analysis, see Table S18 and Table S19, respectively. Both these findings support the hypothesis that AtENT3 provides the apex with root-borne tZR. Based on our findings,

we have proposed an updated working scheme explaining the role of root-borne tZR in the shoot apex. This scheme, depicted in Figure 6F and further discussed below, will be the pivot focus of our future research.

6 Discussion

Ribosylated CKs are the dominant CK form transported through the xylem and phloem (Corbesier et al., 2003; Sakakibara, 2021; Takei et al., 2001) Their effective distribution between the cellular and extracellular compartments, mediated by membrane-bound carriers, is thus a crucial aspect of communication among different tissues and organs. In this work, we address particular differences between the transport kinetics of CK nucleobases and ribosides via radio-accumulation assays in BY-2 cell culture, a plant model system. We show that the uptake kinetics of CKs with isoprenoid chains differ significantly more between nucleobases and ribosides than among compounds with different side chain compositions, highlighting the presence of CK riboside-specific transporters (Figure 1). Conversely, the uptake kinetics of aromatic CKs (BA and BAR) do not differ, suggesting that aromatic CKs are recognized by a different transport system. The specific transport properties of BA and BAR evoke inquiries about the roles of aromatic CKs in plants and the means of maintaining their homeostasis in general.

We further show that the CK uptake occurs via at least two different systems of membrane-bound carriers. One of these systems exclusively recognizes ribosylated substrates. The other one primarily transports nucleobases but not as strictly as the first system. We derive this conclusion from the general trend of our data from accumulation assays, which shows that the inhibition of the CK riboside uptake by nucleobases is weaker than when the roles are reversed (Figure 3). The existence of riboside-specific transporters hypothetically allows plants to regulate the distribution of ribosylated CKs in a targeted manner. Since ribosylated CKs are primarily transported over long distances, the CK riboside-specific carriers could be found within or close to vascular tissues. This particular expression pattern could serve as a clue in the search for other CK riboside transporters in future research.

We used AtENT3 as a representative membrane-bound carrier of CK ribosides to further characterize the CK riboside transport. Our measurements of CK uptake in the *AtENT3*-expressing BY-2 cells showed that AtENT3 transports CK nucleobases and ribosides alike and thus does not belong to the CK riboside-specific carriers (Figure 4). Similar measurements focused on the ability of other AtENTs to distinguish between CK nucleobases and ribosides would allow us to tell whether this trend observed for AtENT3 applies to all AtENTs or whether the family includes other members, that may be specific for CK ribosides. The docked poses of tZ and iP (Figure S1 and S3) show that both nucleobases interact with the Gln62 residue of AtENT3 via a hydrogen bond. Gln62 is conserved among AtENT2-7, while in AtENT1 and 8, the corresponding position is occupied by methionine, an amino acid with an aliphatic side chain that is unlikely to form the mentioned hydrogen bond (Figure 5B). We propose that due to this difference in the amino acid composition, AtENT1 and 8 will not recognize CK nucleobases as substrates, which will be interesting to prove or disprove in future experiments.

The character of the position corresponding to Gln62 in AtENT3 also varies among other ENTs listed in Figure 5B. Notably, this position differs between HsENT1 (methionine) and HsENT2 (glutamine), cobsistent with their previously reported affinities towards nucleobases and

nucleosides. HsENT1 favours uridine, a riboside, over nucleobases adenine, thymine, and hypoxanthine, whereas HsENT2 transports the nucleobases with affinities equal to that towards uridine or greater (Yao et al., 2011). The differential affinity towards nucleobase substrates between HsENT1 and 2 supports the hypothesis that the variable nature of the position corresponding to Gln62 in AtENT3 can affect the substrate specificities of ENTs. Another example is, PfENT1, which has the position Gln62 position occupied by glutamate and transports inosine, a riboside, and hypoxanthine with comparable affinities (Wang et al., 2023).

We have further observed that AtENT3 prefers tZR over iPR (Figure 4). The two substrates differ in the hydroxylation status of their side chains, as tZR is hydroxylated and iPR is not. Through the molecular docking of tZR in the predicted structural model of AtENT3 and subsequent molecular dynamic simulations of the AtENT3-tZR complex, we have identified stable interactions among residues Tyr61, Asp129 and the side-chain hydroxyl group of tZR. These interactions could explain the preference of AtENT3 for tZR. Both Tyr61 and Asp129 are conserved among all AtENTs but not among animal and other ENTs (Figure 5B), suggesting that their presence allows preferential binding of tZ-derived CKs by AtENTs. To investigate these indications further, it would be worth comparing affinities towards tZR and iPR for other AtENTs. as the preference towards the former should be conserved alongside Tyr61 and Asp129 residues. Another option to test the involvement of Tyr61 and Asp129 residues in stabilizing tZR is to measure the transport of tZR mediated by non-plant ENTs.

In the last part of this work, we have addressed the physiological impact of the AtENT3-mediated transport in *A. thaliana* shoots. The membrane transport of CK ribosides has been deemed a necessary step for the activation of tZR coming via xylem from roots up to the shoot apex and subsequent stimulation of *WUS* expression (Davière and Achard, 2017; Landrein et al., 2018; Lopes et al., 2021; Osugi et al., 2017; Sakakibara, 2021). This fact prompted us to investigate whether a change in *AtENT3* expression affects shoot development. Combining publicly available transcriptomic data with our quantitative PCR measurements has revealed that overexpression of *WUS* downregulates expression of *AtENT3* and that the *atent3* mutation downregulates expression of *WUS*. The shoots of *atent3* plants show larger cotyledons than the wild-type plants, which resembles the previously reported phenotype of *wus* mutant seedlings (Hamada et al., 2000; Laux et al., 1996). Nevertheless, this phenotype can also stem from the reduced retention of tZR in *atent3* roots (Korobova et al., 2021).

Other genes affected by *WUS* oversexpression include downregulated *ENT4*, *LOG5*, *LOG6*, *LOG8* (to a lesser extent also *ENT1* and *LOG1*) and upregulated *CKX7*, indicating that the overexpressed *WUS* tends to inhibit CK signalling at several levels as negative feedback. This feedback likely occurs via activation of type-A ARRs, which are typically characterized as CK-repressive (To et al., 2007, 2004). We have seen that overexpression of *WUS* upregulates type-A *ARR4* and *ARR9*. On the other hand, type-A *ARR7* is downregulated, suggesting that ARR7 does not participate in attenuating the incoming CK signal but rather in further regulation of the shoot apex development, consistent with a previous report (Leibfried et al., 2005). The differential effect of *WUS* overexpression on the type-A ARRs could also be a hint of plants being able to discern between CK signalling over long distances (which modulates *WUS* activity in response to environmental cues) and at the local level (which further shapes the SAM) by employing different response regulators for each. The suggested role of AtENT3 in the regulation of *WUS* expression and the subsequent WUS feedback are schematically depicted in Figure 6F, and its further assessment is another

perspective of our future research.

7 Author Contribution

DN, KH, MH, OP designed the experiment and conception. MH, KM performed molecular techniques. PK, DN, KH performed transport assays. PH, DN constructed mathematical model. JL, JS, MP, PK, VM performed phenotypical analysis. DN, VM, and KH wrote the manuscript. All authors read and approved the manuscript.

8 Acknowledgements

The authors wish to thank to Julie Talpová and Anita Bírošíková for excellent technical support and Martin Lepšík and Roman Pleskot for constructive remarks on computational methods.

9 Funding

This work was supported by the project TowArds Next GENeration Crops, reg. no. CZ.02.01.01/00/22_008/0004581 of the ERDF Programme Johannes Amos Comenius.

10 Supplementary Files

Table S1: Sequences of primers used for cloning and quantitative PCR.

Table S2: Parameters for molecular dynamic simulations.

Table S3: Kinetic parameters obtained through the mathematical modelling of accumulations assays with radio-labelled tZ, tZR, iP, iPR, BA, BAR, DHZ, and DHZR in BY-2 cells.

Table S4: Statistical analysis of data from Table S3.

Table S5: Kinetic parameters obtained through the mathematical modelling of accumulation assays with radio-labelled tZ, tZR, iP, and iPR and their non-labelled counterparts at various concentrations as inhibitors.

Table S6: Kinetic parameters obtained through the mathematical modelling of accumulation assays with radio-labelled tZ, tZR, iP, and iPR with our without the addition of 10 μM CCCP at the beginning of the assay.

Table S7: Statistical analysis of data from Table S6.

Table S8: Kinetic parameters obtained through the mathematical modelling of accumulation assays with radio-labelled tZ, tZR, iP, and iPR with the addition of 10 μM CCCP at t = 420 s.

Table S9: Kinetic parameters obtained through the mathematical modelling of accumulation assays with radio-labelled tZ, tZR, iP, iPR, BA, and BAR and various nucleobases and ribosides at the concentration of 20 μM as competitors.

Table S10: Expression levels of tobacco *ENT* homologs in BY-2 cells. Data taken from GSE160438.

Table S11: Kinetic parameters obtained through the mathematical modelling of accumulation assays with radio-labelled tZ, tZR, iP, and iPR in control and induced BY-2 cells harbouring the

AtENT3 gene.

Table S12: Statistical analysis of data from Table S11.

Table S13: Kinetic parameters obtained through the mathematical modelling of accumulation assays with radio-labelled tZR and NBTI, Dipy or CCCP as inhibitors in control and induced BY-2 cells harbouring the *AtENT3* gene.

Table S14: Statistical analysis of data from Table S13.

Table S15: Parameters obtained through processing of images of 8-day-old wild-type and *atent3 A. thaliana* plants grown on the agar.

Table S16: Parameters obtained through processing of images of 8, 11, and 15-day-old wild-type and *atent3 A. thaliana* plants grown in pots.

Table S17: Statistical analysis of areas from Table S16 and Table S17.

Table S18: Relative expression levels of *AtWUS* measured through quantitative PCR in the shoots of 8-day-old wild-type and *atent3 A. thaliana* plants treated with 1 µM tZR in water or the corresponding amount of water.

Table S19: Statistical analysis of data from Table S18.

Supplementary methods: Derivation of models given by equation (1) and equation (2).

Figure S1-S4: The best-docked positions of tZ, tZR, iP, and iPR in the AlphFold-predicted structure of AtENT3.

Figure S5: Distribution of distances and angles during molecular dynamic simulations of the AtENT3-tZR complex.

11 References

Abraham, M., Alekseenko, A., Bergh, C., Blau, C., Briand, E., Doijade, M., Fleischmann, S., Gapsys, V., Garg, G., Gorelov, S., Gouaillardet, G., Gray, A., Irrgang, M.E., Jalalypour, F., Jordan, J., Junghans, C., Kanduri, P., Keller, S., Kutzner, C., Lemkul, J.A., Lundborg, M., Merz, P., Miletić, V., Morozov, D., Páll, S., Schulz, R., Shirts, M., Shvetsov, A., Soproni, B., Spoel, D. van der, Turner, P., Uphoff, C., Villa, A., Wingbermühle, S., Zhmurov, A., Bauer, P., Hess, B., Lindahl, E., 2024. GROMACS 2023.5 Source code. https://doi.org/10.5281/zenodo.11104849

Abraham, M.J., Murtola, T., Schulz, R., Páll, S., Smith, J.C., Hess, B., Lindahl, E., 2015. GROMACS: High performance molecular simulations through multi-level parallelism from laptops to supercomputers. SoftwareX 1–2, 19–25. https://doi.org/10.1016/j.softx.2015.06.001

Alexander, C.R., Dingman, D.W., Schultes, N.P., Mourad, G.S., 2018. The solute transport profile of two Aza-guanine transporters from the Honey bee pathogen Paenibacillus larvae. FEMS Microbiology Letters 365, fny018. https://doi.org/10.1093/femsle/fny018

An, G., Watson, B.D., Stachel, S., Gordon, M.P., Nester, E.W., 1985. New cloning vehicles for transformation of higher plants. EMBO J 4, 277–284.

Best, R.B., Zhu, X., Shim, J., Lopes, P.E.M., Mittal, J., Feig, M., MacKerell, A.D.Jr., 2012. Optimization of the Additive CHARMM All-Atom Protein Force Field Targeting Improved Sampling of the Backbone ϕ, ψ and Side-Chain χ1 and χ2 Dihedral Angles. J. Chem. Theory Comput. 8, 3257–3273. https://doi.org/10.1021/ct300400x

Bishopp, A., Lehesranta, S., Vatén, A., Help, H., El-Showk, S., Scheres, B., Helariutta, K., Mähönen, A.P., Sakakibara, H., Helariutta, Y., 2011. Phloem-Transported Cytokinin Regulates Polar Auxin Transport and Maintains Vascular Pattern in the Root Meristem. Current Biology 21, 927–932. https://doi.org/10.1016/j.cub.2011.04.049

Cavari, B.Z., Avi-Dor, Y., Grossowicz, N., 1967. Effect of carbonyl cyanide m-chlorophenylhydrazone on respiration and respiration-dependent phosphorylation in Escherichia coli. Biochem J 103, 601–608.

Chang, L., Ramireddy, E., Schmülling, T., 2015. Cytokinin as a positional cue regulating lateral root spacing in Arabidopsis. J Exp Bot 66, 4759–4768. https://doi.org/10.1093/jxb/erv252

Corbesier, L., Prinsen, E., Jacqmard, A., Lejeune, P., Van Onckelen, H., Périlleux, C., Bernier, G., 2003. Cytokinin levels in leaves, leaf exudate and shoot apical meristem of Arabidopsis thaliana during floral transition. J Exp Bot 54, 2511–2517. https://doi.org/10.1093/jxb/erg276

Culos, D., Watanabe, M., 1983. The effect of carbonyl cyanide *m*-chlorophenylhydrazone on steroid transport in membrane vesicles of *Pseudomonas testosteroni*. Journal of Steroid Biochemistry 19, 1127–1133. https://doi.org/10.1016/0022-4731(83)90406-5

Cunarro, J., Weiner, M.W., 1975. Mechanism of action of agents which uncouple oxidative phosphorylation: Direct correlation between protoncarrying and respiratory-releasing properties using rat liver mitochondria. Biochimica et Biophysica Acta (BBA) - Bioenergetics 387, 234–240. https://doi.org/10.1016/0005-2728(75)90106-1

Curtis, M.D., Grossniklaus, U., 2003. A gateway cloning vector set for high-throughput functional analysis of genes in planta. Plant Physiol 133, 462–469. https://doi.org/10.1104/pp.103.027979

Davière, J.-M., Achard, P., 2017. Organ communication: Cytokinins on the move. Nature Plants 3, 1–2. https://doi.org/10.1038/nplants.2017.116

De Rybel, B., Adibi, M., Breda, A.S., Wendrich, J.R., Smit, M.E., Novák, O., Yamaguchi, N., Yoshida, S., Isterdael, G.V., Palovaara, J., Nijsse, B., Boekschoten, M.V., Hooiveld, G., Beeckman, T., Wagner, D., Ljung, K., Fleck, C., Weijers, D., 2014. Integration of growth and patterning during vascular tissue formation in Arabidopsis. Science 345. https://doi.org/10.1126/science.1255215

Delbarre, A., Muller, P., Imhoff, V., Guern, J., 1996. Comparison of mechanisms controlling uptake and accumulation of 2,4-dichlorophenoxy acetic acid, naphthalene-1-acetic acid, and indole-3-acetic acid in suspension-cultured tobacco cells. Planta 198, 532–541. https://doi.org/10.1007/BF00262639

Dello Ioio, R., Galinha, C., Fletcher, A.G., Grigg, S.P., Molnar, A., Willemsen, V., Scheres, B., Sabatini, S., Baulcombe, D., Maini, P.K., Tsiantis, M., 2012. A PHABULOSA/Cytokinin Feedback Loop Controls Root Growth in Arabidopsis. Current Biology 22, 1699–1704. https://doi.org/10.1016/j.cub.2012.07.005

Dobránszki, J., Mendler-Drienyovszki, N., 2014. Cytokinin-induced changes in the chlorophyll content and fluorescence of *in vitro* apple leaves. Journal of Plant Physiology 171, 1472–1478.

https://doi.org/10.1016/j.jplph.2014.06.015
Essmann, U., Perera, L., Berkowitz, M.L., Darden, T., Lee, H., Pedersen, L.G., 1995. A smooth particle mesh Ewald method. The Journal of Chemical Physics 103, 8577–8593. https://doi.org/10.1063/1.470117
Girke, C., Daumann, M., Niopek-Witz, S., Möhlmann, T., 2014. Nucleobase and nucleoside transport and integration into plant metabolism. Front. Plant Sci. 5. https://doi.org/10.3389/fpls.2014.00443
Goddard, T.D., Huang, C.C., Meng, E.C., Pettersen, E.F., Couch, G.S., Morris, J.H., Ferrin, T.E., 2018. UCSF ChimeraX: Meeting modern challenges in visualization and analysis. Protein Science 27, 14–25. https://doi.org/10.1002/pro.3235
Hamada, S., Onouchi, H., Tanaka, H., Kudo, M., Liu, Y.-G., Shibata, D., Machida, C., Machida, Y., 2000. Mutations in the WUSCHEL gene of Arabidopsis thaliana result in the development of shoots without juvenile leaves. The Plant Journal 24, 91–101. https://doi.org/10.1046/j.1365-313x.2000.00858.x
Hess, B., 2008. P-LINCS: A Parallel Linear Constraint Solver for Molecular Simulation. J. Chem. Theory Comput. 4, 116–122. https://doi.org/10.1021/ct700200b
Heytler, P.G., 1963. Uncoupling of Oxidative Phosphorylation by Carbonyl Cyanide Phenylhydrazones. I. Some Characteristics of m-CI-CCP Action on Mitochondria and Chloroplasts. Biochemistry 2, 357–361. https://doi.org/10.1021/bi00902a031
Hirose, N., Makita, N., Yamaya, T., Sakakibara, H., 2005. Functional Characterization and Expression Analysis of a Gene, OsENT2, Encoding an Equilibrative Nucleoside Transporter in Rice Suggest a Function in Cytokinin Transport. Plant Physiol 138, 196–206. https://doi.org/10.1104/pp.105.060137
Hirose, N., Takei, K., Kuroha, T., Kamada-Nobusada, T., Hayashi, H., Sakakibara, H., 2008. Regulation of cytokinin biosynthesis, compartmentalization and translocation. J Exp Bot 59, 75–83. https://doi.org/10.1093/jxb/erm157
Hošek, P., Kubeš, M., Laňková, M., Dobrev, P.I., Klíma, P., Kohoutová, M., Petrášek, J., Hoyerová, K., Jiřina, M., Zažímalová, E., 2012. Auxin transport at cellular level: new insights supported by mathematical modelling. J Exp Bot 63, 3815–3827. https://doi.org/10.1093/jxb/ers074
Hu, Y., Patra, P., Pisanty, O., Shafir, A., Belew, Z.M., Binenbaum, J., Ben Yaakov, S., Shi, B., Charrier, L., Hyams, G., Zhang, Y., Trabulsky, M., Caldararu, O., Weiss, D., Crocoll, C., Avni, A., Vernoux, T., Geisler, M., Nour-Eldin, H.H., Mayrose, I., Shani, E., 2023. Multi-Knock—a multi-targeted genome-scale CRISPR toolbox to overcome functional redundancy in plants. Nat. Plants 9, 572–587. https://doi.org/10.1038/s41477-023-01374-4
Humphrey, W., Dalke, A., Schulten, K., 1996. VMD: visual molecular dynamics. J Mol Graph 14, 33–38, 27–28. https://doi.org/10.1016/0263-7855(96)00018-5
Incarbone, M., Bradamante, G., Pruckner, F., Wegscheider, T., Rozhon, W., Nguyen, V., Gutzat, R., Mérai, Z., Lendl, T., MacFarlane, S., Nodine, M., Scheid, O.M., 2023. Salicylic acid and RNA interference mediate antiviral immunity of plant stem cells. Proceedings of the National Academy of Sciences 120, e2302069120. https://doi.org/10.1073/pnas.2302069120
Jamruszka, T., Banasiak, J., Pawela, A., Jarzyniak, K., Xia, J., Biała-Leonhard, W., Plačková, L., Tsering, T., Iacobini, F.R., Novák, O., Geisler, M., Jasiński, M., 2024. Medicago truncatula ABCG40 is a cytokinin importer that negatively regulates lateral root density and nodule number. https://doi.org/10.1101/2022.11.10.516000
Jarzyniak, K., Banasiak, J., Jamruszka, T., Pawela, A., Donato, M.D., Novák, O., Geisler, M., Jasiński, M., 2021. Early stages of legume–rhizobia symbiosis are controlled by ABCG-mediated transport of active cytokinins. Nature Plants 1–9. https://doi.org/10.1038/s41477-021-00873-6
Jumper, J., Evans, R., Pritzel, A., Green, T., Figurnov, M., Ronneberger, O., Tunyasuvunakool, K., Bates, R., Žídek, A., Potapenko, A., Bridgland, A., Meyer, C., Kohl, S.A.A., Ballard, A.J., Cowie, A., Romera-Paredes, B., Nikolov, S., Jain, R., Adler, J., Back, T., Petersen, S., Reiman, D., Clancy, E., Zielinski, M., Steinegger, M., Pacholska, M., Berghammer, T., Bodenstein, S., Silver, D., Vinyals, O., Senior, A.W., Kavukcuoglu, K., Kohli, P., Hassabis, D., 2021. Highly accurate protein structure prediction with AlphaFold. Nature 596, 583–589. https://doi.org/10.1038/s41586-021-03819-2
Karbanova, S., Sorf, A., Jiraskova, L., Lalinska, A., Ptackova, Z., Staud, F., Cerveny, L., 2020. S-(4-Nitrobenzyl)-6-thioinosine (NBMPR) is Not a Selective Inhibitor of Equilibrative Nucleoside Transporters but Also Blocks Efflux Activity of Breast Cancer Resistance Protein. Pharm Res 37, 58. https://doi.org/10.1007/s11095-020-2782-5
Katoh, K., Standley, D.M., 2013. MAFFT Multiple Sequence Alignment Software Version 7: Improvements in Performance and Usability. Molecular Biology and Evolution 30, 772–780. https://doi.org/10.1093/molbev/mst010
Kim, A., Chen, J., Khare, D., Jin, J.-Y., Yamaoka, Y., Maeshima, M., Zhao, Y., Martinoia, E., Hwang, J.-U., Lee, Y.,

2020. Non-intrinsic ATP-binding cassette proteins ABCI19, ABCI20 and ABCI21 modulate cytokinin response at the endoplasmic reticulum in Arabidopsis thaliana. Plant Cell Rep 39, 473–487. https://doi.org/10.1007/s00299-019-02503-0

Ko, D., Kang, J., Kiba, T., Park, J., Kojima, M., Do, J., Kim, K.Y., Kwon, M., Endler, A., Song, W.-Y., Martinoia, E., Sakakibara, H., Lee, Y., 2014. Arabidopsis ABCG14 is essential for the root-to-shoot translocation of cytokinin. Proceedings of the National Academy of Sciences of the United States of America 111, 7150–5. https://doi.org/10.1073/pnas.1321519111

Korobova, A., Kuluev, B., Möhlmann, T., Veselov, D., Kudoyarova, G., 2021. Limitation of Cytokinin Export to the Shoots by Nucleoside Transporter ENT3 and Its Linkage with Root Elongation in Arabidopsis. Cells 10, 350. https://doi.org/10.3390/cells10020350

Landrein, B., Formosa-Jordan, P., Malivert, A., Schuster, C., Melnyk, C.W., Yang, W., Turnbull, C., Meyerowitz, E.M., Locke, J.C.W., Jönsson, H., 2018. Nitrate modulates stem cell dynamics in Arabidopsis shoot meristems through cytokinins. Proceedings of the National Academy of Sciences 115, 1382–1387. https://doi.org/10.1073/pnas.1718670115

Laskowski, R.A., Swindells, M.B., 2011. LigPlot+: Multiple Ligand–Protein Interaction Diagrams for Drug Discovery. J. Chem. Inf. Model. 51, 2778–2786. https://doi.org/10.1021/ci200227u

Laux, T., Mayer, K.F.X., Berger, J., Jürgens, G., 1996. The *WUSCHEL* gene is required for shoot and floral meristem integrity in *Arabidopsis*. Development 122, 87–96. https://doi.org/10.1242/dev.122.1.87

Leibfried, A., To, J.P.C., Busch, W., Stehling, S., Kehle, A., Demar, M., Kieber, J.J., Lohmann, J.U., 2005. WUSCHEL controls meristem function by direct regulation of cytokinin-inducible response regulators. Nature 438, 1172–1175. https://doi.org/10.1038/nature04270

Lemkul, J., 2019. From Proteins to Perturbed Hamiltonians: A Suite of Tutorials for the GROMACS-2018 Molecular Simulation Package [Article v1.0]. LiveCoMS 1. https://doi.org/10.33011/livecoms.1.1.5068

Li, G., Liu, K., Baldwin, S.A., Wang, D., 2003. Equilibrative Nucleoside Transporters of Arabidopsis thaliana: cDNA cloning, expression pattern, and analysis of transport activities. J. Biol. Chem. 278, 35732–35742. https://doi.org/10.1074/jbc.M304768200

Liao, P.-S., Chen, T.-S., Chung, P.-C., 2001. A Fast Algorithm for Multilevel Thresholding. Journal of Information Science and Engineering 17, 713–727.

Lomin, S.N., Krivosheev, D.M., Steklov, M.Y., Arkhipov, D.V., Osolodkin, D.I., Schmülling, T., Romanov, G.A., 2015. Plant membrane assays with cytokinin receptors underpin the unique role of free cytokinin bases as biologically active ligands. J Exp Bot 66, 1851–1863. https://doi.org/10.1093/jxb/eru522

Lopes, F.L., Galvan-Ampudia, C., Landrein, B., 2021. WUSCHEL in the shoot apical meristem: old player, new tricks. Journal of Experimental Botany 72, 1527–1535. https://doi.org/10.1093/jxb/eraa572

Ma, Y., Miotk, A., Šutiković, Z., Ermakova, O., Wenzl, C., Medzihradszky, A., Gaillochet, C., Forner, J., Utan, G., Brackmann, K., Galván-Ampudia, C.S., Vernoux, T., Greb, T., Lohmann, J.U., 2019. WUSCHEL acts as an auxin response rheostat to maintain apical stem cells in Arabidopsis. Nat Commun 10, 5093. https://doi.org/10.1038/s41467-019-13074-9

Mähönen, A.P., Bishopp, A., Higuchi, M., Nieminen, K.M., Kinoshita, K., Törmäkangas, K., Ikeda, Y., Oka, A., Kakimoto, T., Helariutta, Y., 2006. Cytokinin Signaling and Its Inhibitor AHP6 Regulate Cell Fate During Vascular Development. Science 311, 94–98. https://doi.org/10.1126/science.1118875

Mandel, T., Candela, H., Landau, U., Asis, L., Zilinger, E., Carles, C.C., Williams, L.E., 2016. Differential regulation of meristem size, morphology and organization by the ERECTA, CLAVATA and class III HD-ZIP pathways. Development dev.129973. https://doi.org/10.1242/dev.129973

Miller, C.O., Skoog, F., Okumura, F.S., von Saltza, M.H., Strong, F.M., 1956. Isolation, Structure and Synthesis of Kinetin, a Substance Promoting Cell Division. J. Am. Chem. Soc. 78, 1375–1380. https://doi.org/10.1021/ja01588a032

Miyamoto, S., Kollman, P.A., 1992. Settle: An analytical version of the SHAKE and RATTLE algorithm for rigid water models. Journal of Computational Chemistry 13, 952–962. https://doi.org/10.1002/jcc.540130805

Möhlmann, T., Mezher, Z., Schwerdtfeger, G., Neuhaus, H.E., 2001. Characterisation of a concentrative type of adenosine transporter from Arabidopsis thaliana (ENT1,At). FEBS Letters 509, 370–374. https://doi.org/10.1016/S0014-5793(01)03195-7

Müller, K., Dobrev, P.I., Pěnčík, A., Hošek, P., Vondráková, Z., Filepová, R., Malínská, K., Brunoni, F., Helusová, L., Moravec, T., Retzer, K., Harant, K., Novák, O., Hoyerová, K., Petrášek, J., 2021. DIOXYGENASE FOR AUXIN OXIDATION 1 catalyzes the oxidation of IAA amino acid conjugates. Plant Physiol 187, 103–115. https://doi.org/10.1093/plphys/kiab242

Nagata, T., Nemoto, Y., Hasezawa, S., 1992. Tobacco BY-2 Cell Line as the “HeLa” Cell in the Cell Biology of Higher Plants. International Review of Cytology 132, 1–30. https://doi.org/10.1016/S0074-7696(08)62452-3

Nedvěd, D., Hošek, P., Klíma, P., Hoyerová, K., 2021. Differential Subcellular Distribution of Cytokinins: How Does Membrane Transport Fit into the Big Picture? International Journal of Molecular Sciences 22, 3428. https://doi.org/10.3390/ijms22073428

Newell, D.R., O’Connor, P.M., Hilary Calvert, A., Harrap, K.R., 1986. The effect of the nucleoside transport inhibitor dipyridamole on the incorporation of [3H]thymidine in the rat. Biochemical Pharmacology 35, 3871–3877. https://doi.org/10.1016/0006-2952(86)90678-7

Osugi, A., Kojima, M., Takebayashi, Y., Ueda, N., Kiba, T., Sakakibara, H., 2017. Systemic transport of trans-zeatin and its precursor have differing roles in Arabidopsis shoots. Nature Plants 3, 17112. https://doi.org/10.1038/nplants.2017.112

Páll, S., Abraham, M.J., Kutzner, C., Hess, B., Lindahl, E., 2015. Tackling Exascale Software Challenges in Molecular Dynamics Simulations with GROMACS, in: Markidis, S., Laure, E. (Eds.), Solving Software Challenges for Exascale. Springer International Publishing, Cham, pp. 3–27. https://doi.org/10.1007/978-3-319-15976-8_1

Paul, A., Laurila, T., Vuorinen, V., Divinski, S.V., 2014. Fick’s Laws of Diffusion, in: Paul, A., Laurila, T., Vuorinen, V., Divinski, S.V. (Eds.), Thermodynamics, Diffusion and the Kirkendall Effect in Solids. Springer International Publishing, Cham, pp. 115–139. https://doi.org/10.1007/978-3-319-07461-0_3

Pei, J., Grishin, N.V., 2001. AL2CO: calculation of positional conservation in a protein sequence alignment. Bioinformatics 17, 700–712. https://doi.org/10.1093/bioinformatics/17.8.700

Qi, Z., Xiong, L., 2013. Characterization of a Purine Permease Family Gene OsPUP7 Involved in Growth and Development Control in Rice. Journal of Integrative Plant Biology 55, 1119–1135. https://doi.org/10.1111/jipb.12101

Radchuk, V., Belew, Z.M., Gündel, A., Mayer, S., Hilo, A., Hensel, G., Sharma, R., Neumann, K., Ortleb, S., Wagner, S., Muszynska, A., Crocoll, C., Xu, D., Hoffie, I., Kumlehn, J., Fuchs, J., Peleke, F.F., Szymanski, J.J., Rolletschek, H., Nour-Eldin, H.H., Borisjuk, L., 2023. SWEET11b transports both sugar and cytokinin in developing barley grains. The Plant Cell 35, 2186–2207. https://doi.org/10.1093/plcell/koad055

Ravindranath, P.A., Forli, S., Goodsell, D.S., Olson, A.J., Sanner, M.F., 2015. AutoDockFR: Advances in Protein-Ligand Docking with Explicitly Specified Binding Site Flexibility. PLOS Computational Biology 11, e1004586. https://doi.org/10.1371/journal.pcbi.1004586

Richmond, A.E., Lang, A., 1957. Effect of Kinetin on Protein Content and Survival of Detached Xanthium Leaves. Science 125, 650–651. https://doi.org/10.1126/science.125.3249.650-a

Rong, C., Zhang, R., Liu, Y., Chang, Z., Liu, Z., Ding, Y., Ding, C., 2024. Purine permease (PUP) family gene PUP11 positively regulates the rice seed setting rate by influencing seed development. Plant Cell Rep 43, 112. https://doi.org/10.1007/s00299-024-03193-z

Sakakibara, H., 2021. Cytokinin biosynthesis and transport for systemic nitrogen signaling. The Plant Journal 105, 421–430. https://doi.org/10.1111/tpj.15011

Schaller, G.E., Street, I.H., Kieber, J.J., 2014. Cytokinin and the cell cycle. Current Opinion in Plant Biology, SI: Cell signalling and gene regulation 21, 7–15. https://doi.org/10.1016/j.pbi.2014.05.015

Schrödinger, LLC, 2015. The PyMOL Molecular Graphics System, Version 1.8.

Silva-Navas, J., Moreno-Risueno, M.A., Manzano, C., Pallero-Baena, M., Navarro-Neila, S., Téllez-Robledo, B., Garcia-Mina, J.M., Baigorri, R., Gallego, F.J., Pozo, J.C. del, 2015. D-Root: a system for cultivating plants with the roots in darkness or under different light conditions. The Plant Journal 84, 244–255. https://doi.org/10.1111/tpj.12998

Skoog, F., Miller, C.O., 1957. Chemical regulation of growth and organ formation in plant tissues cultured in vitro. Symp Soc Exp Biol 11, 118–130.

Šmeringai, J., Rudolf, J., Trtílek, M., Procházková Schrumpfová, P., Pernisová, M., 2023. Shoot phenotyping of cytokinin receptors mutants revealed fluorescence parameters as early markers of drought stress. https://doi.org/10.1101/2023.11.30.569457

Stoffer-Bittner, A.J., Alexander, C.R., Dingman, D.W., Mourad, G.S., Schultes, N.P., 2018. Functional characterization of the uracil transporter from honeybee pathogen *Paenibacillus larvae*. Microbial Pathogenesis 124, 305–310. https://doi.org/10.1016/j.micpath.2018.08.059

Sun, J., Hirose, N., Wang, X., Wen, P., Xue, L., Sakakibara, H., Zuo, J., 2005. Arabidopsis SOI33/AtENT8 Gene Encodes a Putative Equilibrative Nucleoside Transporter That Is Involved in Cytokinin Transport In Planta. Journal of Integrative Plant Biology 47, 588–603. https://doi.org/10.1111/j.1744-7909.2005.00104.x

Takei, K., Sakakibara, H., Taniguchi, M., Sugiyama, T., 2001. Nitrogen-Dependent Accumulation of Cytokinins in Root

and theTranslocation to Leaf: Implication of Cytokinin Species that Induces GeneExpression of Maize ResponseRegulator. Plant Cell Physiol 42, 85–93. https://doi.org/10.1093/pcp/pce009

Talla, S.K., Panigrahy, M., Kappara, S., Nirosha, P., Neelamraju, S., Ramanan, R., 2016. Cytokinin delays dark-induced senescence in rice by maintaining the chlorophyll cycle and photosynthetic complexes. Journal of Experimental Botany 67, 1839–1851. https://doi.org/10.1093/jxb/erv575

Tessi, T.M., Brumm, S., Winklbauer, E., Schumacher, B., Pettinari, G., Lescano, I., González, C.A., Wanke, D., Maurino, V.G., Harter, K., Desimone, M., 2020. Arabidopsis AZG2 transports cytokinins in vivo and regulates lateral root emergence. New Phytologist 229, 979–993. https://doi.org/10.1111/nph.16943

Tessi, T.M., Maurino, V.G., Shahriari, M., Meissner, E., Novak, O., Pasternak, T., Schumacher, B.S., Ditengou, F., Li, Z., Duerr, J., Flubacher, N.S., Nautscher, M., Williams, A., Kazimierczak, Z., Strnad, M., Thumfart, J.-O., Palme, K., Desimone, M., Teale, W.D., 2023. AZG1 is a cytokinin transporter that interacts with auxin transporter PIN1 and regulates the root stress response. New Phytologist 238, 1924–1941. https://doi.org/10.1111/nph.18879

The GIMP Team, 2024. GNU Image Manipulation Program.

The UniProt Consortium, 2023. UniProt: the Universal Protein Knowledgebase in 2023. Nucleic Acids Research 51, D523–D531. https://doi.org/10.1093/nar/gkac1052

To, J.P.C., Deruère, J., Maxwell, B.B., Morris, V.F., Hutchison, C.E., Ferreira, F.J., Schaller, G.E., Kieber, J.J., 2007. Cytokinin Regulates Type-A Arabidopsis Response Regulator Activity and Protein Stability via Two-Component Phosphorelay. The Plant Cell 19, 3901–3914. https://doi.org/10.1105/tpc.107.052662

To, J.P.C., Haberer, G., Ferreira, F.J., Deruère, J., Mason, M.G., Schaller, G.E., Alonso, J.M., Ecker, J.R., Kieber, J.J., 2004. Type-A Arabidopsis response regulators are partially redundant negative regulators of cytokinin signaling. Plant Cell 16, 658–671. https://doi.org/10.1105/tpc.018978

van der Walt, S.J., Schönberger, J.L., Nunez-Iglesias, J., Boulogne, F., Warner, J.D., Yager, N., Gouillart, E., Yu, T., 2014. scikit-image: image processing in Python. PeerJ 2, e453. https://doi.org/10.7717/peerj.453

Vanommeslaeghe, K., MacKerell, A.D.Jr., 2012. Automation of the CHARMM General Force Field (CGenFF) I: Bond Perception and Atom Typing. J. Chem. Inf. Model. 52, 3144–3154. https://doi.org/10.1021/ci300363c

Vanommeslaeghe, K., Raman, E.P., MacKerell, A.D.Jr., 2012. Automation of the CHARMM General Force Field (CGenFF) II: Assignment of Bonded Parameters and Partial Atomic Charges. J. Chem. Inf. Model. 52, 3155–3168. https://doi.org/10.1021/ci3003649

Virtanen, P., Gommers, R., Oliphant, T.E., Haberland, M., Reddy, T., Cournapeau, D., Burovski, E., Peterson, P., Weckesser, W., Bright, J., Walt, S.J. van der, Brett, M., Wilson, J., Millman, K.J., Mayorov, N., Nelson, A.R.J., Jones, E., Kern, R., Larson, E., Carey, C.J., Polat, İ., Feng, Y., Moore, E.W., VanderPlas, J., Laxalde, D., Perktold, J., Cimrman, R., Henriksen, I., Quintero, E.A., Harris, C.R., Archibald, A.M., Ribeiro, A.H., Pedregosa, F., Mulbregt, P. van, 2020. SciPy 1.0: fundamental algorithms for scientific computing in Python. Nat Methods 17, 261–272. https://doi.org/10.1038/s41592-019-0686-2

Wang, C., Yu, L., Zhang, J., Zhou, Y., Sun, B., Xiao, Q., Zhang, M., Liu, H., Li, Jinhong, Li, Jialu, Luo, Y., Xu, J., Lian, Z., Lin, J., Wang, X., Zhang, P., Guo, L., Ren, R., Deng, D., 2023. Structural basis of the substrate recognition and inhibition mechanism of Plasmodium falciparum nucleoside transporter PfENT1. Nat Commun 14, 1727. https://doi.org/10.1038/s41467-023-37411-1

Ward, J.L., Sherali, A., Mo, Z.-P., Tse, C.-M., 2000. Kinetic and Pharmacological Properties of Cloned Human Equilibrative Nucleoside Transporters, ENT1 and ENT2, Stably Expressed in Nucleoside Transporter-deficient PK15 Cells: ENT2 EXHIBITS A LOW AFFINITY FOR GUANOSINE AND CYTIDINE BUT A HIGH AFFINITY FOR INOSINE *. Journal of Biological Chemistry 275, 8375–8381. https://doi.org/10.1074/jbc.275.12.8375

Waterhouse, A.M., Procter, J.B., Martin, D.M.A., Clamp, M., Barton, G.J., 2009. Jalview Version 2—a multiple sequence alignment editor and analysis workbench. Bioinformatics 25, 1189–1191. https://doi.org/10.1093/bioinformatics/btp033

Werner, T., Motyka, V., Strnad, M., Schmülling, T., 2001. Regulation of plant growth by cytokinin. PNAS 98, 10487–10492. https://doi.org/10.1073/pnas.171304098

Woffendin, C., Plagemann, P.G.W., 1987. Interaction of [3H]dipyridamole with the nucleoside transporters of human erythrocytes and cultured animal cells. J. Membrain Biol. 98, 89–100. https://doi.org/10.1007/BF01871048

Wormit, A., Traub, M., Flörchinger, M., Neuhaus, H.E., Möhlmann, T., 2004. Characterization of three novel members of the Arabidopsis thaliana equilibrative nucleoside transporter (ENT) family. Biochem J 383, 19–26. https://doi.org/10.1042/BJ20040389

Wright, N.J., Lee, S.-Y., 2019. Structures of human ENT1 in complex with adenosine reuptake inhibitors. Nat Struct

Mol Biol 26, 599–606. https://doi.org/10.1038/s41594-019-0245-7

Xiao, Y., Liu, D., Zhang, G., Gao, S., Liu, L., Xu, F., Che, R., Wang, Y., Tong, H., Chu, C., 2019. Big Grain3, encoding a purine permease, regulates grain size via modulating cytokinin transport in rice. Journal of Integrative Plant Biology 61, 581–597. https://doi.org/10.1111/jipb.12727

Xiao, Y., Zhang, J., Yu, G., Lu, X., Mei, W., Deng, H., Zhang, G., Chen, G., Chu, C., Tong, H., Tang, W., 2020. Endoplasmic Reticulum-Localized PURINE PERMEASE1 Regulates Plant Height and Grain Weight by Modulating Cytokinin Distribution in Rice. Front. Plant Sci. 11. https://doi.org/10.3389/fpls.2020.618560

Yang, Q., Zhang, J., Kojima, M., Takebayashi, Y., Uragami, T., Kiba, T., Sakakibara, H., Lee, Y., 2022. ABCG11 modulates cytokinin responses in Arabidopsis thaliana. Front. Plant Sci. 13. https://doi.org/10.3389/fpls.2022.976267

Yang, W., Cortijo, S., Korsbo, N., Roszak, P., Schiessl, K., Gurzadyan, A., Wightman, R., Jönsson, H., Meyerowitz, E., 2021. Molecular mechanism of cytokinin-activated cell division in Arabidopsis. Science 371, 1350–1355. https://doi.org/10.1126/science.abe2305

Yao, S.Y.M., Ng, A.M.L., Cass, C.E., Baldwin, S.A., Young, J.D., 2011. Nucleobase Transport by Human Equilibrative Nucleoside Transporter 1 (hENT1). J Biol Chem 286, 32552–32562. https://doi.org/10.1074/jbc.M111.236117

Zhang, K., Novak, O., Wei, Z., Gou, M., Zhang, X., Yu, Y., Yang, H., Cai, Y., Strnad, M., Liu, C.-J., 2014. Arabidopsis ABCG14 protein controls the acropetal translocation of root-synthesized cytokinins. Nature Communications 5, 1–12. https://doi.org/10.1038/ncomms4274

Zhao, J., Deng, X., Qian, J., Liu, T., Ju, M., Li, J., Yang, Q., Zhu, X., Li, W., Liu, C.-J., Jin, Z., Zhang, K., 2023. *Arabidopsis* ABCG14 forms a homodimeric transporter for multiple cytokinins and mediates long-distance transport of isopentenyladenine-type cytokinins. Plant Communications 4, 100468. https://doi.org/10.1016/j.xplc.2022.100468

Zhao, J., Yu, N., Ju, M., Fan, B., Zhang, Y., Zhu, E., Zhang, M., Zhang, K., 2019. ABC transporter OsABCG18 controls the shootward transport of cytokinins and grain yield in rice. Journal of Experimental Botany 70, 6277–6291. https://doi.org/10.1093/jxb/erz382

Zhao, Y., Stoffler, D., Sanner, M., 2006. Hierarchical and multi-resolution representation of protein flexibility. Bioinformatics 22, 2768–2774. https://doi.org/10.1093/bioinformatics/btl481

Zürcher, E., Liu, J., di Donato, M., Geisler, M., Müller, B., 2016. Plant development regulated by cytokinin sinks. Science 353, 1027–1030.

12 Figures

Figure 1: Characterization of the CK membrane transport in tobacco BY-2 cells. **A**: Estimated values of the influx rate constant (*I*) for different radio-labelled CK tracers obtained by fitting equation (1) into data from radio-accumulation assays. **B-E**: Comparison of the accumulation trends (concentration of the accumulated tracer over time) between CK nucleobases and their ribosylated forms. The curves are aligned by setting $K = 0$ and $c_0 = 2$ nM for each assay. *P*-values obtained from the one-way ANOVA test comparing *I* values for the corresponding pairs of CK nucleobases and ribosides: 0 ($P > 0.1$), * ($0.1 >= P > 0.05$), ** ($0.05 >= P > 0.01$), *** ($P <= 0.01$). Acc.: accumulated.

Figure 2: Saturation of the CK membrane transport in tobacco BY-2 cells. **A-D**: Accumulation trends (concentration of the accumulated tracer in time) of radio-labelled CK in BY2 cell inhibited by increasing concentrations of their non-labelled counterparts. The shape of the curves is determined by the *I* and *E* values obtained by fitting equation (1) into data from radio-accumulation assays. For the visualization purposes, *K* is set to 0 and c_0 to 2 nM for each assay. **E-H**: Dependence of *I* values obtained from the mathematical modelling of radio-accumulation data on the concentration of the non-labelled competitors. The plotted data points are further fitted with equation (3) to obtain the saturation parameters. The fit of equation (3) is represented by grey dashed curves. The *I* values correspond to the curves depicted in A-D. **I-L**: Accumulation trends of radio-labelled CK tracers in presence of 50 µM carbonyl cyanide 3-chlorophenylhydrazone (CCCP). Acc.: accumulated.

Figure 3: Substrate specificity of CK membrane-bound transport systems. **A-D**: Accumulation trends (concentration of the accumulated tracer over time) of radio-labelled CK in BY-2 cell sinhibited by increasing concentrations of chemically diverse non-labelled substances. The shape of the curves is determined by the *I* and *E* values obtained by fitting equation (1) into data from radio-accumulation assays. For the visualization purposes, *K* is set to 0 and c_0 to 2 nM for each assay. **E-H**: Dependence of the *I* values obtained from the mathematical modelling of radio-accumulation data on the concentration of the non-labelled competitors. The plotted data points are further fitted with equation (2) to obtain the saturation parameters. The fit of equation (2) is represented by grey dashed curves. The *I* values correspond to the curves depicted in A-D. **I**: Fold changes of the influx rate constants estimated for various combinations of radio-labelled CK tracers and 20 µM non-labelled competitors. Black cells denote non-tested combinations. Acc.: accumulated.

Figure 4: The effect of *AtENT3* expression on the CK uptake in tobacco BY-2 cells. **A**: Expression of *AtENT* homologues in two day-old BY-2 cultures. The identifiers on the vertical axis correspond to accessions in the NCBI (National Center for Biotechnology Information) Gene database (accessed on 17 April 2024). Data were obtained through the GEO (Gene Expression Omnibus) database under the accession of GSE160438 (Müller et al., 2021). **B-C**: Optimized values of the influx rate constant, *I*, obtained by fitting equation (1) into data from radio-accumulation assays measuring the uptake of radio-labelled CK nucleobases and ribosides in the *AtENT3*-harbouring BY-2 cells under an estradiol-inducible promoter without (ctr) or with the induction (ind) of *AtENT3* expression. **D**: Optimized values of *I* for the uptake of radio-labelled tZR in the *AtENT3*-harbouring BY-2 cells without or with the induction of *AtENT3* expression and without (mock) or with transport inhibitors *S*-(4-nitrobenzyl)-6-thioinosine (NBTI), dipyridamole (DiPy), and carbonyl cyanide 3-chlorophenylhydrazone (CCCP). All inhibitors were applied at a concentration

of 10 µM. *P*-values obtained from the one-way ANOVA test comparing *I* values for induced and control cell lines: 0 (*P* > 0.1), * (0.1 >= *P* > 0.05), ** (0.05 >= *P* > 0.01), *** (*P* <= 0.01).

Figure 5: Computational assessment of the interactions between the AlphaFold-predicted structure of AtENT3 and tZR. **A**: Schematic representation of the best docked pose of tZR in the binding cavity of AtENT3. Green dashed lines represent hydrogen bonds with lengths given in Å. Short red rays represent hydrophobic interactions. Visualized in LigPlot+. **B**: Sequential alignment of plant, animal, parasitic, and yeast ENTs. The residues of AtENT3 interacting with the docked pose of tZR and their homologs are shown in bold. Their conservation among the presented species is depicted by the differential intensity of the blue highlight. Blue vertical lines mark breaks in the sequences. The labels in the header of the alignment denote the residues of AtENT3 found at the given position. The consensus sequences and the logotype of the alignment segments are given at the bottom. Visualized in Jalview. **C**: Superimposition of AtENT3 (tan cylinders) with the docked pose of tZR (green) and the experimental poses of NBTI (light blue) in HsENT1 (PDB code: 6OB6) and inosine (pink) in PfENT1 (PDB code: 7WN1). The amino acid residues of 6OB6 and 7WN1 are hidden. **D**: Sequence conservation of AtENT3 residues interacting with the docked pose of tZR calculated by the AL2CO program (Pei and Grishin, 2001) from the alignment depicted in B. Larger numbers indicate higher conservation. **E**: Hydrogen bonding among tZR, Trp34, Tyr61 and Asp129, and a water molecule in the system equilibrated by molecular dynamics (MD). Hydrogen bonds are depicted as light blue dashed lines. Images C-E are visualized in UCSF ChimeraX. **F**: Fractional occupancies of the MD simulation grid by water molecules. The meshes represent isosurfaces with the fractional occupancy of 90%. Differently coloured meshes correspond to three independent MD simulation runs. Visualized in PyMol. **G**: Representative distributions of atomic distances involving the hydrogen (H5) and oxygen (O5) of the side-chain carboxyl of tZR, a carboxylic oxygen of Asp129 (OD1), the phenolic oxygen of Tyr61 (OH), and the nitrogen-bound hydrogen of Trp34 (HE1).

Figure 6: AtENT3-mediated transport of tZR contributes to the shoot development in *Arabidopsis thaliana*. **A**: Top view images of wild-type and *atent3 A. thaliana* plants grown in pots. Scale bar: 1 cm. **B**: Shoot areas of *A. thaliana* plants grown on the agar and in pots measured through image analysis. **C**: Relative expressions of *AtENT* genes in the shoot apices or apex-enriched tissues of *A. thaliana* retrieved from the Gene Expression Ominubs (GEO) database via accessions GSM4278593-95 (Yang et al., 2021), GSM2104466 and 71 (Mandel et al., 2016), and GSM7764635-36 (Incarbone et al., 2023). The colour scale is normalized from 0 to the maximal value in each column. **D**: Differential expression of genes related to CK transport, metabolism, and signalling in plants ectopically overexpressing *WUSCHEL* (*WUS*) in comparison to control plants. Data obtained from GEO accession GSE122610 (Ma et al., 2019). **E**: Relative expression levels of *WUS* in the shoots of 8 day-old agar-grown *A. thaliana* plants obtained through quantitative PCR. **F**: A schematic proposition of the function of AtENT3-mediated tZR transport in the maintenance of cytokinin homeostasis and WUS activity in the SAM. Black arrows denote movement and conversions of cytokinin species, green arrows activation, and red lines with flat ends inhibition. *P*-values obtained from the one-way ANOVA test comparing wild-type and *atent3* plants: 0 (*P* > 0.1), * (0.1 >= *P* > 0.05), ** (0.05 >= *P* > 0.01), *** (*P* <= 0.01). DAS: days after sowing, LOG: LONELY GUY, CKX: cytokinin dehydrogenase, CLV: CLAVATA.

Figure 1

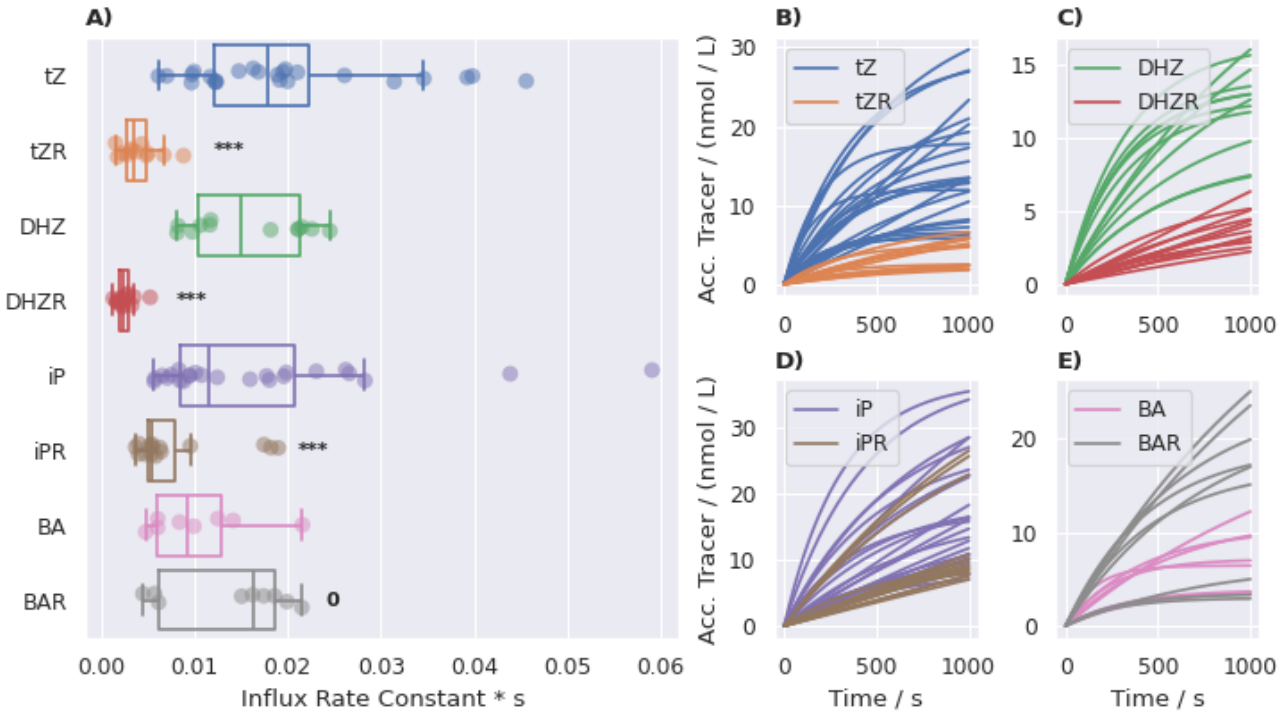

Figure 1: Characterization of the CK membrane transport in tobacco BY-2 cells. **A**: Estimated values of the influx rate constant (*I*) for different radio-labelled CK tracers obtained by fitting equation (1) into data from radio-accumulation assays. **B-E**: Comparison of the accumulation trends (concentration of the accumulated tracer over time) between CK nucleobases and their ribosylated forms. The curves are aligned by setting $K = 0$ and $c_0 = 2$ nM for each assay. *P*-values obtained from the one-way ANOVA test comparing *I* values for the corresponding pairs of CK nucleobases and ribosides: 0 ($P > 0.1$), * ($0.1 >= P > 0.05$), ** ($0.05 >= P > 0.01$), *** ($P <= 0.01$). Acc.: accumulated.

Figure 2

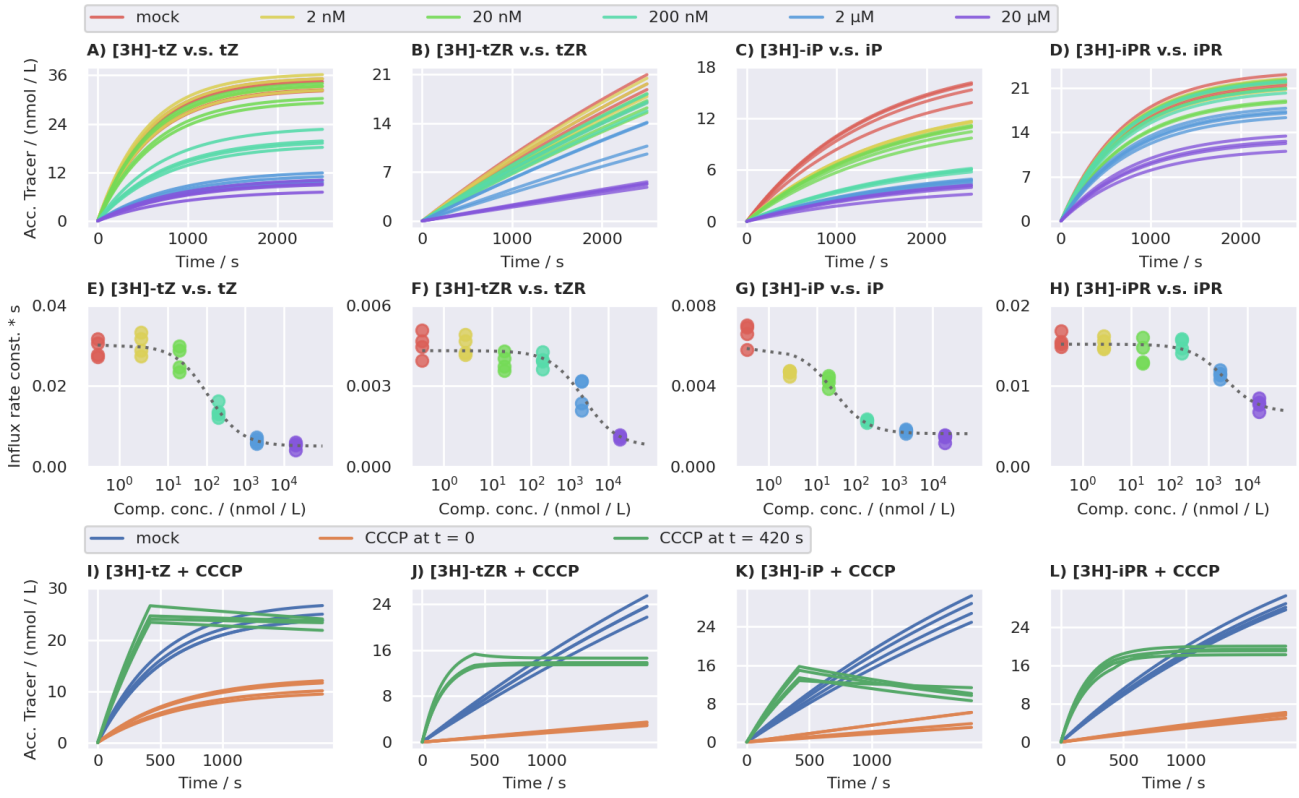

Figure 2: Saturation of the CK membrane transport in tobacco BY-2 cells. **A-D**: Accumulation trends (concentration of the accumulated tracer in time) of radio-labelled CK in BY2 cell inhibited by increasing concentrations of their non-labelled counterparts. The shape of the curves is determined by the *I* and *E* values obtained by fitting equation (1) into data from radio-accumulation assays. For the visualization purposes, *K* is set to 0 and c_0 to 2 nM for each assay. **E-H**: Dependence of *I* values obtained from the mathematical modelling of radio-accumulation data on the concentration of the non-labelled competitors. The plotted data points are further fitted with equation (3) to obtain the saturation parameters. The fit of equation (3) is represented by grey dashed curves. The *I* values correspond to the curves depicted in A-D. **I-L**: Accumulation trends of radio-labelled CK tracers in presence of 50 µM carbonyl cyanide 3-chlorophenylhydrazone (CCCP). Acc.: accumulated.

Figure 3

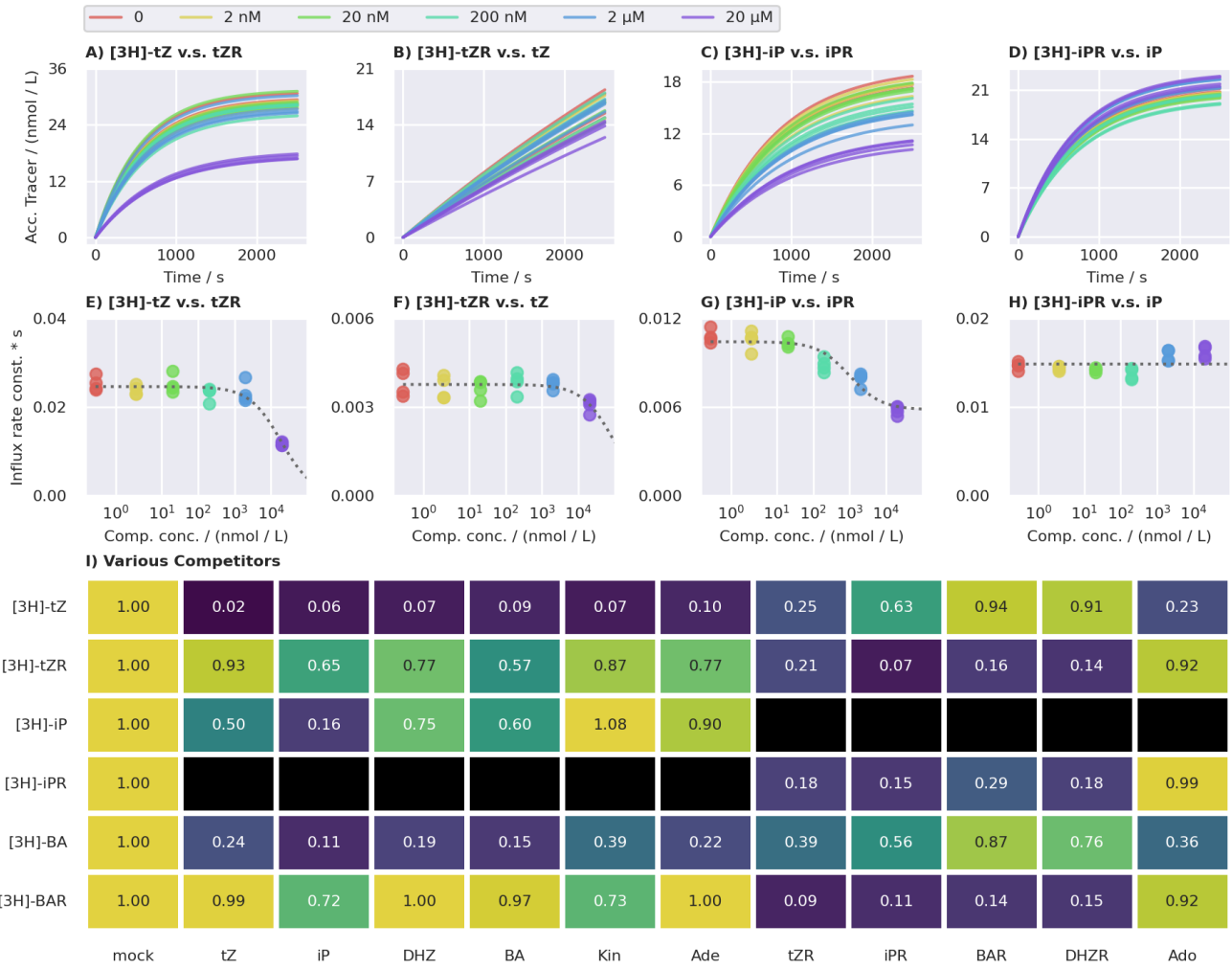

Figure 3: Substrate specificity of CK membrane-bound transport systems. **A-D**: Accumulation trends (concentration of the accumulated tracer over time) of radio-labelled CK in BY-2 cell sinhibited by increasing concentrations of chemically diverse non-labelled substances. The shape of the curves is determined by the *I* and *E* values obtained by fitting equation (1) into data from radio-accumulation assays. For the visualization purposes, *K* is set to 0 and c_0 to 2 nM for each assay. **E-H**: Dependence of the *I* values obtained from the mathematical modelling of radio-accumulation data on the concentration of the non-labelled competitors. The plotted data points are further fitted with equation (2) to obtain the saturation parameters. The fit of equation (2) is represented by grey dashed curves. The *I* values correspond to the curves depicted in A-D. **I**: Fold changes of the influx rate constants estimated for various combinations of radio-labelled CK tracers and 20 µM non-labelled competitors. Black cells denote non-tested combinations. Acc.: accumulated.

Figure 4

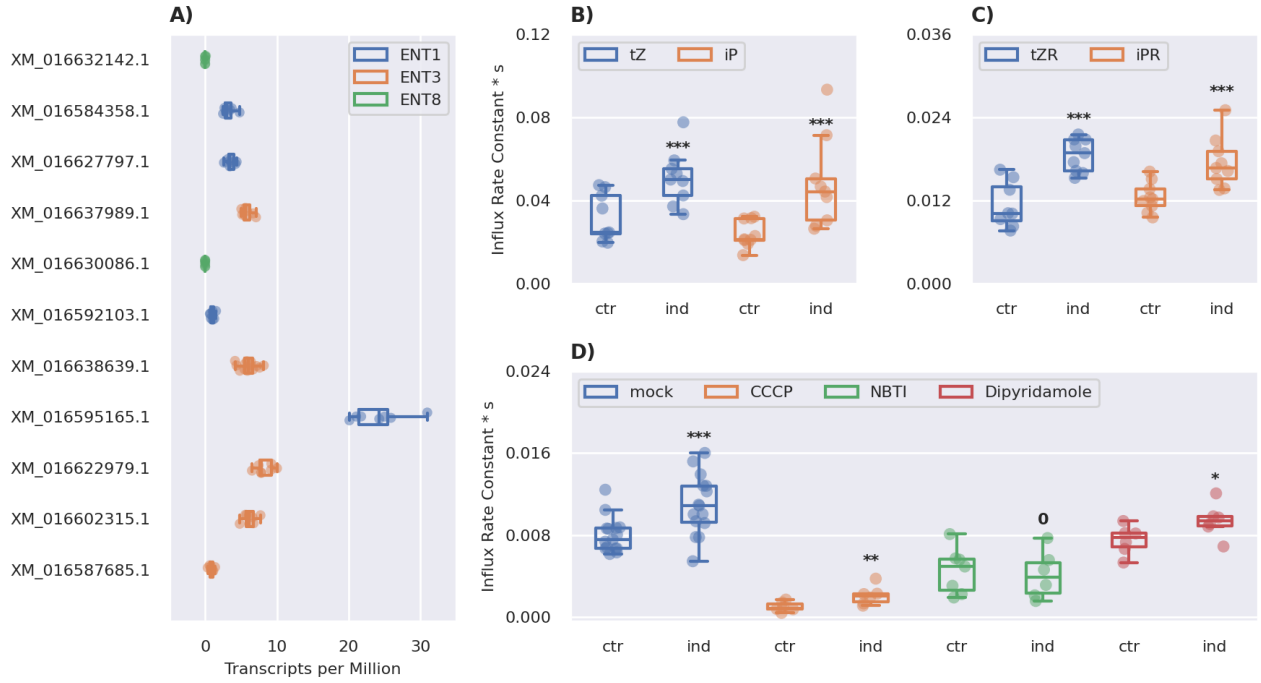

Figure 4: The effect of *AtENT3* expression on the CK uptake in tobacco BY-2 cells. **A**: Expression of *AtENT* homologues in two day-old BY-2 cultures. The identifiers on the vertical axis correspond to accessions in the NCBI (National Center for Biotechnology Information) Gene database (accessed on 17 April 2024). Data were obtained through the GEO (Gene Expression Omnibus) database under the accession of GSE160438 (Müller et al., 2021). **B-C**: Optimized values of the influx rate constant, *I*, obtained by fitting equation (1) into data from radio-accumulation assays measuring the uptake of radio-labelled CK nucleobases and ribosides in the *AtENT3*-harbouring BY-2 cells under an estradiol-inducible promoter without (ctr) or with the induction (ind) of *AtENT3* expression. **D**: Optimized values of *I* for the uptake of radio-labelled tZR in the *AtENT3*-harbouring BY-2 cells without or with the induction of *AtENT3* expression and without (mock) or with transport inhibitors *S*-(4-nitrobenzyl)-6-thioinosine (NBTI), dipyridamole (DiPy), and carbonyl cyanide 3-chlorophenylhydrazone (CCCP). All inhibitors were applied at a concentration of 10 µM. *P*-values obtained from the one-way ANOVA test comparing *I* values for induced and control cell lines: 0 ($P > 0.1$), * ($0.1 >= P > 0.05$), ** ($0.05 >= P > 0.01$), *** ($P <= 0.01$).

Figure 5

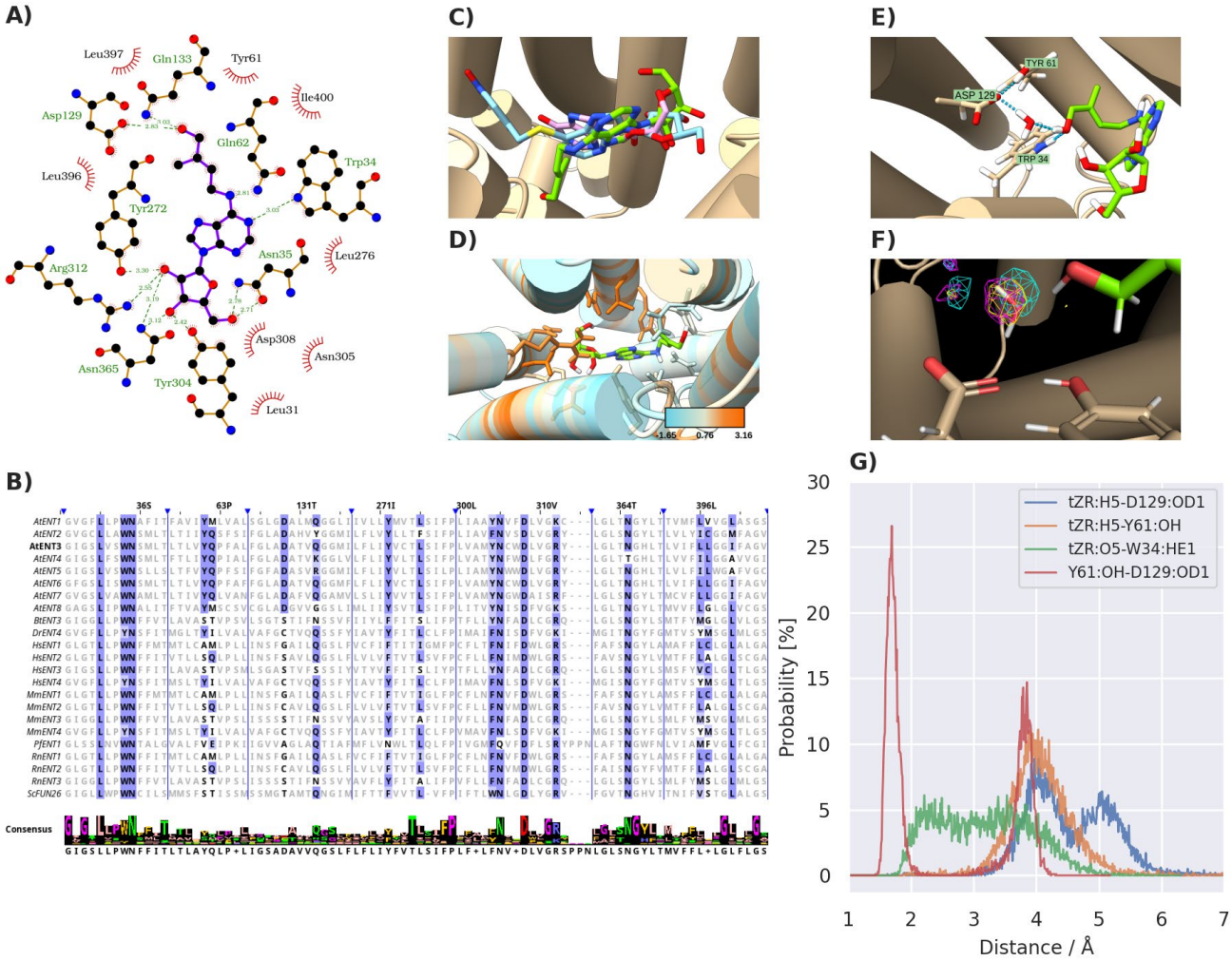

Figure 5: Computational assessment of the interactions between the AlphaFold-predicted structure of AtENT3 and tZR. **A**: Schematic representation of the best docked pose of tZR in the binding cavity of AtENT3. Green dashed lines represent hydrogen bonds with lengths given in Å. Short red rays represent hydrophobic interactions. Visualized in LigPlot+. **B**: Sequential alignment of plant, animal, parasitic, and yeast ENTs. The residues of AtENT3 interacting with the docked pose of tZR and their homologs are shown in bold. Their conservation among the presented species is depicted by the differential intensity of the blue highlight. Blue vertical lines mark breaks in the sequences. The labels in the header of the alignment denote the residues of AtENT3 found at the given position. The consensus sequences and the logotype of the alignment segments are given at the bottom. Visualized in Jalview. **C**: Superimposition of AtENT3 (tan cylinders) with the docked pose of tZR (green) and the experimental poses of NBTI (light blue) in HsENT1 (PDB code: 6OB6) and inosine (pink) in PfENT1 (PDB code: 7WN1). The amino acid residues of 6OB6 and 7WN1 are hidden. **D**: Sequence conservation of AtENT3 residues interacting with the docked pose of tZR calculated by the AL2CO program (Pei and Grishin, 2001) from the alignment depicted in B. Larger numbers indicate higher conservation. **E**: Hydrogen bonding among tZR, Trp34, Tyr61 and Asp129, and a water molecule in

the system equilibrated by molecular dynamics (MD). Hydrogen bonds are depicted as light blue dashed lines. Images C-E are visualized in UCSF ChimeraX. **F**: Fractional occupancies of the MD simulation grid by water molecules. The meshes represent isosurfaces with the fractional occupancy of 90%. Differently coloured meshes correspond to three independent MD simulation runs. Visualized in PyMol. **G**: Representative distributions of atomic distances involving the hydrogen (H5) and oxygen (O5) of the side-chain carboxyl of tZR, a carboxylic oxygen of Asp129 (OD1), the phenolic oxygen of Tyr61 (OH), and the nitrogen-bound hydrogen of Trp34 (HE1).

Figure 6

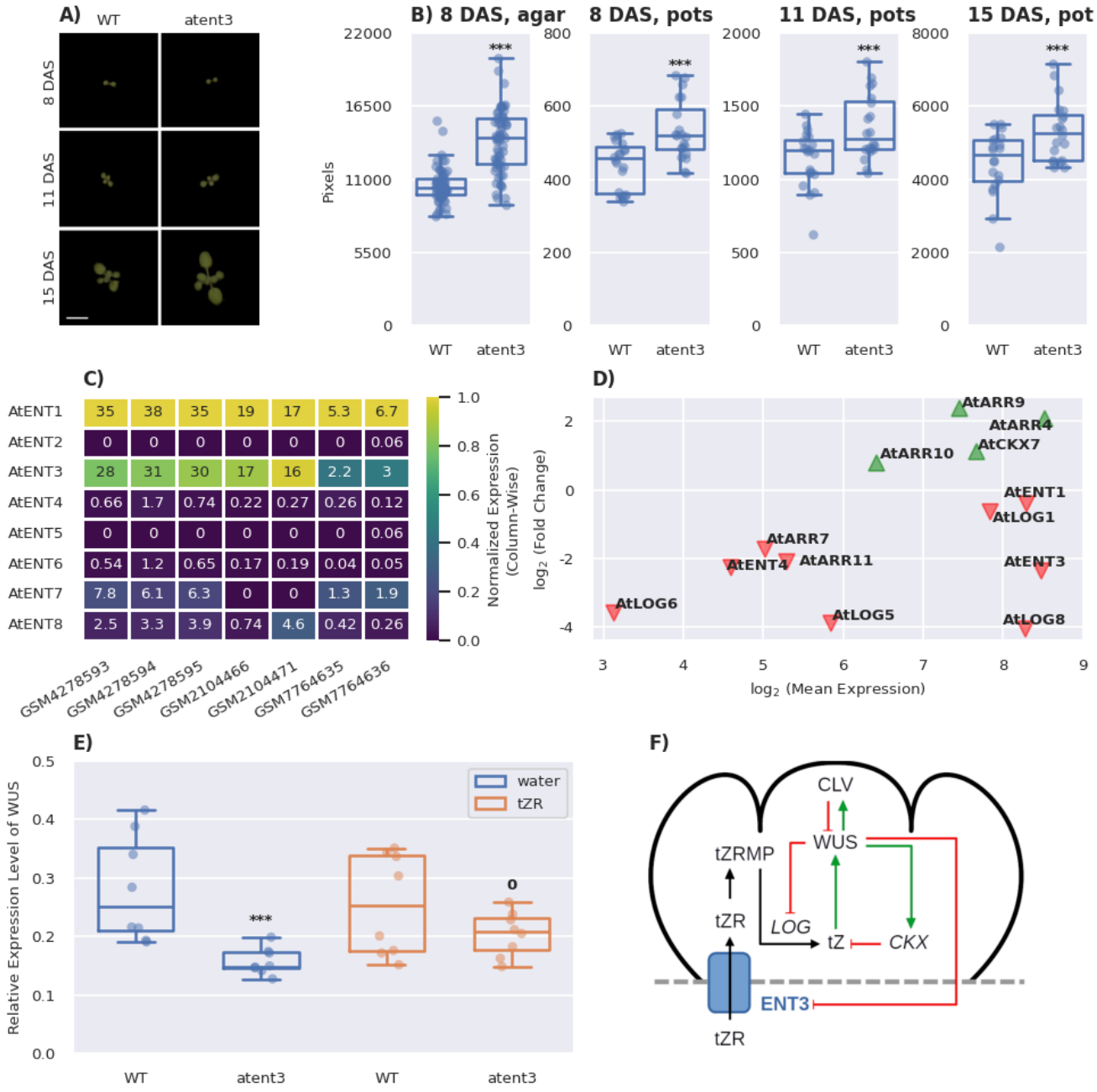

Figure 6: AtENT3-mediated transport of tZR contributes to the shoot development in *Arabidopsis thaliana*. **A**: Top view images of wild-type and *atent3 A. thaliana* plants grown in pots. Scale bar: 1 cm. **B**: Shoot areas of *A. thaliana* plants grown on the agar and in pots measured through image analysis. **C**: Relative expressions of *AtENT* genes in the shoot apices or apex-enriched tissues of *A. thaliana* retrieved from the Gene Expression Ominubs (GEO) database via accessions GSM4278593-95 (Yang et al., 2021), GSM2104466 and 71 (Mandel et al., 2016), and GSM7764635-36 (Incarbone et al., 2023). The colour scale is normalized from 0 to the maximal value in each column. **D**: Differential expression of genes related to CK transport, metabolism, and

signalling in plants ectopically overexpressing *WUSCHEL* (*WUS*) in comparison to control plants. Data obtained from GEO accession GSE122610 (Ma et al., 2019). **E**: Relative expression levels of *WUS* in the shoots of 8 day-old agar-grown *A. thaliana* plants obtained through quantitative PCR. **F**: A schematic proposition of the function of AtENT3-mediated tZR transport in the maintenance of cytokinin homeostasis and WUS activity in the SAM. Black arrows denote movement and conversions of cytokinin species, green arrows activation, and red lines with flat ends inhibition. *P*-values obtained from the one-way ANOVA test comparing wild-type and *atent3* plants: 0 ($P > 0.1$), * ($0.1 >= P > 0.05$), ** ($0.05 >= P > 0.01$), *** ($P <= 0.01$). DAS: days after sowing, LOG: LONELY GUY, CKX: cytokinin dehydrogenase, CLV: CLAVATA.

1 Supplementary Methods

1.1 Derivation of the Transport Model

The model assumes two simultaneous transport processes in the cell suspension culture: the influx of the tracer from the media to the cells and the efflux of the tracer in the opposite direction. We consider both processes to obey the first-order kinetics. This can be mathematically expressed as:

$$\frac{dc_I}{dt} = Ic_E - Ec_I, \tag{S1}$$

where c_I and c_E are the intracellular and extracellular concentrations of the traced CK, respectively, I is the influx rate constant, and E is the efflux rate constant. The sum of the intra- and extracellular concentrations, c_0, is the initial concentration of the tracer applied to the cell suspension, and it remains constant during the assay:

$$c_0 = fc_I + c_E. \tag{S2}$$

The symbol f denotes a factor accounting for the different volumes of the intra- and extracellular environments, which prevents from summing the concentrations directly. With $\bar{v}$ denoting the average volume of a BY-2 cell, previously determined as 3.53×10^{-13} m^3 (Hošek et al., 2012), and ρ denoting the cell suspension density, we can define f as:

$$f = \frac{\bar{v}\rho}{1-\bar{v}\rho} \tag{S3}$$

and rewrite equation (S1) as:

$$\frac{dc_I}{dt} = I(c_0 - fc_I) - Ec_I. \tag{S4}$$

With the initial condition $c_I(0)=0$, we can find the solution to equation (S4) as:

$$\int_0^{c_I} \frac{(-fI-E)\,dc_I}{(-fI-E)c_I + Ic_0} = \int_0^t (-fI-E)\,dt, \tag{S5}$$

$$\ln\frac{Ic_0 - (fI+E)c_I}{Ic_0} = -(fI+E)t, \tag{S6}$$

and finally:

$$c_I(t) = \frac{Ic_0}{fI+E}\left[1 - e^{-t(fI+E)}\right]. \tag{S7}$$

The c_I values calculated from the measured radioactivities are biased due to a portion of the tracer remaining on the cell surfaces. To account for this, we define surface contamination factor K and add term Kc_E to the right side of equation (S7). This yields:

$$c_I(t) = \frac{Ic_0}{fI+E}\left[1 - e^{-t(fI+E)}\right](1-fK) + Kc_0. \tag{S8}$$

1.2 Derivation of the In-Flight Model

In so-called in-flight assays, we applied a chemical to the cell suspension when the accumulation of the radio-labelled tracer was already in progress. We assume the treatment affects the kinetic constants, I and E. The membrane transport in an in-flight assay can be modelled as:

$$\frac{dc_I}{dt}=\begin{cases} Ic_E-Ec_I & \text{if} \quad t\le t' \\ I'c_E-E'c_I & \text{if} \quad t>t' \end{cases}, \tag{S9}$$

where t' is the treatment time and I', E' are the post-treatment values of I, E, respectively. The solution to the first case of equation (S9) is given by equation (S7) and its working implementation, which accounts for the cell surface contamination, by equation (S8). To second case of equation (S9) can be rewritten as:

$$\frac{dc_I}{dt}=I'(c_0-c_I)-E'c_I. \tag{S10}$$

To solve equation (S10), we can use the initial condition $c_I(t')=c'$, where c' is the function value obtained from equation (S7) by setting $t=t'$. With the initial condition, we can write:

$$\int_{c'}^{c_I}\frac{(-fI'-E')dc_I}{(-fI'-E')c_I+I'c_0}=(-fI'-E')\int_{t'}^{t}dt, \tag{S11}$$

which yields:

$$c_I(t)=\frac{I'c_0}{fI'+E'}\left[1-e^{(t'-t)(fI'+E')}\right]+c'e^{(t'-t)(fI'+E')}. \tag{S12}$$

After substituting for c' from equation (S7) and accounting for the cell surface contamination, we can write the integral form of the in-flight model as:

$$c_I(t)=\begin{cases} \dfrac{Ic_0}{fI+E}\left[1-e^{-t(fI+E)}\right](1-fK)+Kc_0 & \text{if} \quad t\le t' \\ \left\{\dfrac{I'c_0}{fI'+E'}\left[1-e^{(t'-t)(fI'+E')}\right]+\dfrac{Ic_0}{fI+E}\left[1-e^{-t'(fI+E)}\right]e^{(t'-t)(fI'+E')}\right\}(1-fK)+Kc_0 & \text{if} \quad t>t' \end{cases}. \tag{S13}$$

Restricting E' to be equal to E yields equation (2) in the main text.

2 Supplementary Figures

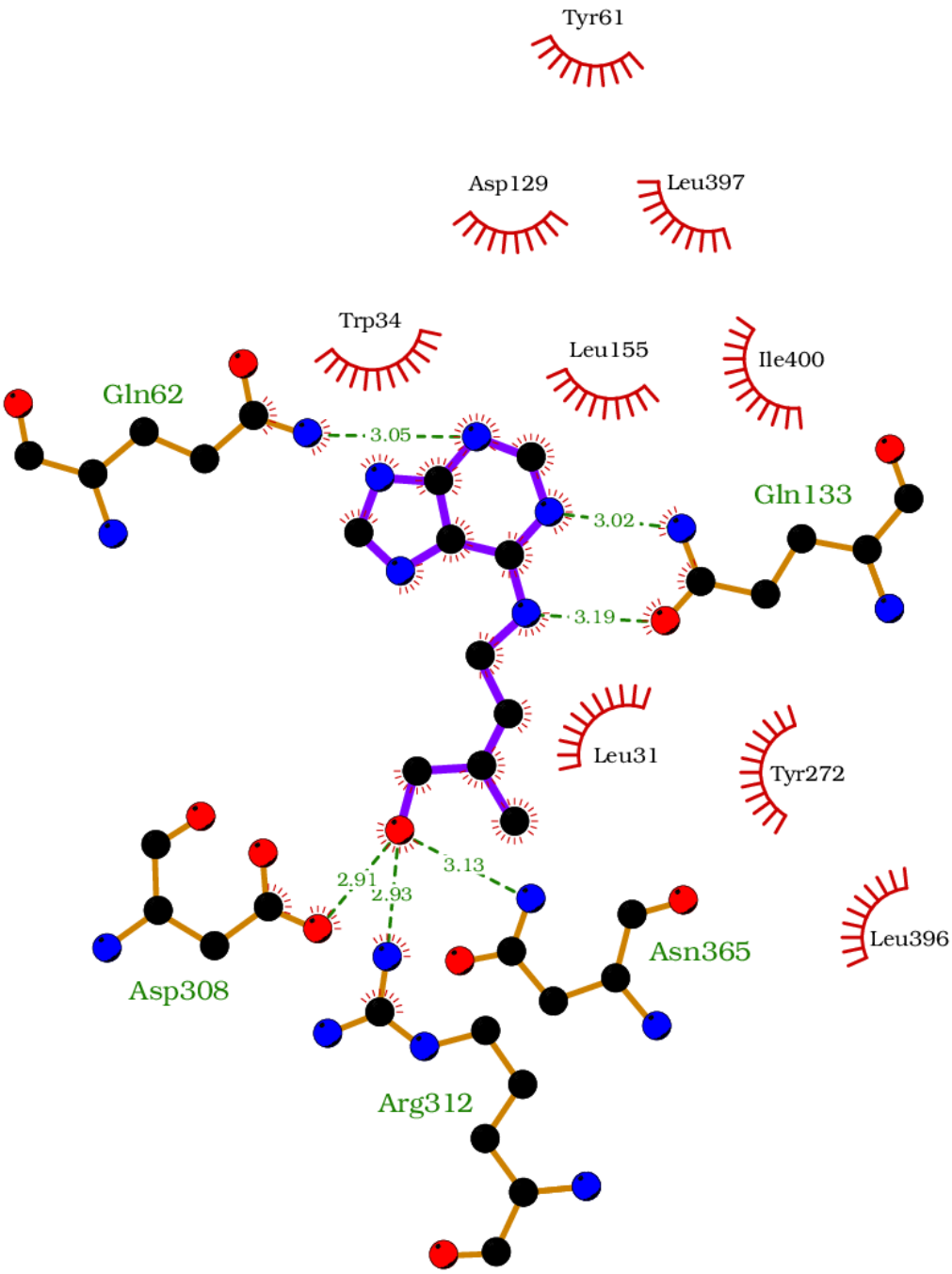

Figure S1: The best-docked pose of trans-zeatin in the AlphaFold-predicted strucutre of AtENT3. Visuazlied in LigPlot+.

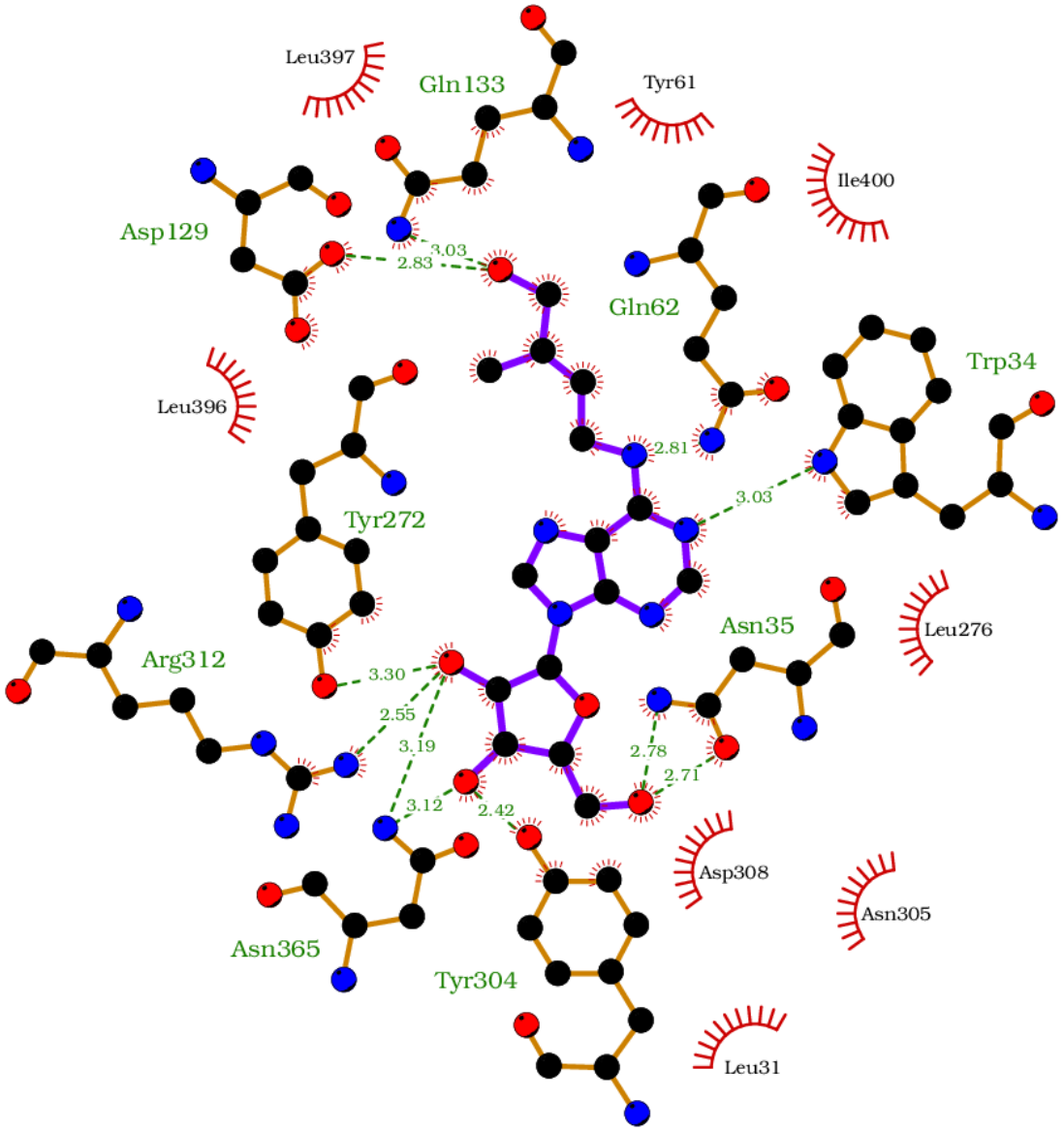

Figure S2: The best-docked pose of trans-zeatin riboside in the AlphaFold-predicted strucutre of AtENT3. Visuazlied in LigPlot+.

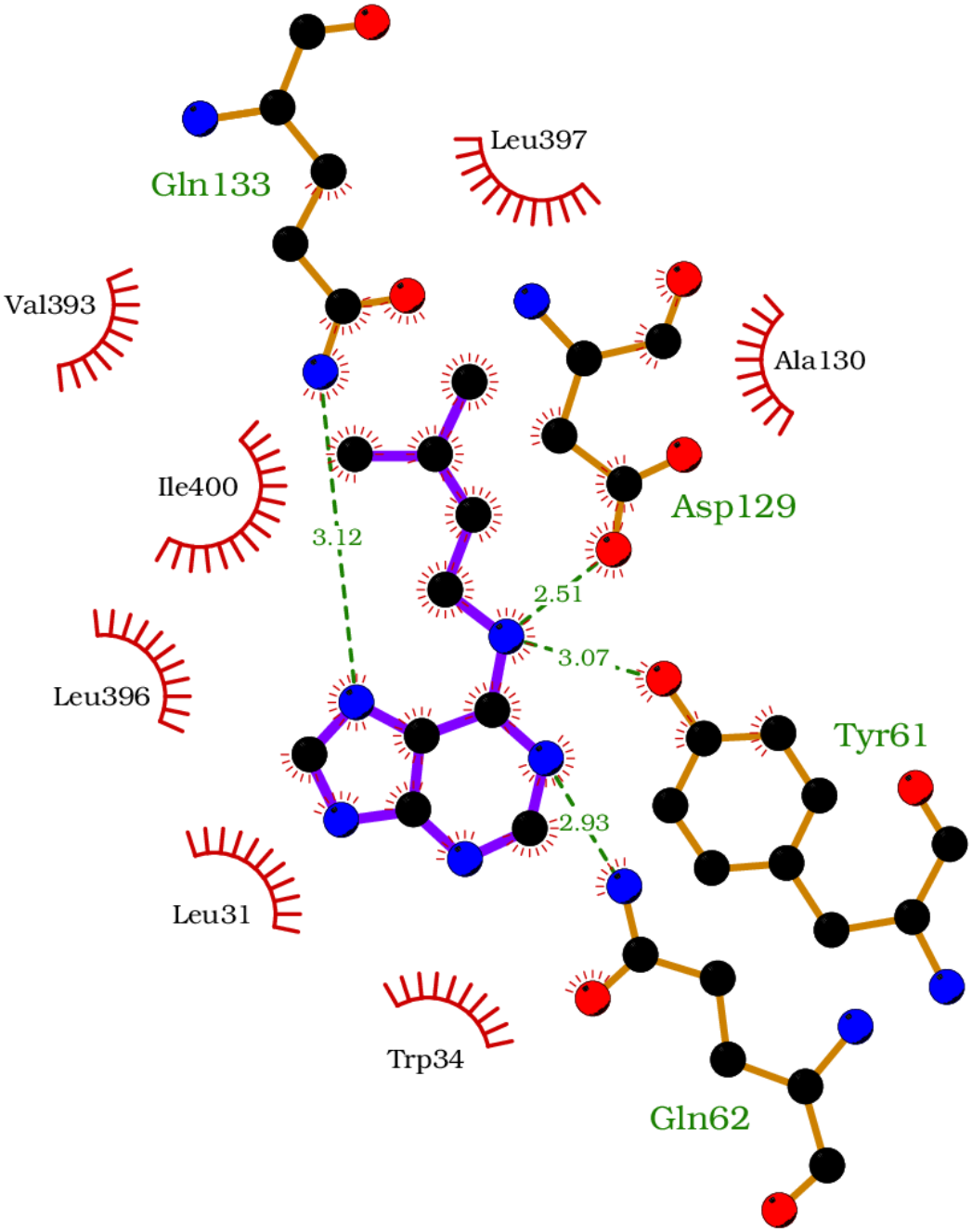

Figure S3: The best-docked pose of isopentenyl adenine in the AlphaFold-predicted strucutre of AtENT3. Visuazlied in LigPlot+.

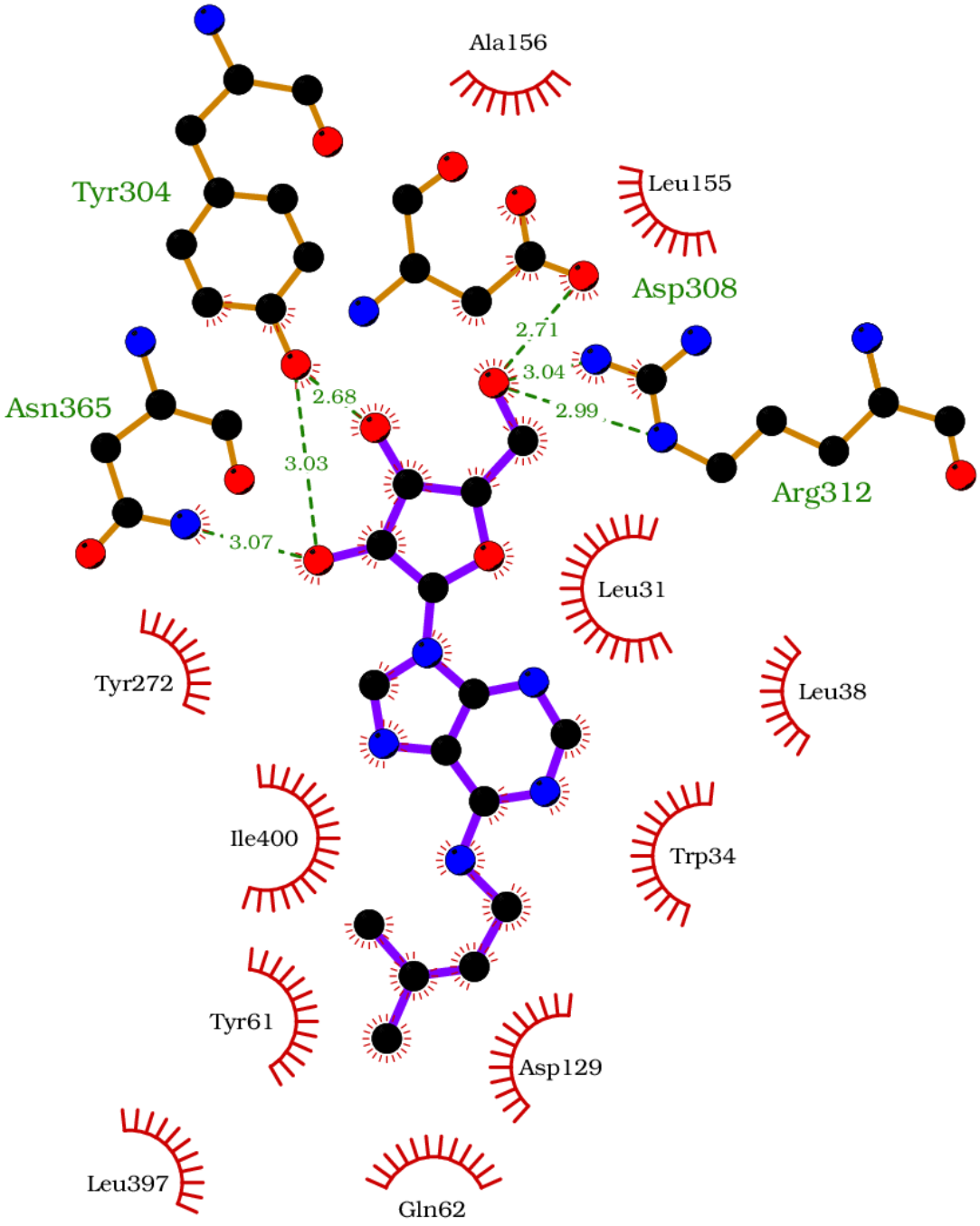

Figure S4: The best-docked pose of isopentenyl adenosine in the AlphaFold-predicted strucutre of AtENT3. Visuazlied in LigPlot+.

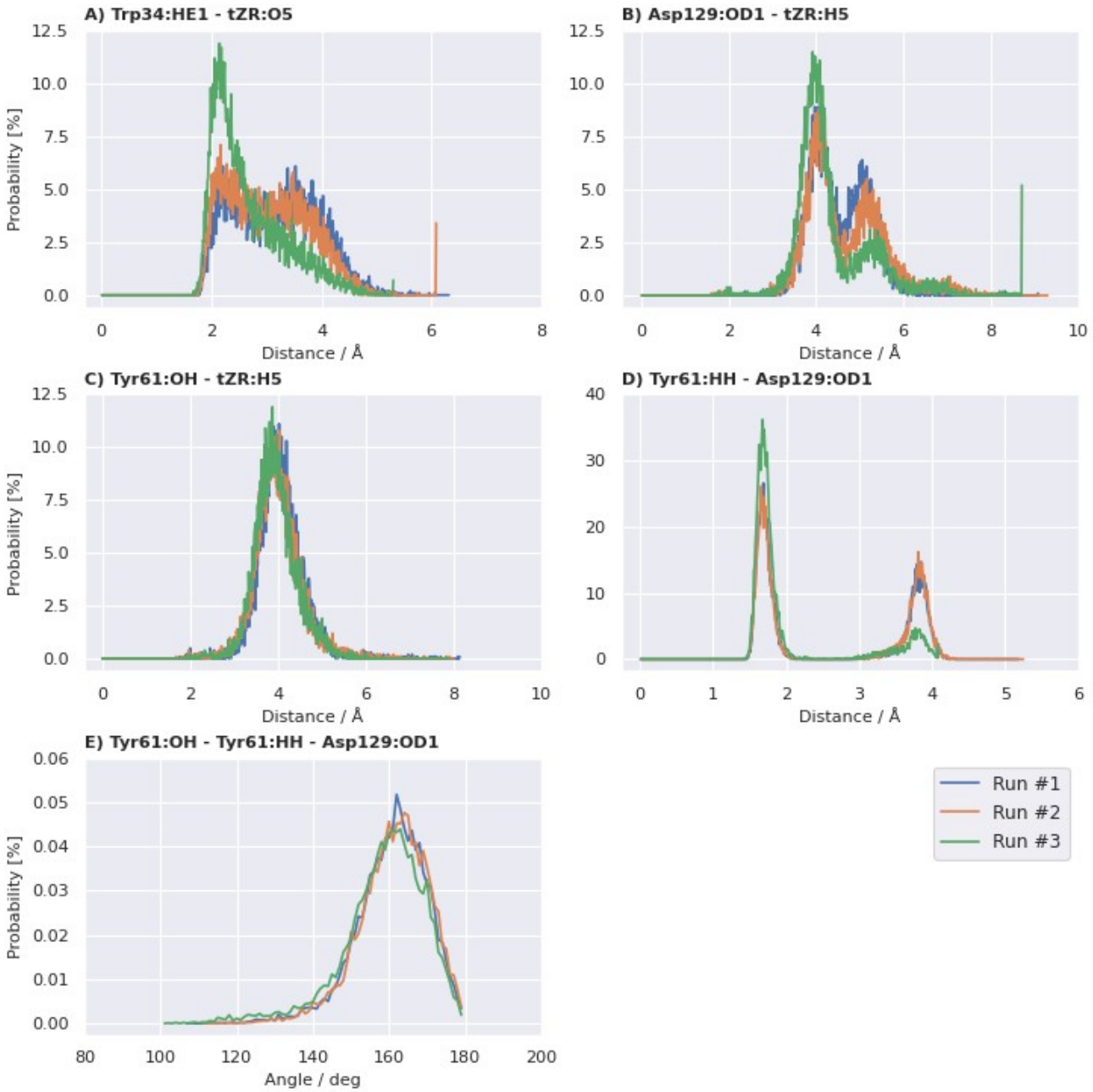

Figure S5: Distributions of chosen distances (A-D) and angles (E) during three independent 100-ns-long molecular dynamic simulations of the complex of AtENT3 with trans-zeatin riboside (tZR) in 150 mM NaCl.

4.3 Cytokinin Dehydrogenase in Xylem Sap Reveals A Direct Link Between Cytokinin Metabolism and Long-Distance Transport

In this manuscript, my colleagues and I demonstrate that CKX is active in oat xylem sap and characterize putative oat CKX isoforms in the context of a bioinformatical analysis of CKX sequences from various monocot species. First, we present a multi-sequence alignment of 492 monocot CKX sequences. These sequences form eight major clusters labelled as class I-VIII for manuscript purposes. Sequences within each class can be characterized with a specific composition of the variable triplet in the semi-conserved FLXRVXXXE motif (i.e. the second, third, and fourth to last residue). The last residue of this triplet can interact with ligands in some cases (Kopečný et al., 2016), indicating that each CKX class comprises enzymes with the same substrate specificity (Figure 1 in the manuscript). For easier reference, we dub the last residue of the variable triplet "VEGAS" based on its five most common identities (i.e. valine, glutamate, glycine, alanine, and serine).

We then compare the active centres of six CKX structures representing six of the eight classes identified through the multi-sequence alignment. We include a newly solved structure of ZmCKX5, which we also report as one of the results of this manuscript. The direct structural comparison supports the previous observation that when glutamine occupies the VEGAS position, it stabilizes a CK nucleobase in the active centre through a hydrogen bond (Kopečný et al., 2016; Malito et al., 2004) (Figure 2 in the manuscript).

Next, we show that the monocot CKX classification partially correlates with the sequence-based predictions of their subcellular localization. Namely, we predict that class II CKXs (variable triplet: NRV) are mainly localized to the cytoplasm, class III (variable triplet: RME) and VII (variable triplet: RDG triplet) to the endoplasmic reticulum, class VI (variable triplet: HGE triplet) to the extracellular space, and class VIII (variable triplet: HKA) to the vacuole. This trend shows that the CKXs with the VEGAS position occupied by glutamate, which efficiently cleave CK nucleobases, are likely localized to compartments where CK nucleobases interact with the CHASE domain of the HK receptors, suggesting that these CKX classes regulate CK signalling by cleaving the biologically active CK form at the site of its action.

We were intrigued to see whether the extracellular class VI CKX isoforms are also present in the xylem and whether they directly regulate the CK flow from roots to shoots. Moreover, considering the assumed specificity of the extracellular CKXs towards CK nucleobases, CKX in the xylem could also be partially responsible for the inability of root-borne tZ to trigger physiological responses in the shoot apex (Sakakibara, 2021). We demonstrate that CKX is active in the xylem sap of several plant species. We further work with the oats since we can detect relatively high CKX activity in its xylem as early as twelve days after germination. We compare substrate specificities of the CKX in oat xylem sap, root, and leaves and show that CKX from the xylem sap and roots prefer tZ over cZ, in contrast to the CKX from leaves (Figure 4 in the manuscript). We identify 27 putative *AsCKX* genes in the oat genome (Kamal et al., 2022) and examine their expression profiles in publicly available transcriptomic datasets. Quantification of the transcriptomic data shows that the predominant *AsCKX* isoforms expressed in oat roots belong to the extracellular class VII (isoforms AsCKX1a, c, and d) and isoforms expressed in leaves to the cytoplasmic class II (isoforms

AsCKX10a, c, and d) (Figure 5 in the manuscript). These expression patterns, in combination with the substrate specificities of CKX from different parts of the plant, imply that cytoplasmic and extracellular CKXs differ in their preferences for tZ and cZ as substrates, which is consistent with previous reports (Šmehilová et al., 2009; Zalabák et al., 2014).

Our results thus indicate that the CKX isoforms responsible for CKX activity in the xylem sap are AsCKX1s and that they are synthesized in roots and subsequently secreted to the xylem. We support this conclusion by showing that most CKX enzymes in the xylem sap are glycosylated and that the AsCKX isoforms predicted to have the most glycosylation sites are AsCKX1s. This finding is consistent with the characteristic glycosylation of the extracellular ZmCKX1 (Franc et al., 2012).

Lastly, we investigate whether CKX activity in the xylem saps responds to changes in nitrate supply and whether the CKX-catalysed cleavage of CKs in the xylem is a part of the mechanism regulating CK distribution between roots and shoots. We show that CKX activity in the xylem sap is proportional to the concentrations of tZ-type CKs in roots and xylem and that both CKX activity and CK concentrations respond to changes in nitrate availability. These results indicate that CK flux from roots to shoots responding to nitrate supply upregulates CKX activity in the xylem.

Personal contribution: I performed the bioinformatical analyses, annotated the putative *AsCKX* genes in the oat genome and quantified the publicly available transcriptomic data. I wrote the manuscript draft and designed the figures.

Cytokinin Dehydrogenase in Xylem Sap: A Direct Link Between Cytokinin Metabolism and Long-Distance Transport

Running head: CKX in xylem sap mediates CK response to nitrate

Authors: Daniel Nedvěd[1,2†], Václav Motyka[1†], David Kopečný[3], Pierre Briozzo[4], Martin Černý[5], Federica Brunoni[6], Karel Müller[1], Ivana Raimanová[7], Petre I. Dobrev[1], and Klára Hoyerová[1*]

[1] Laboratory of Hormonal Regulations in Plants, Institute of Experimental Botany of the Czech Academy of Sciences, Rozvojová 263, 165 00, Prague, Czechia

[2] Department of Experimental Plant Biology, Faculty of Science, Charles University, Viničná 5, 128 44, Prague, Czechia

[3] Department of Experimental Biology, Faculty of Science, Palacký University, Šlechtitelů 27, Olomouc, 779 00, Czechia

[4] INRAE, AgroParisTech, Université Paris-Saclay, Institut Jean-Pierre Bourgin (IJPB), Route de Saint Cyr, F-78026, Versailles, France

[5] Department of Molecular Biology and Radiobiology, Faculty of AgriSciences, Mendel University in Brno, Brno, 613 00, Czechia

[6] Laboratory of Growth Regulators, Faculty of Science, Palacký University & Institute of Experimental Botany of the Czech Academy of Sciences, Šlechtitelů 27, Olomouc, 783 71, Czechia.

[7] Department of Sustainable Arable Land Management and Cropping Systems, Crop Research Institute, Drnovská 507, 161 06 Prague, Czechia

[*] Author for correspondence: hoyerova@ueb.cas.cz

Laboratory of Hormonal Regulations in Plants, Institute of Experimental Botany of the Czech Academy of Sciences, Rozvojová 263, 165 00, Prague, Czechia

[†] These authors contributed equally to this manuscript.

Keywords

Avena sativa, cytokinin dehydrogenase, cytokinin metabolism, cytokinin oxidase, CKX, sequence-based prediction, nitrate, xylem sap

Abbreviations

ABA	abscisic acid
At	mouse-ear cress (*Arabidopsis thaliana*)
Av	oats (*Avena sativa*)
CK	cytokinin
CKX	cytokinin dehydrogenase/oxidase
cZ	*cis*-zeatin
DHZ	dihydrozeatin
FAD	flavine adenine dinucleotide
GO	gene onthology
HPLC	high-pressure liquid chromatohraphy
IAA	indole-3-acetic acid
iP	isopentenyl adenine
iPR	isopentenyl adenosine
LC	liquid chromatography
LOG	LONELY GUY
Lu	flax (*Linum usitatissimum*)
MS	mass spectrometry
NCBI	National Center for Biotechnology Information
NIA	nitrate reductase
NPF	NTR1 / PTR FAMILY
PDB	protein data bank
RMSD	root-mean square deviation
tSNE	t-distributed stochastic neighbour embedding
tZ	*trans*-zeatin
tZR	*trans*-zeatin riboside
Zm	maize (*Zea mays*)

Abstract

Metabolic degradation of plant hormones cytokinins (CKs) co-regulates their homeostasis and signalling. In this work, we employed a large-scale bioinformatical analysis to address a diversity of cytokinin oxidase/dehydrogenase (CKX) substrate specificities previously described in several case studies. We present a three-way correlation of the entire CKX amino acid sequences, a variable motif involved in substrate binding, and subcellular localizations predicted by a deep learning

model. This correlation is conserved in monocotyledonous plants, suggesting that the CKX diversity in a single species allows a precise tuning of the CK homeostasis. Following these findings, we detected CKX activity in xylem sap for the first time, using the oat (*Avena sativa*) as a model plant. Further investigation of the substrate specificity and glycosylation of this xylem-located CKX suggested that it originates in roots. We have identified 27 putative CKXs in oats and attributed the xylem-located activity to the extracellular isoforms AsCKX1a,c,d. Finally, we show that the xylem-located CKX activity responds to the nitrate supply, highlighting its physiological relevance. Taken together, we show that CKX directly modulates root-to-shoot CK translocation through metabolic degradation of the transported CKs.

Introduction

Cytokinins (CKs) are a group of structurally related molecules derived from adenine through substitution on the N6 atom. They act as plant hormones – a subset of plant signalling molecules regulating diverse aspects of plant growth and development (Kieber and Schaller, 2014; Wybouw and De Rybel, 2019; Hu and Shani, 2023). Among others, CKs are involved in the complex system mediating the acquisition and distribution of nitrate, a nitrogen source for plants (Abualia, Riegler and Benkova, 2023). Long-distance transport of CKs from roots to shoots via xylem bears information about nitrate availability in soil, and CKs transported this way are responsible for nitrate assimilation in the shoot (Kiba *et al.*, 2011; Poitout *et al.*, 2018; Roy, 2018; Sakakibara, 2021). CKs further modulate root architecture and expression of nitrate transporters, thus affecting nitrate uptake efficiency (Kiba *et al.*, 2011; Kiba and Krapp, 2016; Varala *et al.*, 2018; Jia and Von Wirén, 2020; Tessi *et al.*, 2020, 2023). Simultaneously, plants regulate CK distribution and activities of enzymes involved in CK biochemistry in response to nitrate availability (Takei *et al.*, 2001, 2004; Maeda *et al.*, 2018; Poitout *et al.*, 2018).

The proper CK signalling depends on processes both maintaining and altering CK equilibrium – transport and conversions between biologically active (i.e. capable of binding to their receptors) and inactive CK forms (reviewed by Kieber and Schaller, 2014; Hluska, Hlusková and Emery, 2021; Nedvěd et al., 2021; Hu and Shani, 2023). The latter consists of a series of biochemical reactions, of which this paper focuses on CK oxidative degradation catalyzed by cytokinin dehydrogenase (CKX; EC 1.5.99.12; also known as cytokinin oxidase or cytokinin oxidase/dehydrogenase). The CKX reaction involves two steps. Firstly, the CK forms a stable oxidized intermediate with an extra double bond compared to the reactant (Popelková *et al.*, 2006; Kopečný *et al.*, 2008, 2016). An electron pair moves from the reactant to the cofactor flavin adenine dinucleotide (FAD) covalently bound to the CKX apoenzyme (Frébortová *et al.*, 2004; Malito *et al.*, 2004). Secondly, the intermediate undergoes hydrolysis, yielding adenine (or its conjugated form, such as adenosine) and

an aldehyde derived from the original N6 substituent (Rhea database accession: 13625) (Pačes, Werstiuk and Hall, 1971; Brownlee, Hall and Whitty, 1975; Hare and van Staden, 1994). CKX thus cleaves the bond between the N6 atom and its substituent.

CKX amino acid sequences contain several residues directly involved in cofactor or substrate binding. Their mutations gravely affect the catalytic properties of the enzyme. A histidine residue found in a conserved motif GSH binds the FAD cofactor and is essential for enzyme activity and stability (Kopečný *et al.*, 2016). An aspartate residue from a conserved motif WTDYL subtracts a hydride from the substrate in the catalytic process (Malito *et al.*, 2004; Kopečný *et al.*, 2016). Several other residues co-determine the shape of the enzyme's binding cavity and provide differential accommodation for various CK species (Kopečný *et al.*, 2016). A semi-conserved motif FL**X**RV**XXX**E (with "**X**" denoting a variable residue) is found along the entrance to the binding cavity, and its penultimate residue accounts for the substrate specificities of different CKX enzymes. A glutamate residue in this position interacts with N9 atoms of CK nucleobases and stabilizes them in the binding cavity. Glutamate-containing variants of CKX, such as maize CKX1 (ZmCKX1) or Arabidopsis CKX2,4 (AtCKX2,4), thus strongly prefer CK nucleobases and also display relatively high enzyme activities *in vitro.* Conversely, when the non-conserved residue is less bulky or polar, the corresponding CKXs are more promiscuous towards CK ribosides and monophosphates, and their enzyme activities are lower (Malito *et al.*, 2004; Frébortová *et al.*, 2007; Galuszka *et al.*, 2007; Kopečný *et al.*, 2016). Other authors have also shown that CKX substrate specificities and enzyme activities correlate with the respective enzyme's subcellular localizations (Šmehilová *et al.*, 2009; Kowalska *et al.*, 2010; Zalabák *et al.*, 2014). Considering sequences of the differentially localized CKXs isoforms studied in these works, one can see correlations among the subcellular localizations and the identity of the variable ligand-binding residue mentioned above.

CKX enzymes also participate in the cross talk of CKs and nitrogen (Reid *et al.*, 2016; Gigli-Bisceglia *et al.*, 2018). Given the specific roles of different CKX forms reported in the works cited earlier, it has intrigued us whether it is possible to pinpoint CKXs regulating the amount and quality of CKs transported from roots to shoots in response to the nitrogen availability in the environment. CKX-mediated regulation of CK long-distance flux has already been suggested (Yang, Yu and Goh, 2002; Brugière *et al.*, 2003; Hoyerová *et al.*, 2007), but the issue has remained unresolved until nowadays. Based on preliminary data, we hypothesize that some CKX proteins are active in the xylem sap and directly affect CKs transported from roots to shoots. Connecting this CKX activity to a CKX isoform with particular substrate specificity would allow us to discuss how CK degradation shapes their long-distance flux and thus information about the nitrogen availability.

Results

Similar CKX Proteins Share a Non-Conserved Sequence Involved in Substrate Binding

Before exploring the relationship between CKX activity and the long-distance transport of CKs, we performed a large-scale bioinformatic analysis of CKX sequences to establish their classification according to their biochemical properties.

To determine whether sequentially similar CKXs share common identities of the ligand-binding variable motifs, we considered 492 CKX sequences from various monocotyledonous species (see Table S1 for the complete list). Through multi-sequential alignment and subsequent dendrogram construction, we identified eight major clusters of sequentially close CKXs (the dendrogram is available in Newick format in Supplementary File 1). For this work, we named these clusters CKX classes I-VIII. We found out that proteins from each class share a specific composition of the non-conserved triplet within the FL**X**RV**XXX**E motif (which comprises, for instance, residues 374-382 in the sequence of ZmCKX1). These characteristic triplets are H**X**S (class I), NRV (class II), RME (class III), H**X**G (class IV), **XX**E (class V), HGE (class VI), RDG (class VII), and HKA (class VIII).

The third residue of this non-conserved triplet can directly interact with the CKX's substrate and at least partially determines the substrate specificity. As we show, this ligand-binding variable residue is in most cases valine, glutamate, glycine, alanine, or serine (Figure 1). For simplicity, we will refer to the non-conserved triplet as the "entrance triplet" (because it is located) and its third residue as the "VEGAS residue" (based on the five most abundant amino acids).

We show that the amino acid composition of the entrance motif correlates with the sequential similarity of CKXs from diverse species and at the same time contains the VEGAS residue, which co-determines the CKX substrate specificity. These findings imply that the possession of several CKX isoforms with slightly different substrate preferences, as show for maize (Šmehilová *et al.*, 2009), Arabidopsis (Kowalska *et al.*, 2010) or rice (Zheng *et al.*, 2023), is a general rule, suggesting that the CKX diversity is a conserved aspect allowing for fine modulation of CK homeostasis.

Crystal Structure of ZmCKX5 Supports the Role of VEGAS Residue in Ligand Recognition

The contribution of VEGAS residue on the shape of the CKX active site and its capability to interact with the substrate (or the lack thereof) can be observed on the enzyme's crystal structures. Up to date, there are publicly available structures of CKXs with the VEGAS position occupied by

serine (ZmCKX2) (Kopečný *et al.*, 2016), glutamate (ZmCKX8 and ZmCKX1) (Malito *et al.*, 2004; Nisler *et al.*, 2021), alanine (ZmCKX4a) (Kopečný *et al.*, 2016), and valine (AtCKX7 and LuCKX7 from flax) (Bae *et al.*, 2008; Wan *et al.*, 2019) and flax CKX7 (LuCKX7) (Wan *et al.*, 2019). These structual studies have revealed that a glutamate at the VEGAS position directly contributes to binding of CK nucleobases, while alanine, valine, and serine do not, suggesting a specific role of glutamate-containing CKXs in degradation of this CK form. However, no such information has been available for glycine-containing isoforms so far.

Here we present the structure of glycine-containing ZmCKX5 (refined up to 1.65 Å resolution, full refinement statistics is given in Table S2), available via Protein Data Bank (PDB) under the code 8QVT. Superimposing the structure of ZmCKX5 onto the structure of ZmCKX1 shows that the proteins are very similar, with root-mean-square deviation (RMSD) values of ~ 1.0 Å and sequence identity of 59 %. Just like other CKX structures, ZmCKX5 displays a classical two-domain topology and carries a covalently linked FAD (for more detail on the structural analysis, see Supplementary File 2). Compared to ZmCKX1, ZmCKX5 is more ordered at the N-terminus where an additional helix can be observed (Figure 2A). Superimpositions of the active sites of the known CKX proteins, together with the ZmCKX5 structure reported here, show that a glycine residue in the VEGAS position doesn't directly interact with *trans*-zeatin (tZ), a CK nucleobase, located in its previously reported position within the CKX active site (Malito *et al.*, 2004) (Figure 2B-D). In other words, our results pinpoint that CKXs with the VEGAS position occupied by a glutamate are likely specialized in cleavage of CK nucleobases, given the formation of additional interactions between the VEGAS glutamate and the substrate.

Sequentially Similar CKX Proteins Share Predicted Subcellular Localizations

In this paper, we have previously reported that sequentially similar CKX classes are characterized by the common entrance triplet, which contributes to the the substrate specificity of the given CKX through the VEGAS residue. Other studies have shown that the differential substrate specificity of CKX enzymes can be linked with the diversity in their subcellular localizations (Šmehilová *et al.*, 2009; Kowalska *et al.*, 2010; Zalabák *et al.*, 2014). Taken together, these findings suggest that different CKX classes, each with their substrate preferences, might also act in specific cellular compartments. So, as the next step, we investigated the correlations between the CKX classification and subcellular localization.

Due to the sparse knowledge of the actual subcellular localizations of the CKX proteins in our dataset, we had them predicted by DeepLoc software (Thumuluri *et al.*, 2022). For each sequence, we obtained prediction scores for ten compartments. To visualize correlations between the CKX

classification and their predicted subcellular localizations, we transformed the DeepLoc scores from 10-dimensional to 2-dimensional space using the t-distributed stochastic neighbour embedding (tSNE) method (van der Maaten and Hinton, 2008). Figure 3A shows the CKX sequences in the transformed space. The plot reveals that class I (H**X**S), II (NRV), VI (HGE), and VIII (HKA) CKXs form distinct clusters. It means the proteins from each of these classes are likely localized in the same compartment. Notably, the class II cluster lies far from the others in the plot, suggesting unique subcellular localization. Less coherent clusters are formed by class III (RME), V (**XX**E), and VII (RDG) CKXs. Finally, class IV CKXs (H**X**G) do not form any cluster and thus probably do not share any characteristic subcellular localization.

Class II CKXs are predicted to be found mainly in the cytoplasm, classes III and VIII CKXs in the ER, and classes V and VIII CKXs in the vacuole. No predominant localization can be assigned to the class I CKXs, although they are unlikely to be found in cytoplasm. Localizations of class IV CKXs show no clear trend, which is in agreement with their lack of clustering in the tSNE-transformed space (Figure 3B-E).

The predictions presented in this part show that the differential subcellular localizations of CKXs with different substrate specificities (co-determined by the VEGAS residue) is a conserved trend, further supporting our previous notion that possessing CKXs of various classes allows their specialization in the overall maintenance of the CK homeostasis.

CKX is Active in Xylem Sap and Displays Substrate Specificity Characteristic for the Root-Derived CKX Isoforms

CKs act as messengers travelling from roots to shoots via xylem, i.e. continual apoplastic space. As shown in previous studies, some CKX isoforms are secreted into the apoplast and are active there (Kowalska *et al*., 2010; Šmehilová *et al*., 2009). In this paper, we have shown that a large group of DeepLoc-predicted extracellular CKXs (class VI) contain a glutamate residue at the VEGAS position and thus likely cleave CK nucleobases with high efficiency. All these facts has lead us to hypothesise that the glutamate-containing CKXs from class VI are active in xylem, which might be a way for plants to regulate the root-to-shoot CK flux. What's more, the activity of class VI CKXs in the xylem sap might be at least partly responsible for the absence of nucleobases among root-to-shoot transported CKs (Osugi *et al.*, 2017; Sakakibara, 2021).

To explore the potential role of CKX in xylem, we measured CKX activity in xylem sap samples from the maize, oat, barley, and wheat. We found the highest CKX activities in maize and oats (Figure 4). We chose the latter for further experiments for two reasons: manipulation with oat plants is less demanding, and we could detect CKX activity in oat xylem sap as early as twelve days after germination.

To further characterize the CKX in xylem, we measured CKX activities in samples isolated from oat xylem sap, oat roots, oat leaves, wheat roots, and wheat leaves. For each sample, we measured activities with three different CK nucleobases: isopentenyl adenine (iP), *trans*-zeatin (tZ), and *cis*-zeatin (cZ). In all sample types, iP was the preferred substrate. CKXs obtained from the oat and wheat roots also favoured tZ over cZ. The same trend applied to CKX from the xylem sap, albeit the difference in activities towards the two zeatins was smaller. Conversely, the leaf CKXs preferred cZ over tZ (Figure 4).

Previous substrate specificity studies on maize CKXs have shown that cZ is preferred over tZ by class V ZmCKX8,9 and class II ZmCKX10; conversely, class VI ZmCKX1 favours tZ over its *cis* counterpart (Šmehilová *et al.*, 2009; Zalabák *et al.*, 2014). This fact, together with the previously reported extracellular localization of ZmCKX1 (Šmehilová *et al.*, 2009; Zalabák *et al.*, 2016), and the similar substrate preferences of the CKX from oat xylem sap, oat roots, and wheat roots (Figure 4) suggest that proteins responsible for the CKX activity in oat xylem are synthesized in roots and homologous to ZmCKX1.

Oat Homologues of ZmCKX1 are Predominantly Expressed in Roots

To provide evidence for the putative role of ZmCKX1 oat homologues in CKX activity in the xylem sap, we first needed to identify and characterize oat *CKX* genes overall. In the annotated oat genome, we found 36 putative *CKX* genes (Kamal *et al.*, 2022; Tinker *et al.*, 2022). Four of them can be expressed in two alternatively splicing variants. Having excluded likely pseudo-genes, we narrowed this list to 27 *AsCKX* isoforms and named them based on their homology with ZmCKXs (see Material and Methods for details). We performed a multi-sequential alignment of the corresponding AsCKX proteins with their maize counterparts. The dendrogram in Figure 4 shows that AsCKXs belong to CKX classes I, II, III, VI, VII, and VIII; ZmCKXs additionally include class V CKXs. We found three oat homologues of ZmCKX1, namely AsCKX1a,c,d; all three belong to class VI and have a glutamate at the VEGAS position.

We have previously hypothesized that the oat homologues of ZmCKX1, i.e. AsCKX1s, are mainly synthesized in roots and secreted into xylem sap. To support this hypothesis, we quantified publicly available *AsCKX* transcript reads in oat leaves, stems, roots, and the pooled samples. In addition, we performed RNA sequencing in our own samples of oat leaf blades and included the data obtained in this way in our analysis. We have found that *AsCKX1s* and *AsCKX4s* are the dominant *CKX* isoforms expressed in roots, followed by three class I *AsCKX2s*. The most expressed forms in the leaves and stems were class II *AsCKX10s*, followed by the remaining *AsCKX2s*, some class III *AsCKX6s*, and *AsCKX4s*. As already implied, the six *AsCKX2s* display two distinct expression

patterns. *AsCKX2a.1,a.2,d.1* are slightly expressed in leaves, while *AsCKX2a.3,d.2,d.3* in stems and roots. The latter are expressed slightly more than the former in the pooled samples (Figure 5).

The prevalent expression of AsCKX1s in roots supports the hypothesis that they are synthesized there and then secreted into the xylem.

AsCKX Proteins in Oat Xylem Sap are Glycosylated

Another characteristic feature of ZmCKX1, besides its subcellular localization and substrate specificity, is its glycosylation pattern. ZmCKX1 is *N*-glycosylated at six positions with 3-25 hexose-long oligosaccharides, more than other CKXs in maize. This glycosylation enhances the enzyme activity and thermal stability of ZmCKX1 (Malito *et al.*, 2004; Kopečný *et al.*, 2008, 2010; Franc *et al.*, 2012). It follows that if the CKX proteins in oat xylem are indeed homologues of ZmCKX1, they are expected to be glycosylated to the similar extent.

To determine the glycosylation of CKX in oat xylem sap, we used Concanavalin A Sepharose 4B chromatography, which allows us to separate glycosylated and non-glycosylated proteins. Most CKX activity in the xylem sap (~ 87 %) was associated with the glycosylated isoforms (Figure 6), in agreement with the extended *N*-glycosylation of ZmCKX1 reported before (Franc *et al.*, 2012). To see whether this glycosylation is possible for AsCKX1s (and thus whether their presence in the xylem sap is consistent with our findings), we used NetNGlyc software (Gupta and Brunak, 2002) to predict *N*-glycosylation sites in the sequences of AsCKXs and ZmCKX1, for which we could compare the predicted sites with those determined experimentally (Franc *et al.*, 2012).

Class VI AsCKX1s and ZmCKX1 contain 4-6 predicted *N*-glycosylation sites, compared to 2-4 sites for class I, one site for class VII and VIII AsCKXs, and no site for class II and III AsCKXs. The seemingly missing sites in the AsCKX1d sequence might be due to the incomplete annotation of the *AsCKX1d* gene, which is also indicated by the relatively shorter length of the AsCKX1d protein sequence (see Table S3). NetNGlyc predicted five of the six experimentally *N*-glycosylation sites of ZmCKX1. The only exception was N294, although the corresponding residues in some AsCKXs were predicted as *N*-glycosylated with satisfactory confidence. Two predicted *N*-glycosylation sites are conserved among class II and VI CKXs, and one additional site among CKXs of classes II, VI, and VII. Interestingly, the different expression patterns of AsCKX2s (Figure 5) also reflect the predicted *N*-glycosylation patterns. The one *N*-glycosylation site predicted for class VIII AsCKXs is unique for them (Figure 6).

These predictions indicate a broad glycosylation of AsCKX1s. Together with the data on CKX glycosylation in the xylem, they support the hypothesis that AsCKX1s are mainly responsible for the CKX activity in the xylem sap.

The CKX Activity in the Xylem Sap Responds to the Increase of the CK Flux Induced by Nitrate Supply

Due to their role in the regulation of CK signalling, expression of *CKX* genes is up-regulated by CKs (Brenner *et al.*, 2012; Gao *et al.*, 2014; Zhou *et al.*, 2020). Therefore, we have expected that an increase of the CK flux from roots to shoots results in higher enzyme activity of CKX in the xylem sap. It has been known that the CK root-to-shoot flux is positively regulated by nitrate supply (Takei *et al.*, 2001, 2004; Poitout *et al.*, 2018; Sakakibara, 2021), which implies that the external nitrate should affect the CKX activity in the xylem sap as well. Showing so would demonstrate that plants actively regulate secretion of CKX proteins to the xylem and that the CKX activity in xylem sap reported in this work has its physiological relevance, rather than being an artefact.

We therefore grew oat plants, supplied them with increasing concentrations of nitrate (16.0, 62.5, 250.0, and 1000.0 µM), and subjected them to various analyses. Firstly, we measured concentrations of different CK types (grouped according to the chemistry of their side chains) in the oat xylem sap, roots, and leaves. In each measurement, tZ-type CKs were the most abundant, followed by cZ-type, iP-type, and dihydrozeatin-type (DHZ-type). The last was detected in the roots and leaves but not the xylem sap. The concentrations of the tZ-type CKs visibly responded to the external nitrate. However, this response was not monotonous. When the nitrate concentration increased from 16.0 to 62.5 µM, the concentration of tZ-type CK in the xylem sap and roots decreased. With further increase in the nitrate concentration, the concentration of tZ-type CKs grew again, eventually surpassing the concentration measured at 16.0 µM nitrate (Figure 7A-C).

Next, we determined the CKX activity in the oat xylem sap. Figure 7D shows that when measured at two pH values (8.5 and 5.1), the CKX activity followed the same trend as previously observed for CK concentrations in the xylem sap (i.e. an initial drop to a minimum followed by an increment).

To ensure that the difference in nitrate supply in the nutrient solution corresponds to the nitrate amounts within the oat plants, we measured nitrate concentrations in oat roots, leaves, and xylem sap, as well as the enzyme activity of nitrate reductase (NIA) in roots and leaves. The results (Figure 7E,F) show that both the nitrate concentration and the NIA activity increase with the external nitrate supply.

We also measured concentrations of two other plant hormones besides CKs, auxin indole-3-acetic acid (IAA; Figure 7G) and abscisic acid (ABA; Figure 7H). IAA in roots behaved similarly to CKs, with the lowest concentrations at 62.5 µM nitrate. ABA showed a similar trend in the xylem sap but a reverse trend in the roots and leaves (i.e. highest concentrations at 62.5 µM nitrate).

These findings indicate that the increase in the CK root-to-shoot flux in response to the nitrate supply is followed by the increase of CKX activity in the xylem and that CK degradation in the xylem is thus regulated.

Material and Methods

Bioinformatical Analysis of CKX Sequences

Known monocot CKX sequences were retrieved from the National Center for Biotechnology Information (NCBI) Identical Protein Groups database (Sayers *et al.*, 2022) (accessed on the 14 February 2023). Oat (*Avena sativa*) CKX sequences were retrieved from the annotated oat cv. Sang reference genome v1.1 (Kamal *et al.*, 2022; Tinker *et al.*, 2022). We selected genes annotated by gene ontology term GO:0019139 (Ashburner *et al.*, 2000; The Gene Ontology Consortium *et al.*, 2023) or by human-readable descriptors containing the sub-strings “cytokinin” followed by “dehydrogenase” or “oxidase”. Conserved domains in the selected genes were translated from nucleotide to protein sequences using the ExPASy translate tool (Gasteiger *et al.*, 2003).

Oat CKXs were named according to their homology with maize (*Zea mays*). Because of the smaller number of ZmCKXs in comparison with AsCKXs, each AsCKX was also identified with the letter “a”, “c”, or “d”, according to its membership in one of the three *A. sativa* chromosome groups (Tomaszewska, Schwarzacher and Heslop-Harrison, 2022). AsCKXs sharing the closest maize homologue and the chromosome group were further annotated with numbers ranging from one onwards.

All multi-sequence alignments presented in this work were generated using MAFFT software with the option --auto (Katoh and Standley, 2013). Tree graphs were generated from the multi-sequence alignment files using IQ-TREE software (Nguyen *et al.*, 2015) with options -st AA, -m TEST, -bb 1000, -alrt 1000 and visualized using the Python package ETE (Huerta-Cepas, Serra and Bork, 2016).

Sequence-Based Predictions

The subcellular localizations of CKX proteins were predicted using DeepLoc (Thumuluri *et al.*, 2022) with ProtT5-XL-Uniref50 transformer (Elnaggar *et al.*, 2022) (denoted as "high quality model" in the DeepLoc web service). For visualization, the prediction scores were transformed from ten-dimensional to two-dimensional space via t-distributed stochastic neighbour embedding (van der Maaten and Hinton, 2008). Glycosylation patterns of CKX proteins were predicted using NetNGlyc (Gupta and Brunak, 2002).

RNA Sequencing and Quantification

Total RNA was isolated from 50–100 mg of 12 day-old plant material using FavorPrep Plant Total RNA Purification kit (Favorgen) and treated with rDNAse (Macherey-Nagel). RNA purity, concentration and integrity were assessed with the RNA Nano 6000 Assay Kit using a Bioanalyzer instrument (Agilent Technologies). For RNA-seq analysis, approximately 5 µg of RNA were submitted for the service procedure provided by the Institute of Applied Biotechnologies. The analysis yielded at least 15 million 150 bps read pairs. Publicly available raw transcripts were accessed via the NCBI Sequence Read Archive (Sayers *et al.*, 2022) and the European Nucleotide Archive (Leinonen *et al.*, 2011). Namely, we used data from projects PRJEB46365 (runs ERR6323384-86), PRJNA916004 (runs SRR22937051-62), PRJNA809080 (runs SRR18094446-57), and PRJNA794002 (runs SRS11553144-65).

Rough reads were quality-filtered using Rcorrector and Trim Galore scripts (Song and Florea, 2015). Transcript abundances were determined using Salmon (Patro *et al.*, 2017) with options --posBias, --seqBias, --gcBias, --numBootstraps 30. The reference index was built from the *A. sativa* v1.1 transcript dataset.

Crystallization and Structure Refinement of ZmCKX5

The *ZmCKX5* gene (Phytozome ID Zm00001d008862) was cloned into a pTYB12 vector and expressed in T7 Express *Escherichia coli* cells (New England Biolabs) at 18 °C overnight. Protein was purified by chitin-based affinity chromatography upon elution with 50 mm DTT to cleave the intein tag and further by gel permeation chromatography on a Superdex S200 column using the NGC liquid chromatography system (Bio-Rad). ZmCKX5 (23 mg mL-1) in 50 mM Tris-HCl, pH 8.0, was crystallized in the condition found using the NeXtal PEGII Suite (Qiagen) containing 0.2 M Li_2SO4, 0.1 M Tris-HCl pH 8.5, 30 % PEG 3000. Crystals were cryoprotected with 15 % glycerol and flash-frozen in liquid nitrogen. Diffraction data were collected at 100 K on the Proxima 2 beamline at the SOLEIL synchrotron (Saint-Aubin, France) at 1.65 Å resolution. Intensities were integrated using the XDS program (Kabsch, 2010). Data quality was assessed using the correlation coefficient *CC*1/2 (Karplus and Diederichs, 2012). The crystal structure of ZmCKX5 was determined by performing molecular replacement with Phaser (Storoni, McCoy and Read, 2004) using a monomer of ZmCKX1 (PDB ID 2QKN) as a search model (Kopečný *et al.*, 2010). The model was refined with BUSTER-TNT (Bricogne *et al.*, 2017), and electron density maps were evaluated using COOT (Emsley and Cowtan, 2004). Structure quality was validated using MolProbity (Chen *et al.*, 2010). Molecular graphics were generated using PyMOL (Schrödinger, LLC, 2015).

Plant Material and Growth Conditions

For the determination of nitrate and CK concentrations and CKX activity, oat plants were grown hydroponically for 12 days in a growth room with 21 °C/15 °C day/night air temperature and 16 h photoperiod (photon flux of 400 µmol m^{-2} s^{-1}). Continuously aerated nutrient solution contained 158 µM $Ca(NO_3)_2$, 70.8 µM KNO_3, 52.5 µM KH_2PO_4, 41.3 µM $MgSO_4$, 47.5 µM KCl, 2.5 µM H_3BO_3, 2 µM Fe-EDTA, 0.2 µM $ZnSO_4$, 0.2 µM $MnSO_4$, 0.05 µM $CuSO_4$, and 0.01 µM $(NH_4)_6Mo_7O_{24}$. For each treatment, 200 L of nutrient solutions were used, corresponding to 2 L per plant. The nutrient solution was changed weekly, and the nitrate concentration was checked and adjusted every other day. Two days before the sampling, the plants were twice transferred to fresh nutrient media containing 16.0, 62.5, 250.0 or 1000.0 µM nitrate and kept there for a day. Missing Ca^{2+} and K^+ were supplied in the form of $CaCl_2$ and KCl.

For other experiments, plants were soaked for 14 h in aerated distilled water and then sown on perlite saturated with double-concentrated Knop's nutrient solution. Plants were grown in a controlled climate growth chamber (Sanyo MLE-350H) at 20 ºC/18 ºC day/night temperature, 80 % air humidity, and 16 h photoperiod with a photon flux density of 300 µmol m^{-2} s^{-1}. Unless stated otherwise, plants were grown for 12 days or until they had two fully developed leaves and one emerging.

Sampling of Xylem Sap, Roots and Shoots

For xylem sap collection, shoots were excised with a razor blade approximately 0.5 cm above the shoot-to-root transition. The excision was performed three hours after the lights went on in the cultivation chamber. The xylem sap released during the first 15 min was discarded. During the following two hours, the sap drops were collected, immediately cooled and kept on ice in closed tubes. Collected sap samples were frozen in liquid nitrogen and stored at -80 °C. Shoots and roots were collected at the same time when the shoots were excised for the collecting of xylem sap, they were frozen in liquid nitrogen and stored under the same conditions.

Determination of Nitrate Content

Leaf and root samples (1 g of fresh weight) were homogenized in liquid nitrogen, extracted with deionized water for 30 min at 90 °C, and filtered. Nitrogen concentrations in plant extracts, nutrient solutions, and xylem sap were determined spectrophotometrically using Skalar San plus analyser (Breda, the Netherlands). The samples were passed through a column of granulated copper-cadmium to reduce nitrate to nitrite. The nitrite was determined spectrophotometrically by measuring the conversion of sulfanilamide and *N*-(1-naphthyl)ethylenediamine dihydrochloride to an azo dye at 540 nm.

Measurement of NIA Activity

Leaf and root samples (1 g of fresh weight) were homogenized in liquid nitrogen and treated with 5 mL of 50 mM Tris-HCl buffer, pH 8.0, containing 3 % bovine serum albumin at 4 °C for 30 min. Insoluble material was removed via centrifugation (1500 × g, 30 min). The NIA activity was determined by measuring the conversion of nitrate to nitrite according to (Gaudinová, 1983).

Cytokinin Analysis

CK-containing fractions were isolated from plant samples via dual-mode solid phase extraction (Dobrev and Kamínek, 2002). CK detection and quantification were carried out using LC/MS/MS system consisting of HTS-Pal auto-sampler with a cooled sample stack (CTC Analytics, Zwingen, Switzerland), Rheos 2200 quaternary HPLC pump (Flux Instruments, Basel, Switzerland), Delta Chrom CTC 100 Column oven (Watrex, Prague, Czechia), and TSQ Quantum Ultra AM triple-quad high-resolution mass spectrometer (Thermo Electron, San Jose, USA) equipped with an electrospray interface. The mass spectrometer was operated in the positive single-reaction monitoring mode.

Measurement of CKX Activity

The CKX activity was measured by an *in vitro* radioisotope assay based on the conversion of [2-^{3}H]iP (prepared by the Isotope Laboratory of the Institute of Experimental Botany AS CR, Prague, Czechia) to [^{3}H]adenine (Motyka *et al.*, 2003). The xylem exudate (20 μL per assay) was used without previous purification. Protein concentration in the xylem sap was determined according to Bradford (1976) using bovine serum albumin as a standard. The substrate and the product were separated as described by Gaudinová et al. (2005). To determine CKX substrate specificity, [2-^{3}H]iP was replaced with [2-^{3}H]tZ or [2-^{3}H]cZ in the standard assay mixture (Gajdošová *et al.*, 2011). All radio-labelled substrates were used at a concentration of 2 μM and a molar activity of 7.4 Bq mol^{-1}.

Determination of CKX Glycosylation

The glycosylation state of CKX in oat xylem sap was determined by Concanavalin A-Sepharose 4B chromatography (Motyka and Kamínek, 1994; Motyka *et al.*, 1996). In the collected fractions, CKX activity was determined as described above.

Discussion

In this work, we address the multifaceted diversity of CKX as a conserved trait enabling selective and fine-tuned regulation of CK homeostasis. Focusing on monocots, we divided 492 CKXs into

eight classes based on their sequential similarity. This CKX classification correlates with the variance of the VEGAS residue-containing “entrance triplet”, i.e. the three consecutive variable residues of the FL**X**RV**XXX**E motif (with VEGAS being the third of them).

This shows that sequentially closely related CKX isoforms are similar in substrate specificities and enzyme activities. Given that the species included in our analysis possess several CKX isoforms belonging to different classes (Figure 1), the individual isoforms likely play specific roles in the regulation of the CK metabolism rather than being simply redundant (although redundancy among isoforms belonging to the same class remains possible). This hypothesis goes along with the differential affinities of maize CKXs towards various CK substrates. ZmCKX2,3 (class I) and ZmCKX4a,b (class VIII) have shown preference towards CK nucleotides and N9-glucosides, while ZmCKX12 (class III), ZmCKX8,9 (class V), and ZmCKX1 (class VI) preferred CK nucleobases, and ZmCKX10 (class II) and ZmCKX5 (class VII) cleaved some N9-derived CKs similarly to the nucleobases (Šmehilová *et al.*, 2009; Zalabák *et al.*, 2014; Kopečný *et al.*, 2016). The CKX substrate specificity about the N9 substitution has been attributed to the varying character of the VEGAS residue and supported by experimentally solved structures of CKXs from different classes (Malito *et al.*, 2004; Bae *et al.*, 2008; Kopečný *et al.*, 2016; Wan *et al.*, 2019; Nisler *et al.*, 2021). As there has been so far no structural model for a CKX with a glycine at the VEGAS position, we have solved the structure of ZmCKX5 (class VII). The superimpositions depicted in Figure 2 confirm the unique capacity of a glutamate residue to interact with a nucleobase substrate.

CKXs also differ in their specificities towards CKs with varying characters of the N6 substituent (i.e. the side chain). For instance, ZmCKX8,9 strongly preferred cZ and tZ, both CKs with a hydroxylated side chain, over non-hydroxylated iP. Conversely, ZmCKX1 preferred iP and tZ over cZ, and ZmCKX10 cleaved all three substrates at similar rates (Šmehilová *et al.*, 2009; Zalabák *et al.*, 2014, 2016; Kopečný *et al.*, 2016). All these proteins have glutamate at the VEGAS position but belong to different classes, showing that the sequence-based substrate specificity of CKX goes beyond the VEGAS residue. The composition of the entrance triplet likely correlates with other sequential (and consequently structural) features responsible for additional fine-tuning of the protein’s substrate specificity. Finding the sequential/structural base for differential affinity towards CKs with diverse side chains in future research would be another great step in our understanding of CKX-mediated modulation of the CK homeostasis.

The ability of CKXs to discriminate CKs with different N6 and N9 substitutions could also contribute to the varying effects of *OsCKX* mutations on endogenous concentrations of *trans*-zeatin riboside (tZR), iP, and isopentenyl adenosine (iPR) in rice (Zheng *et al.*, 2023). Our results suggest that the diversity of CKX isoforms and their substrate specificities is conserved among the monocot

491 species, if not the plant kingdom as a whole, considering that similar trends were observed in
492 *Arabidopsis* (Frébortová *et al.*, 2007; Galuszka *et al.*, 2007; Kowalska *et al.*, 2010).
493 We also saw a correlation between the CKX classification and the predicted subcellular
494 localizations, further backing the idea of the CKX family consisting of similar yet functionally
495 specialized members. Our *in silico* analysis shows four main trends: class II CKXs (entrance triplet
496 NRV) are predominantly predicted to be localized to the cytoplasm, class III CKXs (entrance triplet
497 RME) to the ER, class VI CKXs (entrance triplet HGE) to the extracellular space, and class VIII
498 CKXs (entrance triplet HKA) to the vacuole (Figure 3). This rough model is consistent with
499 previously determined localizations of ZmCKX1,4a,9,10 or OsCKX3,11 (Šmehilová *et al.*, 2009;
500 Zalabák *et al.*, 2016; Zhang *et al.*, 2021; Huang *et al.*, 2023). On the other hand, the reported
501 subcellular localization of ZmCKX11,12 is vacuolar (Zalabák *et al.*, 2016), while their
502 classification as class III and the presence of RME entrance triplet suggest localization to the ER
503 (Figure 3, 4).
504 Considering the correlations between different substrate specificities and subcellular localizations
505 allows us to discuss the role of CKX in the context of the diverse and tightly regulated CK
506 distribution at the cellular level. We present class II CKXs as the main representatives of CKXs
507 localized to the cytoplasm. With a valine at the VEGAS position, they are equipped for cleavage of
508 conjugated CKs. In addition, we show that class II CKXs in oats, AsCKX10s, are the dominant
509 CKX class in stems and leaves (Figure 5). This is in agreement with the reported expression pattern
510 of the cytoplasmic ZmCKX10 (Šmehilová *et al.*, 2009). It follows that the role of cytoplasmic
511 CKXs may consist in cleavage of CKs travelling from roots to shoots as conjugates. Moreover,
512 given the cytoplasmic localization of LONELY GUY, an enzyme catalysing the final step of the
513 biosynthesis of CK nucleobases (Kurakawa *et al.*, 2007; Kuroha *et al.*, 2009; Chen *et al.*, 2022),
514 populating the cytoplasm with valine-containing CKX isoforms may allow the local CK production
515 in shoots to run independently of the degradation of the CKs transported from roots. This
516 hypothesis assumes existence of membrane transporters facilitating the uptake of conjugated CKs
517 (which are both bulky and polar) from the apoplast into the cells. CKXs isoforms localized to the
518 vacuole (mostly those of class VIII), are equipped for the cleavage of conjugated CKs as well,
519 thanks to the alanine residue at their VEGAS position. Considering the existence of vacuole-stored
520 CKs (Jiskrová *et al.*, 2016), plants might use the CKX-catalysed cleavage to recycle adenine
521 species. Mobilization of adenine derivatives from vacuole is crucial for growth and pollen
522 germination (Bernard *et al.*, 2011). The dominant CKX classes in the ER and extracellular space
523 (classes III and VI, resp.) are characterized with a glutamate at the VEGAS position, implying that
524 they effectively cleave CK nucleobases. Since CK nucleobases are the biologically active CK form
525 and their receptors have been found both on the ER membrane (Wulfetange *et al.*, 2011) and the

plasmatic membrane (Antoniadi *et al.*, 2020), the most apparent role of the class III and VI consists in attenuation of CK signalling via CK degradation. With C*KX* gene expression being positively regulated by CKs (Brenner *et al.*, 2012; Gao *et al.*, 2014; Zhou *et al.*, 2020), the degradation of CK nucleobases can occur as a part of a negative feedback loop.

The extracellular class VI CKXs have also come across as good candidates for proteins catalysing the CKX activity observed in the oat xylem sap. We have supported this notion by showing that the class VI CKXs in oats, namely AsCKX1a,c,d are mainly expressed in roots (Figure 5), as expected for proteins excreted to the xylem and subsequently travelling via the transpiration stream. Moreover, the high *N*-glycosylation potential of AsCKX1s is consistent with the determined glycosylation state of CKXs present in the oat xylem sap (Figure 6). We have further attempted to identify proteins in xylem sap using proteomics. While not providing us with conclusive results, the targeted analysis of peptides suggested the presence of AsCKX1a, AsCKX2d.1, and AsCKX4c (see Table S4-S6). Degradation of CK nucleobases by glutamate-containing CKXs in the xylem might contribute to the fact that CKs transported from roots to shoots are predominantly in the form or ribosides and phosphates (Beveridge *et al.*, 1997; Takei *et al.*, 2001; Sakakibara, 2021).

As summarized in the Introduction, CKs in the xylem act as messengers carrying information about nitrate availability in the environment (Kiba *et al.*, 2011; Ruffel *et al.*, 2016; Poitout *et al.*, 2018; Roy, 2018; Sakakibara, 2021). Given that *CKX* expression is induced by CKs (Brenner *et al.*, 2012; Gao *et al.*, 2014; Zhou *et al.*, 2020), the increase of the CK root-to-shoot flux in response to nitrate should result in the corresponding increase of the CKX activity in the xylem sap. This would be another example of CKX mediating negative feedback on CK signalling (and this time also on CK long distance transport). To confirm this assumption, we examined the changes in CK concentrations and CKX activity in oat plants exposed to different concentrations of nitrate. In agreement with previous findings (Takei *et al.*, 2001; Poitout *et al.*, 2018), we observed a significant response to nitrate among tZ-type CKs, which were the most abundant in our samples. The concentrations of these CKs varied in the oat roots and xylem but not in the leaves, suggesting that the leaves possess mechanisms to compensate for the increased CK influx from the roots (such as degradation of conjugated CKs by cytoplasmic CKXs as discussed above). We also show that the nitrate-dependent changes in CK concentrations in the roots and xylem sap correlate with the changes in the activity of xylem-located CKXs, showing that CKX in the xylem sap indeed responds to concentrations of transported CKs (Figure 7A-D). As described above, we have attributed the xylem-located CKX activity to AsCKX1s, which can cleave biologically active CK nucleobases. An increase in the xylem-located CKX activity might also contribute to a previously observed nitrogen-induced shift in the tZR/tZ ratio in the xylem (Osugi *et al.*, 2017; Sakakibara, 2021).

It is apparent from Figure 7B-D that the responses of root and xylem-located CKs and xylem-located CKX were not monotonous but rather passed through a minimum between the lowest and the highest nitrate concentrations tested. One possible explanation of these trends involves a variable efficiency of nitrate perception depending on the nitrate supply. This property has been attributed to NRT1 / PTR FAMILY 6.3 (NPF6.3) protein, which functions as both a nitrate transporter and receptor (Liu, Huang and Tsay, 1999; Ho *et al.*, 2009; Krouk *et al.*, 2010; Wang *et al.*, 2018). When the nitrate supply increases from low to high, NPF6.3 switches from a high- to a low-affinity state. The molecular mechanism of the switch involves the dephosphorylation of a threonine residue (T101) and the formation of an NPF6.3 dimer. When the nitrate availability diminishes, T101 gets phosphorylated, and the NPF6.3 dimer dissociates (Parker and Newstead, 2014; Sun *et al.*, 2014; Tsay, 2014; Sun and Zheng, 2015). This mechanism of affinity reversal allows us to hypothesize that with growing nitrate supply, there is a point at which a portion of the NPF6.3 population has switched from the high- to the low-affinity state, and the said growth in nitrate supply is not sufficient to compensate for this change. Such a point would explain the observed minima in CK and CKX responses to the nitrate.

Besides CKs and CKX, we also saw that the differences in nitrate supply affected the concentrations of IAA (an auxin) and ABA in the roots and xylem sap. IAA followed the same trend as CKs (Figure 7H). ABA showed the same trend in the xylem sap but a reversed one in the roots (Figure 7I). The latter suggests an antagonistic relation between ABA and CKs, which might be relevant to the previously reported inhibitory effect of ABA on nitrate uptake (Harris and Ondzighi-Assoume, 2017; Su *et al.*, 2021).

Finding that CKX is active in the xylem sap and regulated in response to the CK flux allows us to incorporate CK degradation into contemporary models of CK long-distance transport and root-to-shoot signalling (Nedvěd *et al.*, 2021; Sakakibara, 2021; Hu and Shani, 2023). CK cleavage in the apoplast can be a manner of suppressing the CK signalling, alongside CK transport into cells. Given our assumption that the xylem-located CKXs preferentially cleave CK nucleobases as their substrates, the exact fate of CK ribosides, the main form of the xylem-located CKs, remains yet to be uncovered.

Data Availability

Structure coordinates have been deposited to the Protein Data Bank (PDB) as 8QVT.

Author Contribution

DN, VM, and KH designed the experiment and conception. DN, VM, DK, PB, MČ, FB, KM, and IR performed the experiments. PID performed metabolical analysis. DN, VM, and KH wrote the manuscript. All authors read and approved the manuscript.

Acknowledgements

The authors wish to thank to Stanislav Vosolsobě for his advice on the bioinformatical analyses, Eva Kobzová for her assistance in plant cultivation, Marie Korecká for her help in collecting the xylem sap, and Selgen® company for providing seeds necessary for our experimental work.

Funding

This work was supported by the Jean d'Alembert fellowship as part of France 2030 program ANR-11-IDEX-0003, the Mobility grant 8J23FR011 from the Ministry of Education, Youth and Sports of the Czech Republic, and the project TowArds Next GENeration Crops, reg. no. CZ.02.01.01/00/22_008/0004581 of the ERDF Programme Johannes Amos Comenius.

Supplementary Files

Supplementary tables are provided in file “SupplementaryTables.xlsx”. Supplementary files 1 and 2 are provided separately.

Table S1: CKX protein sequences used in the bioinformatical analysis. The “ID” column consists of the Sang v1.1 gene names for *Avena sativa* and the NCBI Protein accessions for other species.

Table S2: Refinement statistics for the crystallization of ZmCKX5.

Table S3: Naming of the AsCKX isoforms. The corresponding CKX classes, lengths of mRNAs and proteins are given as well.

Table S4: Proteome profiling in oat xylem sap.

Table S5: Targeted proteomic analysis of oat xylem sap against AsCKXs.

Table S6: Targeted proteomic analysis of oat xylem sap against all oat proteins.

Supplementary File 1: A tree graph in the Newick format used to construct the dendrogram in Figure 1.

Supplementary File 2: Structural analysis of ZmCKX5, proteomic analyses in oat xylem sap.

References

Abualia, R., Riegler, S. and Benkova, E. (2023) 'Nitrate, Auxin and Cytokinin—A Trio to Tango', *Cells*, 12(12), p. 1613. Available at: https://doi.org/10.3390/cells12121613.

Antoniadi, I. *et al.* (2020) 'Cell-surface receptors enable perception of extracellular cytokinins', *Nature Communications*, 11(1), p. 4284. Available at: https://doi.org/10.1038/s41467-020-17700-9.

Ashburner, M. *et al.* (2000) 'Gene Ontology: tool for the unification of biology', *Nature Genetics*, 25(1), pp. 25–29. Available at: https://doi.org/10.1038/75556.

Bae, E. *et al.* (2008) 'Crystal structure of Arabidopsis thaliana cytokinin dehydrogenase', *Proteins: Structure, Function, and Bioinformatics*, 70(1), pp. 303–306. Available at: https://doi.org/10.1002/prot.21678.

Bernard, C. *et al.* (2011) 'Equilibrative nucleoside transporter 1 (ENT1) is critical for pollen germination and vegetative growth in Arabidopsis', *Journal of Experimental Botany*, 62(13), pp. 4627–4637. Available at: https://doi.org/10.1093/jxb/err183.

Beveridge, C.A. *et al.* (1997) 'The shoot controls zeatin riboside export from pea roots. Evidence from the branching mutant rms4', *The Plant Journal*, 11(2), pp. 339–345. Available at: https://doi.org/10.1046/j.1365-313X.1997.11020339.x.

Bradford, M.M. (1976) 'A rapid and sensitive method for the quantitation of microgram quantities of protein utilizing the principle of protein-dye binding', *Analytical Biochemistry*, 72, pp. 248–254. Available at: https://doi.org/10.1006/abio.1976.9999.

Brenner, W.G. *et al.* (2012) 'Gene Regulation by Cytokinin in Arabidopsis', *Frontiers in Plant Science*, 3. Available at: https://doi.org/10.3389/fpls.2012.00008.

Bricogne, G. *et al.* (2017) 'BUSTER'. Cambridge, United Kingdom: Global Phasing Ltd.

Brownlee, B.G., Hall, R.H. and Whitty, C.D. (1975) '3-Methyl-2-butenal: An Enzymatic Degradation Product of the Cytokinin, N^6-(Δ^2-Isopentenyl)adenine', *Canadian Journal of Biochemistry*, 53(1), pp. 37–41. Available at: https://doi.org/10.1139/o75-006.

Brugière, N. *et al.* (2003) 'Cytokinin Oxidase Gene Expression in Maize Is Localized to the Vasculature, and Is Induced by Cytokinins, Abscisic Acid, and Abiotic Stress', *Plant Physiology*, 132(3), pp. 1228–1240. Available at: https://doi.org/10.1104/pp.102.017707.

Chen, L. *et al.* (2022) 'The LONELY GUY gene family: from mosses to wheat, the key to the formation of active cytokinins in plants', *Plant Biotechnology Journal*, 20(4), pp. 625–645. Available at: https://doi.org/10.1111/pbi.13783.

Chen, V.B. *et al.* (2010) 'MolProbity: all-atom structure validation for macromolecular crystallography', *Acta Crystallographica Section D: Biological Crystallography*, 66(Pt 1), pp. 12–21. Available at: https://doi.org/10.1107/S0907444909042073.

Dobrev, P.I. and Kamínek, M. (2002) 'Fast and efficient separation of cytokinins from auxin and abscisic acid and their purification using mixed-mode solid-phase extraction', *Journal of Chromatography A*, 950(1–2), pp. 21–29. Available at: https://doi.org/10.1016/S0021-9673(02)00024-9.

Elnaggar, A. *et al.* (2022) 'ProtTrans: Toward Understanding the Language of Life Through Self-Supervised Learning', *IEEE Transactions on Pattern Analysis and Machine Intelligence*, 44(10), pp. 7112–7127. Available at: https://doi.org/10.1109/TPAMI.2021.3095381.

Emsley, P. and Cowtan, K. (2004) 'Coot: model-building tools for molecular graphics', *Acta Crystallographica. Section D, Biological Crystallography*, 60(Pt 12 Pt 1), pp. 2126–2132. Available at: https://doi.org/10.1107/S0907444904019158.

Franc, V. *et al.* (2012) 'Analysis of N-glycosylation in maize cytokinin oxidase/dehydrogenase 1 using a manual microgradient chromatographic separation coupled offline to MALDI-TOF/TOF mass spectrometry', *Journal of Proteomics*, 75(13), pp. 4027–4037. Available at: https://doi.org/10.1016/j.jprot.2012.05.013.

Frébortová, J. *et al.* (2004) 'Catalytic reaction of cytokinin dehydrogenase: preference for quinones as electron acceptors.', *The Biochemical journal*, 380(Pt 1), pp. 121–30. Available at: https://doi.org/10.1042/BJ20031813.

Frébortová, J. *et al.* (2007) 'Functional expression and purification of cytokinin dehydrogenase from Arabidopsis thaliana (AtCKX2) in Saccharomyces cerevisiae', *Biologia Plantarum*, 51(4), pp. 673–682. Available at: https://doi.org/10.1007/s10535-007-0141-6.

Gajdošová, S. *et al.* (2011) 'Distribution, biological activities, metabolism, and the conceivable function of cis-zeatin-type cytokinins in plants', *Journal of Experimental Botany*, 62(8), pp. 2827–2840. Available at: https://doi.org/10.1093/jxb/erq457.

Galuszka, P. *et al.* (2007) 'Biochemical Characterization of Cytokinin Oxidases/Dehydrogenases from Arabidopsis thaliana Expressed in Nicotiana tabacum L.', *Journal of Plant Growth Regulation*, 26(3), pp. 255–267. Available at: https://doi.org/10.1007/s00344-007-9008-5.

Gao, S. *et al.* (2014) 'CYTOKININ OXIDASE/DEHYDROGENASE4 Integrates Cytokinin and Auxin Signaling to Control Rice Crown Root Formation', *Plant Physiology*, 165(3), pp. 1035–1046. Available at: https://doi.org/10.1104/pp.114.238584.

Gasteiger, E. *et al.* (2003) 'ExPASy: the proteomics server for in-depth protein knowledge and analysis', *Nucleic Acids Research*, 31(13), pp. 3784–3788. Available at: https://doi.org/10.1093/nar/gkg563.

Gaudinová, A. (1983) 'The effect of NO3- and NH4+ ions on enzymes involved in nitrogen assimilation in Pisum sativum L', *Biologia plantarum*, 25(6), p. 440. Available at: https://doi.org/10.1007/BF02903144.

Gaudinová, A. *et al.* (2005) 'The Involvement of Cytokinin Oxidase/Dehydrogenase and Zeatin Reductase in Regulation of Cytokinin Levels in Pea (Pisum sativum L.) Leaves', *Journal of Plant Growth Regulation*, 24(3), pp. 188–200. Available at: https://doi.org/10.1007/s00344-005-0043-9.

Gigli-Bisceglia, N. *et al.* (2018) 'Cell wall integrity modulates *Arabidopsis thaliana* cell cycle gene expression in a cytokinin- and nitrate reductase-dependent manner', *Development*, p. dev.166678. Available at: https://doi.org/10.1242/dev.166678.

Gupta, R. and Brunak, S. (2002) 'Prediction of glycosylation across the human proteome and the correlation to protein function', *Pac Symp Biocomput*, pp. 310–22.

Hare, P.D. and van Staden, J. (1994) 'Cytokinin oxidase: Biochemical features and physiological significance', *Physiologia Plantarum*, 91(1), pp. 128–136. Available at: https://doi.org/10.1111/j.1399-3054.1994.tb00668.x.

Harris, J.M. and Ondzighi-Assoume, C.A. (2017) 'Environmental nitrate signals through abscisic acid in the root tip', *Plant Signaling & Behavior*, 12(1), p. e1273303. Available at: https://doi.org/10.1080/15592324.2016.1273303.

Hluska, T., Hlusková, L. and Emery, R.J. (2021) 'The Hulks and the Deadpools of the Cytokinin Universe: A Dual Strategy for Cytokinin Production, Translocation, and Signal Transduction', *Biomolecules*, 11(2), p. 209. Available at: https://doi.org/10.3390/biom11020209.

Ho, C.-H. *et al.* (2009) 'CHL1 Functions as a Nitrate Sensor in Plants', *Cell*, 138(6), pp. 1184–1194. Available at: https://doi.org/10.1016/j.cell.2009.07.004.

Hoyerová, K. *et al.* (2007) 'Cytokinin oxidase/dehydrogenase activity in oat xylem sap'. *3rd International Symposium on Plant Neurobiology*, Štrbské pleso, Slovakia.

Hu, Y. and Shani, E. (2023) 'Cytokinin activity – transport and homeostasis at the whole plant, cell, and subcellular levels', *New Phytologist*, 239(5), pp. 1603–1608. Available at: https://doi.org/10.1111/nph.19001.

Huang, P. *et al.* (2023) 'Cytokinins regulate rice lamina joint development and leaf angle', *Plant Physiology*, 191(1), pp. 56–69. Available at: https://doi.org/10.1093/plphys/kiac401.

Huerta-Cepas, J., Serra, F. and Bork, P. (2016) 'ETE 3: Reconstruction, Analysis, and Visualization of Phylogenomic Data', *Molecular Biology and Evolution*, 33(6), pp. 1635–1638. Available at: https://doi.org/10.1093/molbev/msw046.

Jia, Z. and Von Wirén, N. (2020) 'Signaling pathways underlying nitrogen-dependent changes in root system architecture: from model to crop species', *Journal of Experimental Botany*. Edited by G. Xu, 71(15), pp. 4393–4404. Available at: https://doi.org/10.1093/jxb/eraa033.

Jiskrová, E. *et al.* (2016) 'Extra- and intracellular distribution of cytokinins in the leaves of monocots and dicots', *New Biotechnology*, 33(5, Part B), pp. 735–742. Available at: https://doi.org/10.1016/j.nbt.2015.12.010.

Kabsch, W. (2010) 'XDS', *Acta Crystallographica Section D: Biological Crystallography*, 66(2), pp. 125–132. Available at: https://doi.org/10.1107/S0907444909047337.

Kamal, N. *et al.* (2022) 'The mosaic oat genome gives insights into a uniquely healthy cereal crop', *Nature*, pp. 1–7. Available at: https://doi.org/10.1038/s41586-022-04732-y.

Karplus, P.A. and Diederichs, K. (2012) 'Linking crystallographic model and data quality', *Science (New York, N.Y.)*, 336(6084), pp. 1030–1033. Available at: https://doi.org/10.1126/science.1218231.

Katoh, K. and Standley, D.M. (2013) 'MAFFT Multiple Sequence Alignment Software Version 7: Improvements in Performance and Usability', *Molecular Biology and Evolution*, 30(4), pp. 772–780. Available at: https://doi.org/10.1093/molbev/mst010.

Kiba, T. *et al.* (2011) 'Hormonal control of nitrogen acquisition: roles of auxin, abscisic acid, and cytokinin', *Journal of Experimental Botany*, 62(4), pp. 1399–1409. Available at: https://doi.org/10.1093/jxb/erq410.

Kiba, T. and Krapp, A. (2016) 'Plant Nitrogen Acquisition Under Low Availability: Regulation of Uptake and Root Architecture', *Plant and Cell Physiology*, 57(4), pp. 707–714. Available at: https://doi.org/10.1093/pcp/pcw052.

Kieber, J.J. and Schaller, G.E. (2014) 'Cytokinins', *The Arabidopsis Book*, 12, p. e0168. Available at: https://doi.org/10.1199/tab.0168.

Kopečný, D. *et al.* (2008) 'Mechanism-Based Inhibitors of Cytokinin Oxidase/Dehydrogenase Attack FAD Cofactor', *Journal of Molecular Biology*, 380(5), pp. 886–899. Available at: https://doi.org/10.1016/j.jmb.2008.05.044.

Kopečný, D. *et al.* (2010) 'Phenyl- and benzylurea cytokinins as competitive inhibitors of cytokinin oxidase/dehydrogenase: A structural study', *Biochimie*, 92(8), pp. 1052–1062. Available at: https://doi.org/10.1016/j.biochi.2010.05.006.

Kopečný, D. *et al.* (2016) 'Kinetic and structural investigation of the cytokinin oxidase/dehydrogenase active site', *The FEBS Journal*, 283(2), pp. 361–377. Available at: https://doi.org/10.1111/febs.13581.

Kowalska, M. *et al.* (2010) 'Vacuolar and cytosolic cytokinin dehydrogenases of Arabidopsis thaliana: Heterologous expression, purification and properties', *Phytochemistry*, 71(17), pp. 1970–1978. Available at: https://doi.org/10.1016/j.phytochem.2010.08.013.

Krouk, G. *et al.* (2010) 'Nitrate-regulated auxin transport by NRT1.1 defines a mechanism for nutrient sensing in plants', *Developmental Cell*, 18(6), pp. 927–937. Available at: https://doi.org/10.1016/j.devcel.2010.05.008.

Kurakawa, T. *et al.* (2007) 'Direct control of shoot meristem activity by a cytokinin-activating enzyme', *Nature*, 445, pp. 652–655. Available at: https://doi.org/10.1038/nature05504.

Kuroha, T. *et al.* (2009) 'Functional analyses of LONELY GUY cytokinin-activating enzymes reveal the importance of the direct activation pathway in Arabidopsis.', *The Plant cell*, 21(10), pp. 3152–69. Available at: https://doi.org/10.1105/tpc.109.068676.

Leinonen, R. *et al.* (2011) 'The European Nucleotide Archive', *Nucleic Acids Research*, 39(Database issue), pp. D28–D31. Available at: https://doi.org/10.1093/nar/gkq967.

Liu, K.H., Huang, C.Y. and Tsay, Y.F. (1999) 'CHL1 is a dual-affinity nitrate transporter of Arabidopsis involved in multiple phases of nitrate uptake.', *The Plant Cell*, 11(5), pp. 865–874.

van der Maaten, L. and Hinton, G. (2008) 'Viualizing data using t-SNE', *Journal of Machine Learning Research*, 9, pp. 2579–2605.

Maeda, Y. *et al.* (2018) 'A NIGT1-centred transcriptional cascade regulates nitrate signalling and incorporates phosphorus starvation signals in Arabidopsis', *Nature Communications*, 9(1), p. 1376. Available at: https://doi.org/10.1038/s41467-018-03832-6.

Malito, E. *et al.* (2004) 'Structures of Michaelis and Product Complexes of Plant Cytokinin Dehydrogenase: Implications for Flavoenzyme Catalysis', *Journal of Molecular Biology*, 341(5), pp. 1237–1249. Available at: https://doi.org/10.1016/J.JMB.2004.06.083.

Motyka, V. *et al.* (1996) 'Changes in Cytokinin Content and Cytokinin Oxidase Activity in Response to Derepression of ipt Gene Transcription in Transgenic Tobacco Calli and Plants', *Plant Physiology*, 112(3), pp. 1035–1043. Available at: https://doi.org/10.1104/pp.112.3.1035.

Motyka, V. *et al.* (2003) 'Cytokinin-induced upregulation of cytokinin oxidase activity in tobacco includes changes in enzyme glycosylation and secretion', *Physiologia Plantarum*, 117(1), pp. 11–21. Available at: https://doi.org/10.1034/j.1399-3054.2003.1170102.x.

Motyka, V. and Kamínek, M. (1994) 'Cytokinin oxidase from auxin- and cytokinin-dependent callus cultures of tobacco (Nicotiana tabacum L.)', *Journal of Plant Growth Regulation*, 13(1), pp. 1–9. Available at: https://doi.org/10.1007/BF00210700.

Nedvěd, D. *et al.* (2021) 'Differential Subcellular Distribution of Cytokinins: How Does Membrane Transport Fit into the Big Picture?', *International Journal of Molecular Sciences*, 22(7), p. 3428. Available at: https://doi.org/10.3390/ijms22073428.

Nguyen, L.-T. *et al.* (2015) 'IQ-TREE: A Fast and Effective Stochastic Algorithm for Estimating Maximum-Likelihood Phylogenies', *Molecular Biology and Evolution*, 32(1), pp. 268–274. Available at: https://doi.org/10.1093/molbev/msu300.

Nisler, J. *et al.* (2021) 'Diphenylurea-derived cytokinin oxidase/dehydrogenase inhibitors for biotechnology and agriculture', *Journal of Experimental Botany*, 72(2), pp. 355–370. Available at: https://doi.org/10.1093/jxb/eraa437.

Osugi, A. *et al.* (2017) 'Systemic transport of trans-zeatin and its precursor have differing roles in Arabidopsis shoots', *Nature Plants*, 3(8), p. 17112. Available at: https://doi.org/10.1038/nplants.2017.112.

Pačes, V., Werstiuk, E. and Hall, R.H. (1971) 'Conversion of N6-(A2-Isopentenyl)adenosine to Adenosine by Enzyme Activity in Tobacco Tissue', *Plant Physiol*, 48, pp. 775–778.

Parker, J.L. and Newstead, S. (2014) 'Molecular basis of nitrate uptake by the plant nitrate transporter NRT1.1', *Nature*, 507(7490), pp. 68–72. Available at: https://doi.org/10.1038/nature13116.

Patro, R. *et al.* (2017) 'Salmon provides fast and bias-aware quantification of transcript expression', *Nature Methods*, 14(4), pp. 417–419. Available at: https://doi.org/10.1038/nmeth.4197.

Poitout, A. *et al.* (2018) 'Responses to Systemic Nitrogen Signaling in Arabidopsis Roots Involve *trans* -Zeatin in Shoots', *The Plant Cell*, 30(6), pp. 1243–1257. Available at: https://doi.org/10.1105/tpc.18.00011.

Popelková, H. *et al.* (2006) 'Kinetic and chemical analyses of the cytokinin dehydrogenase-catalysed reaction: correlations with the crystal structure', *Biochemical Journal*, 398(Pt 1), pp. 113–124. Available at: https://doi.org/10.1042/BJ20060280.

Reid, D.E. *et al.* (2016) 'CYTOKININ OXIDASE/DEHYDROGENASE3 Maintains Cytokinin Homeostasis during Root and Nodule Development in *Lotus japonicus*', *Plant Physiology*, 170(2), pp. 1060–1074. Available at: https://doi.org/10.1104/pp.15.00650.

Roy, S. (2018) 'Nitrate Ahoy! Shoot Cytokinin Signals Integrate Growth Responses with Nitrogen Availability', *The Plant Cell*, 30(6), pp. 1169–1170. Available at: https://doi.org/10.1105/tpc.18.00453.

Ruffel, S. *et al.* (2016) 'Long-distance nitrate signaling displays cytokinin dependent and independent branches', *Journal of Integrative Plant Biology*, 58(3), pp. 226–229. Available at: https://doi.org/10.1111/jipb.12453.

Sakakibara, H. (2021) 'Cytokinin biosynthesis and transport for systemic nitrogen signaling', *The Plant Journal*, 105(2), pp. 421–430. Available at: https://doi.org/10.1111/tpj.15011.

Sayers, E.W. *et al.* (2022) 'Database resources of the national center for biotechnology information', *Nucleic Acids Research*, 50(D1), pp. D20–D26. Available at: https://doi.org/10.1093/nar/gkab1112.

Schrödinger, LLC (2015) 'The PyMOL Molecular Graphics System, Version 1.8'.

Šmehilová, M. *et al.* (2009) 'Subcellular localization and biochemical comparison of cytosolic and secreted cytokinin dehydrogenase enzymes from maize', *Journal of Experimental Botany*, 60(9), pp. 2701–2712. Available at: https://doi.org/10.1093/jxb/erp126.

Song, L. and Florea, L. (2015) ‘Rcorrector: efficient and accurate error correction for Illumina RNA-seq reads’, *GigaScience*, 4, p. 48. Available at: https://doi.org/10.1186/s13742-015-0089-y.

Storoni, L.C., McCoy, A.J. and Read, R.J. (2004) ‘Likelihood-enhanced fast rotation functions’, *Acta Crystallographica Section D*, 60(3), pp. 432–438. Available at: https://doi.org/10.1107/S0907444903028956.

Su, H. *et al.* (2021) ‘Abscisic acid signaling negatively regulates nitrate uptake via phosphorylation of NRT1.1 by SnRK2s in Arabidopsis’, *Journal of Integrative Plant Biology*, 63(3), pp. 597–610. Available at: https://doi.org/10.1111/jipb.13057.

Sun, J. *et al.* (2014) ‘Crystal structure of the plant dual-affinity nitrate transporter NRT1.1’, *Nature*, 507(7490), pp. 73–77. Available at: https://doi.org/10.1038/nature13074.

Sun, J. and Zheng, N. (2015) ‘Molecular Mechanism Underlying the Plant NRT1.1 Dual-Affinity Nitrate Transporter’, *Frontiers in Physiology*, 6. Available at: https://www.frontiersin.org/articles/10.3389/fphys.2015.00386 (Accessed: 29 October 2023).

Takei, K. *et al.* (2001) ‘Nitrogen-Dependent Accumulation of Cytokinins in Root and theTranslocation to Leaf: Implication of Cytokinin Species that Induces GeneExpression of Maize ResponseRegulator’, *Plant and Cell Physiology*, 42(1), pp. 85–93. Available at: https://doi.org/10.1093/pcp/pce009.

Takei, K. *et al.* (2004) ‘AtIPT3 is a Key Determinant of Nitrate-Dependent Cytokinin Biosynthesis in Arabidopsis’, *Plant and Cell Physiology*, 45(8), pp. 1053–1062. Available at: https://doi.org/10.1093/pcp/pch119.

Tessi, T.M. *et al.* (2020) ‘Arabidopsis AZG2 transports cytokinins in vivo and regulates lateral root emergence’, *New Phytologist*, 229(2), pp. 979–993. Available at: https://doi.org/10.1111/nph.16943.

Tessi, T.M. *et al.* (2023) ‘AZG1 is a cytokinin transporter that interacts with auxin transporter PIN1 and regulates the root stress response’, *New Phytologist*, 238(5), pp. 1924–1941. Available at: https://doi.org/10.1111/nph.18879.

The Gene Ontology Consortium *et al.* (2023) ‘The Gene Ontology knowledgebase in 2023’, *Genetics*, 224(1), p. iyad031. Available at: https://doi.org/10.1093/genetics/iyad031.

Thumuluri, V. *et al.* (2022) ‘DeepLoc 2.0: multi-label subcellular localization prediction using protein language models’, *Nucleic Acids Research*, 50(W1), pp. W228–W234. Available at: https://doi.org/10.1093/nar/gkac278.

Tinker, N.A. *et al.* (2022) ‘Genome analysis in Avena sativa reveals hidden breeding barriers and opportunities for oat improvement’, *Communications Biology*, 5(1), p. 474. Available at: https://doi.org/10.1038/s42003-022-03256-5.

Tomaszewska, P., Schwarzacher, T. and Heslop-Harrison, J.S. (Pat) (2022) ‘Oat chromosome and genome evolution defined by widespread terminal intergenomic translocations in polyploids’, *Frontiers in Plant Science*, 13, p. 1026364. Available at: https://doi.org/10.3389/fpls.2022.1026364.

Tsay, Y.-F. (2014) ‘How to switch affinity’, *Nature*, 507(7490), pp. 44–45. Available at: https://doi.org/10.1038/nature13063.

Varala, K. *et al.* (2018) ‘Temporal transcriptional logic of dynamic regulatory networks underlying nitrogen signaling and use in plants’, *Proceedings of the National Academy of Sciences*, 115(25), pp. 6494–6499. Available at: https://doi.org/10.1073/pnas.1721487115.

Wan, L. *et al.* (2019) ‘Structural and functional insights into the modulation of the activity of a flax cytokinin oxidase by flax rust effector AvrL567-A’, *Molecular Plant Pathology*, 20(2), pp. 211–222. Available at: https://doi.org/10.1111/mpp.12749.

Wang, Y.-Y. *et al.* (2018) ‘Nitrate Transport, Signaling, and Use Efficiency’, *Annual Review of Plant Biology*, 69(1), pp. 85–122. Available at: https://doi.org/10.1146/annurev-arplant-042817-040056.

Wulfetange, K. *et al.* (2011) ‘The cytokinin receptors of Arabidopsis are located mainly to the endoplasmic reticulum’, *Plant Physiology*, 156(4), pp. 1808–1818. Available at: https://doi.org/10.1104/pp.111.180539.

Wybouw, B. and De Rybel, B. (2019) ‘Cytokinin – A Developing Story’, *Trends in Plant Science*, 24(2), pp. 177–185. Available at: https://doi.org/10.1016/j.tplants.2018.10.012.

Yang, S.H., Yu, H. and Goh, C.J. (2002) 'Isolation and characterization of the orchid cytokinin oxidase DSCKX1 promoter', *Journal of Experimental Botany*, 53(376), pp. 1899–1907. Available at: https://doi.org/10.1093/jxb/erf055.

Zalabák, D. *et al.* (2014) 'Biochemical characterization of the maize cytokinin dehydrogenase family and cytokinin profiling in developing maize plantlets in relation to the expression of cytokinin dehydrogenase genes', *Plant Physiology and Biochemistry*, 74, pp. 283–293. Available at: https://doi.org/10.1016/j.plaphy.2013.11.020.

Zalabák, D. *et al.* (2016) 'Maize cytokinin dehydrogenase isozymes are localized predominantly to the vacuoles', *Plant Physiology and Biochemistry*, 104, pp. 114–124. Available at: https://doi.org/10.1016/j.plaphy.2016.03.013.

Zhang, W. *et al.* (2021) 'Cytokinin oxidase/dehydrogenase OsCKX11 coordinates source and sink relationship in rice by simultaneous regulation of leaf senescence and grain number', *Plant Biotechnology Journal*, 19(2), pp. 335–350. Available at: https://doi.org/10.1111/pbi.13467.

Zheng, X. *et al.* (2023) 'Loss-function mutants of OsCKX gene family based on CRISPR-Cas systems revealed their diversified roles in rice', *The Plant Genome*, 16(2), p. e20283. Available at: https://doi.org/10.1002/tpg2.20283.

Zhou, Z. *et al.* (2020) 'Transcriptome Analysis of the Cytokinin Response in Medicago truncatula', *Journal of Plant Biology*, 63(3), pp. 189–202. Available at: https://doi.org/10.1007/s12374-020-09244-8.

Figure legends

Figure 1: Sequence-based classification of CKXs. **Left**: A tree graph of monocot CKX protein sequences. Each leaf represents a single sequence. The coloured portions of the tree represent eight CKX classes established in this work, annotated as I-VIII. **Top right**: The sequence logo of the semi-conserved FL**X**RV**XXX**E motif with the "entrance triplet" marked by a grey rectangle. Created with WebLogo (Crooks *et al.*, 2004). **Bottom right**: The most common amino acids at each position of the entrance triplet per each CKX class. The occurrence of the residues at the given position and in the given classes are presented in parentheses. If the occurrence of the most common residue is less than 50 %, it is considered variable and labelled "**X**" in the main text. The third position, depicted in the bold font, is the VEGAS residue, which can directly interact with the substrate.

Figure 2: Structure-based substrate specificities of CKXs from different classes. **A**: A structural comparison between ZmCKX5 (dark blue, this work / PDB 8QVT) and ZmCKX1 (light blue, PDB 1W1R). The helix–loop–helix region from residues 294–325 in ZmCKX1 (shown with black arrow) is disordered in ZmCKX5. An additional N-terminal helix in ZmCKX5 is also shown. **B-D**: Detailed overviews at the entrance to the active site in CKXs from six classes. Superimpositions of ZmCKX5 on ZmCKX1, ZmCKX2 (red, PDB 4ML8) on ZmCKX4a (violet, PDB 4O95), and ZmCKX8 (cyan, PDB 6YAQ) on AtCKX7 (orange, PDB 2EXR) are shown. The entrance motif is in the red rectangle, and the VEGAS residues are labelled.

Figure 3: Subcellular localizations of monocotyledonous CKXs predicted by DeepLoc with ProtT5 transformer. **A**: t-Distributed stochastic neighbour embeddings (tSNE) of the DeepLoc prediction scores. Each point represents a single CKX sequence. Each sequence is labelled by its class and the corresponding representative motif of the given class. **B-E**: DeepLoc scores of the individual CKX sequences for the cytoplasm, extracellular space, endoplasmic reticulum (ER), and vacuole. Higher scores indicate higher prediction confidence. Red crosses denote outlying points.

Figure 4: Cytokinin dehydrogenase in the oat (*Avena sativa*). **Left**: A dendrogram depicting classification of oat and maize CKXs, alongside LuCKX7 and AtCKX7. For each isoform, the three letter-long entrance motif is shown. The classes are annotated by Roman numerals placed around the graph. **Top right**: CKX activity measured in the xylem saps of different plant species. The ages of the plants are given in days after germination (DAG). **Bottom right**: Substrate specificities of CKXs isolated from different parts of oats and maize. iP: isopentenyl adenine, tZ: *trans*-zeatin, cZ: *cis*-zeatin.

Figure 5: *AsCKX* expression patterns in oat leaves, stems, roots, and pooled samples. The data represent means of normalized counts obtained via RNA sequencing, and values are given in transcripts per million. The data were obtained either in this work or from publicly available

sequence reads; in the latter case, the corresponding project accessions are provided in the column headers. The *AsCKX* genes are further annotated with the CKX classes and the corresponding characteristic entrance motifs.

Figure 6: Glycosylation of oat CKXs. **Left**: Absorbance at 280 nm and CKX activity measured in fractions eluted during Concavalin A-Sepharose 4B chromatography. The arrow annotates elution of glycosylated proteins by applying 200 mM methylmannose. **Right**: Prediction of *N*-glycosylation sites for AsCKXs and ZmCKX1 via NetNGlyc. The light blue cells represent asparagine residues (identified by their numbers given inside the cells) predicted as N-glycosylated with at least 50 % confidence. Residues in each column are aligned among all CKX sequences included in the graphics. For ZmCKX1, the bold numbers represent residues that were experimentally identified as N-glycosylated. CKX classification and the representative entrance motifs are shown on the right side of the graphics. AsCKXs from classes II and III have been excluded, as they are not predicted to be N-glycosylated.

Figure 7: Various responses to different nitrate supply in oats. **A**: CK concentrations in leaves. **B**: CK concentrations in roots. **C**: CK concentrations in xylem sap. **D**: CKX activity in xylem sap at two pH values (nitrate supply ranging from 16 to 1000 µM). **E**: Nitrate concentrations in leaves, roots, and xylem sap. **F**: Nitrate reductase activity in leaves and roots. **G**: Indole-3-acetic acid concentrations in leaves, roots, and xylem sap. **H**: Abscisic acid concentrations in leaves, roots, and xylem sap. tZ: *trans*-zeatin, cZ: *cis*-zeatin, iP: isopentenyladenine, DHZ: dihydrozeatin.

Figure 1

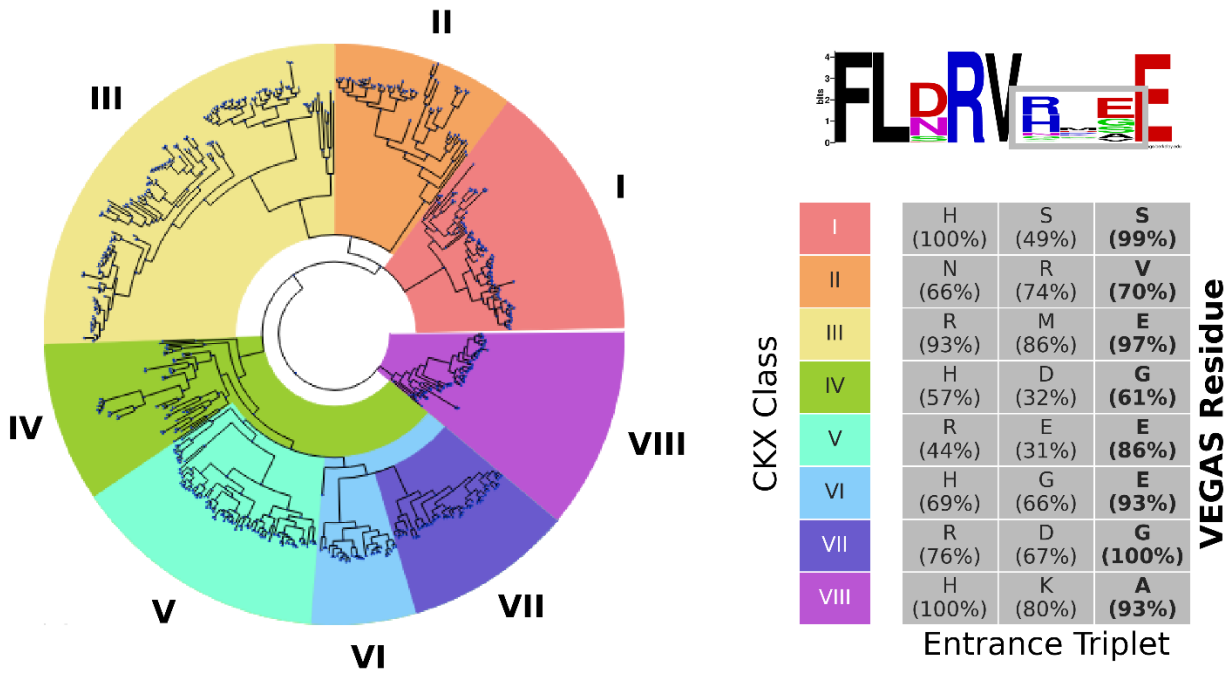

Figure 1: Sequence-based classification of CKXs. **Left**: A tree graph of monocot CKX protein sequences. Each leaf represents a single sequence. The coloured portions of the tree represent eight CKX classes established in this work, annotated as I-VIII. **Top right**: The sequence logo of the semi-conserved FL**X**RV**XXX**E motif with the "entrance triplet" marked by a grey rectangle. Created with WebLogo (Crooks *et al.*, 2004). **Bottom right**: The most common amino acids at each position of the entrance triplet per each CKX class. The occurrence of the residues at the given position and in the given classes are presented in parentheses. If the occurrence of the most common residue is less than 50 %, it is considered variable and labelled "**X**" in the main text. The third position, depicted in the bold font, is the VEGAS residue, which can directly interact with the substrate.

Figure 2

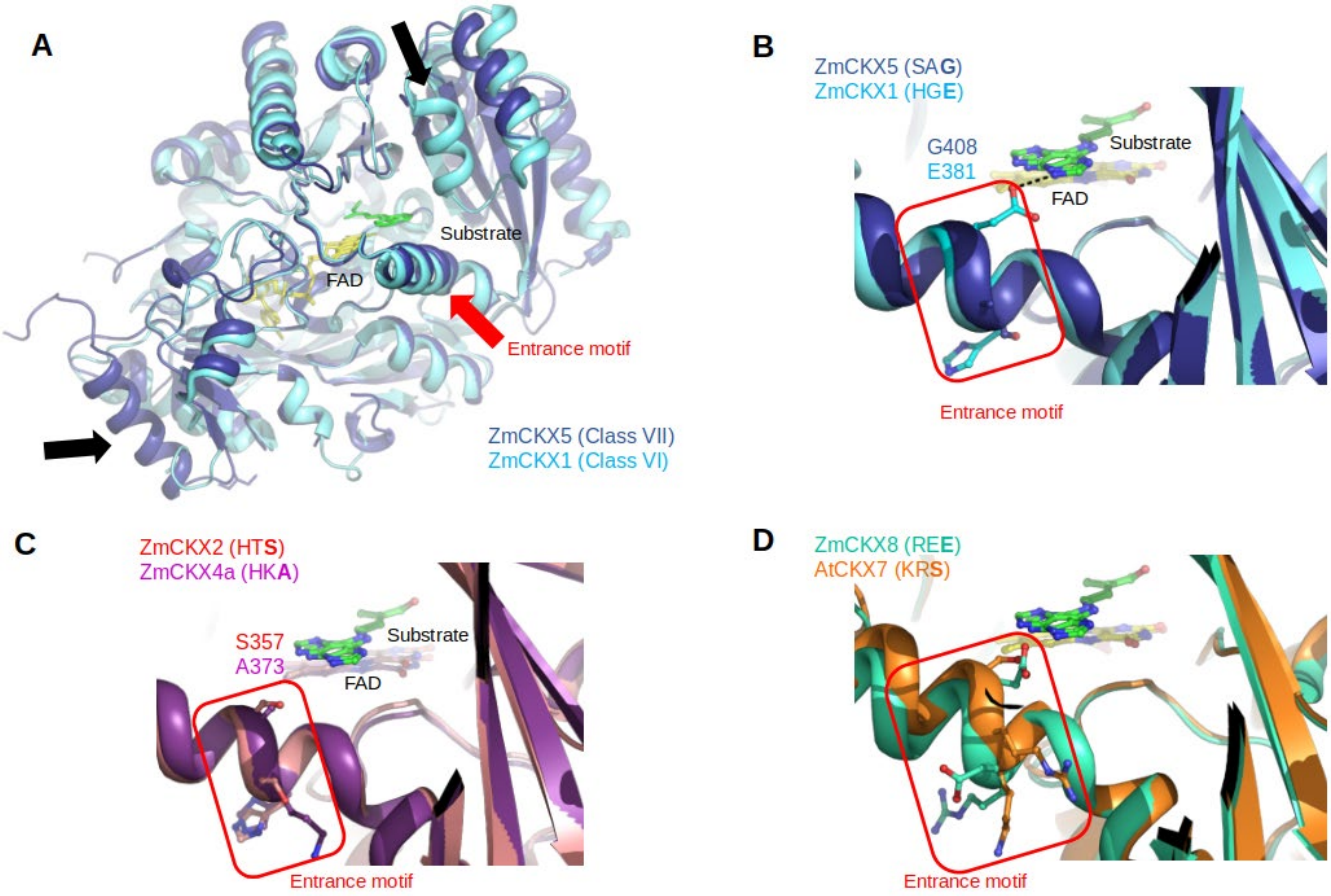

Figure 2: Structure-based substrate specificities of CKXs from different classes. **A**: A structural comparison between ZmCKX5 (dark blue, this work / PDB 8QVT) and ZmCKX1 (light blue, PDB 1W1R). The helix–loop–helix region from residues 294–325 in ZmCKX1 (shown with black arrow) is disordered in ZmCKX5. An additional N-terminal helix in ZmCKX5 is also shown. **B-D**: Detailed overviews at the entrance to the active site in CKXs from six classes. Superimpositions of ZmCKX5 on ZmCKX1, ZmCKX2 (red, PDB 4ML8) on ZmCKX4a (violet, PDB 4O95), and ZmCKX8 (cyan, PDB 6YAQ) on AtCKX7 (orange, PDB 2EXR) are shown. The entrance motif is in the red rectangle, and the VEGAS residues are labelled.

Figure 3

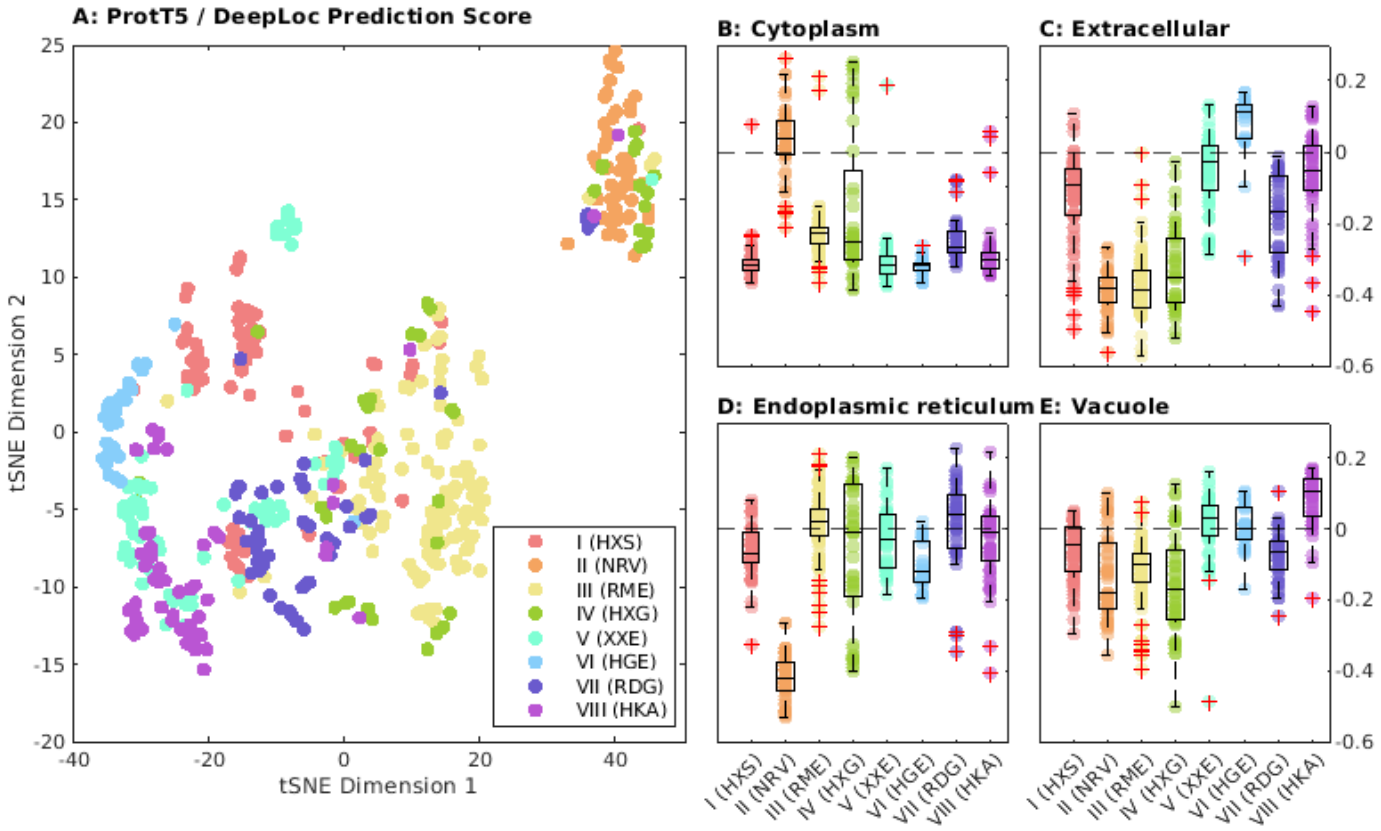

Figure 3: Subcellular localizations of monocotyledonous CKXs predicted by DeepLoc with ProtT5 transformer. **A**: t-Distributed stochastic neighbour embeddings (tSNE) of the DeepLoc prediction scores. Each point represents a single CKX sequence. Each sequence is labelled by its class and the corresponding representative motif of the given class. **B-E**: DeepLoc scores of the individual CKX sequences for the cytoplasm, extracellular space, endoplasmic reticulum (ER), and vacuole. Higher scores indicate higher prediction confidence. Red crosses denote outlying points.

Figure 4

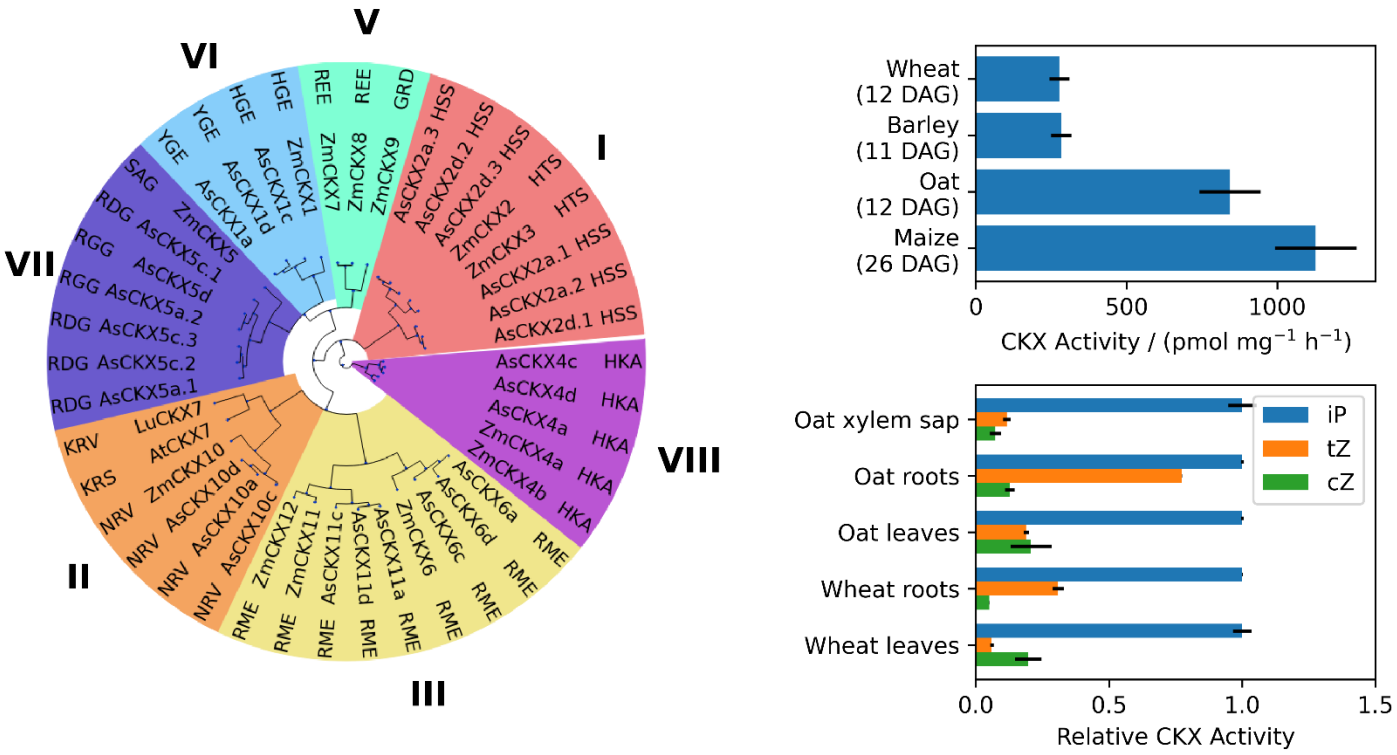

Figure 4: Cytokinin dehydrogenase in the oat (*Avena sativa*). **Left**: A dendrogram depicting classification of oat and maize CKXs, alongside LuCKX7 and AtCKX7. For each isoform, the three letter-long entrance motif is shown. The classes are annotated by Roman numerals placed around the graph. **Top right**: CKX activity measured in the xylem saps of different plant species. The ages of the plants are given in days after germination (DAG). **Bottom right**: Substrate specificities of CKXs isolated from different parts of oats and maize. iP: isopentenyl adenine, tZ: *trans*-zeatin, cZ: *cis*-zeatin.

Figure 5

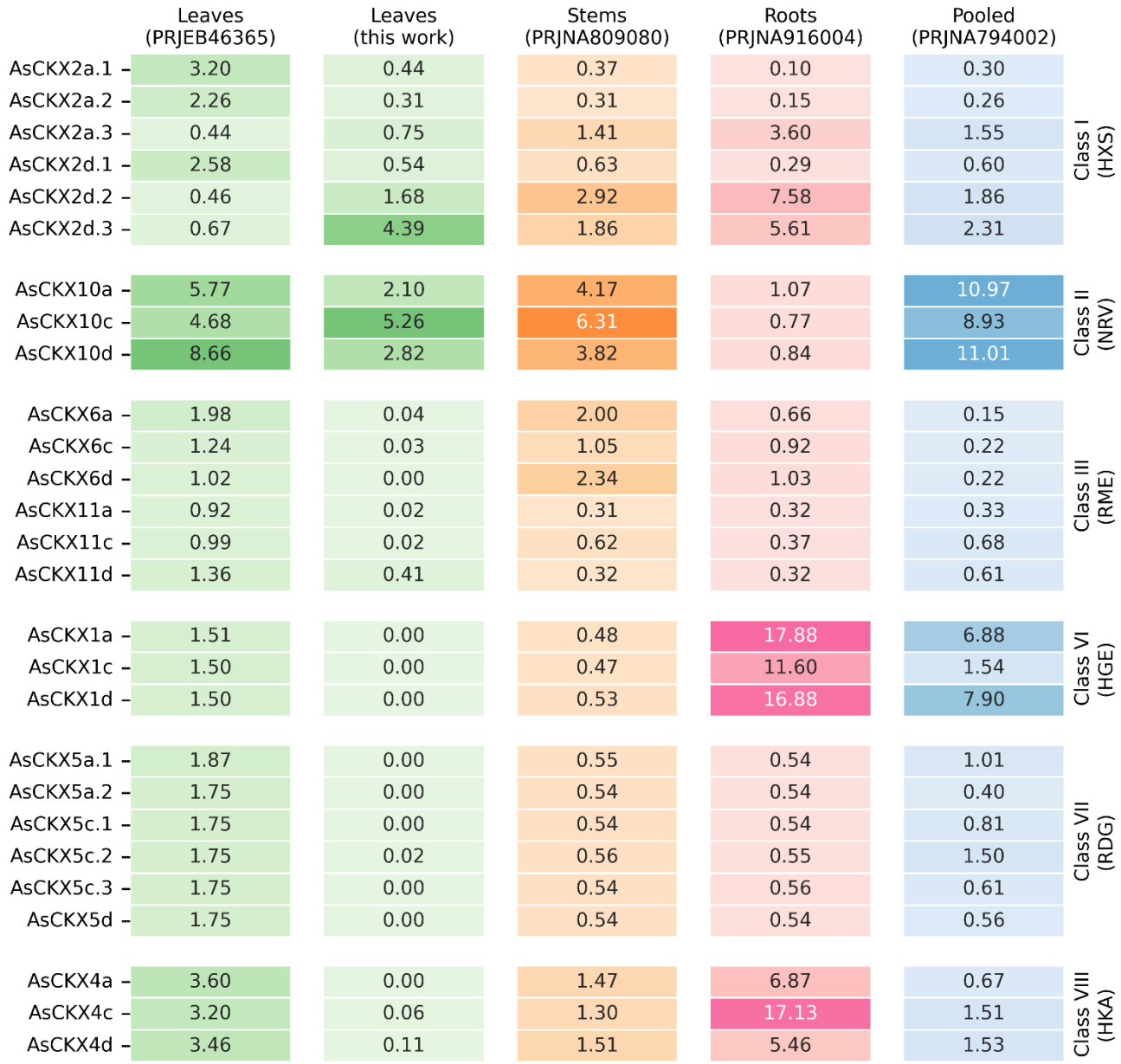

Figure 5: *AsCKX* expression patterns in oat leaves, stems, roots, and pooled samples. The data represent means of normalized counts obtained via RNA sequencing, and values are given in transcripts per million. The data were obtained either in this work or from publicly available sequence reads; in the latter case, the corresponding project accessions are provided in the column headers. The *AsCKX* genes are further annotated with the CKX classes and the corresponding characteristic entrance motifs.

Figure 6

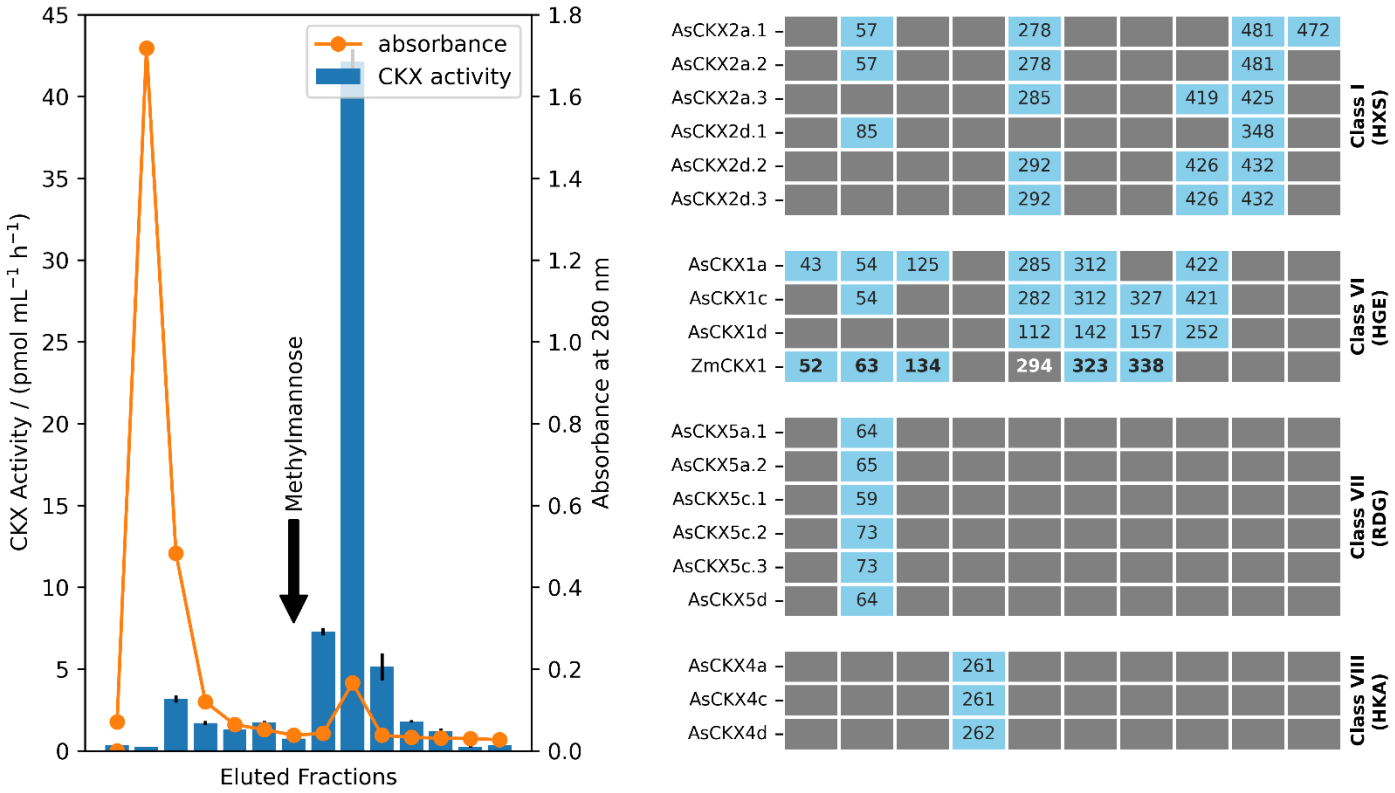

Figure 6: Glycosylation of oat CKXs. **Left**: Absorbance at 280 nm and CKX activity measured in fractions eluted during Concavalin A-Sepharose 4B chromatography. The arrow annotates elution of glycosylated proteins by applying 200 mM methylmannose. **Right**: Prediction of *N*-glycosylation sites for AsCKXs and ZmCKX1 via NetNGlyc. The light blue cells represent asparagine residues (identified by their numbers given inside the cells) predicted as N-glycosylated with at least 50 % confidence. Residues in each column are aligned among all CKX sequences included in the graphics. For ZmCKX1, the bold numbers represent residues that were experimentally identified as N-glycosylated. CKX classification and the representative entrance motifs are shown on the right side of the graphics. AsCKXs from classes II and III have been excluded, as they are not predicted to be N-glycosylated.

Figure 7

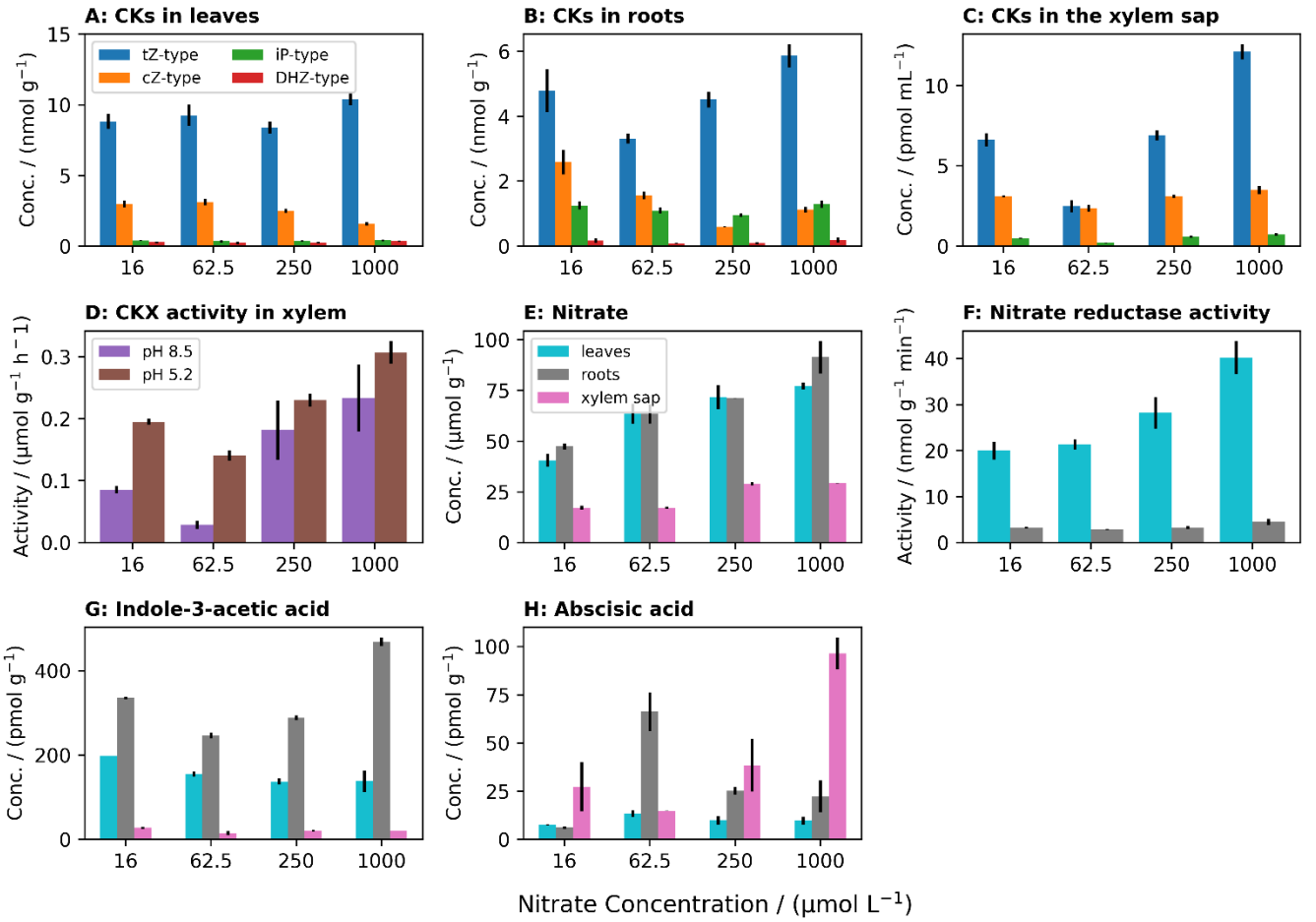

Figure 7: Various responses to different nitrate supply in oats. **A**: CK concentrations in leaves. **B**: CK concentrations in roots. **C**: CK concentrations in xylem sap. **D**: CKX activity in xylem sap at two pH values (nitrate supply ranging from 16 to 1000 µM). **E**: Nitrate concentrations in leaves, roots, and xylem sap. **F**: Nitrate reductase activity in leaves and roots. **G**: Indole-3-acetic acid concentrations in leaves, roots, and xylem sap. **H**: Abscisic acid concentrations in leaves, roots, and xylem sap. tZ: *trans*-zeatin, cZ: *cis*-zeatin, iP: isopentenyladenine, DHZ: dihydrozeatin.

5 Discussion

5.1 In Search of Riboside-Specific Cytokinin Transporters

CK ribosides are the main form of CKs travelling from roots to shoots via the xylem. Considering that the direct biological activity of CK ribosides (i.e. binding to the HK receptors and triggering downstream responses) is in the current state of knowledge unlikely (Hothorn et al., 2011; Lomin et al., 2015; Romanov and Schmülling, 2021) one can assume that ribosylated CKs mainly serve to carry information about the nutrient status in the soil to the upper parts of the plant without triggering unwanted CK response on the way. The inability of the non-ribosylated root-borne tZ to regulate physiological responses in the shoot apex suggests that ribosylation further protects the root-to-shoot translocated CKs from their CKX-catalysed cleavage in the SAM area (Davière and Achard, 2013; Osugi et al., 2017; Sakakibara, 2021), and as I show in this thesis, also from the CKX activity in xylem itself. Another effect of CK ribosylation is that ribosylated CKs are less likely to freely diffuse across biological membranes (as summarized in 4.1), and thus less likely to leak from the xylem.

As CK ribosides do not trigger CK responses by themselves, they must be activated once they arrive at their destination in the plant shoot. One possible activation mechanism involves hydrolysis of CK ribosides catalysed by CPN1, a cell wall-bound hydrolase. This reaction occurs in the apoplast (Kojima et al., 2023). The released CK nucleobase can bind to the plasma membrane-bound receptors or enter the cell, move to the endoplasmic reticulum, and activate the CK signalling pathway from here. Another option involves phosphorylation of the CK nucleoside molecule, followed by LOG-catalysed activation. Considering the cytoplasmic localization of LOG enzymes (Kuroha et al., 2009), this activation pathway requires the uptake of ribosylated CKs from the apoplast to the cytoplasm. Once activated, the CK molecule can enter the plasmatic reticule or return to the apoplast to activate the downstream signalling elements. Grafting experiments showed that wild-type stock does not rescue the reduced SAM size of the *atlog1-7 s*eptuple mutant scion, indicating that the pathway involving CK riboside uptake and LOG-catalysed activation is at least in some situations irreplaceable (Davière and Achard, 2013; Osugi et al., 2017; Sakakibara, 2021). The importance of LOG-catalysed activation is further highlighted by *CPN1* being expressed in panicles and leaves in rice and by the relatively mild effects of the *cpn1* mutation on panicle morphology (Kojima et al., 2023).

In Chapter 4.2, I show that two types of membrane-bound carriers can mediate the cellular uptake of ribosylated CKs. The two carrier types differ in their ability to transport CK nucleobases alongside ribosides. Both could be involved in the uptake of root-borne CK ribosides, mainly tZR, from the apoplast in shoots; the concentration of tZR in the xylem is greater than that of tZ, which should limit the inhibition effect of tZ on the uptake of tZR mediated by the nucleobase-recognizing carriers. Employing the nucleobase-recognizing carrier type described in Chapter 4.2 could also enable the uptake of both tZR and tZ from the apoplast, thus increasing the efficiency of the root-borne CK signal. As Sakakibara (2021) suggests, the joint uptake of root-borne tZ and tZR could occur in leaves.

Direct characterization of the transport activity of AtENT3, a carrier shown to affect the root-to-shoot translocation of CKs (Korobova et al., 2021), reveals that this transporter belongs

among carriers that recognize both CK nucleobases and ribosides, leaving the identity of the strictly riboside-specific carriers open. The *AtENT3* gene is also one of two *AtENTs* whose homologs are expressed in the BY-2 cells, in which my colleagues and I observed the discussed transport of CK ribosides. The remaining *ENTs* expressed in the BY-2 cells are annotated as homologs of *AtENT1*, suggesting that AtENT1 belongs among the CK riboside-specific carriers.

Li and colleagues (2003) tested the specificity of AtENT1 towards non-CK substrates using competition assays with radio-labelled adenosine in a yeast expression system. They show that AtENT1 transports ribosides (adenosine, guanosine, cytidine, uridine, and thymidine) and 2'-deoxyribosides but not nucleobases (adenine, guanine, cytosine, uracil, and hypoxanthine). This report supports the hypothesis that AtENT1 might transport CK ribosides but not CK nucleobases. A direct confirmation of this hypothesis is still required because CK nucleobases could use their side chains to form extra interactions with their transporters, unlike adenine and other nucleobases.

If we show that AtENT1 is a CK riboside-specific carrier, it will be worth examining whether its inability to transport CK nucleobases can be explained by different amino acids in the active sites of AtENT1 and AtENT3. As shown in Chapter 4.2, the major difference among the generally conserved active site amino acids is at the position corresponding to Gln62 in AtENT3. In AtENT2-7, this position is occupied by glutamine, an amino acid with a polar side chain, which can stabilize a ligand via hydrogen bonding. Conversely, in AtENT1 and AtENT8, this position is occupied by methionine, whose side chain is hydrophobic. Moreover, when grouped by sequential similarity, AtENT1 with AtENT8 and AtENT2-7 form two distinct clusters, suggesting that the amino-acid diversity at the position corresponding to Gln62 in AtENT3 correlates with the AtENT3 diversity in general (Li et al., 2003).

Molecular docking of tZ and iP into AtENT3 shows that Gln62 can interact with both of them (Figure S1 and S3 in Chapter 4.2), supporting the hypothesis that the amino acid at this position might determine whether an ENT protein can bind and transport nucleobases or not. Moreover, Girke and colleagues (2015) have shown that AtENT7, one of the glutamine-containing members of AtENTs, transports non-CK nucleobases and ribosides with similar affinities, in contrast with AtENT1 (Li et al., 2003). Wormit and colleagues (2004) reported that nucleobases only mildly inhibit the uptake of adenosine mediated by AtENT7, which might suggest a different interpretation than the results published by Girke et al. (2015). It will be thus worth scanning the substrate specificities of all AtENTs under the same experimental conditions to describe their relative differences.

The amino acid diversity at the position corresponding to Gln62 in AtENT3 occurs not only among AtENTs but also among ENTs from non-plant species depicted in Figure 5 in Chapter 4.2, suggesting that the sequence-based classification of ENTs as nucleobase-recognizing or riboside-specific (not only in relation to CK substrates) could be widespread. As for human ENTs, the position corresponding to Gln62 in AtENT3 is occupied by methionine and isoleucine (both amino acids with hydrophobic side chains) in HsENT1 and HsENT4, respectively, and by glutamine and threonine (both amino acids with polar side chains) in HsENT2 and HsENT3, respectively. Transport assays performed with human ENTs have revealed that while HsENT1 transports nucleobases, it does so significantly less readily than HsENT2, while both transport ribosides as well (Yao et al., 2011, 2002; Young et al., 2008). HsENT3 transport both ribosides and nucleobases (Baldwin et al., 2005). The active sites of HsENT1 and HsENT2 differ in additional residues alongside the one corresponding to Gln62 in AtENT3; Ala88 and Gly154 in HsENT1 correspond to

Ser75 and Ser141 in HsENT2 (as well as Tyr61 and Asp129 in AtENT3), respectively. These two serine residues might further increase the potential of the HsENT2 active site to interact with nucleobases via hydrogen bonding. The trend among the substrate preferences of HsENT1-3 supports the hypothesis that the identity of the residue corresponding to Gln62 in AtENT3 co-determines the substrate specificity of an ENT protein. The case of HsENT4 is less straightforward. Concerning canonical nucleobases and ribosides, HsENT4 transports adenosine but not adenine, whereas its mouse homolog, MmENT4, transports both these substances. Nevertheless, HsENT4 also recognizes a variety of non-ribosylated amines, namely epinephrine, norepinephrine, dopamine, serotonin, and histamine (Barnes et al., 2006; Engel et al., 2004). While not derived from nucleobases, the structures of these amines might resemble CKs since they consist of an aromatic cycle and a side chain carrying at least one polar atomic group. Unlike HsENT1-3, HsENT4 possesses a tyrosine residue at the position corresponding to Tyr61 in AtENT3 (Tyr112 in HsENT4), which I suggest to interact with the side chain of hydroxylated CKs (Chapter 4.2). Therefore, HsENT4 could bind amine-containing compounds through its Tyr112 residue independently of its specificities for nucleobases and ribosides.

5.2 Elusive Thermodynamics of the AtENT3-Mediated Transport

Another finding presented in Chapter 4.2 says that the AtENT3-mediated transport of tZR does not change when treated with 10µM CCCP (unlike the treatment with 10µM NBTI and dipyridamole, which cancels or diminishes the effect of *AtENT3* expression), even though the overall tZR uptake in BY-2 cells significantly drops. This finding is consistent with a previous report by Li and colleagues (Li et al., 2003) showing that 5µM CCCP and 1mM dinitrophenol (DNP) only mildly affect the AtENT3-mediated uptake of adenosine and uridine. For comparison, treating AtENT1 with 1mM DNP abolishes the AtENT1-mediated adenosine uptake (Möhlmann et al., 2001).

The resistance of AtENT3 towards CCCP might indicate that AtENT3 mediates facilitated diffusion rather than proton gradient-dependent transport, in contrast to how my colleagues and I review the thermodynamics of AtENTs in Chapter 4.1. However, this interpretation clashes with other reports showing that the rate of AtENT3-mediated adenosine transport changes with pH, and conversely, intracellular pH decreases in the presence of adenosine, both of which point towards adenosine-proton symport (Traub et al., 2007; Wormit et al., 2004). The dependence of the AtENT3-mediated adenosine transport rate on pH contrasts with AtENT7, which mediates adenosine uniport (Girke et al., 2015; Wormit et al., 2004).

The seemingly contradicting conclusions about the thermodynamic aspect of the AtENT3-mediated transport might indicate that the proton gradient stimulates the adenosine uptake by AtENT3 but is not necessary for the transport to occur. Such interpretation would be consistent with the fact that AtENT3 retains at least 60% of its optimal adenosine uptake rate in pH ranging from 5.5 to 8.0, but the transport activity of AtENT1 almost drops to zero in the alkali environment (Wormit et al., 2004).

The transport mechanism of AtENT3 might be similar to that of HsENT4, which can transport adenosine and its derivative 2-chloroadenosine at neutral and acidic pH, but in the latter case, the transport rate is much higher. Curiously, the HsENT4-mediated transport of serotonin is

independent of pH, indicating that the transport mode of one ENT protein towards different substrates might vary (Barnes et al., 2006; Tandio et al., 2019). Previously, I have hypothesized that the binding mode between HsENT4 and biologically active amines such as serotonin could be similar to the computationally modelled binding mode between AtENT3 and tZR shown in Chapter 4.2, given that the Tyr112 residue in HsENT4 aligns with the tZR-binding Tyr61 in AtENT3 and that the side chains of serotonin and tZR might play similar roles in interaction with their respective transporters. It follows that similarly to HsENT4 and serotonin, AtENT3 might transport tZR in a different mode than adenosine or uridine independently of the proton gradient. This dual action of AtENT3 would further explain the observed insensitivity of AtENT3-mediated tZR uptake to CCCP. We can promptly address this hypothesis by performing the accumulation assays described in Chapter 4.2 at various pH.

5.3 Multifaceted Function of AtENT3: One Task in Diverse Locations

In this thesis, I address the AtENT3-mediated CK transport in relation to tZR uptake from the apoplast. This uptake is necessary for the LOG-catalysed activation of root-borne tZR in shoots (Sakakibara, 2021). The LOG-activated CKs regulate the fate of SAM cells by inducing *WUS* expression (Landrein et al., 2018; Lopes et al., 2021; Sakakibara, 2021). My colleagues and I demonstrate the involvement of AtENT3 in the uptake of root-borne tZR by showing that the *WUS* expression in *atent3 A. thaliana* seedling shoots is lower than in the wild type. Treating the *atent3* seedlings with tZR rescues the decreased *WUS* expression, supporting the hypothesis that the change in *WUS* expression occurs due to the limited tZR access. Moreover, publicly available transcriptomic data show that *AtENT3* is, alongside *AtENT1*, expressed in the shoot apex area and that ectopic over-expression of *WUS* downregulates the expression of *AtENT3*, together with *AtENT4*, *AtLOG5*, *AtLOG6*, and *AtLOG8*, and upregulates the expression of *AtCKX7*, suggesting that WUS attenuates the incoming CK signal by various means (Figure 6 in Chapter 4.2).

Based on the results presented in Chapter 4.2, I conclude that AtENT3 mediates the uptake of root-borne tZR from the xylem in shoots. Korobova and colleagues (2021) have previously reported that AtENT3 contributes to CK retention in roots. In both situations, AtENT3 is a membrane-bound carrier that mediates CK transport from the apoplast to the cytoplasm, but its action in roots and shoots implies different effects on CK distribution throughout the plant. In roots, AtENT3 negatively regulates root-to-shoot CK translocation and CK-mediated responses by retaining root-borne CKs that would otherwise travel to shoots and activate downstream elements of the two-component signalling cascade there. Conversely, in shoots, AtENT3 enables LOG-catalysed activation of root-borne CKs, thus promoting CK-mediated responses and demonstrating that in the context of a specific physiological process, a single protein can play even antagonistic roles based just on its localization.

The AtENT3-mediated uptake of tZ-type CKs in roots implies that in *aten3* mutants, a larger portion of CKs is transported from roots to shoots. Korobova and colleagues (2021) confirm this assumption by showing that when supplied with exogenous tZR, *atent3* mutant plants have less tZ-type CKs in roots and more in shoots compared to wild-type plants. This change in CK distribution could be related to the phenotypes presented in Chapter 4.2. The *atent3* plants have larger cotyledons and leaves compared to the wild type, opposite to the smaller leaves of plants with less

CK content in the shoots due to overexpressed *CKX* (Holst et al., 2011; Werner et al., 2001) or multiple *ipt* mutations (Miyawaki et al., 2006), suggesting that the observed phenotype of *atent3* is caused by increased CK signalling in *atent3* shoots, although the CK effect on leaf size depends on other contextual variables and can be both positive and negative (Skalák et al., 2019; Wu et al., 2021). Considering that the *atent3* mutation hinders the LOG-catalysed activation of root-borne CKs, the probable CK-positive phenotype is likely mediated by CPN1-activated CKs. This activation pathway could be boosted not only by the increased influx of root-borne CKs but also by their decreased uptake into the cells and, thus, higher accumulation in the apoplast, where CPN1 is active (Kojima et al., 2023); i.e. consequences of the loss of *atent3* function in roots and shoots might add to one another, resulting in the apparent CK-positive response in the *atent3* shoots.

5.4 Transcriptomic Data Suggest Complex AtENT3 Regulation by Cytokinins

The opposing functions of root- and shoot-localized AtENT3 proteins can potentially clash. Plants might prevent this clash by employing different mechanisms to regulate the *AtENT3* expression in roots and shoots. The WUS-mediated downregulation of *AtENT3* in shoots could be an example of this differential regulation since the *WUS* expression is restricted to specific areas of the SAM. As the *WUS* expression is upregulated by CKs (Lopes et al., 2021), it follows that in shoots, CKs act as negative regulators of the AtENT3-mediated transport and that AtENT3 is subject to negative feedback mediated by its substrate. A similar mechanism in roots would mean that CK retention in roots diminishes when the CK content in the xylem increases, for instance, in response to increased nitrate supply. In this hypothetical situation, the plant loses a way to regulate the already boosted root-to-shoot CK flux. On the contrary, if CKs regulate *AtENT3* expression in roots positively, an increase in CK root-to-shoot flux activates AtENT3-mediated retention of CKs in roots and decreases the amount of CKs travelling to shoots. It means that different responses of the *AtENT3* expression to CKs would allow CKs to effectuate negative feedback to their translocation both in roots and shoots by modulating AtENT3 activity. This hypothesis could be addressed by measuring *AtENT3* expression in CK-treated and control plants with roots and shoots separated.

Publicly available transcriptomic data accessible via Electronic Fluorescent Pictograph (eFP) Browser (Winter et al., 2007) show that treating whole 7-day-old *A. thaliana* seedlings with 1μM tZ leads to a 1.69-fold increase of *AtENT3* expression one hour after the treatment (compared to the non-treated control). After the next two hours, *AtENT3* expression in the treated seedlings is 5.10 times lower than in the control. This trend might be consistent with the assumed CK-mediated regulation of *AtENT3* expression. Its early rise might reflect the *AtENT3* upregulation in roots due to CK treatment, and the later drop might occur as a portion of the tZ used for the treatment translocates to shoots and downregulates the *AtENT3* expression there. Another experiment in the eFP Browser shows that treating 21-day-old *A. thaliana* plants with 20μM tZ leads to a 1.58-fold increase of *AtENT3* expression three hours after the treatment. The different responses to tZ in younger and older plants might be due to different root-to-shoot ratios of the base *AtENT3* expression levels.

Other datasets available through the eFP Browser provide transcriptomic data obtained during tissue regeneration and *de novo* organogenesis. In *A. thaliana* hypocotyl explants, tissue

differentiation is an outcome of auxin-CK interplay (Kubo and Kakimoto, 2000; Pernisová et al., 2009), implying that changes in the *AtENT3* expression during these processes might provide additional insight into its regulation by CK. Che and colleagues (2006) measured gene expression levels in root *A. thaliana* root explants cultivated on callus induction medium (containing auxin and CK in 11:1 ratio), shoot induction medium (containing auxin and CK in 9:50 ratio) or root induction medium (containing only auxin). *AtENT3* expression decreases in the explants cultivated on shoot induction medium and increases in the explants cultivated on the other two media types. The former trend supports the hypothesis that CKs downregulate the *AtENT3* expression in shoots. The latter trend does not directly address the issue of whether CKs upregulate the *AtENT3* expression in roots but indicates that AtENT3 might be regulated by auxin or possibly auxin-to-CK ratio. The involvement of auxin in AtENT3 regulation is further supported by *AtENT3* upregulation in roots treated with 10μM 1-naphthylacetic acid (NAA; an auxin) in assays studying lateral root initiation (De Rybel et al., 2012; Vanneste et al., 2005) and *AtENT3* upregulation in root meristem during its regeneration after removal of the stem cell niche, a process marked by increased auxin signalling and reorganization of the auxin transport network (Sena et al., 2009).

Che and colleagues (2006) further show that *AtENT6*[1], the closest relative of *AtENT3* (Li et al., 2003), is more than 10-fold downregulated due to the mutation of the *RELATED TO AP2 6L* (*RAP2.6L*) gene. *RAP2.6L* encodes a transcription factor expressed during early shoot development (Che et al., 2006) and might thus regulate CK homeostasis in shoots by controlling the AtENT3-mediated CK transport. In addition, *RAP2.6L* responds to stress hormones abscisic acid, jasmonic acid, salicylic acid, and ethylene (Krishnaswamy et al., 2011) and might thus contribute to their interactions with CKs.

Chatfield and colleagues (2013) induced the regeneration of *A. thaliana* lateral root primordia into shoot meristem by consecutive treatment with 10μM NAA and 4.4μM iP. Since shoot regeneration from root tissues involves *WUS* expression (Gallois et al., 2004; Gordon et al., 2007), the authors performed the same experiment with the *wus* mutant and measured gene expression levels in the roots of wild-type and *wus* seedlings. In both sample types, *AtENT3* expression significantly decreases after a two-day-long iP treatment, a time point corresponding to the initiation of the *WUS* expression in the wild-type lateral root primordia (Chatfield et al., 2013). These findings support the negative regulation of AtENT3 by WUS, suggested in Chapter 4.2. However, they also imply that CKs can downregulate *AtENT3* expression in a WUS-independent manner. Interestingly, the CK treatment stimulates *RAP2.6L* expression both in wild-type and *wus* plants, which means that the expression trends of *AtENT3* and *RAP2.6L* are opposite, contrary to the reported downregulation of *AtENT3* in *rap2.6l* mutant plants (Che et al., 2006).

5.5 Metabolic Regulation of Cytokinin Distribution in Response to Nitrate Supply

My colleagues and I show that CK distribution among roots and shoots in oats is further regulated by the CKX-catalysed cleavage of CKs in the xylem. The CKX present in oat xylem prefers tZ to cZ, consistent with the substrate preferences of CKXs derived from roots (Figure 4 in

1 Che and colleagues (2006) used Affymetrix ATH1 GeneChips microarrays to measure gene expression levels. The corresponding probe set ID annotation, accessible via GEO as GPL198, maps both *AtENT6* (At4g05110) and *AtENT3* (At4g05120) to the same probe set, namely 255261_s_at, and the discussed change in expression might thus be relevant to both genes.

Chapter 4.3) and the previously reported preferences of extracellular CKX isoforms, notably ZmCKX1 (Šmehilová et al., 2009; Zalabák et al., 2014). We have therefore hypothesized that the CKX activity observed in oat xylem sap is mostly effectuated by oat homologs of ZmCKX1, dubbed AsCKX1a, AsCKX1c, and AsCKX1d, which are synthesized in roots and subsequently secreted to the xylem. This hypothesis is supported by the expression pattern of AsCKXs, showing that *AsCKX1s* are predominantly expressed in roots (Figure 5 in Chapter 4.3), and glycosylation of the CKX isoforms active in oat xylem sap (Figure 6 in Chapter 4.3), which is consistent with the function-determining glycosylation of ZmCKX1 (Franc et al., 2012). Proteomic analysis that could confirm or specify the role of AsCKX1s in xylem sap is underway.

ZmCKX1 has been repeatedly reported to efficiently cleave CK nucleobases and, to a lesser extent, ribosides (Kopečný et al., 2016; Šmehilová et al., 2009; Zalabák et al., 2014), which are the two predominant forms of tZ in xylem (Sakakibara, 2021; Takei et al., 2001b). This substrate specificity suggests that homologs of ZmCKX1 could be efficient regulators of the root-to-shoot CK flux. CK nucleobases, being the favourite substrate type of the CKX isoforms active in xylem, might contribute to the prevalence of tZR over tZ in xylem sap. Moreover, assuming that the CK fraction of the xylem sap is consecutively subject to CKX-catalysed cleavage, the amount of biologically active CK nucleobases travelling from roots to shoots might progressively decrease with the distance travelled, resulting in a gradient of CK signal alongside the basipetal axis of the plant.

In Chapter 4.3, my colleagues and I further show that concentrations of tZ-type in roots and xylem sap but not in leaves respond to nitrate supply, which is consistent with previous reports that nitrate positively regulates root-to-shoot CK transport (Takei et al., 2001b) as well as expression of genes involved in the biosynthesis of tZ-type CKs (Maeda et al., 2018; Miyawaki et al., 2004; Ramireddy et al., 2014; Takei et al., 2004a, 2004b). In general, the concentrations of tZ-type CKs increase with nitrate supply, but this trend is not linear and passes through a minimum between nitrate concentrations of 16.0 and 250.0μM (Figure 7 in Chapter 4.3). This trend might be, broadly speaking, a result of multiple signalling pathways simultaneously regulating biosynthesis and the export of tZ-type CKs in roots. Another possible explanation concerns the nitrate transporter/receptor NFP6.3. This protein exists in two forms; with limited nitrate supply, NFP6.3 is a protomer with a high affinity for nitrate. As the nitrate becomes plentiful, NFP6.3 dimerizes, and its affinity towards nitrate lowers (Parker and Newstead, 2014; Sun et al., 2014; Sun and Zheng, 2015). Considering this nitrate-dependent dimerization, there might be a range in which an increase in nitrate supply results in a decreased nitrate transport/sensing capacity of NFP6.3 (further discussed in the manuscript in Chapter 4.3). Unlike tZ-type CKs, cZ-type CKs in leaves and roots respond to the increasing nitrate supply negatively. Considering that cZ-type CKs are likely products of tRNA degradation (Kasahara et al., 2004; Miyawaki et al., 2004), their down-regulation by bountiful nitrate supply is consistent with tRNA mobilization during nitrogen starvation (Melino et al., 2018). The opposing trends of tZ- and cZ-type CK responses to nitrate supply suggest that the tZ-to-cZ ratio reflects the amount of available nitrogen and that cZ might act as a messenger of nitrogen starvation, which is consistent with the previously reported involvement of cZ in stress responses and stress resistance (Eisermann et al., 2020; Schäfer et al., 2015; Silva-Navas et al., 2019).

The response of CKX activity in xylem sap mirrors that of tZ-type CKs, indicating that the CKX-catalysed degradation of CKs travelling from roots to shoots is mediated and linked to current

CK concentrations (Figure 7 in Chapter 4.3). Since *CKX* genes are upregulated by CKs (Brenner et al., 2012; Gao et al., 2014; Zhou et al., 2020), the increased CKX activity in xylem likely represents negative feedback to the increased CK concentrations in xylem sap. Nitrate-mediated upregulation of the CKX activity in xylem sap is consistent with a report showing that one CKX isoform in *A. thaliana*, AtCKX4, responds positively to nitrate and is negatively regulated by the NIGT1 repressor (Maeda et al., 2018). Consistently with this finding, Ramireddy and colleagues (2014) show that the nitrate-mediated expression changes of *AtCKX4* are the most prominent of all *AtCKX* genes. The similarity search algorithm available via the UniProtKB database (The UniProt Consortium, 2023) reveals that AtCKX4 is the closest *A. thaliana* homolog of ZmCKX1 and thus expected to be responsible for the CKX activity in xylem, further supporting the link between CKX in xylem and nitrate. *AtCKX4* expression is not altered due to repression of the nitrate-responding transcription factor NLP6 (Maeda et al., 2018), suggesting that the positive response of CKX in the xylem to nitrate is a consequence of the elevated CK concentrations, rather than *AtCKX4* expression being directly mediated by nitrate (although involvement of another nitrate-responding transcription factor is not ruled out). The report by Maeda and colleagues (2018) shows that *AtENT3* is downregulated by nitrate and NIGT1, too. Other reports have shown that plant ENTs are generally upregulated during nitrogen starvation, possibly to increase cellular uptake of nucleosides that are further metabolized and provide nitrogen (Li et al., 2003; Ľuptáková et al., 2024; Melino et al., 2018). In roots, AtENT3 downregulation by increased nitrate supply could result in decreased CK retention and thus enhanced CK root-to-shoot flux, which raises a question of whether the AtENT3-mediated negative feedback to increased CK concentrations suggested above can indeed occur. It is worth testing AtENT3's response to nitrate with roots and shoots separated to better understand how these responses could potentially clash with the putative regulation pathways suggested above. It should not be ignored that the negative response of AtENT3 to nitrate might also be mediated by CKs, similar to AtCKX4.

6 Conclusions

Based on the results presented in this thesis, I conclude that:

1. CK ribosides are transported across the plasma membrane by at least two types of membrane-bound carriers, of which one transports both CK nucleobases and ribosides, whereas the other is riboside-specific
2. AtENT3 transports CK nucleobases and ribosides, preferring tZR over iPR. This preference can be explained by Tyr61 and Asp129 residues, conserved among AtENTs but not among ENTs from non-plant species and interacting with the side-chain hydroxyl group of tZR.
3. The *atent3* mutation results in the downregulation of *WUS* expression in shoots and affects the shoot phenotype; conversely, *AtENT3* expression is downregulated by WUS, indicating that AtENT3 at least partially mediates CK uptake necessary for the LOG-catalysed activation of root-borne CK ribosides in shoots.
4. CKX is active in xylem sap, and root-borne CKs travelling to shoots are, therefore, subject to metabolic degradation, which allows plants to regulate the CK flux in the xylem. The CKX isoforms responsible for this regulation are likely homologs of ZmCKX1 (such as AtCKX4 in *A. thaliana*). CKX activity in the xylem mirrors the CK concentrations, confirming that this activity is regulated.

I summarize these findings in the context of the current state of the art in **Figure 2**.

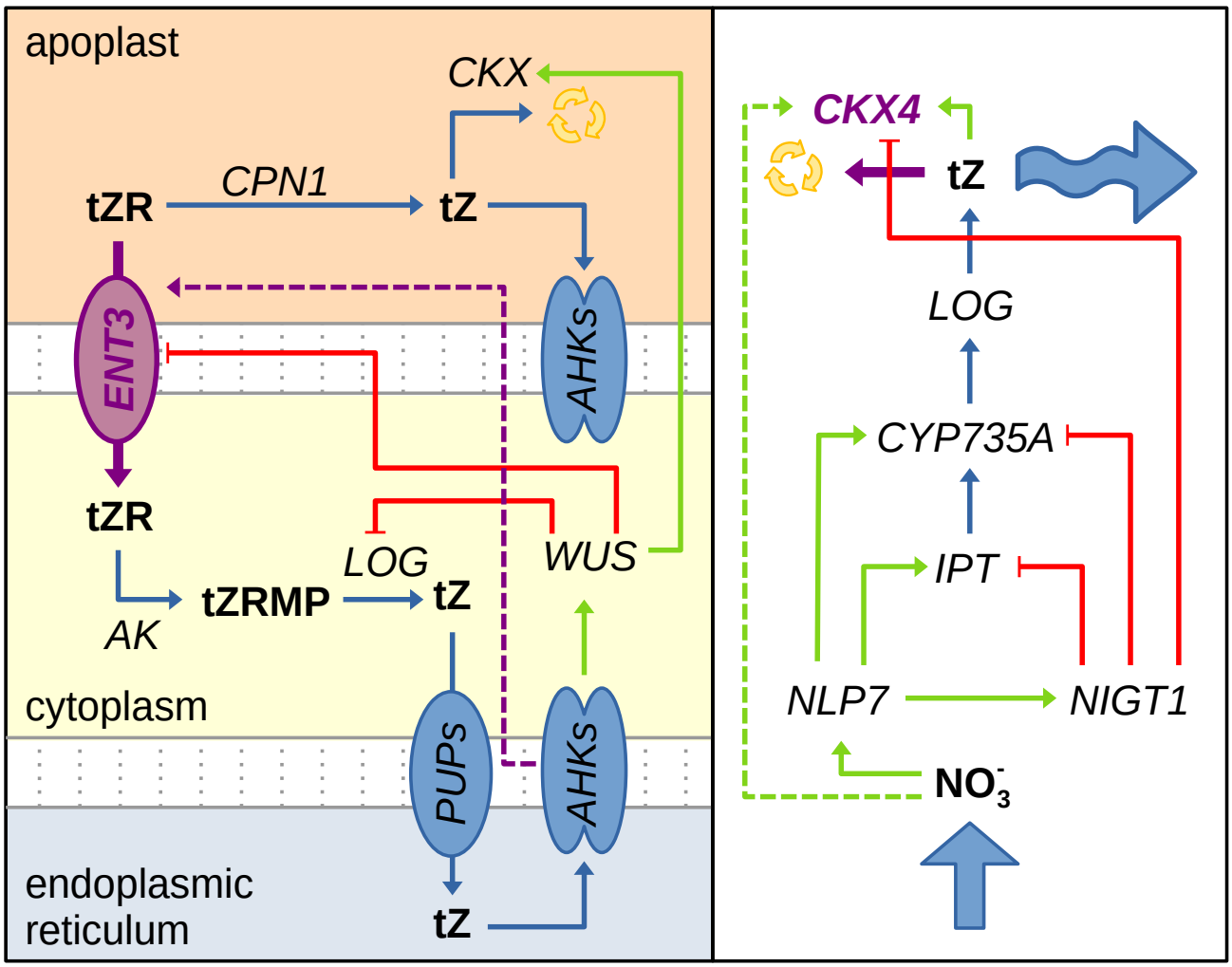

Figure 2: Findings from this thesis implemented into working models of mechanisms contributing to regulation and maintenance of CK distribution. **Left**: AtENT3 mediates tZR uptake from the apoplast to the cytoplasm. In the cytoplasm, tZR is activated via AK and LOG to tZ, which can enter the endoplasmic reticulum to activate AHKs. Importers of tZ to the endoplasmic reticulum include homologs of OsPUP1 and OsPUP7. The LOG-catalysed activation pathway allows CKs to stimulate *WUS* expression in the SAM. WUS provides negative feedback to CK signalization by inhibiting the LOG and AtENT3 activity and stimulating CKX-catalysed CK degradation. CK signalling could also regulate AtENT3 in a WUS-independent manner. The exact mechanism of this regulation remains to be explained (dashed arrow line). Alternatively, tZR can be converted to tZ by CPN1 in the apoplast and activate plasma membrane-bound AHKs, although this pathway seems insufficient to stimulate *WUS* expression. For simplicity, CKX activity is depicted in the apoplast only. **Right**: Increased nitrate supply in roots stimulates expression of CK biosynthetic genes responsive to the NLP7 transcription factor and NIGT1 repressor. The synthesized CKs (here represented by tZ) can be transported to shoots via xylem (wavy arrow) or degraded by AtCKX7 (a homolog of ZmCKX1). *AtCKX7* expression is stimulated by nitrate via a yet unknown pathway and repressed by NIGT1.

7 References

Abualia, R., Ötvös, K., Novák, O., Bouguyon, E., Domanegg, K., Krapp, A., Nacry, P., Gojon, A., Lacombe, B., Benková, E., 2022. Molecular framework integrating nitrate sensing in root and auxin-guided shoot adaptive responses. Proc. Natl. Acad. Sci. U.S.A. 119, e2122460119. https://doi.org/10.1073/pnas.2122460119

Abualia, R., Riegler, S., Benkova, E., 2023. Nitrate, Auxin and Cytokinin—A Trio to Tango. Cells 12, 1613. https://doi.org/10.3390/cells12121613

Allen, M., Qin, W., Moreau, F., Moffatt, B., 2002. Adenine phosphoribosyltransferase isoforms of Arabidopsis and their potential contributions to adenine and cytokinin metabolism. Physiologia Plantarum 115, 56–68. https://doi.org/10.1034/j.1399-3054.2002.1150106.x

Alvarez, J.M., Schinke, A.-L., Brooks, M.D., Pasquino, A., Leonelli, L., Varala, K., Safi, A., Krouk, G., Krapp, A., Coruzzi, G.M., 2020. Transient genome-wide interactions of the master transcription factor NLP7 initiate a rapid nitrogen-response cascade. Nat Commun 11, 1157. https://doi.org/10.1038/s41467-020-14979-6

Anantharaman, V., Aravind, L., 2001. The CHASE domain: a predicted ligand-binding module in plant cytokinin receptors and other eukaryotic and bacterial receptors. Trends in Biochemical Sciences 26, 579–582. https://doi.org/10.1016/S0968-0004(01)01968-5

Antoniadi, I., Novák, O., Gelová, Z., Johnson, A., Plíhal, O., Simerský, R., Mik, V., Vain, T., Mateo-Bonmatí, E., Karady, M., Pernisová, M., Plačková, L., Opassathian, K., Hejátko, J., Robert, S., Friml, J., Doležal, K., Ljung, K., Turnbull, C., 2020. Cell-surface receptors enable perception of extracellular cytokinins. Nature Communications 11, 4284. https://doi.org/10.1038/s41467-020-17700-9

Argueso, C.T., Kieber, J.J., 2024. Cytokinin: From autoclaved DNA to two-component signaling. The Plant Cell koad327. https://doi.org/10.1093/plcell/koad327

Argyros, R.D., Mathews, D.E., Chiang, Y.-H., Palmer, C.M., Thibault, D.M., Etheridge, N., Argyros, D.A., Mason, M.G., Kieber, J.J., Schaller, G.E., 2008. Type B Response Regulators of Arabidopsis Play Key Roles in Cytokinin Signaling and Plant Development. Plant Cell 20, 2102–2116. https://doi.org/10.1105/tpc.108.059584

Arkhipova, T.N., Veselov, S.U., Melentiev, A.I., Martynenko, E.V., Kudoyarova, G.R., 2005. Ability of bacterium Bacillus subtilis to produce cytokinins and to influence the growth and endogenous hormone content of lettuce plants. Plant Soil 272, 201–209. https://doi.org/10.1007/s11104-004-5047-x

Armstrong, D.J., Burrows, W.J., Evans, P.K., Skoog, F., 1969. Isolation of cytokinins from tRNA. Biochemical and Biophysical Research Communications 37, 451–456. https://doi.org/10.1016/0006-291X(69)90936-X

Arnau, J.A., Tadeo, F.R., Guerri, J., Primo-Millo, E., 1999. Cytokinins in peach: Endogenous levels during early fruit development. Plant Physiology and Biochemistry 37, 741–750. https://doi.org/10.1016/S0981-9428(00)86687-5

Åstot, C., Doležal, K., Nordström, A., Wang, Q., Kunkel, T., Moritz, T., Chua, N.-H., Sandberg, G., 2000. An alternative cytokinin biosynthesis pathway. Proceedings of the National Academy of Sciences of the United States of America 97, 14778–83. https://doi.org/10.1073/pnas.260504097

Baldwin, S.A., Yao, S.Y.M., Hyde, R.J., Ng, A.M.L., Foppolo, S., Barnes, K., Ritzel, M.W.L., Cass, C.E., Young, J.D., 2005. Functional Characterization of Novel Human and Mouse Equilibrative Nucleoside Transporters (hENT3 and mENT3) Located in Intracellular Membranes *. Journal of Biological Chemistry 280, 15880–15887. https://doi.org/10.1074/jbc.M414337200

Barnes, K., Dobrzynski, H., Foppolo, S., Beal, P.R., Ismat, F., Scullion, E.R., Sun, L., Tellez, J., Ritzel, M.W.L., Claycomb, W.C., Cass, C.E., Young, J.D., Billeter-Clark, R., Boyett, M.R., Baldwin, S.A., 2006. Distribution and Functional Characterization of Equilibrative Nucleoside Transporter-4, a Novel Cardiac Adenosine Transporter Activated at Acidic pH. Circulation Research. https://doi.org/10.1161/01.RES.0000238359.18495.42

Bassil, N.V., Mok, Dws., Mok, M.C., 1993. Partial Purification of a cis-trans-Isomerase of Zeatin from Immature Seed of Phaseolus vulgaris L. Plant Physiol. 102, 867–872. https://doi.org/10.1104/pp.102.3.867

Besnard, F., Rozier, F., Vernoux, T., 2014. The AHP6 cytokinin signaling inhibitor mediates an auxin-cytokinin crosstalk that regulates the timing of organ initiation at the shoot apical meristem. Plant Signaling & Behavior 9, e28788. https://doi.org/10.4161/psb.28788

Bishopp, A., Lehesranta, S., Vatén, A., Help, H., El-Showk, S., Scheres, B., Helariutta, K., Mähönen, A.P., Sakakibara, H., Helariutta, Y., 2011. Phloem-Transported Cytokinin Regulates Polar Auxin Transport and Maintains Vascular Pattern in the Root Meristem. Current Biology 21, 927–932. https://doi.org/10.1016/j.cub.2011.04.049

Boswell-Casteel, R.C., Hays, F.A., 2017. Equilibrative Nucleoside Transporters – A Review. Nucleosides Nucleotides Nucleic Acids 36, 7–30. https://doi.org/10.1080/15257770.2016.1210805

Brenner, W.G., Ramireddy, E., Heyl, A., Schmülling, T., 2012. Gene Regulation by Cytokinin in Arabidopsis. Front. Plant Sci. 3. https://doi.org/10.3389/fpls.2012.00008
Brownlee, B.G., Hall, R.H., Whitty, C.D., 1975. 3-Methyl-2-butenal: An Enzymatic Degradation Product of the Cytokinin, N^6-(Δ^2-Isopentenyl)adenine. Can. J. Biochem. 53, 37–41. https://doi.org/10.1139/o75-006
Brzobohatý, B., Moore, I., Kristoffersen, P., Bako, L., Campos, N., Schell, J., Palme, K., 1993. Release of active cytokinin by a beta-glucosidase localized to the maize root meristem. Science 262, 1051–1054. https://doi.org/10.1126/science.8235622
Bürkle, L., Cedzich, A., Döpke, C., Stransky, H., Okumoto, S., Gillissen, B., Kühn, C., Frommer, W.B., 2003. Transport of cytokinins mediated by purine transporters of the PUP family expressed in phloem, hydathodes, and pollen of Arabidopsis. The Plant Journal 34, 13–26. https://doi.org/10.1046/j.1365-313X.2003.01700.x
Caesar, K., Thamm, A.M.K., Witthöft, J., Elgass, K., Huppenberger, P., Grefen, C., Horak, J., Harter, K., 2011. Evidence for the localization of the Arabidopsis cytokinin receptors AHK3 and AHK4 in the endoplasmic reticulum. J Exp Bot 62, 5571–5580. https://doi.org/10.1093/jxb/err238
Cedzich, A., Stransky, H., Schulz, B., Frommer, W.B., 2008. Characterization of Cytokinin and Adenine Transport in Arabidopsis Cell Cultures 148, 1857–1867. https://doi.org/10.1104/pp.108.128454
Chang, L., Ramireddy, E., Schmülling, T., 2015. Cytokinin as a positional cue regulating lateral root spacing in Arabidopsis. J Exp Bot 66, 4759–4768. https://doi.org/10.1093/jxb/erv252
Chatfield, S.P., Capron, R., Severino, A., Penttila, P.-A., Alfred, S., Nahal, H., Provart, N.J., 2013. Incipient stem cell niche conversion in tissue culture: using a systems approach to probe early events in WUSCHEL-dependent conversion of lateral root primordia into shoot meristems. The Plant Journal 73, 798–813. https://doi.org/10.1111/tpj.12085
Che, P., Lall, S., Nettleton, D., Howell, S.H., 2006. Gene Expression Programs during Shoot, Root, and Callus Development in Arabidopsis Tissue Culture. Plant Physiology 141, 620–637. https://doi.org/10.1104/pp.106.081240
Chen, C.-M., Kristopeit, S.M., 1981a. Metabolism of Cytokinin: Dephosphorylation of Cytokinin Ribonucleotide by 5'-Nucleotidases From Wheat Germ Cytosol. Plant physiology 67, 494–498. https://doi.org/10.1104/PP.67.3.494
Chen, C.-M., Kristopeit, S.M., 1981b. Metabolism of Cytokinin: Deribosylation of Cytokinin Ribonucleoside by Adenosine Nucleosidase from Wheat Germ Cells. Plant Physiol 68, 1020–1023.
Chen, L., Zhao, J., Song, J., Jameson, P.E., 2021. Cytokinin glucosyl transferases, key regulators of cytokinin homeostasis, have potential value for wheat improvement. Plant Biotechnology Journal 19, 878–896. https://doi.org/10.1111/pbi.13595
Chen, L.-Q., 2014. SWEET sugar transporters for phloem transport and pathogen nutrition. New Phytologist 201, 1150–1155. https://doi.org/10.1111/nph.12445
Corbesier, L., Prinsen, E., Jacqmard, A., Lejeune, P., Van Onckelen, H., Périlleux, C., Bernier, G., 2003. Cytokinin levels in leaves, leaf exudate and shoot apical meristem of Arabidopsis thaliana during floral transition. J Exp Bot 54, 2511–2517. https://doi.org/10.1093/jxb/erg276
Cronin, H., Draelos, Z.D., 2010. Original Contribution: Top 10 botanical ingredients in 2010 anti-aging creams. Journal of Cosmetic Dermatology 9, 218–225. https://doi.org/10.1111/j.1473-2165.2010.00516.x
Cutcliffe, J.W., Hellmann, E., Heyl, A., Rashotte, A.M., 2011. CRFs form protein–protein interactions with each other and with members of the cytokinin signalling pathway in Arabidopsis via the CRF domain. Journal of Experimental Botany 62, 4995–5002. https://doi.org/10.1093/jxb/err199
Davière, J.-M., Achard, P., 2013. Gibberellin signaling in plants. Development 140, 1147–1151. https://doi.org/10.1242/dev.087650
De Rybel, B., Adibi, M., Breda, A.S., Wendrich, J.R., Smit, M.E., Novák, O., Yamaguchi, N., Yoshida, S., Isterdael, G.V., Palovaara, J., Nijsse, B., Boekschoten, M.V., Hooiveld, G., Beeckman, T., Wagner, D., Ljung, K., Fleck, C., Weijers, D., 2014. Integration of growth and patterning during vascular tissue formation in Arabidopsis. Science 345. https://doi.org/10.1126/science.1255215
De Rybel, B., Audenaert, D., Xuan, W., Overvoorde, P., Strader, L.C., Kepinski, S., Hoye, R., Brisbois, R., Parizot, B., Vanneste, S., Liu, X., Gilday, A., Graham, I.A., Nguyen, L., Jansen, L., Njo, M.F., Inzé, D., Bartel, B., Beeckman, T., 2012. A role for the root cap in root branching revealed by the non-auxin probe naxillin. Nat Chem Biol 8, 798–805. https://doi.org/10.1038/nchembio.1044
Dello Ioio, R., Galinha, C., Fletcher, A.G., Grigg, S.P., Molnar, A., Willemsen, V., Scheres, B., Sabatini, S., Baulcombe, D., Maini, P.K., Tsiantis, M., 2012. A PHABULOSA/Cytokinin Feedback Loop Controls Root Growth in Arabidopsis. Current Biology 22, 1699–1704. https://doi.org/10.1016/j.cub.2012.07.005
Deng, Y., Dong, H., Mu, J., Ren, B., Zheng, B., Ji, Z., Yang, W.-C., Liang, Y., Zuo, J., 2010. *Arabidopsis* Histidine Kinase CKI1 Acts Upstream of HISTIDINE PHOSPHOTRANSFER PROTEINS to Regulate Female Gametophyte Development and Vegetative Growth. The Plant Cell 22, 1232–1248. https://doi.org/10.1105/tpc.108.065128

Dobisova, T., Hrdinova, V., Cuesta, C., Michlickova, S., Urbankova, I., Hejatkova, R., Zadnikova, P., Pernisova, M., Benkova, E., Hejatko, J., 2017. Light Controls Cytokinin Signaling via Transcriptional Regulation of Constitutively Active Sensor Histidine Kinase CKI1. Plant Physiol. 174, 387–404. https://doi.org/10.1104/pp.16.01964

Dobránszki, J., Mendler-Drienyovszki, N., 2014. Cytokinin-induced changes in the chlorophyll content and fluorescence of *in vitro* apple leaves. Journal of Plant Physiology 171, 1472–1478. https://doi.org/10.1016/j.jplph.2014.06.015

Eisermann, I., Motyka, V., Kümmel, S., Dobrev, P.I., Hübner, K., Deising, H.B., Wirsel, S.G.R., 2020. *CgIPT1* is required for synthesis of *cis*-zeatin cytokinins and contributes to stress tolerance and virulence in *Colletotrichum graminicola*. Fungal Genetics and Biology 143, 103436. https://doi.org/10.1016/j.fgb.2020.103436

El-Showk, S., Ruonala, R., Helariutta, Y., 2013. Crossing paths: cytokinin signalling and crosstalk. Development (Cambridge, England) 140, 1373–83. https://doi.org/10.1242/dev.086371

Emery, R.J.N., Ma, Q., Atkins, C.A., 2000. The Forms and Sources of Cytokinins in Developing White Lupine Seeds and Fruits. Plant Physiology 123, 1593–1604. https://doi.org/10.1104/pp.123.4.1593

Engel, K., Zhou, M., Wang, J., 2004. Identification and Characterization of a Novel Monoamine Transporter in the Human Brain *. Journal of Biological Chemistry 279, 50042–50049. https://doi.org/10.1074/jbc.M407913200

Entsch, B., Parker, C.W., Letham, D.S., 1983. An enzyme from lupin seeds forming alanine derivatives of cytokinins. Phytochemistry 22, 375–381. https://doi.org/10.1016/0031-9422(83)83008-8

Esteves, F., Rueff, J., Kranendonk, M., 2021. The Central Role of Cytochrome P450 in Xenobiotic Metabolism—A Brief Review on a Fascinating Enzyme Family. Journal of Xenobiotics 11, 94–114. https://doi.org/10.3390/jox11030007

Evidente, A., Fujii, T., Iacobellis, N.S., Riva, S., Sisto, A., Surico, G., 1991. Structure-activity relationships of zeatin cytokinins produced by plant pathogenicPseudomonades. Phytochemistry 30, 3505–3510. https://doi.org/10.1016/0031-9422(91)80055-6

Faiss, M., Zalubilová, J., Strnad, M., Schmülling, T., 1997. Conditional transgenic expression of the ipt gene indicates a function for cytokinins in paracrine signaling in whole tobacco plants. The Plant Journal 12, 401–415. https://doi.org/10.1046/j.1365-313X.1997.12020401.x

Franc, V., Šebela, M., Řehulka, P., Končitíková, R., Lenobel, R., Madzak, C., Kopečný, D., 2012. Analysis of N-glycosylation in maize cytokinin oxidase/dehydrogenase 1 using a manual microgradient chromatographic separation coupled offline to MALDI-TOF/TOF mass spectrometry. Journal of Proteomics 75, 4027–4037. https://doi.org/10.1016/j.jprot.2012.05.013

Frébortová, J., Fraaije, M.W., Galuszka, P., Sebela, M., Pec, P., Hrbác, J., Novák, O., Bilyeu, K.D., English, J.T., Frébort, I., 2004. Catalytic reaction of cytokinin dehydrogenase: preference for quinones as electron acceptors. The Biochemical journal 380, 121–30. https://doi.org/10.1042/BJ20031813

Gajdošová, S., Spíchal, L., Kamínek, M., Hoyerová, K., Novák, O., Dobrev, P.I., Galuszka, P., Klíma, P., Gaudinová, A., Žižková, E., Hanuš, J., Dančák, M., Trávníček, B., Pešek, B., Krupička, M., Vaňková, R., Strnad, M., Motyka, V., 2011. Distribution, biological activities, metabolism, and the conceivable function of cis-zeatin-type cytokinins in plants. Journal of Experimental Botany 62, 2827–2840. https://doi.org/10.1093/jxb/erq457

Gallois, J.-L., Nora, F.R., Mizukami, Y., Sablowski, R., 2004. WUSCHEL induces shoot stem cell activity and developmental plasticity in the root meristem. Genes Dev. 18, 375–380. https://doi.org/10.1101/gad.291204

Galuszka, P., Popelkova, H., Werner, T., Frébortová, J., Pospisílová, H., Mik, V., Köllmer, I., Schmülling, T., Frébort, I., 2007. Biochemical characterization of cytokinin Oxidases/Dehydrogenases from *Arabidopsis thaliana* expressed in *Nicotiana tabacum* L. Journal of Plant Growth Regulation 26, 255–267. https://doi.org/10.1007/s00344-007-9008-5

Gao, S., Fang, J., Xu, F., Wang, W., Sun, X., Chu, J., Cai, B., Feng, Y., Chu, C., 2014. CYTOKININ OXIDASE/DEHYDROGENASE4 Integrates Cytokinin and Auxin Signaling to Control Rice Crown Root Formation. Plant Physiology 165, 1035–1046. https://doi.org/10.1104/pp.114.238584

Gaudinová, A., Dobrev, P.I., Šolcová, B., Novák, O., Strnad, M., Friedecký, D., Motyka, V., 2005. The Involvement of Cytokinin Oxidase/Dehydrogenase and Zeatin Reductase in Regulation of Cytokinin Levels in Pea (Pisum sativum L.) Leaves. J Plant Growth Regul 24, 188–200. https://doi.org/10.1007/s00344-005-0043-9

Gibb, M., Kisiala, A.B., Morrison, E.N., Emery, R.J.N., 2020. The Origins and Roles of Methylthiolated Cytokinins: Evidence From Among Life Kingdoms. Front. Cell Dev. Biol. 8, 605672. https://doi.org/10.3389/fcell.2020.605672

Gillissen, B., Bürkle, L., André, B., Kühn, C., Rentsch, D., Brandl, B., Frommer, W.B., 2000. A New Family of High-Affinity Transporters for Adenine, Cytosine, and Purine Derivatives in Arabidopsis. Plant Cell 12, 291–300.

Girke, C., Arutyunova, E., Syed, M., Traub, M., Möhlmann, T., Lemieux, M.J., 2015. High yield expression and purification of equilibrative nucleoside transporter 7 (ENT7) from Arabidopsis thaliana. Biochimica et Biophysica Acta (BBA) - General Subjects 1850, 1921–1929. https://doi.org/10.1016/j.bbagen.2015.06.003
Girke, C., Daumann, M., Niopek-Witz, S., Möhlmann, T., 2014. Nucleobase and nucleoside transport and integration into plant metabolism. Front. Plant Sci. 5. https://doi.org/10.3389/fpls.2014.00443
Golovko, A., Sitbon, F., Tillberg, E., Nicander, B., 2002. Identification of a tRNA isopentenyltransferase gene from Arabidopsis thaliana. Plant Mol Biol 49, 161–169. https://doi.org/10.1023/A:1014958816241
Gordon, S.P., Chickarmane, V.S., Ohno, C., Meyerowitz, E.M., 2009. Multiple feedback loops through cytokinin signaling control stem cell number within the Arabidopsis shoot meristem. Proceedings of the National Academy of Sciences 106, 16529–16534. https://doi.org/10.1073/pnas.0908122106
Gordon, S.P., Heisler, M.G., Reddy, G.V., Ohno, C., Das, P., Meyerowitz, E.M., 2007. Pattern formation during de novo assembly of the Arabidopsisshoot meristem. Development 134, 3539–3548. https://doi.org/10.1242/dev.010298
Haberlandt, G., 1913. Zur Physiologie der Zellteilung, Sitzungsberichte der K. Preussischen Akademie der Wissenschaften zu Berlin. Kgl. Akademie d. Wissenschaften Reimer, Berlin, Berlin.
Haidoune, M., Mornet, R., Laloue, M., 1990. Synthesis of 6-(3-methylpyrrol-1-yl)-9-β-D-ribofuranosyl purine, a novel metabolite of zeatin riboside. Tetrahedron Letters 31, 1419–1422. https://doi.org/10.1016/S0040-4039(00)88821-8
Hall, R.H., 1970. N6-(δ2-Isopentenyl)adenosine: Chemical Reactions, Biosynthesis, Metabolism, and Significance to the Structure and Function of †RNA, in: Davidson, J.N., Cohn, W.E. (Eds.), Progress in Nucleic Acid Research and Molecular Biology. Academic Press, pp. 57–86. https://doi.org/10.1016/S0079-6603(08)60561-9
Hall, R.H., Csonka, L., David, H., McLennan, B., 1967. Cytokinins in the Soluble RNA of Plant Tissues. Science 156, 69–71. https://doi.org/10.1126/science.156.3771.69
Hamada, S., Onouchi, H., Tanaka, H., Kudo, M., Liu, Y.-G., Shibata, D., Machida, C., Machida, Y., 2000. Mutations in the WUSCHEL gene of Arabidopsis thaliana result in the development of shoots without juvenile leaves. The Plant Journal 24, 91–101. https://doi.org/10.1046/j.1365-313x.2000.00858.x
Hare, P.D., van Staden, J., 1994. Cytokinin oxidase: Biochemical features and physiological significance. Physiologia Plantarum 91, 128–136. https://doi.org/10.1111/j.1399-3054.1994.tb00668.x
Hejátko, J., Ryu, H., Kim, G.-T., Dobešová, R., Choi, S., Choi, S.M., Souček, P., Horák, J., Pekárová, B., Palme, K., Brzobohatý, B., Hwang, I., 2009. The Histidine Kinases CYTOKININ-INDEPENDENT1 and ARABIDOPSIS HISTIDINE KINASE2 and 3 Regulate Vascular Tissue Development in *Arabidopsis* Shoots. The Plant Cell 21, 2008–2021. https://doi.org/10.1105/tpc.109.066696
Heyl, A., Schmülling, T., 2003. Cytokinin signal perception and transduction. Current Opinion in Plant Biology 6, 480–488. https://doi.org/10.1016/S1369-5266(03)00087-6
Higuchi, M., Pischke, M.S., Mähönen, A.P., Miyawaki, K., Hashimoto, Y., Seki, M., Kobayashi, M., Shinozaki, K., Kato, T., Tabata, S., Helariutta, Y., Sussman, M.R., Kakimoto, T., 2004. In planta functions of the Arabidopsis cytokinin receptor family. Proceedings of the National Academy of Sciences 101, 8821–8826. https://doi.org/10.1073/pnas.0402887101
Hirose, N., Makita, N., Yamaya, T., Sakakibara, H., 2005. Functional Characterization and Expression Analysis of a Gene, OsENT2, Encoding an Equilibrative Nucleoside Transporter in Rice Suggest a Function in Cytokinin Transport. Plant Physiol 138, 196–206. https://doi.org/10.1104/pp.105.060137
Hirose, N., Takei, K., Kuroha, T., Kamada-Nobusada, T., Hayashi, H., Sakakibara, H., 2008. Regulation of cytokinin biosynthesis, compartmentalization and translocation. J Exp Bot 59, 75–83. https://doi.org/10.1093/jxb/erm157
Hluska, T., Dobrev, P.I., Tarkowská, D., Frébortová, J., Zalabák, D., Kopečný, D., Plíhal, O., Kokáš, F., Briozzo, P., Zatloukal, M., Motyka, V., Galuszka, P., 2016. Cytokinin metabolism in maize: Novel evidence of cytokinin abundance, interconversions and formation of a new trans-zeatin metabolic product with a weak anticytokinin activity. Plant Science 247, 127–137. https://doi.org/10.1016/j.plantsci.2016.03.014
Hluska, T., Šebela, M., Lenobel, R., Frébort, I., Galuszka, P., 2017. Purification of Maize Nucleotide Pyrophosphatase/Phosphodiesterase Casts Doubt on the Existence of Zeatin Cis–Trans Isomerase in Plants. Front. Plant Sci. 8. https://doi.org/10.3389/fpls.2017.01473
Holst, K., Schmülling, T., Werner, T., 2011. Enhanced cytokinin degradation in leaf primordia of transgenic *Arabidopsis* plants reduces leaf size and shoot organ primordia formation. Journal of Plant Physiology, Regulation of plant primary metabolism 168, 1328–1334. https://doi.org/10.1016/j.jplph.2011.03.003
Horák, J., Grefen, C., Berendzen, K.W., Hahn, A., Stierhof, Y.-D., Stadelhofer, B., Stahl, M., Koncz, C., Harter, K., 2008. The Arabidopsis thaliana response regulator ARR22 is a putative AHP phospho-histidine phosphatase expressed in the chalaza of developing seeds. BMC Plant Biol 8, 77. https://doi.org/10.1186/1471-2229-8-77
Horgan, R., Hewett, E.W., Horgan, J.M., Purse, J., Wareing, P.F., 1975. A new cytokinin from Populus x robusta. Phytochemistry 14, 1005–1008. https://doi.org/10.1016/0031-9422(75)85176-4

Hošek, P., Hoyerová, K., Kiran, N.S., Dobrev, P.I., Zahajská, L., Filepová, R., Motyka, V., Müller, K., Kamínek, M., 2020. Distinct metabolism of N-glucosides of isopentenyladenine and trans-zeatin determines cytokinin metabolic spectrum in Arabidopsis. New Phytologist 225, 2423–2438. https://doi.org/10.1111/nph.16310

Hošek, P., Kubeš, M., Laňková, M., Dobrev, P.I., Klíma, P., Kohoutová, M., Petrášek, J., Hoyerová, K., Jiřina, M., Zažímalová, E., 2012. Auxin transport at cellular level: new insights supported by mathematical modelling. J Exp Bot 63, 3815–3827. https://doi.org/10.1093/jxb/ers074

Hothorn, M., Dabi, T., Chory, J., 2011. Structural basis for cytokinin recognition by Arabidopsis thaliana histidine kinase 4. Nat Chem Biol 7, 766–768. https://doi.org/10.1038/nchembio.667

Hou, B., Lim, E.-K., Higgins, G.S., Bowles, D.J., 2004. N-Glucosylation of Cytokinins by Glycosyltransferases of Arabidopsis thaliana. J. Biol. Chem. 279, 47822–47832. https://doi.org/10.1074/jbc.M409569200

Hoyerová, K., Hošek, P., 2020. New Insights Into the Metabolism and Role of Cytokinin N-Glucosides in Plants. Front Plant Sci 11. https://doi.org/10.3389/fpls.2020.00741

Hradilová, J., Malbeck, J., Brzobohatý, B., 2007. Cytokinin Regulation of Gene Expression in the AHP Gene Family in Arabidopsis thaliana. J Plant Growth Regul 26, 229–244. https://doi.org/10.1007/s00344-007-9011-x

Hu, Y., Patra, P., Pisanty, O., Shafir, A., Belew, Z.M., Binenbaum, J., Ben Yaakov, S., Shi, B., Charrier, L., Hyams, G., Zhang, Y., Trabulsky, M., Caldararu, O., Weiss, D., Crocoll, C., Avni, A., Vernoux, T., Geisler, M., Nour-Eldin, H.H., Mayrose, I., Shani, E., 2023. Multi-Knock—a multi-targeted genome-scale CRISPR toolbox to overcome functional redundancy in plants. Nat. Plants 9, 572–587. https://doi.org/10.1038/s41477-023-01374-4

Hu, Y., Shani, E., 2023. Cytokinin activity – transport and homeostasis at the whole plant, cell, and subcellular levels. New Phytologist 239, 1603–1608. https://doi.org/10.1111/nph.19001

Hutchison, C.E., Kieber, J.J., 2002. Cytokinin Signaling in Arabidopsis. Plant Cell 14, S47–S59. https://doi.org/10.1105/tpc.010444

Hutchison, C.E., Li, J., Argueso, C., Gonzalez, M., Lee, E., Lewis, M.W., Maxwell, B.B., Perdue, T.D., Schaller, G.E., Alonso, J.M., Ecker, J.R., Kieber, J.J., 2006. The Arabidopsis Histidine Phosphotransfer Proteins Are Redundant Positive Regulators of Cytokinin Signaling. Plant Cell 18, 3073–3087. https://doi.org/10.1105/tpc.106.045674

Hwang, I., Sheen, J., 2001. Two-component circuitry in Arabidopsis cytokinin signal transduction. Nature 413, 383–389. https://doi.org/10.1038/35096500

Hwang, J.-U., Song, W.-Y., Hong, D., Ko, D., Yamaoka, Y., Jang, S., Yim, S., Lee, E., Khare, D., Kim, K., Palmgren, M., Yoon, H.S., Martinoia, E., Lee, Y., 2016. Plant ABC Transporters Enable Many Unique Aspects of a Terrestrial Plant's Lifestyle. Molecular Plant, Membrane Transport 9, 338–355. https://doi.org/10.1016/j.molp.2016.02.003

Ionescu, I.A., López-Ortega, G., Burow, M., Bayo-Canha, A., Junge, A., Gericke, O., Moller, B.L., Sánchez-Pérez, R., 2017. Transcriptome and Metabolite Changes during Hydrogen Cyanamide-Induced Floral Bud Break in Sweet Cherry. Frontiers in Plant Science 8. https://doi.org/10.3389/fpls.2017.01233

Ishida, K., Yamashino, T., Mizuno, T., 2008a. Expression of the Cytokinin-Induced Type-A Response Regulator Gene *ARR9* Is Regulated by the Circadian Clock in *Arabidopsis thaliana*. Bioscience, Biotechnology, and Biochemistry 72, 3025–3029. https://doi.org/10.1271/bbb.80402

Ishida, K., Yamashino, T., Yokoyama, A., Mizuno, T., 2008b. Three Type-B Response Regulators, ARR1, ARR10 and ARR12, Play Essential but Redundant Roles in Cytokinin Signal Transduction Throughout the Life Cycle of Arabidopsis thaliana. Plant and Cell Physiology 49, 47–57. https://doi.org/10.1093/pcp/pcm165

Islam, F., Yasmeen, T., Arif, M.S., Ali, S., Ali, B., Hameed, S., Zhou, W., 2016. Plant growth promoting bacteria confer salt tolerance in Vigna radiata by up-regulating antioxidant defense and biological soil fertility. Plant Growth Regul 80, 23–36. https://doi.org/10.1007/s10725-015-0142-y

Jamruszka, T., Banasiak, J., Pawela, A., Jarzyniak, K., Xia, J., Biała-Leonhard, W., Plačková, L., Tsering, T., Iacobini, F.R., Novák, O., Geisler, M., Jasiński, M., 2024. Medicago truncatula ABCG40 is a cytokinin importer that negatively regulates lateral root density and nodule number. https://doi.org/10.1101/2022.11.10.516000

Jarzyniak, K., Banasiak, J., Jamruszka, T., Pawela, A., Donato, M.D., Novák, O., Geisler, M., Jasiński, M., 2021. Early stages of legume–rhizobia symbiosis are controlled by ABCG-mediated transport of active cytokinins. Nature Plants 1–9. https://doi.org/10.1038/s41477-021-00873-6

Jin, S.-H., Ma, X.-M., Kojima, M., Sakakibara, H., Wang, Y.-W., Hou, B.-K., 2013. Overexpression of glucosyltransferase UGT85A1 influences trans-zeatin homeostasis and trans-zeatin responses likely through O-glucosylation. Planta 237, 991–999. https://doi.org/10.1007/s00425-012-1818-4

Jumper, J., Evans, R., Pritzel, A., Green, T., Figurnov, M., Ronneberger, O., Tunyasuvunakool, K., Bates, R., Žídek, A., Potapenko, A., Bridgland, A., Meyer, C., Kohl, S.A.A., Ballard, A.J., Cowie, A., Romera-Paredes, B., Nikolov, S., Jain, R., Adler, J., Back, T., Petersen, S., Reiman, D., Clancy, E., Zielinski, M., Steinegger, M., Pacholska, M., Berghammer, T., Bodenstein, S., Silver, D., Vinyals, O., Senior, A.W., Kavukcuoglu, K., Kohli, P.,

Hassabis, D., 2021. Highly accurate protein structure prediction with AlphaFold. Nature 596, 583–589. https://doi.org/10.1038/s41586-021-03819-2
Kakimoto, T., 2001. Identification of Plant Cytokinin Biosynthetic Enzymes as Dimethylallyl Diphosphate:ATP/ADP Isopentenyltransferases. Plant and Cell Physiology 42, 677–685. https://doi.org/10.1093/pcp/pce112
Kakimoto, T., 1996. CKI1, a Histidine Kinase Homolog Implicated in Cytokinin Signal Transduction. Source: Science, New Series 274, 982–985. https://doi.org/10.1126/science.274.5289.982
Kamal, N., Tsardakas Renhuldt, N., Bentzer, J., Gundlach, H., Haberer, G., Juhász, A., Lux, T., Bose, U., Tye-Din, J.A., Lang, D., van Gessel, N., Reski, R., Fu, Y.-B., Spégel, P., Ceplitis, A., Himmelbach, A., Waters, A.J., Bekele, W.A., Colgrave, M.L., Hansson, M., Stein, N., Mayer, K.F.X., Jellen, E.N., Maughan, P.J., Tinker, N.A., Mascher, M., Olsson, O., Spannagl, M., Sirijovski, N., 2022. The mosaic oat genome gives insights into a uniquely healthy cereal crop. Nature 1–7. https://doi.org/10.1038/s41586-022-04732-y
Kamínek, M., 2015. Tracking the Story of Cytokinin Research. J Plant Growth Regul 34, 723–739. https://doi.org/10.1007/s00344-015-9543-4
Kang, N.Y., Cho, C., Kim, J., 2013. Inducible Expression of Arabidopsis Response Regulator 22 (ARR22), a Type-C ARR, in Transgenic Arabidopsis Enhances Drought and Freezing Tolerance. PLOS ONE 8, e79248. https://doi.org/10.1371/journal.pone.0079248
Kasahara, H., Takei, K., Ueda, N., Hishiyama, S., Yamaya, T., Kamiya, Y., Yamaguchi, S., Sakakibara, H., 2004. Distinct Isoprenoid Origins of cis- and trans-Zeatin Biosyntheses in Arabidopsis. J. Biol. Chem. 279, 14049–14054. https://doi.org/10.1074/jbc.M314195200
Khablak, S.H., Spivak, S.I., Pastukhova, N.L., Yemets, A.I., Blume, Ya.B., 2024. Cytokinin Oxidase/Dehydrogenase as an Important Target for Increasing Plant Productivity. Cytol. Genet. 58, 115–125. https://doi.org/10.3103/S0095452724020051
Kiba, T., Aoki, K., Sakakibara, H., Mizuno, T., 2004. Arabidopsis Response Regulator, ARR22, Ectopic Expression of Which Results in Phenotypes Similar to the wol Cytokinin-Receptor Mutant. Plant and Cell Physiology 45, 1063–1077. https://doi.org/10.1093/pcp/pch128
Kiba, T., Takebayashi, Y., Kojima, M., Sakakibara, H., 2019. Sugar-induced de novo cytokinin biosynthesis contributes to Arabidopsis growth under elevated CO2. Sci Rep 9, 7765. https://doi.org/10.1038/s41598-019-44185-4
Kiba, T., Takei, K., Kojima, M., Sakakibara, H., 2013. Side-Chain Modification of Cytokinins Controls Shoot Growth in Arabidopsis. Developmental Cell 27, 452–461. https://doi.org/10.1016/j.devcel.2013.10.004
Kiba, T., Yamada, H., Sato, S., Kato, T., Tabata, S., Yamashino, T., Mizuno, T., 2003. The Type-A Response Regulator, ARR15, Acts as a Negative Regulator in the Cytokinin-Mediated Signal Transduction in Arabidopsis thaliana. Plant Cell Physiol 44, 868–874. https://doi.org/10.1093/pcp/pcg108
Kieber, J.J., Schaller, G.E., 2018. Cytokinin signaling in plant development. Development 145. https://doi.org/10.1242/dev.149344
Kieber, J.J., Schaller, G.E., 2010. The Perception of Cytokinin: A Story 50 Years in the Making | Plant Physiology. Plant Physiology 154, 487–492. https://doi.org/10.1104/pp.110.161596
Kim, A., Chen, J., Khare, D., Jin, J.-Y., Yamaoka, Y., Maeshima, M., Zhao, Y., Martinoia, E., Hwang, J.-U., Lee, Y., 2020. Non-intrinsic ATP-binding cassette proteins ABCI19, ABCI20 and ABCI21 modulate cytokinin response at the endoplasmic reticulum in Arabidopsis thaliana. Plant Cell Rep 39, 473–487. https://doi.org/10.1007/s00299-019-02503-0
Kline, L.K., Fittler, F., Hall, R.H., 1969. N^6-(Δ^2-isopentenyl)adenosine. Biosynthesis in transfer ribonucleic acid in vitro. Biochemistry 8, 4361–4371. https://doi.org/10.1021/bi00839a021
Ko, D., Kang, J., Kiba, T., Park, J., Kojima, M., Do, J., Kim, K.Y., Kwon, M., Endler, A., Song, W.-Y., Martinoia, E., Sakakibara, H., Lee, Y., 2014. Arabidopsis ABCG14 is essential for the root-to-shoot translocation of cytokinin. Proceedings of the National Academy of Sciences of the United States of America 111, 7150–5. https://doi.org/10.1073/pnas.1321519111
Kojima, M., Makita, N., Miyata, K., Yoshino, M., Iwase, A., Ohashi, M., Surjana, A., Kudo, T., Takeda-Kamiya, N., Toyooka, K., Miyao, A., Hirochika, H., Ando, T., Shomura, A., Yano, M., Yamamoto, T., Hobo, T., Sakakibara, H., 2023. A cell wall–localized cytokinin/purine riboside nucleosidase is involved in apoplastic cytokinin metabolism in Oryza sativa. Proceedings of the National Academy of Sciences 120, e2217708120. https://doi.org/10.1073/pnas.2217708120
Kopečná, M., Blaschke, H., Kopečný, D., Vigouroux, A., Koncitíková, R., Novák, O., Kotland, O., Strnad, M., Moréra, S., von Schwartzenberg, K., 2013. Structure and function of nucleoside hydrolases from Physcomitrella patens and maize catalyzing the hydrolysis of purine, pyrimidine, and cytokinin ribosides. Plant physiology 163, 1568–83. https://doi.org/10.1104/pp.113.228775
Kopečný, D., Končitíková, R., Popelka, H., Briozzo, P., Vigouroux, A., Kopečná, M., Zalabák, D., Šebela, M., Skopalová, J., Frébort, I., Moréra, S., 2016. Kinetic and structural investigation of the cytokinin oxidase/dehydrogenase active site. The FEBS Journal 283, 361–377. https://doi.org/10.1111/febs.13581

Kopečný, D., Šebela, M., Briozzo, P., Spíchal, L., Houba-Hérin, N., Mašek, V., Joly, N., Madzak, C., Anzenbacher, P., Laloue, M., 2008. Mechanism-Based Inhibitors of Cytokinin Oxidase/Dehydrogenase Attack FAD Cofactor. Journal of Molecular Biology 380, 886–899. https://doi.org/10.1016/j.jmb.2008.05.044

Koprna, R., De Diego, N., Dundálková, L., Spíchal, L., 2016. Use of cytokinins as agrochemicals. Bioorganic & Medicinal Chemistry, Recent Developments in Agrochemistry 24, 484–492. https://doi.org/10.1016/j.bmc.2015.12.022

Korobova, A., Kuluev, B., Möhlmann, T., Veselov, D., Kudoyarova, G., 2021. Limitation of Cytokinin Export to the Shoots by Nucleoside Transporter ENT3 and Its Linkage with Root Elongation in Arabidopsis. Cells 10, 350. https://doi.org/10.3390/cells10020350

Kowalska, M., Galuszka, P., Frébortová, J., Šebela, M., Béres, T., Hluska, T., Šmehilová, M., Bilyeu, K.D., Frébort, I., 2010. Vacuolar and cytosolic cytokinin dehydrogenases of Arabidopsis thaliana: Heterologous expression, purification and properties. Phytochemistry 71, 1970–1978. https://doi.org/10.1016/j.phytochem.2010.08.013

Krishnaswamy, S., Verma, S., Rahman, M.H., Kav, N.N.V., 2011. Functional characterization of four APETALA2-family genes (RAP2.6, RAP2.6L, DREB19 and DREB26) in Arabidopsis. Plant Mol Biol 75, 107–127. https://doi.org/10.1007/s11103-010-9711-7

Krouk, G., Lacombe, B., Bielach, A., Perrine-Walker, F., Malinska, K., Mounier, E., Hoyerova, K., Tillard, P., Leon, S., Ljung, K., Zazimalova, E., Benkova, E., Nacry, P., Gojon, A., 2010. Nitrate-regulated auxin transport by NRT1.1 defines a mechanism for nutrient sensing in plants. Dev Cell 18, 927–937. https://doi.org/10.1016/j.devcel.2010.05.008

Kubiasová, K., Montesinos, J.C., Šamajová, O., Nisler, J., Mik, V., Semerádová, H., Plíhalová, L., Novák, O., Marhavý, P., Cavallari, N., Zalabák, D., Berka, K., Doležal, K., Galuszka, P., Šamaj, J., Strnad, M., Benková, E., Plíhal, O., Spíchal, L., 2020. Cytokinin fluoroprobe reveals multiple sites of cytokinin perception at plasma membrane and endoplasmic reticulum. Nature Communications 11, 4285. https://doi.org/10.1038/s41467-020-17949-0

Kubo, M., Kakimoto, T., 2000. The CYTOKININ-HYPERSENSITIVE genes of Arabidopsis negatively regulate the cytokinin-signaling pathway for cell division and chloroplast development. The Plant Journal 23, 385–394. https://doi.org/10.1046/j.1365-313x.2000.00796.x

Kurakawa, T., Ueda, N., Maekawa, M., Kobayashi, K., Kojima, M., Nagato, Y., Sakakibara, H., Kyozuka, J., 2007. Direct control of shoot meristem activity by a cytokinin-activating enzyme. Nature 445, 652–655. https://doi.org/10.1038/nature05504

Kuroha, T., Tokunaga, H., Kojima, M., Ueda, N., Ishida, T., Nagawa, S., Fukuda, H., Sugimoto, K., Sakakibara, H., 2009. Functional analyses of LONELY GUY cytokinin-activating enzymes reveal the importance of the direct activation pathway in Arabidopsis. The Plant cell 21, 3152–69. https://doi.org/10.1105/tpc.109.068676

Laloue, M., Terrine, C., Guern, J., 1977. Cytokinins: Metabolism and Biological Activity of N-(Delta-Isopentenyl)adenosine and N-(Delta-Isopentenyl)adenine in Tobacco Cells and Callus. Plant physiology 59, 478–83.

Landrein, B., Formosa-Jordan, P., Malivert, A., Schuster, C., Melnyk, C.W., Yang, W., Turnbull, C., Meyerowitz, E.M., Locke, J.C.W., Jönsson, H., 2018. Nitrate modulates stem cell dynamics in Arabidopsis shoot meristems through cytokinins. Proceedings of the National Academy of Sciences 115, 1382–1387. https://doi.org/10.1073/pnas.1718670115

Le Hir, R., Sorin, C., Chakraborti, D., Moritz, T., Schaller, H., Tellier, F., Robert, S., Morin, H., Bako, L., Bellini, C., 2013. ABCG9, ABCG11 and ABCG14 ABC transporters are required for vascular development in Arabidopsis. The Plant Journal 76, 811–824. https://doi.org/10.1111/tpj.12334

Leonard, N.J., Playtis, A.J., Skoog, F., Schmitz, R.Y., 1971. Stereoselective synthesis of cis-zeatin. J. Am. Chem. Soc. 93, 3056–3058. https://doi.org/10.1021/ja00741a046

Leopold, A.C., Kawase, M., 1964. Benzyladenine Efffcts on Bean Leaf Growth and Senescence. American Journal of Botany 51, 294–298. https://doi.org/10.1002/j.1537-2197.1964.tb06633.x

Letham, D.S., 1973. Cytokinins from Zea mays. Phytochemistry 12, 2445–2455. https://doi.org/10.1016/0031-9422(73)80453-4

Letham, D.S., 1963. Zeatin, a factor inducing cell division isolated from Zea mays. Life Sciences 2, 569–573. https://doi.org/10.1016/0024-3205(63)90108-5

Li, G., Liu, K., Baldwin, S.A., Wang, D., 2003. Equilibrative Nucleoside Transporters of Arabidopsis thaliana: cDNA cloning, expression pattern, and analysis of transport activities. J. Biol. Chem. 278, 35732–35742. https://doi.org/10.1074/jbc.M304768200

Liu, J., Moore, S., Chen, C., Lindsey, K., 2017. Crosstalk Complexities between Auxin, Cytokinin, and Ethylene in Arabidopsis Root Development: From Experiments to Systems Modeling, and Back Again. Molecular Plant 10, 1480–1496. https://doi.org/10.1016/j.molp.2017.11.002

Lomin, S.N., Krivosheev, D.M., Steklov, M.Y., Arkhipov, D.V., Osolodkin, D.I., Schmülling, T., Romanov, G.A., 2015. Plant membrane assays with cytokinin receptors underpin the unique role of free cytokinin bases as biologically active ligands. J Exp Bot 66, 1851–1863. https://doi.org/10.1093/jxb/eru522

Lopes, F.L., Galvan-Ampudia, C., Landrein, B., 2021. WUSCHEL in the shoot apical meristem: old player, new tricks. Journal of Experimental Botany 72, 1527–1535. https://doi.org/10.1093/jxb/eraa572

Ľuptáková, E., Vigouroux, A., Končitíková, R., Kopečná, M., Zalabák, D., Novák, O., Salcedo Sarmiento, S., Ćavar Zeljković, S., Kopečný, D.J., von Schwartzenberg, K., Strnad, M., Spíchal, L., De Diego, N., Kopečný, D., Moréra, S., 2024. Plant nucleoside N-ribohydrolases: riboside binding and role in nitrogen storage mobilization. The Plant Journal 117, 1432–1452. https://doi.org/10.1111/tpj.16572

MacLeod, J.K., Summons, R.E., Parker, C.W., Letham, D.S., 1975. Lupinic acid, a purinyl amino acid and a novel metabolite of zeatin. J. Chem. Soc., Chem. Commun. 809–810. https://doi.org/10.1039/C39750000809

Maeda, Y., Konishi, M., Kiba, T., Sakuraba, Y., Sawaki, N., Kurai, T., Ueda, Y., Sakakibara, H., Yanagisawa, S., 2018. A NIGT1-centred transcriptional cascade regulates nitrate signalling and incorporates phosphorus starvation signals in Arabidopsis. Nat Commun 9, 1376. https://doi.org/10.1038/s41467-018-03832-6

Mähönen, A.P., Bishopp, A., Higuchi, M., Nieminen, K.M., Kinoshita, K., Törmäkangas, K., Ikeda, Y., Oka, A., Kakimoto, T., Helariutta, Y., 2006. Cytokinin Signaling and Its Inhibitor AHP6 Regulate Cell Fate During Vascular Development. Science 311, 94–98. https://doi.org/10.1126/science.1118875

Malito, E., Coda, A., Bilyeu, K.D., Fraaije, M.W., Mattevi, A., 2004. Structures of Michaelis and Product Complexes of Plant Cytokinin Dehydrogenase: Implications for Flavoenzyme Catalysis. Journal of Molecular Biology 341, 1237–1249. https://doi.org/10.1016/J.JMB.2004.06.083

Mansfield, T.A., Schultes, N.P., Mourad, G.S., 2009. AtAzg1 and AtAzg2 comprise a novel family of purine transporters in Arabidopsis. FEBS Letters 583, 481–486. https://doi.org/10.1016/j.febslet.2008.12.048

Marchive, C., Roudier, F., Castaings, L., Bréhaut, V., Blondet, E., Colot, V., Meyer, C., Krapp, A., 2013. Nuclear retention of the transcription factor NLP7 orchestrates the early response to nitrate in plants. Nat Commun 4, 1713. https://doi.org/10.1038/ncomms2650

Marhavý, P., Duclercq, J., Weller, B., Feraru, E., Bielach, A., Offringa, R., Friml, J., Schwechheimer, C., Murphy, A., Benková, E., 2014. Cytokinin Controls Polarity of PIN1-Dependent Auxin Transport during Lateral Root Organogenesis. Current Biology 24, 1031–1037. https://doi.org/10.1016/j.cub.2014.04.002

Martin, R.C., Mok, M.C., Shaw, G., Mok, D.W.S., 1989. An Enzyme Mediating the Conversion of Zeatin to Dihydrozeatin in Phaseolus Embryos 1. Plant Physiol 90, 1630–1635.

Melino, V.J., Casartelli, A., George, J., Rupasinghe, T., Roessner, U., Okamoto, M., Heuer, S., 2018. RNA Catabolites Contribute to the Nitrogen Pool and Support Growth Recovery of Wheat. Front. Plant Sci. 9. https://doi.org/10.3389/fpls.2018.01539

Meunier, B., de Visser, S.P., Shaik, S., 2004. Mechanism of Oxidation Reactions Catalyzed by Cytochrome P450 Enzymes. Chem. Rev. 104, 3947–3980. https://doi.org/10.1021/cr020443g

Miller, C.O., Skoog, F., Okumura, F.S., von Saltza, M.H., Strong, F.M., 1956. Isolation, Structure and Synthesis of Kinetin, a Substance Promoting Cell Division. J. Am. Chem. Soc. 78, 1375–1380. https://doi.org/10.1021/ja01588a032

Miller, C.O., Skoog, F., Okumura, F.S., von Saltza, M.H., Strong, F.M., 1955a. Structure and Synthesis of Kinetin. J. Am. Chem. Soc. 77, 2662–2663. https://doi.org/10.1021/ja01614a108

Miller, C.O., Skoog, F., von Saltza, M.H., Strong, F.M., 1955b. Kinetin, a Cell Division Factor From Deoxyribonucleic Acid. J. Am. Chem. Soc. 77, 1392. https://doi.org/10.1021/ja01610a105

Miyawaki, K., Matsumoto-Kitano, M., Kakimoto, T., 2004. Expression of cytokinin biosynthetic isopentenyltransferase genes in Arabidopsis: tissue specificity and regulation by auxin, cytokinin, and nitrate. The Plant Journal 37, 128–138. https://doi.org/10.1046/j.1365-313X.2003.01945.x

Miyawaki, K., Tarkowski, P., Matsumoto-Kitano, M., Kato, T., Sato, S., Tarkowska, D., Tabata, S., Sandberg, G., Kakimoto, T., 2006. Roles of Arabidopsis ATP/ADP isopentenyltransferases and tRNA isopentenyltransferases in cytokinin biosynthesis. Proceedings of the National Academy of Sciences of the United States of America 103, 16598–603. https://doi.org/10.1073/pnas.0603522103

Moffatt, B.A., Wang, L., Allen, M.S., Stevens, Y.Y., Qin, W., Snider, J., Von Schwartzenberg, K., 2000. Adenosine Kinase of Arabidopsis. Kinetic Properties and Gene Expression. Plant Physiology 124, 1775–1785. https://doi.org/10.1104/pp.124.4.1775

Möhlmann, T., Mezher, Z., Schwerdtfeger, G., Neuhaus, H.E., 2001. Characterisation of a concentrative type of adenosine transporter from Arabidopsis thaliana (ENT1,At). FEBS Letters 509, 370–374. https://doi.org/10.1016/S0014-5793(01)03195-7

Mok, M.C., Martin, R.C., Dobrev, P.I., Vanková, R., Ho, P.S., Yonekura-Sakakibara, K., Sakakibara, H., Mok, D.W.S., 2005. Topolins and Hydroxylated Thidiazuron Derivatives Are Substrates of Cytokinin O-Glucosyltransferase

with Position Specificity Related to Receptor Recognition. Plant Physiol 137, 1057–1066. https://doi.org/10.1104/pp.104.057174
Mougel, C., Zhulin, I.B., 2001. CHASE: an extracellular sensing domain common to transmembrane receptors from prokaryotes, lower eukaryotes and plants. Trends in Biochemical Sciences 26, 582–584. https://doi.org/10.1016/S0968-0004(01)01969-7
Murakoshi, I., Ikegami, F., Ookawa, N., Haginiwa, J., Letham, Davids., 1977. Enzymatic Synthesis of Lupinic Acid, a Novel Metabolite of Zeatin in Higher Plants. Chemical & Pharmaceutical Bulletin 25, 520–522. https://doi.org/10.1248/cpb.25.520
Nagata, T., Nemoto, Y., Hasezawa, S., 1992. Tobacco BY-2 Cell Line as the “HeLa” Cell in the Cell Biology of Higher Plants. International Review of Cytology 132, 1–30. https://doi.org/10.1016/S0074-7696(08)62452-3
Nedvěd, D., Hošek, P., Klíma, P., Hoyerová, K., 2021. Differential Subcellular Distribution of Cytokinins: How Does Membrane Transport Fit into the Big Picture? International Journal of Molecular Sciences 22, 3428. https://doi.org/10.3390/ijms22073428
Nishimura, C., Ohashi, Y., Sato, S., Kato, T., Tabata, S., Ueguchi, C., 2004. Histidine Kinase Homologs That Act as Cytokinin Receptors Possess Overlapping Functions in the Regulation of Shoot and Root Growth in Arabidopsis. Plant Cell 16, 1365–1377. https://doi.org/10.1105/tpc.021477
Osugi, A., Kojima, M., Takebayashi, Y., Ueda, N., Kiba, T., Sakakibara, H., 2017. Systemic transport of trans-zeatin and its precursor have differing roles in Arabidopsis shoots. Nature Plants 3, 17112. https://doi.org/10.1038/nplants.2017.112
Othman, E.M., Naseem, M., Awad, E., Dandekar, T., Stopper, H., 2016. The Plant Hormone Cytokinin Confers Protection against Oxidative Stress in Mammalian Cells. PLoS One 11. https://doi.org/10.1371/journal.pone.0168386
Pačes, V., Werstiuk, E., Hall, R.H., 1971. Conversion of N6-(A2-Isopentenyl)adenosine to Adenosine by Enzyme Activity in Tobacco Tissue. Plant Physiol 48, 775–778.
Parker, J.L., Newstead, S., 2014. Molecular basis of nitrate uptake by the plant nitrate transporter NRT1.1. Nature 507, 68–72. https://doi.org/10.1038/nature13116
Pernisová, M., Klíma, P., Horák, J., Válková, M., Malbeck, J., Souček, P., Reichman, P., Hoyerová, K., Dubová, J., Friml, J., Za, E., žímalová, Hejátko, J., 2009. Cytokinins modulate auxin-induced organogenesis in plants via regulation of the auxin efflux. PNAS 106, 3609–3614. https://doi.org/10.1073/pnas.0811539106
Pertry, I., Václavíková, K., Depuydt, S., Galuszka, P., Spíchal, L., Temmerman, W., Stes, E., Schmülling, T., Kakimoto, T., Montagu, M.C.E.V., Strnad, M., Holsters, M., Tarkowski, P., Vereecke, D., 2009. Identification of Rhodococcus fascians cytokinins and their modus operandi to reshape the plant. PNAS 106, 929–934. https://doi.org/10.1073/pnas.0811683106
Pertry, I., Václavíková, K., Gemrotová, M., Spíchal, L., Galuszka, P., Depuydt, S., Temmerman, W., Stes, E., De Keyser, A., Riefler, M., Biondi, S., Novák, O., Schmülling, T., Strnad, M., Tarkowski, P., Holsters, M., Vereecke, D., 2010. Rhodococcus fascians Impacts Plant Development Through the Dynamic Fas-Mediated Production of a Cytokinin Mix. MPMI 23, 1164–1174. https://doi.org/10.1094/MPMI-23-9-1164
Pils, B., Heyl, A., 2009. Unraveling the Evolution of Cytokinin Signaling. Plant Physiology 151, 782–791. https://doi.org/10.1104/pp.109.139188
Poitout, A., Crabos, A., Petřík, I., Novák, O., Krouk, G., Lacombe, B., Ruffel, S., 2018. Responses to Systemic Nitrogen Signaling in Arabidopsis Roots Involve *trans* -Zeatin in Shoots. Plant Cell 30, 1243–1257. https://doi.org/10.1105/tpc.18.00011
Popelková, H., Fraaije, M.W., Novák, O., Frébortová, J., Bilyeu, K.D., Frébort, I., 2006. Kinetic and chemical analyses of the cytokinin dehydrogenase-catalysed reaction: correlations with the crystal structure. Biochem J 398, 113–124. https://doi.org/10.1042/BJ20060280
Punwani, J.A., Hutchison, C.E., Schaller, G.E., Kieber, J.J., 2010. The subcellular distribution of the Arabidopsis histidine phosphotransfer proteins is independent of cytokinin signaling. The Plant Journal 62, 473–482. https://doi.org/10.1111/j.1365-313X.2010.04165.x
Qi, Z., Xiong, L., 2013. Characterization of a Purine Permease Family Gene OsPUP7 Involved in Growth and Development Control in Rice. Journal of Integrative Plant Biology 55, 1119–1135. https://doi.org/10.1111/jipb.12101
Radchuk, V., Belew, Z.M., Gündel, A., Mayer, S., Hilo, A., Hensel, G., Sharma, R., Neumann, K., Ortleb, S., Wagner, S., Muszynska, A., Crocoll, C., Xu, D., Hoffie, I., Kumlehn, J., Fuchs, J., Peleke, F.F., Szymanski, J.J., Rolletschek, H., Nour-Eldin, H.H., Borisjuk, L., 2023. SWEET11b transports both sugar and cytokinin in developing barley grains. The Plant Cell 35, 2186–2207. https://doi.org/10.1093/plcell/koad055
Radhika, V., Ueda, N., Tsuboi, Y., Kojima, M., Kikuchi, J., Kudo, T., Sakakibara, H., 2015. Methylated Cytokinins from the Phytopathogen Rhodococcus fascians Mimic Plant Hormone Activity. Plant Physiology 169, 1118–1126. https://doi.org/10.1104/pp.15.00787

Raines, T., Shanks, C., Cheng, C.-Y., McPherson, D., Argueso, C.T., Kim, H.J., Franco-Zorrilla, J.M., López-Vidriero, I., Solano, R., Vaňková, R., Schaller, G.E., Kieber, J.J., 2016. The cytokinin response factors modulate root and shoot growth and promote leaf senescence in Arabidopsis. The Plant Journal 85, 134–147. https://doi.org/10.1111/tpj.13097

Ramireddy, E., Chang, L., Schmülling, T., 2014. Cytokinin as a mediator for regulating root system architecture in response to environmental cues. Plant Signaling & Behavior 9, e27771. https://doi.org/10.4161/psb.27771

Rashotte, A.M., Mason, M.G., Hutchison, C.E., Ferreira, F.J., Schaller, G.E., Kieber, J.J., 2006. A subset of Arabidopsis AP2 transcription factors mediates cytokinin responses in concert with a two-component pathway. Proceedings of the National Academy of Sciences 103, 11081–11085. https://doi.org/10.1073/pnas.0602038103

Richmond, A.E., Lang, A., 1957. Effect of Kinetin on Protein Content and Survival of Detached Xanthium Leaves. Science 125, 650–651. https://doi.org/10.1126/science.125.3249.650-a

Romanov, G.A., Lomin, S.N., Schmülling, T., 2006. Biochemical characteristics and ligand-binding properties of Arabidopsis cytokinin receptor AHK3 compared to CRE1/AHK4 as revealed by a direct binding assay. Journal of Experimental Botany 57, 4051–4058. https://doi.org/10.1093/jxb/erl179

Romanov, G.A., Schmülling, T., 2021. On the biological activity of cytokinin free bases and their ribosides. Planta 255, 27. https://doi.org/10.1007/s00425-021-03810-1

Rong, C., Zhang, R., Liu, Y., Chang, Z., Liu, Z., Ding, Y., Ding, C., 2024. Purine permease (PUP) family gene PUP11 positively regulates the rice seed setting rate by influencing seed development. Plant Cell Rep 43, 112. https://doi.org/10.1007/s00299-024-03193-z

Sakai, H., Honma, T., Aoyama, T., Sato, S., Kato, T., Tabata, S., Oka, A., 2001. ARR1, a Transcription Factor for Genes Immediately Responsive to Cytokinins. Science 294, 1519–1521. https://doi.org/10.1126/science.1065201

Sakakibara, H., 2021. Cytokinin biosynthesis and transport for systemic nitrogen signaling. The Plant Journal 105, 421–430. https://doi.org/10.1111/tpj.15011

Sakakibara, H., Kasahara, H., Ueda, N., Kojima, M., Takei, K., Hishiyama, S., Asami, T., Okada, K., Kamiya, Y., Yamaya, T., Yamaguchi, S., Macmillan, J., 2005. Agrobacterium tumefaciens increases cytokinin production in plastids by modifying the biosynthetic pathway in the host plant. PNAS 102, 9972–9977. https://doi.org/10.1073/pnas.0500793102

Salomé, P.A., To, J.P.C., Kieber, J.J., McClung, C.R., 2005. *Arabidopsis* Response Regulators ARR3 and ARR4 Play Cytokinin-Independent Roles in the Control of Circadian Period. The Plant Cell 18, 55–69. https://doi.org/10.1105/tpc.105.037994

Schäfer, M., Brütting, C., Canales, I.M., Großkinsky, D.K., Vankova, R., Baldwin, I.T., Meldau, S., 2015. The role of cis-zeatin-type cytokinins in plant growth regulation and mediating responses to environmental interactions. J Exp Bot 66, 4873–4884. https://doi.org/10.1093/jxb/erv214

Schaller, G.E., Street, I.H., Kieber, J.J., 2014. Cytokinin and the cell cycle. Current Opinion in Plant Biology, SI: Cell signalling and gene regulation 21, 7–15. https://doi.org/10.1016/j.pbi.2014.05.015

Schoor, S., Farrow, S., Blaschke, H., Lee, S., Perry, G., Von Schwartzenberg, K., Emery, N., Moffatt, B., 2011. Adenosine Kinase Contributes to Cytokinin Interconversion in Arabidopsis. Plant Physiology 157, 659–672. https://doi.org/10.1104/pp.111.181560

Schweizer, U., Bohleber, S., Fradejas-Villar, N., 2017. The modified base isopentenyladenosine and its derivatives in tRNA. RNA Biol 14, 1197–1208. https://doi.org/10.1080/15476286.2017.1294309

Sena, G., Wang, X., Liu, H.-Y., Hofhuis, H., Birnbaum, K.D., 2009. Organ regeneration does not require a functional stem cell niche in plants. Nature 457, 1150–1153. https://doi.org/10.1038/nature07597

Silva-Navas, J., Conesa, C.M., Saez, A., Navarro-Neila, S., Garcia-Mina, J.M., Zamarreño, A.M., Baigorri, R., Swarup, R., del Pozo, J.C., 2019. Role of cis-zeatin in root responses to phosphate starvation. New Phytologist 224, 242–257. https://doi.org/10.1111/nph.16020

Šimura, J., Antoniadi, I., Široká, J., Tarkowská, D., Strnad, M., Ljung, K., Novák, O., 2018. Plant Hormonomics: Multiple Phytohormone Profiling by Targeted Metabolomics. Plant Physiology 177, 476–489. https://doi.org/10.1104/pp.18.00293

Skalák, J., Vercruyssen, L., Claeys, H., Hradilová, J., Cerny, M., Novák, O., Placková, L., Saiz-Fernández, I., Skaláková, P., Coppens, F., Dhondt, S., Koukalová, S., Zouhar, J., Inzé, D., Brzobohaty, B., 2019. Multifaceted activity of cytokinin in leaf development shapes its size and structure in Arabidopsis. Plant Journal 97, 805–824. https://doi.org/10.1111/tpj.14285

Skoog, F., Miller, C.O., 1957. Chemical regulation of growth and organ formation in plant tissues cultured in vitro. Symp Soc Exp Biol 11, 118–130.

Šmehilová, M., Dobrůšková, J., Novák, O., Takáč, T., Galuszka, P., 2016. Cytokinin-Specific Glycosyltransferases Possess Different Roles in Cytokinin Homeostasis Maintenance. Front Plant Sci 7. https://doi.org/10.3389/fpls.2016.01264

Šmehilová, M., Galuszka, P., Bilyeu, K.D., Jaworek, P., Kowalska, M., Šebela, M., Sedlářová, M., English, J.T., Frébort, I., 2009. Subcellular localization and biochemical comparison of cytosolic and secreted cytokinin dehydrogenase enzymes from maize. Journal of Experimental Botany 60, 2701–2712. https://doi.org/10.1093/jxb/erp126

Sørensen, J.L., Benfield, A.H., Wollenberg, R.D., Westphal, K., Wimmer, R., Nielsen, M.R., Nielsen, K.F., Carere, J., Covarelli, L., Beccari, G., Powell, J., Yamashino, T., Kogler, H., Sondergaard, T.E., Gardiner, D.M., 2017. The cereal pathogen Fusarium pseudograminearum produces a new class of active cytokinins during infection. Mol Plant Pathol 19, 1140–1154. https://doi.org/10.1111/mpp.12593

Spíchal, L., 2012. Cytokinins - recent news and views of evolutionally old molecules. Functional Plant Biology 39, 267–284. https://doi.org/10.1071/FP11276

Spíchal, L., Rakova, N.Y., Riefler, M., Mizuno, T., Romanov, G.A., Strnad, M., Schmülling, T., 2004. Two Cytokinin Receptors of Arabidopsis thaliana, CRE1/AHK4 and AHK3, Differ in their Ligand Specificity in a Bacterial Assay. Plant Cell Physiol 45, 1299–1305. https://doi.org/10.1093/pcp/pch132

Stolz, A., Riefler, M., Lomin, S.N., Achazi, K., Romanov, G.A., Schmülling, T., 2011. The specificity of cytokinin signalling in Arabidopsis thaliana is mediated by differing ligand affinities and expression profiles of the receptors. The Plant Journal 67, 157–168. https://doi.org/10.1111/j.1365-313X.2011.04584.x

Strnad, M., 1997. The aromatic cytokinins. Physiologia Plantarum 101, 674–688. https://doi.org/10.1111/J.1399-3054.1997.TB01052.X

Strnad, M., Peters, W., Hanuš, J., Beck, E., 1994. Ortho-topolin-9-glucoside, an aromatic cytokinin from Populus x canadensis cv Robusta leaves. Phytochemistry, The international journal of plant biochemistry 37, 1059–1062. https://doi.org/10.1016/S0031-9422(00)89528-X

Sun, J., Bankston, J.R., Payandeh, J., Hinds, T.R., Zagotta, W.N., Zheng, N., 2014. Crystal structure of the plant dual-affinity nitrate transporter NRT1.1. Nature 507, 73–77. https://doi.org/10.1038/nature13074

Sun, J., Hirose, N., Wang, X., Wen, P., Xue, L., Sakakibara, H., Zuo, J., 2005. Arabidopsis SOI33/AtENT8 Gene Encodes a Putative Equilibrative Nucleoside Transporter That Is Involved in Cytokinin Transport In Planta. Journal of Integrative Plant Biology 47, 588–603. https://doi.org/10.1111/j.1744-7909.2005.00104.x

Sun, J., Zheng, N., 2015. Molecular Mechanism Underlying the Plant NRT1.1 Dual-Affinity Nitrate Transporter. Frontiers in Physiology 6.

Sun, W., Shahrajabian, M.H., Soleymani, A., 2024. The Roles of Plant-Growth-Promoting Rhizobacteria (PGPR)-Based Biostimulants for Agricultural Production Systems. Plants 13, 613. https://doi.org/10.3390/plants13050613

Sweere, U., Eichenberg, K., Lohrmann, J., Mira-Rodado, V., Bäurle, I., Kudla, J., Nagy, F., Schäfer, E., Harter, K., 2001. Interaction of the Response Regulator ARR4 with Phytochrome B in Modulating Red Light Signaling. Science 294, 1108–1111. https://doi.org/10.1126/science.1065022

Szydlowski, N., Bürkle, L., Pourcel, L., Moulin, M., Stolz, J., Fitzpatrick, T.B., 2013. Recycling of pyridoxine (vitamin B6) by PUP1 in Arabidopsis. The Plant Journal 75, 40–52. https://doi.org/10.1111/tpj.12195

Takei, K., Sakakibara, H., Sugiyama, T., 2001a. Identification of Genes Encoding Adenylate Isopentenyltransferase, a Cytokinin Biosynthesis Enzyme, in Arabidopsis thaliana. J. Biol. Chem. 276, 26405–26410. https://doi.org/10.1074/jbc.M102130200

Takei, K., Sakakibara, H., Taniguchi, M., Sugiyama, T., 2001b. Nitrogen-Dependent Accumulation of Cytokinins in Root and theTranslocation to Leaf: Implication of Cytokinin Species that Induces GeneExpression of Maize ResponseRegulator. Plant Cell Physiol 42, 85–93. https://doi.org/10.1093/pcp/pce009

Takei, K., Ueda, N., Aoki, K., Kuromori, T., Hirayama, T., Shinozaki, K., Yamaya, T., Sakakibara, H., 2004a. AtIPT3 is a Key Determinant of Nitrate-Dependent Cytokinin Biosynthesis in Arabidopsis. Plant Cell Physiol 45, 1053–1062. https://doi.org/10.1093/pcp/pch119

Takei, K., Yamaya, T., Sakakibara, H., 2004b. Arabidopsis CYP735A1 and CYP735A2 encode cytokinin hydroxylases that catalyze the biosynthesis of trans-Zeatin. The Journal of biological chemistry 279, 41866–72. https://doi.org/10.1074/jbc.M406337200

Talla, S.K., Panigrahy, M., Kappara, S., Nirosha, P., Neelamraju, S., Ramanan, R., 2016. Cytokinin delays dark-induced senescence in rice by maintaining the chlorophyll cycle and photosynthetic complexes. Journal of Experimental Botany 67, 1839–1851. https://doi.org/10.1093/jxb/erv575

Tandio, D., Vilas, G., Hammond, J.R., 2019. Bidirectional transport of 2-chloroadenosine by equilibrative nucleoside transporter 4 (hENT4): Evidence for allosteric kinetics at acidic pH. Sci Rep 9, 13555. https://doi.org/10.1038/s41598-019-49929-w

Tarkowská, D., Doležal, K., Tarkowski, P., Åstot, C., Holub, J., Fuksová, K., Schmülling, T., Sandberg, G., Strnad, M., 2003. Identification of new aromatic cytokinins in Arabidopsis thaliana and Populus × canadensis leaves by LC-(+)ESI-MS and capillary liquid chromatography/frit–fast atom bombardment mass spectrometry. Physiologia Plantarum 117, 579–590. https://doi.org/10.1034/j.1399-3054.2003.00071.x

Tessi, T.M., Brumm, S., Winklbauer, E., Schumacher, B., Pettinari, G., Lescano, I., González, C.A., Wanke, D., Maurino, V.G., Harter, K., Desimone, M., 2020. Arabidopsis AZG2 transports cytokinins in vivo and regulates lateral root emergence. New Phytologist 229, 979–993. https://doi.org/10.1111/nph.16943

Tessi, T.M., Maurino, V.G., Shahriari, M., Meissner, E., Novak, O., Pasternak, T., Schumacher, B.S., Ditengou, F., Li, Z., Duerr, J., Flubacher, N.S., Nautscher, M., Williams, A., Kazimierczak, Z., Strnad, M., Thumfart, J.-O., Palme, K., Desimone, M., Teale, W.D., 2023. AZG1 is a cytokinin transporter that interacts with auxin transporter PIN1 and regulates the root stress response. New Phytologist 238, 1924–1941. https://doi.org/10.1111/nph.18879

The UniProt Consortium, 2023. UniProt: the Universal Protein Knowledgebase in 2023. Nucleic Acids Research 51, D523–D531. https://doi.org/10.1093/nar/gkac1052

To, J.P.C., Deruère, J., Maxwell, B.B., Morris, V.F., Hutchison, C.E., Ferreira, F.J., Schaller, G.E., Kieber, J.J., 2007. Cytokinin Regulates Type-A Arabidopsis Response Regulator Activity and Protein Stability via Two-Component Phosphorelay. The Plant Cell 19, 3901–3914. https://doi.org/10.1105/tpc.107.052662

To, J.P.C., Haberer, G., Ferreira, F.J., Deruère, J., Mason, M.G., Schaller, G.E., Alonso, J.M., Ecker, J.R., Kieber, J.J., 2004. Type-A Arabidopsis Response Regulators Are Partially Redundant Negative Regulators of Cytokinin Signaling. Plant Cell 16, 658–671. https://doi.org/10.1105/tpc.018978

Traub, M., Flörchinger, M., Piecuch, J., Kunz, H., Weise-Steinmetz, A., Deitmer Joachim W., Ekkehard Neuhaus H., Möhlmann Torsten, 2007. The fluorouridine insensitive 1 (fur1) mutant is defective in equilibrative nucleoside transporter 3 (ENT3), and thus represents an important pyrimidine nucleoside uptake system in Arabidopsis thaliana. The Plant Journal 49, 855–864. https://doi.org/10.1111/j.1365-313X.2006.02998.x

Tsay, Y.-F., 2014. How to switch affinity. Nature 507, 44–45. https://doi.org/10.1038/nature13063

Vanneste, S., De Rybel, B., Beemster, G.T.S., Ljung, K., De Smet, I., Van Isterdael, G., Naudts, M., Iida, R., Gruissem, W., Tasaka, M., Inzé, D., Fukaki, H., Beeckman, T., 2005. Cell Cycle Progression in the Pericycle Is Not Sufficient for SOLITARY ROOT/IAA14-Mediated Lateral Root Initiation in *Arabidopsis thaliana*. The Plant Cell 17, 3035–3050. https://doi.org/10.1105/tpc.105.035493

Verrier, P.J., Bird, D., Burla, B., Dassa, E., Forestier, C., Geisler, M., Klein, M., Kolukisaoglu, Ü., Lee, Y., Martinoia, E., Murphy, A., Rea, P.A., Samuels, L., Schulz, B., Spalding, E.P., Yazaki, K., Theodoulou, F.L., 2008. Plant ABC proteins – a unified nomenclature and updated inventory. Trends in Plant Science 13, 151–159. https://doi.org/10.1016/j.tplants.2008.02.001

Voller, J., Béres, T., Zatloukal, M., Džubák, P., Hajdúch, M., Doležal, K., Schmülling, T., Miroslav, S., 2019. Anti-cancer activities of cytokinin ribosides. Phytochem Rev 18, 1101–1113. https://doi.org/10.1007/s11101-019-09620-4

Voller, J., Zatloukal, M., Lenobel, R., Doležal, K., Béreš, T., Kryštof, V., Spíchal, L., Niemann, P., Džubák, P., Hajdúch, M., Strnad, M., 2010. Anticancer activity of natural cytokinins: A structure–activity relationship study. Phytochemistry 71, 1350–1359. https://doi.org/10.1016/j.phytochem.2010.04.018

Vylíčilová, H., Bryksová, M., Matušková, V., Doležal, K., Plíhalová, L., Strnad, M., 2020. Naturally Occurring and Artificial N9-Cytokinin Conjugates: From Synthesis to Biological Activity and Back. Biomolecules 10, 832. https://doi.org/10.3390/biom10060832

Wang, C., Yu, L., Zhang, J., Zhou, Y., Sun, B., Xiao, Q., Zhang, M., Liu, H., Li, Jinhong, Li, Jialu, Luo, Y., Xu, J., Lian, Z., Lin, J., Wang, X., Zhang, P., Guo, L., Ren, R., Deng, D., 2023. Structural basis of the substrate recognition and inhibition mechanism of Plasmodium falciparum nucleoside transporter PfENT1. Nat Commun 14, 1727. https://doi.org/10.1038/s41467-023-37411-1

Wang, J., Ma, X.-M., Kojima, M., Sakakibara, H., Hou, B.-K., 2013. Glucosyltransferase UGT76C1 finely modulates cytokinin responses via cytokinin N-glucosylation in Arabidopsis thaliana. Plant Physiology and Biochemistry 65, 9–16. https://doi.org/10.1016/J.PLAPHY.2013.01.012

Wang, J., Ma, X.-M., Kojima, M., Sakakibara, H., Hou, B.-K., 2011. N-Glucosyltransferase UGT76C2 is Involved in Cytokinin Homeostasis and Cytokinin Response in Arabidopsis thaliana. Plant and Cell Physiology 52, 2200–2213. https://doi.org/10.1093/pcp/pcr152

Wang, R., Okamoto, M., Xing, X., Crawford, N.M., 2003. Microarray Analysis of the Nitrate Response in Arabidopsis Roots and Shoots Reveals over 1,000 Rapidly Responding Genes and New Linkages to Glucose, Trehalose-6-Phosphate, Iron, and Sulfate Metabolism. Plant Physiology 132, 556–567. https://doi.org/10.1104/pp.103.021253

Wang, T.L., Horgan, R., 1978. Dihydrozeatin riboside, a minor cytokinin from the leaves of Phaseolus vulgaris L. Planta 140, 151–153. https://doi.org/10.1007/BF00384914

Werner, T., Motyka, V., Strnad, M., Schmülling, T., 2001. Regulation of plant growth by cytokinin. PNAS 98, 10487–10492. https://doi.org/10.1073/pnas.171304098

Werner, T., Schmülling, T., 2009. Cytokinin action in plant development. Current Opinion in Plant Biology, Cell signalling and gene regulation 12, 527–538. https://doi.org/10.1016/j.pbi.2009.07.002

Wildman, S.A., Crippen, G.M., 1999. Prediction of Physicochemical Parameters by Atomic Contributions. J. Chem. Inf. Comput. Sci. 39, 868–873. https://doi.org/10.1021/ci990307l
Wilkens, S., 2015. Structure and mechanism of ABC transporters. F1000Prime Rep 7, 14. https://doi.org/10.12703/P7-14
Winter, D., Vinegar, B., Nahal, H., Ammar, R., Wilson, G.V., Provart, N.J., 2007. An "Electronic Fluorescent Pictograph" Browser for Exploring and Analyzing Large-Scale Biological Data Sets. PLOS ONE 2, e718. https://doi.org/10.1371/journal.pone.0000718
Wirtz, M., Hell, R., 2006. Functional analysis of the cysteine synthase protein complex from plants: Structural, biochemical and regulatory properties. Journal of Plant Physiology 163, 273–286. https://doi.org/10.1016/j.jplph.2005.11.013
Wormit, A., Traub, M., Flörchinger, M., Neuhaus, H.E., Möhlmann, T., 2004. Characterization of three novel members of the Arabidopsis thaliana equilibrative nucleoside transporter (ENT) family. Biochem J 383, 19–26. https://doi.org/10.1042/BJ20040389
Wright, N.J., Lee, S.-Y., 2019. Structures of human ENT1 in complex with adenosine reuptake inhibitors. Nat Struct Mol Biol 26, 599–606. https://doi.org/10.1038/s41594-019-0245-7
Wu, W., Du, K., Kang, X., Wei, H., 2021. The diverse roles of cytokinins in regulating leaf development. Hortic Res 8, 118. https://doi.org/10.1038/s41438-021-00558-3
Wulfetange, K., Lomin, S.N., Romanov, G.A., Stolz, A., Heyl, A., Schmülling, T., 2011. The cytokinin receptors of Arabidopsis are located mainly to the endoplasmic reticulum. Plant Physiol 156, 1808–1818. https://doi.org/10.1104/pp.111.180539
Xiao, Y., Liu, D., Zhang, G., Gao, S., Liu, L., Xu, F., Che, R., Wang, Y., Tong, H., Chu, C., 2019. Big Grain3, encoding a purine permease, regulates grain size via modulating cytokinin transport in rice. Journal of Integrative Plant Biology 61, 581–597. https://doi.org/10.1111/jipb.12727
Xiao, Y., Zhang, J., Yu, G., Lu, X., Mei, W., Deng, H., Zhang, G., Chen, G., Chu, C., Tong, H., Tang, W., 2020. Endoplasmic Reticulum-Localized PURINE PERMEASE1 Regulates Plant Height and Grain Weight by Modulating Cytokinin Distribution in Rice. Front. Plant Sci. 11. https://doi.org/10.3389/fpls.2020.618560
Xu, L., Jia, W., Tao, X., Ye, F., Zhang, Yan, Ding, Z.J., Zheng, S.J., Qiao, S., Su, N., Zhang, Yu, Wu, S., Guo, J., 2024. Structures and mechanisms of the Arabidopsis cytokinin transporter AZG1. Nat. Plants 10, 180–191. https://doi.org/10.1038/s41477-023-01590-y
Yamada, H., Suzuki, T., Terada, K., Takei, K., Ishikawa, K., Miwa, K., Yamashino, T., Mizuno, T., 2001. The Arabidopsis AHK4 Histidine Kinase is a Cytokinin-Binding Receptor that Transduces Cytokinin Signals Across the Membrane. Plant Cell Physiol 42, 1017–1023. https://doi.org/10.1093/pcp/pce127
Yang, Q., Zhang, J., Kojima, M., Takebayashi, Y., Uragami, T., Kiba, T., Sakakibara, H., Lee, Y., 2022. ABCG11 modulates cytokinin responses in Arabidopsis thaliana. Front. Plant Sci. 13. https://doi.org/10.3389/fpls.2022.976267
Yao, S.Y.M., Ng, A.M.L., Cass, C.E., Baldwin, S.A., Young, J.D., 2011. Nucleobase Transport by Human Equilibrative Nucleoside Transporter 1 (hENT1). J Biol Chem 286, 32552–32562. https://doi.org/10.1074/jbc.M111.236117
Yao, S.Y.M., Ng, A.M.L., Vickers, M.F., Sundaram, M., Cass, C.E., Baldwin, S.A., Young, J.D., 2002. Functional and Molecular Characterization of Nucleobase Transport by Recombinant Human and Rat Equilibrative Nucleoside Transporters 1 and 2: CHIMERIC CONSTRUCTS REVEAL A ROLE FOR THE ENT2 HELIX 5–6 REGION IN NUCLEOBASE TRANSLOCATION *. Journal of Biological Chemistry 277, 24938–24948. https://doi.org/10.1074/jbc.M200966200
Young, J.D., Yao, S.Y.M., Sun, L., Cass, C.E., Baldwin, S.A., 2008. Human equilibrative nucleoside transporter (ENT) family of nucleoside and nucleobase transporter proteins. Xenobiotica 38, 995–1021. https://doi.org/10.1080/00498250801927427
Zalabák, D., Galuszka, P., Mrízová, K., Podlešáková, K., Gu, R., Frébortová, J., 2014. Biochemical characterization of the maize cytokinin dehydrogenase family and cytokinin profiling in developing maize plantlets in relation to the expression of cytokinin dehydrogenase genes. Plant Physiology and Biochemistry 74, 283–293. https://doi.org/10.1016/j.plaphy.2013.11.020
Zdarska, M., Dobisová, T., Gelová, Z., Pernisová, M., Dabravolski, S., Hejátko, J., 2015. Illuminating light, cytokinin, and ethylene signalling crosstalk in plant development: Fig. 1. EXBOTJ 66, 4913–4931. https://doi.org/10.1093/jxb/erv261
Zhang, K., Novak, O., Wei, Z., Gou, M., Zhang, X., Yu, Y., Yang, H., Cai, Y., Strnad, M., Liu, C.-J., 2014. Arabidopsis ABCG14 protein controls the acropetal translocation of root-synthesized cytokinins. Nature Communications 5, 1–12. https://doi.org/10.1038/ncomms4274
Zhang, X., Chen, Y., Lin, X., Hong, X., Zhu, Y., Li, W., He, W., An, F., Guo, H., 2013. Adenine Phosphoribosyl Transferase 1 is a Key Enzyme Catalyzing Cytokinin Conversion from Nucleobases to Nucleotides in Arabidopsis. Molecular Plant 6, 1661–1672. https://doi.org/10.1093/mp/sst071

Zhao, J., Deng, X., Qian, J., Liu, T., Ju, M., Li, J., Yang, Q., Zhu, X., Li, W., Liu, C.-J., Jin, Z., Zhang, K., 2023. *Arabidopsis* ABCG14 forms a homodimeric transporter for multiple cytokinins and mediates long-distance transport of isopentenyladenine-type cytokinins. Plant Communications 4, 100468. https://doi.org/10.1016/j.xplc.2022.100468

Zhao, J., Yu, N., Ju, M., Fan, B., Zhang, Y., Zhu, E., Zhang, M., Zhang, K., 2019. ABC transporter OsABCG18 controls the shootward transport of cytokinins and grain yield in rice. Journal of Experimental Botany 70, 6277–6291. https://doi.org/10.1093/jxb/erz382

Zheng, B., Deng, Y., Mu, J., Ji, Z., Xiang, T., Niu, Q.-W., Chua, N.-H., Zuo, J., 2006. Cytokinin affects circadian-clock oscillation in a phytochrome B- and Arabidopsis response regulator 4-dependent manner. Physiologia Plantarum 127, 277–292. https://doi.org/10.1111/j.1399-3054.2006.00660.x

Zhou, Z., Liu, H., Ma, C., Chao, Y., Han, L., 2020. Transcriptome Analysis of the Cytokinin Response in Medicago truncatula. J. Plant Biol. 63, 189–202. https://doi.org/10.1007/s12374-020-09244-8

Zschiedrich, C.P., Keidel, V., Szurmant, H., 2016. Molecular Mechanisms of Two-Component Signal Transduction. Journal of Molecular Biology 428, 3752–3775. https://doi.org/10.1016/j.jmb.2016.08.003

Zürcher, E., Liu, J., di Donato, M., Geisler, M., Müller, B., 2016. Plant development regulated by cytokinin sinks. Science 353, 1027–1030.

Zwack, P.J., De Clercq, I., Howton, T.C., Hallmark, H.T., Hurny, A., Keshishian, E.A., Parish, A.M., Benkova, E., Mukhtar, M.S., Van Breusegem, F., Rashotte, A.M., 2016. Cytokinin Response Factor 6 Represses Cytokinin-Associated Genes during Oxidative Stress. Plant Physiol. pp.00415.2016. https://doi.org/10.1104/pp.16.00415